Dissertation
zur Erlangung des akademischen Grades
Doktor der Naturwissenschaften

Baryogenesis Originating from Lepton Number Violation Induced by Right-Handed Majorana Neutrinos

Sinan Zeißner
geboren in Herdecke

Dortmund, 2021

Lehrstuhl für Theoretische Physik III
Fakultät Physik
Technische Universität Dortmund

Erstgutachter:	Prof. Dr. Heinrich Päs
Zweitgutachter:	Jun.-Prof. Dr. Emmanuel Stamou
Abgabedatum:	08. März 2021
Disputation:	21. Juni 2021

Abstract

In this thesis, different ways to use right-handed Majorana neutrinos to explain the active neutrino masses as well as the baryon number asymmetry observed in our universe are investigated. It is shown that the induced lepton number violation can assist baryon number asymmetry generating models, whose asymmetry without additional lepton number violation is completely washed out by sphaleron transitions. Extending this investigation to the scotogenic model, also the relic dark matter abundance observed in our universe can be explained. Furthermore, different mechanisms for generating a lepton number asymmetry directly via interactions involving right-handed Majorana neutrinos are investigated. It is discussed that for models in which the Yukawa couplings of the neutrino sector can be larger than in the type-I seesaw mechanism, the parameter space for thermal leptogenesis is enlarged. Moreover, it is pointed out that considering thermal mass corrections, only an induced mass degeneracy of right-chiral neutrinos enables new prospects of leptogenesis.

Additionally, loop corrections for massive vector bosons interacting with each other are investigated in time-dependent perturbation theory. Studying the case of two interacting massive vector bosons in a simple example in detail, it is shown that the degree of divergence in the S-matrix is the same as expected from R_ξ gauge.

Kurzfassung

In dieser Arbeit werden verschiedene Möglichkeiten untersucht, wie rechtshändige Majorananeutrios zur Erzeugung der beobachteten Baryonzahlasymmetrie beitragen können. Es wird gezeigt, dass die induzierte Leptonenzahlverletzung Baryonenzahlasymmetrie erzeugende Modelle unterstützen kann, bei denen die erzeugte Asymmetrie ohne zusätzliche Leptonenzahlverletzung durch Sphaleronenübergänge wieder ausgelöscht wird. Um zusätzlich die beobachtete Dunkle Materie Dichte zu erklären, wird diese Untersuchung auf das Scotogenic Modell erweitert. Des Weiteren werden verschiedene Mechanismen einer direkten Leptonenzahlasymmetrieerzeugung durch Interaktionen mit rechtshändigen Majorananeutrinos untersucht. Es wird diskutiert, dass sich für Modelle, bei denen größere Yukawakopplungen als im Type-I Seesaw-Mechanismus möglich sind, der Parameterbereich für thermische Leptogenese vergrößern. Außerdem wird gezeigt, dass unter Beachtung thermischer Massenkorrekturen nur eine induzierte Massendegenerierung von rechtschiralen Neutrinos neue Möglichkeiten für Leptogenese eröffnet.

Unabhängig davon werden Schleifenkorrekturen von miteinander wechselwirkenden massiven Vektorbosonen in zeitabhängiger Störungstheorie betrachtet und dabei der Spezialfall von zwei wechselwirkenden massiven Vektorbosonen genauer untersucht. Für ein einfaches Beispiel wird gezeigt, dass der Divergenzgrad der S-Matrix der Erwartung aus der R_ξ-Eichung entspricht.

Contents

Acronyms

B	baryon number
BBN	Big Bang nucleosynthesis
BSM	beyond the Standard Model
CKM	Cabibbo-Kobayashi-Maskawa
CMB	cosmic microwave background
DM	dark matter
EV	expectation value
EWPT	electroweak phase transition
EWSB	electroweak symmetry breaking
FO	flavor oscillation
GR	general theory of relativity
GUT	Grand Unified Theory
L	lepton number
MSW	Mikheyev-Smirnov-Wolfenstein
QFT	quantum field theory
QM	quantum mechanics
PMNS	Pontecorvo-Maki-Nakagawa-Sakata
RGE	renormalization group equation
SM	Standard Model
SR	special theory of relativity
SSB	spontaneous symmetry breaking
TFT	thermal quantum field theory
VEV	vacuum expectation value
2HDM	two-Higgs-doublet model

Abbreviations

$\mathsf{H}(t)$	Hubble expansion rate
T_c	critical temperature
T_{Sph}	temperature where sphaleron transitions become inefficient

px	$=$	$p^\mu x_\mu$
dx	$=$	d^4x
$d\tilde{k}_i$	$=$	$\delta(k^2 - m_i^2)dk/(2\pi)^4$
$\delta^4(p^\mu - k^\mu)$	$=$	$\delta(p-k)$
$d\Omega^2$	$=$	$d\theta^2 + \sin^2\theta d\varphi^2$

In this thesis all equations are given in Planck units:

$$c = \hbar = G = k_B = 1\,.$$

1 Introduction

The Standard Model (SM) of particle physics – summarizing all of our knowledge about observed particles and their interaction which can be put together into a consistent theory – is consistent with most experimental observations referring to particle interactions. However, some observations cannot be explained by the SM, requiring extensions of the model which are often called physics beyond the Standard Model (BSM). One open question e.g. is the origin of the neutrino masses observed in neutrino oscillation experiments, cf. e.g. reference [1, 72]. Moreover, the observed relic baryon number (B) asymmetry as well as the relic dark matter (DM) abundance, cf. e.g. reference [2], cannot be explained by the SM only.

In this thesis, extensions of the SM addressing these three problems related to the particle content of the SM are investigated. The focus lies on right-handed Majorana neutrinos which can naturally explain the smallness of the observed active neutrino masses and at the same time would naturally cause lepton number (L) violating processes. These L violating processes can e.g. be used to assist sources of B violation which individually cannot explain the observed B asymmetry. Furthermore, under certain circumstances, L violation on its own can generate a non-vanishing L asymmetry which is partly converted to a B asymmetry by sphaleron transitions.

Moreover, the temperature dependent effective Higgs potential is calculated and the equations of motion for fields after spontaneous symmetry breaking are investigated. Additionally, loop contributions for massive vector bosons interacting with each other are considered in time-dependent perturbation theory. For a simple example, it appears that the loop contributions deviate from the naive expectation. It is discussed that this deviation is essential when investigating the degree of diverges in the S-matrix.

First, in chapter 2, quantum field theory (QFT) is introduced and subtleties in the consideration of local interaction terms arising from theories including massive vector bosons interacting with each other are investigated. Afterwards, gauge theories are discussed with an emphasis on gauge fixing and spontaneously broken symmetries. Furthermore, the SM of particle physics is presented and flavor oscillation as well as CP violation – a key element of baryogenesis – are introduced. After that, in chapter 3, the focus is shifted to thermal systems including many particles. In this chapter, among others, the Boltzmann equations describing the time evolution of number densities and particle-antiparticle asymmetries are derived. Subsequently, in chapter 4, the time evolution of the B asymmetry is investigated in a general setup. In particular, sphaleron transitions, which, as part of the SM, build the framework for all baryogenesis scenarios, are discussed.

Following this, extensions of the SM which are of relevance to this thesis are presented. First, in chapter 5, right-handed Majorana neutrinos are introduced, the induced rate of lepton number violation is calculated, and the basic concept of thermal leptogenesis is briefly discussed. Afterwards,

in chapter 6, an extended Higgs sector is investigated and thermal corrections to the effective Higgs potential are discussed. In particular, the inert Higgs model – a two-Higgs-doublet model (2HDM) with an imposed Z_2 symmetry – and the scotogenic model – the inert Higgs model extended by right-handed Majorana neutrinos – are investigated. The scotogenic model suggests itself in light of this thesis because it includes a DM candidate and allows for larger Yukawa coupling of the neutrino sector without being in conflict with the Planck bound on the sum of the active neutrino masses, cf. reference [2]. Consequently, the enlarged parameter space of the Yukawa couplings of the neutrino sector allows e.g. for new prospects of leptogenesis and, as a byproduct, also the observed relic DM abundance can be explained.

Subsequently, in chapter 7, the interplay of $B-L$ asymmetry conserving GUT baryogenesis, lepton number violation induced by right-handed Majorana neutrinos, and sphaleron transitions is presented in detail. For this, L violation represents an essential ingredient because the $B-L$ conserving sphaleron transitions would completely wash out the initial $B-L$ conserving B asymmetry without having an additional source of $B-L$ violation. First, all relevant parts of the time evolution of the baryon number asymmetry are brought together and, afterwards, the parameter space is investigated for various benchmark points. Last, in chapter 8, various possibilities to realize leptogenesis based on right-handed Majorana neutrinos are investigated. For this, the focus lies on Majorana masses in the region below 10^{10} GeV, which are insufficient to generate the observed B asymmetry in the simplest version of thermal leptogenesis. In particular, thermal leptogenesis in light of the scotogenic model is briefly investigated and, afterwards, possibilities of enlarging CP violation with the help of thermally induced mass degeneracy is investigated.
Finally, in chapter 9, the main results of this thesis are summarized.

2 Quantum Field Theory in the Vacuum

Physics is a natural science examining fundamental phenomena of nature to find patterns which are expressed as laws and equations. In order to develop fundamental theories, the basic assumption is made that not only individual but all phenomena of nature follow laws.
An essential principle of physics is that the laws of nature are universal, i.e. applicable always and everywhere. This homogeneity of space and time yields the conservation of momentum and energy. Furthermore, it is assumed that the laws of nature know no direction – they are isotropic in space. This causes the conservation of the angular momentum. In addition, it is assumed that the description of nature is independent of the choice of the inertial frame of reference.

The special theory of relativity (SR) combines these basic principles with the observation that the speed of light in vacuum is identical for all observers. Consequently, light can neither be a massive particle nor a wave propagating in a medium (Lorentz ether theory). SR claims that massless particles always travel with the speed of light while massive particles can only asymptotically reach it with increasing energy. In addition, the transformation from one inertial frame of reference to another – known as Lorentz transformation – does not shift time and space independently, cf. equation (A.2). Consequently, space and time cannot be treated separately but as a unit called spacetime.

The assumption that gravity and acceleration are locally indistinguishable leads to the general theory of relativity (GR) which states that spacetime itself does not exist independently of its content. The connection between spacetime geometry and the energy-momentum tensor is described by the Einstein field equations (A.3). These equations state that massive objects curve the surrounding space and that the space expands depending on its energy content, cf. equation (A.5). The first prediction can be observed as gravitational lensing while the second one leads to the Big Bang theory which has among others been confirmed by the observation of the cosmic microwave background (CMB) and the validation of the Big Bang nucleosynthesis (BBN) predictions.

In general, the content of the universe is observed to be structured into bound objects. During interactions with high enough energies, the substructure of the objects can be observed. Objects which have no substructure are elementary particles.
In classical mechanics, free objects can be fully described by their mass, momentum, and position in spacetime. Furthermore, in classical electrodynamics fields appear which can be excited to oscillations propagating at the speed of light. However, observations show that this classical picture breaks down when considering very light objects such as elementary particles. In addition, it cannot explain the photoelectric effect. To explain observation, the concept of particles and waves as discrete and continuous objects, respectively, have to be abandoned. Quantum mechanics (QM) combines both concepts, meaning that all objects have to be described by a time-dependent position probability amplitude function $\psi(x,t)$ called wave function. As a consequence, objects can only either carry a discrete momentum or be localized in space but not both at once.

In the following, in section 2.1, the well-known relativistic equations of motion for scalar bosons, vector bosons, and spin-1/2 fermions are motivated. Afterwards, in section 2.2, the essentials of QFT are introduced and the calculation of transition amplitudes based on time-dependent perturbation theory is investigated. This introduction is done in preparation of the investigation of thermal systems, cf. chapter 3, and the calculation of propagators and loop contributions in time-dependent perturbation theory, cf. section 2.3. Especially for the latter, a fundamental comprehension of the basics of QFT is of special relevance in order to classify the found discrepancy between loop contributions from massive vector bosons derived in time-dependent perturbation theory and the naively expected result. Afterwards, in support of the results from time-dependent perturbation theory, in section 2.4, the path integral formalism is introduced and investigated in detail for massive vector bosons.
Because the validity of the derived loop contribution of massive vector bosons is supported by the fact that the degree of divergence in the S-matrix is the same as expected from R_ξ gauge, the basic concepts of renormalization are summarized in section 2.5. Furthermore, the resulting scale dependence of the coupling constants being usually expressed in the form of renormalization group equations (RGEs) is relevant for the leptogenesis model considered in chapter 7.

In the SM, massive vector bosons only arise from spontaneously broken gauge symmetries. The usual method to prove the renormalizability of a theory including massive vector bosons arising from spontaneously broken gauge symmetries is to apply the gauge-fixing procedure. To investigate this in more detail, first of all, the basic concepts of gauge symmetries and the gauge-fixing procedure are introduced in section 2.6. Afterwards, in section 2.7, the equations of motion for fields after spontaneous symmetry breaking (SSB) are investigated.

Afterwards, in section 2.8, the SM of particle physics is introduced. Following, in section 2.9, the appearance of the observed flavor oscillations is briefly explained. Finally, in section 2.10, the effective equation of motion resulting from a non-vanishing interaction rate is introduced and the resulting CP violation is investigated.

2.1 Introduction Into Relativistic Quantum Mechanics

Inspired by the observation that the energy of a single photon is given by the frequency times the Planck constant $h = 2\pi$[1] ($E = 2\pi\nu = \omega$), the wave function of a photon – i.e. the wave function of light – is written as

$$\psi(x) := \psi(t, \vec{x}) \propto \exp\left[-i\left(\omega t - \vec{k}\vec{r}\right)\right] = \exp\left[-i\left(Et - \vec{k}\vec{r}\right)\right] = e^{-ipx}\,, \tag{2.1}$$

where the equivalence of the wave vector ($\vec{k}$) and momentum vector ($\vec{p}$) is required by Lorentz invariance and the common abbreviation $px = p^\mu x_\mu$ is used. Based on this, the wave function of free massive objects in position space are written as a superposition of energy eigenstates ($\propto e^{-ipx}$):

$$\psi(x) = \int \frac{d^3\vec{p}}{(2\pi)^3} c\,(\vec{p})\, e^{-ipx}\,, \tag{2.2}$$

[1] In this thesis all equations are given in Planck units ($c = \hbar = G = k_B = 1$).

with $E_i = \sqrt{\vec{p}^{\,2} + m_i^2}$. As a consequence, objects cannot be localized and carry a definite momentum at the same time. This result can be formalized in the uncertainty principle[2]

$$\sigma_x^2 \, \sigma_p^2 = \langle (\hat{x} - \langle \hat{x} \rangle)^2 \rangle \, \langle (\hat{p} - \langle \hat{p} \rangle)^2 \rangle \geq \frac{1}{4} \,, \tag{2.3}$$

with the standard deviation of position σ_x and momentum σ_p. Moreover, the expectation value of an operator in position space is defined as

$$\langle \hat{O}(t) \rangle = \langle \psi(t) | \hat{O}(t) | \psi(t) \rangle = \int d^3x \, \psi^*(x) \, \hat{O}(x) \, \psi(x) \,, \tag{2.4}$$

where $\psi(x)$ and $\hat{O}(x)$ are the position space representation of $|\psi(t)\rangle$ and $\hat{O}(t)$, respectively:

$$\psi(x) = \langle \vec{x} | \psi(t) \rangle \ , \tag{2.5}$$

with $|\vec{x}\rangle$ being the eigenstate of position operator:

$$\hat{x} \, |\vec{x}\rangle = \vec{x} \, |\vec{x}\rangle \ . \tag{2.6}$$

Besides, the position operator, one can also define a momentum operator and Hamiltonian with corresponding eigenstates:

$$\hat{p} \, |\vec{p}\rangle = \vec{p} \, |\vec{p}\rangle \qquad \text{and} \qquad \hat{\mathrm{H}} \, |E\rangle = E \, |E\rangle \ . \tag{2.7}$$

According to equation (2.1), the spatial derivative of the wave function is proportional to the momentum. Based on this, the momentum operator in position space can be expressed as

$$\langle \vec{x} | \hat{p} | \psi \rangle = -i \nabla \psi(x) \,. \tag{2.8}$$

Moreover, the time derivative is proportional to the energy, meaning that the time evolution of a state vector is determined by the Hamiltonian:

$$\hat{\mathrm{H}}_S \, |\psi_S(t)\rangle = i \frac{\partial}{\partial t} \, |\psi_S(t)\rangle = i \frac{\partial}{\partial t} U(t) \, |\psi_S(0)\rangle \ , \tag{2.9}$$

where the Schrödinger picture (S) with time-dependent state vectors is used. However, in QM, only expectation values of operators are observable. Consequently, the time evolution can also be absorbed into the operators,

$$\hat{O}_H(t) := U^\dagger(t) \hat{O}_S(t) U(t) \qquad \Rightarrow \qquad \frac{d}{dt} \hat{O}_H(t) - U^\dagger(t) \frac{\partial \hat{O}_S(t)}{\partial t} U(t) = i \big[\hat{\mathrm{H}}_H, \hat{O}_H \big] \,, \tag{2.10}$$

known as Heisenberg picture (H), meaning that the state vectors are time independent.

Due to the energy-momentum relation, the time evolution of a free particle can be expressed in terms of the Hamiltonian. Furthermore, considering an external spacetime dependent potential $V(x)$, it also contributes to the total amount of energy. In the non-relativistic limit $E \approx m + \vec{p}^{\,2}/(2m)$ this leads to the Schrödinger equation, cf. equation (A.6).

[2] Note that the uncertainty principle not only holds for deviation of position and momentum but for all pairs of complementary variables.

However, due to the insufficiency for the description of highly energetic ($|\vec{p}| \gtrsim m$) or massless particles, a relativistic generalization of the Schrödinger equation is needed. Using the relativistic energy-momentum relation $E = \sqrt{\vec{p}^{\,2} + m^2}$ instead of the non-relativistic one leads to the intuitive ansatz

$$i\frac{\partial}{\partial t}\psi(x) = \sqrt{-\nabla^2 + m^2}\,\psi(x)\,. \tag{2.11}$$

But this equation treats time and space derivatives differently which is not what is expected from a relativistic equation of motion. Furthermore, the series expansion of the square root in power of ∇^2 leads to a non-local expression [64]. This problem can be circumvented by squaring the operators on both sides, resulting in the Klein-Gordon equation (A.7) which is sufficient to describe wave functions that transform as Lorentz scalars.

Particles with non-vanishing spin and therefore an orientation in space have to be described by multi-component wave functions which do not transform trivially under a Lorentz transformation. In general, the wave function of massive spin-1 particles can be expressed in terms of a plain wave times one of the three orthogonal polarization vectors describing the Lorentz structure, cf. equation (A.59). The time evolution of the single polarization can be expressed by the Klein-Gordon equation. By including a projection operator ($\Pi^\mu{}_\nu\,\varepsilon^\nu_\lambda = \varepsilon^\mu_\lambda$ and $\Pi^\mu{}_\nu\,p^\nu = 0$) to ensure that only observable particle states are eigenstates, the equation of motion for a massive spin-1 particles can be expressed by the Proca equation (A.9).

More advanced, considering a theory which also includes massless vector bosons, only two polarization vectors $\varepsilon^\mu_{t_{1,2}}$ fulfill the defining conditions (A.59) are observable. However, these polarization vectors are not definite anymore because a term proportional to the four-momentum p^μ can be added without altering the defining conditions. In addition, these terms proportional to p^μ also appear in Lorentz transformations:

$$\Lambda^\nu{}_\mu\,\varepsilon^\mu_{t_{1,2}} = \alpha_1\,\varepsilon^\nu_{t_1} + \sqrt{1-\alpha_1}\,\varepsilon^\nu_{t_2} + \alpha_2\,p^\nu\,, \tag{2.12}$$

which yields a non-Lorentz invariant polarization sum[3]. As a consequence, massless vector bosons can only give rise to a Lorentz invariant theory if the time evolution is invariant under the transformation $\varepsilon^\mu \to \varepsilon^\mu + \alpha\,p^\mu$. It can be shown that this condition is fulfilled when the Lagrangian is invariant under the transformation (A.25) leading to the concept of gauge theories, cf. section 2.6.

For spin-1/2 particles, the Lorentz structure is given by so called spinors Ψ which neither transform as Lorentz scalars nor as Lorentz vectors, cf. equation (A.17). In contrast to bosons (particles with integer spin), the time evolution for fermions (particles with half odd integer spin) is not based on the Klein-Gordon equation. This is because the probability current resulting from the Klein-Gordon equation is not positive definite. In QM, this is problematic for all kinds of particles but in QFT, the probability current becomes a charge current which can be negative. On the other hand, unlike for bosons, the number of fermions is conserved, requiring a theory with a positive definite probability current.
Actually, the Klein-Gordon equation is not positive definite due to the squared time derivative implying that a linear equation in time would circumvent this problem. As Paul Dirac noticed first,

[3] Actually, the problem arises because p^μ is not a valid base vector for massless particles ($p^2 = 0$).

this can be done in a Lorentz invariant way by writing down the equation of motion in matrix form. Consequently, the time evolution of spin-1/2 fermions is described by the Dirac equation (A.8).

However, besides the problem of a negative probability current resulting from the Klein-Gordon equation, positive as well as negative energy eigenstates occur from all derived equations of motion because they are all base on the relation $E^2 = \vec{p}^{\,2} + m^2$. This fact makes arbitrarily small energies possible as soon as interaction terms allow for the transition between eigenstates of the free equation of motion.
Furthermore, QM is unable to describe systems with variable particle number, meaning that only transitions between energy eigenstates induced by external forces can be described but not e.g. the emission of a photon.

2.2 Introduction Into the Basic Concepts of Quantum Field Theory

To overcome the issues of QM mentioned in the previous section, QFT was developed. Because in QFT, states with variable particle number are considered, it is convenient to distinguish between the particle content and the state of the individual particles. Note that in this context, as for the rest of this work, the term *particle* does not refer to a classical object but to eigenstates of the free Hamiltonian.

2.2.1 Essentials of Quantum Field Theory

Starting with the investigation of a non-interacting theory, a multi-particle system with arbitrary particle content can be fully described by a state vector $|F\rangle$ containing information about the particle content in momentum space. To determine the time evolution of the system, the information about the particle content needs to be converted into a set of wave functions. For this reason, an operator $\psi(x)$ is included, generating the quantum mechanical wave functions whose time evolution is determined by the quantum-mechanical equations of motion introduced in the previous section. Thus, only $\psi(x)$ is time dependent, meaning that here, the Heisenberg picture is considered. Moreover, another operator $\psi^\dagger(x)$ can be added which converts the set of wave functions back to a state vector:

$$i\,\psi^\dagger(x)\,\frac{d}{dt}\psi(x)\,|F\rangle = \psi^\dagger(x)\,\hat{\mathrm{H}}(x)\,\psi(x)\,|F\rangle\ . \tag{2.13}$$

Because the time evolution of each particle species is described by a different Hamiltonian, it makes sense to decompose $\psi(x)$ into so called quantum field operators for each particle species $\psi_i(x)$, cf. equation (A.39), which only generates the wave functions of the corresponding particle content. Using this, the time evolution of $|F\rangle$ can be written as a sum of Hamiltonian for each particle species:

$$i\,\psi^\dagger(x)\,\frac{d}{dt}\psi(x)\,|F\rangle = i\sum_i \psi_i^\dagger(x)\,\frac{d}{dt}\psi_i(x)\,|F\rangle = \sum_i \psi_i^\dagger(x)\,\hat{\mathrm{H}}_i(x)\,\psi_i(x)\,|F\rangle\ . \tag{2.14}$$

For a detailed derivation of quantum field operators, cf. appendix A.4.

It is useful to consider the complex conjugate of the equations of motion in order to find an interpretation for the negative energy eigenvalues arising from the relativistic equations of motion. As long as only the free equation of motion is considered, the resulting equation of motion of the conjugated wave functions is basically equivalent to the initial equation of motion. However, considering an interacting theory with particles that are charged under a gauge symmetry, cf. section 2.6, the equation of motion in the complex-conjugated picture differs by a sign in front of the gauge interaction term. Thus, the complex-conjugated picture describes the time evolution of a particle with opposite charge and is for this reason also called charge-conjugated picture. Such a particle with an equivalent free equation of motion but negative charge is known as the antiparticle. Thus, the negative energy solutions which correspond to positive energy solutions in the charge-conjugated picture, can be interpreted as antiparticles traveling in the inverse time direction. In QFT, this interpretation can be implemented by defining the quantum field operator such that it not only produces a particle state but also annihilates an antiparticle state, cf. equation (A.55).

This interpretation of negative energy eigenstates as antiparticles is proven by the fact that for each particle which is charged, meaning that it transforms non-trivially under a symmetry transformation (e.g. gauge symmetries), an associated antiparticle can be observed. Furthermore, writing down particle content changing interactions in terms of the quantum field operators given in (A.55), the production and annihilation of particle-antiparticle pairs is predicted. Additionally, at each vertex, either a particle can be produced or an antiparticle can be annihilated, both with the same coupling strength. Both of these predictions are in agreement with observations.

A big advantage of QFT is that, due to the introduction of creation and annihilation operators, particle number violating interactions can be added easily. Generally, using the basic assumption that the state vector at any given time can be expressed as a superposition of eigenstates of the free Hamiltonian, any interaction can be written in terms of a local transition probability among state vectors:

$$\hat{\mathrm{H}}_I = \sum_{F,F'} c_{F\to F'} \left|F'\right\rangle \left\langle F\right| \,. \tag{2.15}$$

In QFT, such an interaction term can be expressed by the local action of multiple quantum field operators:

$$\hat{\mathcal{H}}_I(x) = \sum_k \alpha_k \, \psi^\dagger_{j_m}(x) \ldots \psi^\dagger_{j_1}(x) \, \psi_{i_n}(x) \ldots \psi_{i_1}(x) \,, \tag{2.16}$$

where k sums all different interaction terms[4]. Note that including particle content changing interactions, $|F\rangle$ as well as $\psi(x)$ are time dependent. In detail, the time dependence of $\psi(x)$ is determined by the free equation of motion ($\hat{\mathrm{H}}_0$) while the time dependence of $|F\rangle$ is only determined by the particle content changing interactions ($\hat{\mathrm{H}}_I$). Thus, in the following, as not mentioned otherwise, the time evolution in the interaction picture is considered, cf. equation (A.30).

[4]Note that both expressions of the interaction Hamiltonian are not synonymous because (2.15) only shows the general structure of transition terms while (2.16) correspond to a Lorentz invariant theory allowing to express general transition amplitudes in terms of the coupling constants α_k and the particle content of the state vectors.

2.2.2 Calculation of Transition Rates in Quantum Field Theory

Considering transition amplitudes between eigenstates of the free equation of motion, time-dependent perturbation theory, for details cf. appendix A.3, can be used to express these transition amplitudes between different state vectors – known as *S-matrix* – as

$$\begin{aligned}\mathcal{S}_{F\to F'} &= \sum_n \frac{(-i)^n}{n!} \langle F'|\mathcal{T}\left(\int dx' (\hat{\mathcal{H}}_I)_D(x')\right)^n |F\rangle \\ &= \sum_{n,m_n} A \int \prod_{i=1}^{n} dx'_i \, \langle F'|\mathcal{T}\psi_{1_1}(x'_1)\dots\psi_{n_{k_n}}(x'_n)|F\rangle \ , \end{aligned} \tag{2.17}$$

where n runs over all orders in perturbation theory, m_n runs over all combinations of different interaction terms being part of $(\hat{\mathcal{H}}_I)_D(x')$, and A is a prefactor containing coupling constants. Note that here, the particle content of $|F\rangle$ is not assumed to have a distinct momentum but a momentum distribution and for $|F'\rangle$, only the content but not the momentum is assumed to be distinct. The reason for this definition is that the resulting transition probabilities can be used to describe the time evolution of thermal systems, cf. section 3.2.
Defining $|F''\rangle$ as the state vector with the joint particle content of $|F\rangle$ and $|F'\rangle$, the field operators can be divided into a set of field operators $\psi_{i_k}(x'_{i_k})$ whose action adjusts the particle content of $|F\rangle$ and $|F''\rangle$, another set of field operators $\psi_{f_l}(x'_{f_l})$ whose action adjusts the particle content of $|F'\rangle$ and $|F''\rangle$ and a set of remaining field operators $\psi'_{1_1}(x'_1)\dots\ \psi'_{n_{j_n}}(x'_n)$ which together do not alter the particle content[5].
Furthermore, defining $x_i = x'_i - x'_m$ for $i \neq m$, one is only left with a x'_m dependence in the plain waves of $\psi_{i_k}(x'_{i_k})$ and $\psi_{f_l}(x'_{f_l})$ because it cancels out in the remaining part. Consequently, the corresponding spacetime integral enforces four-momentum conservation in the limit $t_{\text{initial}} \to -\infty$ and $t_{\text{final}} \to \infty$. Using this and only considering the connected part of the S-matrix[6] the transition amplitude becomes

$$\mathcal{S}_{F\to F'} = \int \prod_k d\tilde{p}_{i_k} \prod_l d\tilde{p}_{f_l} \, \langle F'| \prod_l a^\dagger_{f_l}(\vec{p}_{f_l}) \prod_k a_{i_k}(\vec{p}_{i_k})|F\rangle \, \mathcal{A}_{F\to F'} \, , \tag{2.18}$$

where the abbreviation $d\tilde{p}_i = \delta(p^2 - m_i^2)dp = d^3p/(2\pi)^3/(2E_i)$ is used and the wave function part of the quantum field operator $\tilde{\psi}_{i,\vec{k}}(x)$, cf. equation (A.43), acting on the external states is part of $\mathcal{A}_{F\to F'}$ being defined as

$$\begin{aligned}\mathcal{A}_{F\to F'} &= \sum_{n,m_n} A \int \prod_{i=1, i\neq m}^{n} dx_i \prod_l \tilde{\psi}_{f_l,\vec{k}_{f_l}}(x_{f_l}) \prod_k \tilde{\psi}_{i_k,\vec{k}_{i_k}}(x_{i_k}) \\ &\qquad \times \langle F''|\mathcal{T}\psi'_{1_1}(x_1)\dots\psi'_{n_{j_n}}(x_n)|F''\rangle \, (2\pi)^4\delta^4\Big(\sum_k k_{i_k} - \sum_l k_{f_l}\Big) \\ &:= i\mathcal{M}_{F\to F'}(2\pi)^4\delta^4\Big(\sum_k k_{i_k} - \sum_l k_{f_l}\Big) , \end{aligned} \tag{2.19}$$

[5] When rearranging the quantum field operator, one has to take care of the Lorentz and the spinor structure by including according summation indices

[6] The connected part of the S-matrix only considers amplitudes which can be visualized by a connected diagram, cf. appendix A.3.2.

with $x_m = 0$ and $\mathcal{M}_{F\to F'}$ being the *matrix element*. Note that it is convenient to visualize the elements of the perturbation series by diagrams, cf. appendix A.3.2.

Next, for the calculation of the transition probability, one uses

$$\left(\int dx\, e^{i(p_f-p_i)x}\right)^2 = \int dx\, e^{i(p_f-p_i)x}(2\pi)^4\delta^4\big(p_i-p_f\big) = VT(2\pi)^4\delta^4\big(p_i-p_f\big)\,, \tag{2.20}$$

with VT being the spacetime volume. In addition, using (A.48) and (A.45) or (A.47), respectively,

$$\begin{aligned}\Big|\int \prod_k d\tilde{p}_{i_k} \prod_l d\tilde{p}_{f_l}\, \langle F'| \prod_l a^\dagger_{f_l}(\vec{p}_{f_l}) \prod_k a_{i_k}(\vec{p}_{i_k})|F\rangle \Big|^2 \\ = \int \prod_k d\tilde{p}_{i_k} f^F_{i_k}(\vec{p}_{i_k}) \prod_l d\tilde{p}_{f_l} \left(1 \pm f^{F''}_{f_l}(\vec{p}_{f_l})\right)\,,\end{aligned} \tag{2.21}$$

is obtained, where $f^F_i(\vec{p}_i)$ denotes the distribution function corresponding to the state $|F\rangle$[7] and the sign in front of the second distribution function is determined by the particle species: $+$ for bosons and $-$ for fermions.
Hence, the transition probability per spacetime volume can be expressed as

$$p_{F\to F'} = \int \prod_k d\tilde{p}_{i_k} f_{i_k}(\vec{p}_{i_k}) \prod_l d\tilde{p}_{f_l} \big[1 \pm f_{f_l}(\vec{p}_{f_l})\big] |\mathcal{M}_{F\to F'}|^2 (2\pi)^4\delta^4\Big(\sum_k k_{i_k} - \sum_l k_{f_l}\Big)\,. \tag{2.22}$$

At this point, it makes sense to introduce the well-known C, P, and T transformations which are of special relevance in light of this thesis. First of all, the time reversal transformation (T) invert the time $t \to -t$ which in the context of transition amplitudes relates $\mathcal{S}_{F\to F'}$ and $\mathcal{S}_{F'\to F}$. Consequently, the transition probabilities for both processes, $F \to F'$ and $F' \to F$, are equal if T is conserved. In analogy, the parity transformation (P) inverts space $\vec{x} \to -\vec{x}$ relating transition amplitudes with chirality-flipped particle content and the charge conjugation (C) links transition amplitudes where the particle content is replaced by the corresponding antiparticles. Note, however, historically charge conjugation is defined such that actually both together C and P transformations convert particles into their antiparticles. Because the negative energy solutions of the free equation of motion arising from a Lorentz invariant theory where interpreted as antiparticles traveling backwards in time, resulting in an according definition of the quantum field operators, cf. equation (A.39), it is implied that a combination of C, P, and T transformation leave the time evolution invariant which is well-known as CPT theorem.

Turning back to vacuum QFT, single scattering processes are studied isolated from the environment which means that $|F''\rangle = |0\rangle$ and, as a consequence, $f^{F''}_{f_l} = 0$ are implied. Furthermore, for $|F''\rangle = |0\rangle$, $|\mathcal{M}_{F\to F'}|^2$ is independent of the state vector and the square of $\mathcal{A}_{F\to F'}$ becomes equivalent to the square of $\mathcal{S}_{F\to F'}$ because the expression in equation (2.21) is one.
Considering simple processes involving only one or two incoming particles with fixed momentum,

[7] Note that in general, the product of distribution functions become non-trivial when multiple field operators of the same species contribute. This is due to the fact that the creation and annihilation operators alter the particle content, implying that the next creation or annihilation operator acts on a field with modified particle content. However, in most cases, it is a reasonable approximation to assume independent distribution functions of the individual incoming and outgoing particles.

it is convenient to define the differential decay width in the rest frame of the decaying particle ($f_i(\vec{p}_i) = \delta^3(\vec{p}_i)/V$)

$$d\Gamma_{i\to f_1\dots f_n} = V p_{i\to f_1\dots f_n} = \frac{|\mathcal{M}_{i\to f_1\dots f_n}|^2}{2m_i}(2\pi)^4\delta^4\left(p_i - \sum_l p_{f_l}\right)\prod_l d\tilde{p}_{f_l}\,, \tag{2.23}$$

and the differential cross section

$$d\sigma_{i_1i_2\to f_1\dots f_n} = \frac{V p_{i_1i_2\to f_1\dots f_n}}{|\vec{v}_{i_1}|} = \frac{|\mathcal{M}_{i_1i_2\to f_1\dots f_n}|^2}{2\lambda\left[s, m_{i_1}^2, m_{i_2}^2\right]}(2\pi)^4\delta^4\left(p_{i_1} + p_{i_2} - \sum_l p_{f_l}\right)\prod_l d\tilde{p}_{f_l}\,, \tag{2.24}$$

with $\lambda[a,b,c]$ being defined in (D.5). In the case of only two outgoing particles ($n = 2$) both expressions can be further simplified to

$$d\Gamma_{i\to f_1f_2} = \frac{|\mathcal{M}_{i\to f_1f_2}|^2}{32\pi^2}\frac{|\vec{p}_{f_1}|}{m_i^2}d\Omega\,, \tag{2.25}$$

$$d\sigma_{i_1i_2\to f_1f_2} = \frac{|\mathcal{M}_{i_1i_2\to f_1f_2}|^2}{64\pi^2 s}\frac{|\vec{p}_{f_1}|}{|\vec{p}_{i_1}|}d\Omega\,. \tag{2.26}$$

2.3 Derivation of Propagators and Loops in Time-Dependent Perturbation Theory

According to equation (2.19), the simplest non-trivial matrix element appearing in the perturbation series only contains two quantum field operators acting on a vacuum state. This case is closely related to propagators, which are of special importance since more complex terms of the perturbation series can be expressed in terms of propagators.
In this section, first of all, the propagator and loop contributions for scalar bosons are investigated in time-dependent perturbation theory to get familiar with the formalism. Afterwards, it is discussed that for massive vector bosons, local interaction terms appear in the interaction Hamiltonian, which guarantees the Lorentz invariance of transition amplitudes. Subsequently, this investigation is extended to a theory containing two massive vector bosons interacting with each other. In a simple example, it is demonstrated that loop contributions only including massive vector bosons deviate from what is naively expected. Moreover, it is discussed that this deviation is essential in the investigation of the degree of divergence in the S-matrix.

2.3.1 Propagators for Scalar Bosons and Spin-1/2 Fermions and Introduction of Loop Contributions

In general, the vacuum propagator in position space is defined by the action of two quantum field operators on the vacuum state. Hence, the propagator of scalar fields, cf. equation (A.57a), is given by

$$\langle 0|\,\mathcal{T}\phi(x+y)\phi^\dagger(y)\,|0\rangle = \int d\tilde{k}\left(\Theta(t)e^{-ikx} + \Theta(-t)e^{ikx}\right)\,, \tag{2.27}$$

where the bosonic commutation relation, cf. equation (A.45), and the normalization of the vacuum ($\langle 0|0\rangle = 1$) are used. Furthermore, $\Theta(x)$ is the Heaviside step function defined in equation (D.9). Next, it is convenient to use the residue theorem to rewrite equation (2.27) into the well-known form of the spacetime propagator, cf. equation (A.60):

$$\langle 0|\,\mathcal{T}\phi(x+y)\phi^\dagger(y)\,|0\rangle = \lim_{\epsilon\to 0^+}\int \frac{dk}{(2\pi)^4}\frac{i}{k_0^2-(E_k-i\epsilon)^2}e^{-ikx}\,. \tag{2.28}$$

Note that deriving the propagator in this way, the intuitive interpretation is difficult because starting from operators describing observable particles which fulfill the energy-momentum relation known as *on-shell*, a propagator is obtained which can transfer four-momentum which does not fulfill the energy-momentum relation – known as *off-shell*. However, as investigated in appendix A.6, the propagator in the given form arises from the quantum mechanical interference of the exchange of a particle from y to $x+y$ for positive x_0 and the exchange of an antiparticle from $y+x$ to y for negative x_0, where both, the particle and the antiparticle, fulfill the energy-momentum relation.

Besides, so called *tree-level* processes where two separated spacetime points are interconnected by a single propagator, also so-called *loop* contributions appear in the perturbation theory where separated spacetime points are interconnected by multiple propagators. In the simplest case of a tree-level processes where external currents only couple at two spacetime points being interconnected by a scalar boson propagator, the matrix-element is proportional to the propagator in momentum space:

$$\mathcal{M} \propto \int dx\,\langle 0|\,\mathcal{T}\phi(x+y)\phi^\dagger(y)\,|0\rangle\,e^{ipx} = \frac{i}{p^2-m^2}\,, \tag{2.29}$$

where p is the sum of the incoming and outgoing four-momenta, respectively.
In contrast, for the simplest loop process where external currents couple at two spacetime points but are interconnected by two scalar boson propagators, the matrix-element becomes

$$\begin{aligned}\mathcal{M} &\propto \int dx\,\langle 0|\,\mathcal{T}\phi_1(x+y)\phi_2(x+y)\phi_1^\dagger(y)\phi_2^\dagger(y)\,|0\rangle\,e^{ipx}\\ &= \lim_{\epsilon\to 0^+}\int \frac{dk}{(2\pi)^4}\frac{i}{k^2-m_1^2+i\epsilon}\frac{i}{(p-k)^2-m_2^2+i\epsilon}\,,\end{aligned} \tag{2.30}$$

where, for simplicity, two different scalar fields (ϕ_1 and ϕ_2) are considered here. Note that the remaining momentum integral in loop contributions can be divergent. Addressing this issue, renormalization can be used to absorb the divergences by redefining the Hamiltonian, cf. section 2.5.

Considering spin-1/2 fermions, the propagator in position space is

$$\langle 0|\,\mathcal{T}\Psi(x+y)\overline{\Psi}(y)\,|0\rangle = \int d\tilde{k}\left(\Theta(t)(\not{k}+m)e^{-ikx}-\Theta(-t)(\not{k}-m)e^{ikx}\right)\,. \tag{2.31}$$

Making use of the residue theorem, the propagator in the well-known form, cf. equation (A.61), is obtained.

2.3.2 Derivation of the Massive Vector Boson Propagator

The propagator for massive vector bosons in position space is given by

$$\begin{aligned}&\langle 0|\,\mathcal{T}A^\mu(x+y)(A^\nu)^\dagger(y)\,|0\rangle \\ &\qquad=\sum_\lambda\int d\tilde{k}_A\left(\Theta(t)\epsilon^\mu_\lambda(\vec{k})(\epsilon^\nu_\lambda(\vec{k}))^\dagger e^{-ikx}+\Theta(-t)(\epsilon^\mu_\lambda(\vec{k}))^\dagger\epsilon^\nu_\lambda(\vec{k})e^{ikx}\right).\end{aligned}\tag{2.32}$$

Evaluating the polarization sum for massive vector bosons,

$$\sum_\lambda\epsilon^\mu_\lambda(\vec{k})(\epsilon^\nu_\lambda(\vec{k}))^\dagger=\sum_\lambda(\epsilon^\mu_\lambda(\vec{k}))^\dagger\epsilon^\nu_\lambda(\vec{k})=-g^{\mu\nu}+\frac{k_A^\mu k_A^\nu}{m_A^2}\,,\tag{2.33}$$

the propagator becomes

$$\langle 0|\,\mathcal{T}A^\nu(x+y)(A^\mu)^\dagger(y)\,|0\rangle=\int d\tilde{k}_A\left(-g^{\mu\nu}+\frac{k_A^\mu k_A^\nu}{m_A^2}\right)\left(\Theta(t)e^{-ikx}+\Theta(-t)e^{ikx}\right),\tag{2.34}$$

where the energy of a four-momentum with an index A is determined by the energy-momentum relation: $\vec{k}_A=\vec{k}$ and $k_A^0=E_k=\sqrt{\vec{k}^{\,2}+m_A^2}$.

However, for massive vector bosons, the propagator in the well-known form, cf. equation (A.62), cannot simply be derived by making use of the residue theorem because the energy integration path has to be closed e.g. by adding a path which, for positive and negative x_0, leads from $k_0\to\infty$ over $k_0\to\pm i\infty$ to $k_0\to-\infty$, respectively[8]. For the scalar bosons and spin-1/2 fermions, the propagators in the well-known form are obtained, as the remaining part of the integrand ($1/(k_0^2-E_k^2+i\epsilon)$ and $(\not{k}+m)/(k_0^2-E_k^2+i\epsilon)$) converges to zero for $k_0\to\pm\infty$, implying that the contribution of the path closing the integration curve vanishes. In contrast, considering massive vector bosons, the remaining part of the integrand converges to

$$\lim_{k_0\to\pm\infty}\left(g_{\mu\nu}-\frac{k_\mu k_\nu}{m_A^2}\right)\frac{-i}{k_0^2-E_k^2+i\epsilon}=-i\,\frac{g_{\mu0}g_{\nu0}}{m_A^2}\,,\tag{2.35}$$

meaning that the contribution of the integration path closing the integration curve cannot be ignored.

Thus, the polarization sum has to be excluded from the energy integral when using the residue theorem, meaning that the propagator is given by the on-shell polarization sum times the scalar boson propagator:

$$\langle 0|\,\mathcal{T}A^\nu(x+y)(A^\mu)^\dagger(y)\,|0\rangle=\int\frac{dk}{(2\pi)^4}\left(g^{\mu\nu}-\frac{k_A^\mu k_A^\nu}{m_A^2}\right)\frac{-i}{k^2-m_A^2+i\epsilon}e^{-ikx}\,,\tag{2.36}$$

which can also be written as, cf. equation (D.15),

$$\langle 0|\,\mathcal{T}A^\nu(x+y)(A^\mu)^\dagger(y)\,|0\rangle=\int\frac{dk}{(2\pi)^4}\left[\left(g^{\mu\nu}-\frac{k^\mu k^\nu}{m_A^2}\right)\frac{-i}{k^2-m_A^2+i\epsilon}-\frac{ig^{\mu0}g^{\nu0}}{m_A^2}\right]e^{-ikx}\,.\tag{2.37}$$

[8] The path is chosen such that the exponential function and, for this reason, the integrand does not diverge but becomes exponentially suppressed in the limit $k_0\to\pm i\infty$.

However, this propagator is not Lorentz invariant, cf. e.g. reference [68, pp. 274-278], which means that something must be missing because the Proca Lagrangian, cf. equation (A.18c), determining the time evolution of massive vector bosons is Lorentz invariant.
Because the propagator is only relevant for an interaction theory, to address this issue, a general Lorentz invariant interaction term is added to the Proca Lagrangian

$$\mathcal{L}(x) = -\frac{1}{4}F_{\mu\nu}F^{\mu\nu} + \frac{m^2}{2}A_\mu(x)A^\mu(x) - J_\mu(x)A^\mu(x)\,. \tag{2.38}$$

Evaluating the corresponding Hamiltonian, an additional local interaction term arises in the interaction Hamiltonian [68, pp. 320-323]:

$$\hat{\mathrm{H}}_I(x) = J_\mu(x)A^\mu(x) + \frac{[J_0(x)]^2}{m_A^2}\,. \tag{2.39}$$

Thus, adding the contributions of the local interaction term and the non-local interaction term, the naively expected Lorentz invariant S-matrix is obtained[9]:

$$\begin{aligned}\mathcal{S}_{F\to F'} &= \frac{(-i)^2}{2}\int dy \int dx\, \langle F'|\mathcal{T}J_\mu(x+y)A^\mu(x+y)A^\nu(y)J_\nu(y)|F\rangle - i\int dy \frac{\langle F'|[J^0(y)]^2|F\rangle}{2m_A^2} \\ &= \frac{(-i)^2}{2}\int dy \int dx\, \langle F'|\mathcal{T}J_\mu(x+y)J_\nu(y)|F\rangle \int \frac{dk}{(2\pi)^4}\left(g^{\mu\nu} - \frac{k^\mu k^\nu}{m_A^2}\right)\frac{-i}{k^2 - m_A^2 + i\epsilon}e^{-ikx} \\ &\quad - \frac{i}{2m_A^2}\int dy\, \langle F'|[J^0(y)]^2|F\rangle \left(1 - \int dx \int dk\, e^{-ikx}\right),\end{aligned} \tag{2.40}$$

where the bottom row is zero ($\int dx \int dk\, e^{-ikx} = \int dx\, \delta(x) = 1$).

Similarly, considering interaction terms involving derivatives of scalar boson field operators, the resulting propagator is given by

$$\langle 0|\mathcal{T}[\partial^\mu\phi(x+y)][\partial^\nu\phi(y)]|0\rangle = \int \frac{dk}{(2\pi)^4}\frac{k_\phi^\mu k_\phi^\nu}{m^2}\frac{i}{k^2 - m_\phi^2 + i\epsilon}e^{-ikx}\,, \tag{2.41}$$

with $k_\phi^0 = \sqrt{\vec{k}^2 + m_\phi^2}$. Furthermore, a similar local interaction term – $\hat{\mathrm{H}}_I(x) = J_0^2(x)/(2m_\phi^2)$ – is obtained, ensuring that the S-matrix is Lorentz invariant.

2.3.3 Detailed Investigation of Transition Amplitudes Involving Self Interactions of Massive Vector Bosons

For now, only an interaction term involving a single massive vector boson has been considered, cf. equation (2.39). Thus, the obtained local interaction term only ensures the Lorentz invariance of the S-matrix for a theory including no interaction terms involving multiple massive vector bosons. Thus, to generalize the investigation made in reference [68, pp. 320-323], in the following, a

[9] Note that here, the vacuum QFT approximation $\langle F''|A^\mu(x+y)A^\nu(y)|F''\rangle = \langle 0|A^\mu(x+y)A^\nu(y)|0\rangle$ is used, which is sufficient because the additional thermal contributions do not break the Lorentz symmetry.

generalized interaction Lagrangian containing two massive vector bosons interacting with each other is studied in detail:

$$\mathcal{L}_I(x) = -J_A^\mu(x)A_{H,\mu}(x) - J_B^\mu(x)B_{H,\mu}(x) - J^{\mu\nu}(x)A_{H,\mu}(x)B_{H,\nu}(x)\,, \tag{2.42}$$

with $A_H^\mu(x)$ and $B_H^\mu(x)$ being two different massive vector fields and $J_A^\mu(x)$, $J_B^\mu(x)$, and $J^{\mu\nu}(x)$ being independent of $A_H^\mu(x)$ and $B_H^\mu(x)$. Note that here, the fields carry the subscript H to highlight that the fields in the Heisenberg-picture and not in the interaction-picture are considered[10]. Moreover, it should be mentioned that the following derivation of the interaction Hamiltonian is derived in close relation to reference [68, pp. 320-323], meaning that the single steps are adjusted to the generalized interaction Lagrangian and the different signature of the Minkowski space used in this thesis, cf. equation (A.1).
To derive the interaction Hamiltonian, first of all, the conjugated fields need to be calculated:

$$\Pi_{A,H}^\mu(x) = \frac{\partial\mathcal{L}(x)}{\partial(\partial_0 A_{H,\mu}(x))} = -F_A^{0\mu} = \begin{cases} 0 & \mu = 0 \\ -\partial^0 A_H^\mu(x) + \partial^\mu A_H^0(x) & \mu = i \end{cases}, \tag{2.43a}$$

$$\Pi_{B,H}^\mu(x) = \frac{\partial\mathcal{L}(x)}{\partial(\partial_0 B_{H,\mu}(x))} = -F_B^{0\mu} = \begin{cases} 0 & \mu = 0 \\ -\partial^0 B_H^\mu(x) + \partial^\mu B_H^0(x) & \mu = i \end{cases}. \tag{2.43b}$$

Because $\Pi_{A,H}^0(x)$ and $\Pi_{B,H}^0(x)$ vanish, $A_H^0(x)$ and $B_H^0(x)$ are only auxiliary fields which need to be replaced by their solutions when changing to the Hamilton formalism[11]. For determining the replacement, the Euler-Lagrange equations for $A_H^0(x)$ and $B_H^0(x)$ are considered,

$$m_A^2 A_H^0(x) - J_A^0(x) - J^0{}_\nu(x)B_H^\nu(x) = -\partial_\mu F_A^{\mu 0}\,, \tag{2.44a}$$

$$m_B^2 B_H^0(x) - J_B^0(x) - J_\mu{}^0(x)A_H^\mu(x) = -\partial_\mu F_B^{\mu 0}\,, \tag{2.44b}$$

which, using equation (2.43), can be written as

$$A_H^0(x) = \frac{1}{m_A^2}\left(\nabla\vec{\Pi}_{A,H}(x) + J_A^0(x) + J^0{}_\nu(x)B_H^\nu(x)\right), \tag{2.45a}$$

$$B_H^0(x) = \frac{1}{m_A^2}\left(\nabla\vec{\Pi}_{B,H}(x) + J_B^0(x) + J_\mu{}^0(x)A_H^\mu(x)\right). \tag{2.45b}$$

[10] In the QFT Lagrangian, the fields are always considered in the Heisenberg picture because the resulting equations of motion (Euler-Lagrange equations) also include the interaction terms. In contrast, in the interaction picture, the equations of motion of the fields are only determined by the free equation of motion.

[11] This can be understood from the fact that the Lagrangian does not contain time-derivatives of $A_H^0(x)$ and $B_H^0(x)$, implying that equation (2.45) cannot arise from Hamilton's equations.

Because $A^0_H(x)$ depends on $B^0_H(x)$ and vice versa, both can be determined iteratively, implying that both are replaced by an infinite series:

$$A^0_H(x) = \frac{1}{m_A^2}\Bigg(\nabla\vec{\Pi}_{A,H}(x) + J^0_A(x) + J^0{}_i(x)B^i_H(x) + \frac{J^0{}_0(x)}{m_B^2}\left(\nabla\vec{\Pi}_{B,H}(x) + J^0_B(x) + J_i{}^0(x)A^i_H(x) + \frac{J_0{}^0(x)}{m_A^2}\ldots\right)\Bigg) \tag{2.46a}$$

$$=: \frac{1}{m_A^2}\left(\nabla\vec{\Pi}_{A,H}(x) + J'^0_A(x)\right), \tag{2.46b}$$

$$B^0_H(x) = \frac{1}{m_B^2}\Bigg(\nabla\vec{\Pi}_{B,H}(x) + J^0_B(x) + J_i{}^0(x)A^i_H(x) + \frac{J_0{}^0(x)}{m_A^2}\left(\nabla\vec{\Pi}_{A,H}(x) + J^0_A(x) + J^0{}_i(x)B^i_H(x) + \frac{J^0{}_0(x)}{m_B^2}\ldots\right)\Bigg) \tag{2.46c}$$

$$=: \frac{1}{m_B^2}\left(\nabla\vec{\Pi}_{B,H}(x) + J'^0_B(x)\right). \tag{2.46d}$$

Using this, the Hamiltonian can be evaluated, cf. equation (A.77).
Following reference [68, p. 321], changing from the Heisenberg-picture to the interaction-picture ($\vec{A}_H(x) \to \vec{A}(x)$, $\vec{\Pi}_{A,H}(x) \to \vec{\Pi}_A(x)$, $\vec{B}_H(x) \to \vec{B}(x)$ and $\vec{\Pi}_{B,H}(x) \to \vec{\Pi}_B(x)$), the obtained Hamiltonian can be split into a free Hamiltonian

$$\hat{\mathrm{H}}_0 = \int d^3x\,\frac{1}{2}\left(\vec{\Pi}_A(x)^2 + \frac{1}{m_A^2}\left[\nabla\vec{\Pi}_A(x)\right]^2 + \left[\nabla\times\vec{A}(x)\right]^2 + m_A^2\vec{A}(x)^2\right) + \int d^3x\,\frac{1}{2}\left(\vec{\Pi}_B(x)^2 + \frac{1}{m_B^2}\left[\nabla\vec{\Pi}_B(x)\right]^2 + \left[\nabla\times\vec{B}(x)\right]^2 + m_B^2\vec{B}(x)^2\right), \tag{2.47}$$

determining the time evolution of the fields, and an interaction part

$$\begin{aligned}\hat{\mathcal{H}}_I(x) = {} & -\vec{J}_A(x)\vec{A}(x) - \vec{J}_B(x)\vec{B}(x) + J^{ij}(x)A^i(x)B^j(x) - \frac{1}{2m_A^2}\left[J'^0_A(x)\right]^2 - \frac{1}{2m_B^2}\left[J'^0_B(x)\right]^2 \\ & + \frac{1}{m_A^2}\left[J^0_A(x) - J^{0j}(x)B^j(x)\right]\left[\nabla\vec{\Pi}_A(x) + J'^0_A(x)\right] \\ & + \frac{1}{m_B^2}\left[J^0_B(x) - J^{i0}(x)A^i(x)\right]\left[\nabla\vec{\Pi}_B(x) + J'^0_B(x)\right] \\ & + \frac{1}{m_A^2m_B^2}J^{00}(x)\left[\nabla\vec{\Pi}_A(x) + J'^0_A(x)\right]\left[\nabla\vec{\Pi}_B(x) + J'^0_B(x)\right].\end{aligned} \tag{2.48}$$

Finally, as argued in reference [68, pp. 321-322], in the interaction-picture, $A^0(x)$ and $B^0(x)$ can be reintroduced by defining

$$A^0(x) := \frac{1}{m_A^2}\nabla\vec{\Pi}_A(x) \qquad \text{and} \qquad B^0(x) := \frac{1}{m_B^2}\nabla\vec{\Pi}_B(x)\,. \tag{2.49}$$

Using this definition, the equations of motion for $A^\mu(x)$ and $B^\mu(x)$ become the Proca equation, cf. equation (A.9), on which the definition of the field operator for massive vector bosons, cf. equation (A.57c), considered previously for the derivation of the propagator is based on. Furthermore, the

interaction Hamiltonian density becomes, cf. equation (A.81),

$$\begin{aligned}\hat{\mathcal{H}}_I(x) = {} & J_A^\mu(x)A_\mu(x) + J_B^\mu(x)B_\mu(x) + J^{\mu\nu}(x)A_\mu(x)B_\nu(x) + \frac{\left[J_A^0(x)\right]^2}{2m_A^2} + \frac{\left[J_B^0(x)\right]^2}{2m_B^2} \\ & + \frac{J_A^0(x)J^{0\nu}(x)B_\nu(x)}{m_A^2} + \frac{J_B^0(x)J^{\mu 0}(x)A_\mu(x)}{m_B^2} + \frac{J_A^0(x)J^{00}(x)J_B^0(x)}{m_A^2 m_B^2} \\ & + \frac{(J^{0\nu}(x)B_\nu(x))^2}{2m_A^2} + \frac{(J^{\mu 0}(x)A_\mu(x))^2}{2m_B^2} + \dots \quad . \end{aligned} \tag{2.50}$$

Including the local interaction terms, it can be shown that, as expected, at tree level, the well-known Lorentz invariant result is obtained. Considering e.g. the simplest amplitude involving the vector boson self coupling ($\mathcal{S} \sim J_A^\mu(x)J^{\nu\sigma}(x)J_B^\rho(x)$), there are four contributing parts:

$$\begin{aligned}\mathcal{S}_{F\to F'} = {} & (-i)^3 \int dx \int dy \int dz\, \langle F'|\mathcal{T} J_A^\mu(x+y)A_\mu(x+y)A_\nu(y)J^{\nu\sigma}(y)B_\sigma(y+z)B_\rho(y+z)J_B^\rho(y+z)|F\rangle \\ & + (-i)^2 \int dy \int dz\, \langle F'|\mathcal{T} \frac{J_A^0(y)J_0{}^\nu(y)}{m_A^2} B_\nu(y)B_\mu(y+z)J_B^\mu(y+z)|F\rangle \\ & + (-i)^2 \int dx \int dy\, \langle F'|\mathcal{T} J_A^\mu(x+y)A_\mu(x+y)A_\nu(y)\frac{J^\nu{}_0(y)J_B^0(y)}{m_B^2}|F\rangle \\ & - i \int dy\, \langle F'|\frac{J_A^0(y)J_{00}(y)J_B^0(y)}{m_A^2 m_B^2}|F\rangle \ . \end{aligned} \tag{2.51}$$

Replacing all pairs of field operators by the propagator given in equation (2.37), the local contributions cancel out and the naively expected Lorentz invariant S-matrix is obtained:

$$\begin{aligned}\mathcal{S}_{F\to F'} = {} & (-i)^3 \int dx \int dy \int dz\, \langle F'|J_A^\mu(x+y)J^{\nu\sigma}(y)J_B^\rho(y+z)|F\rangle \\ & \times \int \frac{dk}{(2\pi)^4}\left(g_{\mu\nu} - \frac{k_\mu k_\nu}{m_A^2}\right)\frac{-i}{k^2 - m_A^2}e^{-ikx} \int \frac{dq}{(2\pi)^4}\left(g_{\sigma\rho} - \frac{q_\sigma q_\rho}{m_B^2}\right)\frac{-i}{q^2 - m_B^2}e^{-iqz}\,. \end{aligned} \tag{2.52}$$

2.3.4 Implications on Loop Contributions Involving Multiple Massive Vector Bosons

Next, loop contributions only containing massive vector boson propagators are investigated. Considering the interaction Lagrangian (2.42), for the simplest loop contribution only containing massive vector bosons ($\mathcal{S} \sim J^{\mu\sigma}(x)J^{\nu\rho}(x)$), the naively expected S-matrix is given by

$$\begin{aligned}\mathcal{S}_{F\to F'}^{\text{naive}} = {} & \frac{(-i)^2}{2} \int dx \int dy\, \langle F'|\mathcal{T} J_{\mu\sigma}(x+y)J_{\nu\rho}(y)|F\rangle \\ & \times (-i)^2 \int \frac{dk}{(2\pi)^4}\frac{g^{\mu\nu} - \frac{k^\mu k^\nu}{m_A^2}}{k^2 - m_A^2}e^{-ikx} \int \frac{dq}{(2\pi)^4}\frac{g^{\sigma\rho} - \frac{q^\sigma q^\rho}{m_B^2}}{q^2 - m_B^2}e^{-iqx}\,, \end{aligned} \tag{2.53}$$

where the external currents are interconnected by the Lorentz invariant part of the propagators, cf. equation (A.62), because all local contributions are expected to cancel. However, the naively expected loop contributions lead to difficulties related to the degree of the divergence of the S-matrix. The reason for that is that, in the naive form, loop contributions with an arbitrary number

of external currents diverge. This issue can be seen e.g. when vanishing external momenta are considered. In this case, the external currents can be expressed in terms of the metric and the loop four-momentum k^μ: $J^{\mu\sigma} = f_1(k^2)g^{\mu\sigma} + f_2(k^2)k^\mu k^\sigma$. Thus, the loop integrand containing n massive vector bosons scales (for $f_2(k^2) = 0$) at least like $(f_1(k^2)/m_{A,B}^2)^n$ for large k^2, implying that the loop diverges independent of n if $f_1(k^2)$ contains elements which are not suppressed for large k^2 (e.g. $f_1(k^2) \propto 1$). Thus, the power-counting arguments cannot be used to prove the renormalizability of a theory, cf. reference [69, p. 299][12].

However, investigating the loop contribution from equation (2.53) in more detail, there are three different contributing parts[13]:

$$\begin{aligned}
\mathcal{S}_{F\to F'} = \frac{(-i)^4}{2}\int dx \int dy\, \langle F'|\mathcal{T} J_{\mu\sigma}(x+y)J_{\nu\rho}(y)|F\rangle \\
\times \int \frac{dk}{(2\pi)^4}\left[\frac{g^{\mu\nu} - \frac{k^\mu k^\nu}{m_A^2}}{k^2 - m_A^2} + \frac{g^{\mu 0}g^{\nu 0}}{m_A^2}\right] e^{-ikx} \int \frac{dq}{(2\pi)^4}\left[\frac{g^{\sigma\rho} - \frac{q^\sigma q^\rho}{m_B^2}}{q^2 - m_B^2} + \frac{g^{\sigma 0}g^{\rho 0}}{m_B^2}\right] e^{-iqx} \\
+ (-i)^2 \int dx \left[\frac{1}{m_A^2}\langle F'|\mathcal{T} J_{0\sigma}(x)J_{0\rho}(x)|F\rangle \int \frac{dq}{(2\pi)^4}\left[\frac{g^{\sigma\rho} - \frac{q^\sigma q^\rho}{m_B^2}}{q^2 - m_B^2} + \frac{g^{\sigma 0}g^{\rho 0}}{m_B^2}\right] e^{-iqx}\right. \\
\left. + \frac{1}{m_B^2}\langle F'|\mathcal{T} J_{\mu 0}(x)J_{\nu 0}(x)|F\rangle \int \frac{dk}{(2\pi)^4}\left[\frac{g^{\mu\nu} - \frac{k^\mu k^\nu}{m_A^2}}{k^2 - m_A^2} + \frac{g^{\mu 0}g^{\nu 0}}{m_A^2}\right] e^{-ikx}\right] \\
= \mathcal{S}_{F\to F'}^{\text{naive}} - \frac{1}{m_A^2 m_B^2}\int dx\, \langle F'|\mathcal{T}\big[J_{00}(x)\big]^2|F\rangle\ . \qquad (2.54)
\end{aligned}$$

Thus, deriving the loop contribution for massive vector bosons properly, a result differing from the naive expectation is obtained because local interaction terms of the form $\sim [J_{00}(x)]^n$ do not appear in the interaction Hamiltonian, cf. equation (2.50). However, the remaining loop contribution is still Lorentz invariant which becomes more obvious when the matrix element is rewritten as

$$\begin{aligned}
\mathcal{S}_{F\to F'} = -\frac{(-i)^3}{4}\int dx \int dy\, \langle F'|\mathcal{T} J_{\mu\sigma}(x+y)J_{\nu\rho}(y)|F\rangle \int \frac{dq}{(2\pi)^4}\left[\int d\tilde{k}_A \left(g^{\mu\nu} - \frac{k_A^\mu k_A^\nu}{m_A^2}\right)\right. \\
\left. \times \frac{g^{\sigma\rho} - \frac{q^\sigma q^\rho}{m_B^2}}{q^2 - m_B^2} e^{-i(k_A+q)x} + \int d\tilde{k}_B \left(g^{\sigma\rho} - \frac{k_B^\sigma k_B^\rho}{m_B^2}\right)\frac{g^{\mu\nu} - \frac{q^\mu q^\nu}{m_A^2}}{q^2 - m_A^2} e^{-i(k_B+q)x}\right]. \qquad (2.55)
\end{aligned}$$

On first sight, equation (2.55) does not seem Lorentz invariant because of the appearance of on-shell four-momenta. Moreover, for the corresponding massive vector boson, only one momentum integral occurs ($d\tilde{k}_{A,B}$). However, one of the propagators in each loop can be on-shell without breaking the Lorentz invariance because the remaining four-momentum integrals (dq in equation (2.55)) ensure four-momentum conservation in each vertex. Intuitively, this can be understood from the fact that cutting one propagator of a loop diagram results in a different diagram with the loop particle as an external particle (on-shell). The contribution of the resulting diagram is Lorentz invariant because the other loop propagators are given in the naive, Lorentz-invariant form.

[12] More precisely, in reference [7], it is stated that the Green functions in unitary gauge are not renormalizable, meaning that divergences do not cancel until the S-matrix is evaluated.

[13] Considering more complex matrix-elements ($\mathcal{S} \sim [J^{\mu\nu}(x)]^{2n}$) that an alike result is obtained: $\mathcal{S}_{F\to F'}^{\text{naive}} - 1/(m_A^2 m_B^2)^n \int dx\, \langle F'|[J_{00}(x)]^{2n}|F\rangle$, which can be rewritten into a similar form as given in equation (2.55).

Moreover, considering vanishing external momenta again, the external current can be expressed as $J^{\mu\sigma} = f(k_{A,B}^2)g^{\mu\sigma} + g(k_{A,B}^2)k_{A,B}^{\mu}k_{A,B}^{\sigma}$, implying that the sum over all Lorentz indices is independent of $k_{A,B}^{\mu}$:

$$\left(f_1(k_{A,B}^2)g^{\mu_1\nu_1} + g_1(k_{A,B}^2)k_{A,B}^{\mu_1}k_{A,B}^{\nu_1}\right)\left(g^{\nu_1\mu_2} - \frac{k_{A,B}^{\nu_1}k_{A,B}^{\mu_2}}{m_{A,B}^2}\right)\dots\left(g^{\nu_n\mu_1} - \frac{k_{A,B}^{\nu_n}k_{A,B}^{\mu_1}}{m_{A,B}^2}\right) = 3\prod_i f_i(k_{A,B}^2)\,. \tag{2.56}$$

Thus, considering the local interaction terms properly, the propagator part of the loop containing n massive vector bosons scales as $1/(k^2)^n$, implying that the usual power-counting argument can be used to prove renormalizability. Hence, as expected, the degree of divergence in the S-matrix is the same as expected from R_ξ gauge. Note that the propagator part scaling like $1/(k^2)^n$ can be seen from the fact that, after evaluating the Lorentz sum, the residue theorem can be used to rewrite the loop momentum integral $(d\tilde{k})$ into the typically investigated four-momentum integral form (dk).

However, to make statements about the degree of divergences in the S-matrix of general theories, this investigation needs to be extended for a more general interaction Lagrangian of a form containing an arbitrary number of massive vector fields A_i:

$$\mathcal{L}_I(x) = -\sum_i J_i^{\mu}(x)A_{i,H,\mu}(x) - \sum_j J_{ij}^{\mu\nu}(x)A_{i,H,\mu}(x)A_{j,H,\nu}(x) + \mathcal{O}(A^3)\,. \tag{2.57}$$

However, without evaluating the corresponding interaction Hamiltonian in detail, following the previous calculation, it can be seen that local interaction terms of the form $[J^{00}]^n$ are still absent in the interaction Hamiltonian, meaning that for self-interacting massive vector bosons as well as for multiple massive vector bosons interacting with each other, a deviation of the properly derived loop contribution from the naive expectation is expected. Nevertheless, it should be proven that no further subtleties especially with respect to higher order interaction terms $\sim \mathcal{O}(A^3)$ occur.

Because nowadays, the path integral formalism is typically used for the calculation of transition amplitudes, the loop contribution of interest will be discussed in the path integral formalism in the next section.

2.3.5 Implications on Massless Vector Bosons

Finally, considering massless vector bosons, their contribution to the perturbation series is determined by the massless limit of the massive vector bosons. The reason for that is that the Lagrangian and therefore the equations of motion of both only differ by the mass term. On first sight, taking the massless limit for the propagator is non-trivial because of the $k^\mu k^\nu/m_A^2$ term. However, as has been discussed in section 2.1, massless vector bosons can only appear in gauge theories, meaning that the gauge invariance enforces $J^\mu(x)k_\mu = 0$. Consequently, the $k^\mu k^\nu/m_A^2$ term can simply be ignored or replaced by $k^\mu k^\nu/k^2$, meaning that the propagator in the most general form is given by equation (A.63).

However, this propagator causes problems again when loop contributions only containing massless vector bosons are considered because in the loop, they count as four degrees of freedom while only

two are physical. The reason for that is that the polarization sum does not only sum over the physical polarizations, cf. equation (A.59), but also includes unphysical polarizations. As a consequence, the naively expected loop contribution contradicts the optical theorem [60, pp. 510-512]. Following the previous investigation for massive vector bosons, it is indicated that also for massless vector bosons, one of the propagators in the loop is given by the propagator only including the physical polarizations. In this case, also the loop contribution is determined by the massless limit of the massive vector bosons case, cf. equation (2.55). The reason for that is again the conservation of the gauge current, implying that the contribution of the unphysical polarizations vanishes as long as one of the gauge bosons is on-shell. Thus, contracting the Lorentz indices, a simple loop contribution induced e.g. by two different massless vector bosons (A and B) interacting with each other becomes

$$\begin{aligned}\mathcal{S}_{F\to F'} = &-\frac{(-i)^3}{2}\int dx \int dy\, \langle F'|\mathcal{T} J_{\mu\nu}(x+y)J^{\mu\nu}(y)|F\rangle \\ &\times \int \frac{dq}{(2\pi)^4}\left[\int d\tilde{k}_A \frac{1}{q^2} e^{-i(k_A+q)x} + \int d\tilde{k}_B \frac{1}{q^2} e^{-i(k_B+q)x}\right].\end{aligned} \tag{2.58}$$

Note that the $d\tilde{k}$ integral cannot simply be rewritten into a four-momentum integral because only when one of the gauge bosons is on-shell, the conservation of the gauge current guaranties that only physical polarizations contribute[14].

2.4 Path Integral for Quantum Field Theory

In this section, first of all, the aspects of the path integral formalism relevant for QM are briefly introduced and, afterwards, the usual method for calculating transition amplitudes in QFT in the path integral formalism is discussed for scalar boson fields[15]. Finally, the path integral for quantum fields – with a focus on massive vector bosons – is investigated in detail. In particular, it is discussed that, including interaction terms involving multiple vector bosons, the path integral cannot be written in the naively expected form.

2.4.1 Path Integral for Quantum Mechanics

It can be shown that a transition amplitude between eigenstates of the position operator $\hat{x}\,|x_i\rangle = x_i\,|x_i\rangle$ in QM can be expressed by the path integral

$$\langle x_f, t_f|x_i, t_i\rangle = \int \mathcal{D}x\,\mathcal{D}p\,\exp\left[i\int_{t_i}^{t_f} dt\left(p(t)\dot{x}(t) - \hat{\mathrm{H}}(p(t),x(t))\right)\right] := \int \mathcal{D}x\,\mathcal{D}p\, e^{iS}\,, \tag{2.59}$$

[14] This can be understood from the fact that $J_{\mu\nu}(x)$, in general, contains spacetime derivatives acting on the momentum integrals, meaning that $J_{\mu\nu}(x)$ is not necessarily independent of the loop momenta.

[15] The introduction to the path integral formalism and the following derivation of the scalar boson propagator are closely related to the derivations in sections 6 and 8 of reference [64].

where $x(t)$ and $p(t)$ are defined by the action of the position and momentum operators

$$\hat{x}\,|\psi(t)\rangle = x(t)\,|\psi(t)\rangle \qquad \text{and} \qquad \hat{p}\,|\psi(t)\rangle = p(t)\,|\psi(t)\rangle\ , \tag{2.60}$$

and the path integral integrates over all phase-space paths ($\mathcal{D}x\,\mathcal{D}p$) which fulfill the boundary conditions $x(t_{i,f}) = x_{i,f}$.

To see the benefit of the path integral formalism, more generalized forms of transition amplitudes which also include the action of operators can be considered:

$$\langle x_f, t_f|\mathcal{T}\,\hat{x}(t_1)\dots\hat{x}(t_n)\,\hat{p}(t'_1)\dots\hat{p}(t'_{n'})|x_i,t_i\rangle = \int \mathcal{D}x\,\mathcal{D}p\; x(t_1)\dots x(t_n)\,p(t'_1)\dots p(t'_{n'})\,e^{iS}\,, \tag{2.61}$$

with $t_i \le t_1,\dots,t_n,t'_1,\dots,t'_{n'} \le t_f$. Using the modification $\hat{\mathrm{H}}(p(t),x(t)) \to \hat{\mathrm{H}}(p(t),x(t)) - f(t)x(t) - h(t)p(t)$, the generalized transition amplitude can be rewritten in terms of functional derivatives:

$$\langle x_f, t_f|\mathcal{T}\hat{x}(t_1)\dots\hat{p}(t'_{n'})|x_i,t_i\rangle = (-i)^{n+n'}\frac{\delta}{\delta f(t_1)}\dots\frac{\delta}{\delta h(t'_{n'})}\,\langle x_f,t_f|x_i,t_i\rangle_{f,h}\Big|_{f=h=0}\,, \tag{2.62}$$

with $\langle\dots|\dots\rangle_{f,h}$ referring to the modified amplitude and the functional derivative being defined as

$$\frac{\delta}{\delta f(t')}g(f(t)) = \frac{\partial g(f(t))}{\partial f(t)}\delta(t-t')\,. \tag{2.63}$$

Furthermore, it is convenient to consider the transition amplitude of the ground state ($|0\rangle$) and take the limit $t_{i,f} \to \mp\infty$. Additionally, using the modification $\hat{\mathrm{H}} \to (1-i\epsilon)\hat{\mathrm{H}}$, cf. appendix A.6,

$$\begin{aligned}\langle 0|0\rangle_{f,h} &= \lim_{t_i\to-\infty,t_f\to\infty}\int dx_f dx_i\,\langle 0|x_f,t_f\rangle\,\langle x_f,t_f|x_i,t_i\rangle_{f,h}\,\langle x_i,t_i|0\rangle \\ &= \int \mathcal{D}x\,\mathcal{D}p\,\exp\left[i\int_{-\infty}^{\infty}dt\left(p(t)\dot{x}(t) - (1-i\epsilon)\hat{\mathrm{H}}(p(t),x(t)) + f(t)x(t) + h(t)p(t)\right)\right]\,,\end{aligned} \tag{2.64}$$

is obtained. Next, as in time-dependent perturbation theory, considering transition amplitudes between eigenstates of the free Hamiltonian in the limit $\int dt\,\hat{\mathrm{H}}_I(p(t),x(t)) \ll 1$, the interaction Hamiltonian can be excluded from the path integral by exchanging $p(t)$ and $x(t)$ by functional derivatives:

$$\begin{aligned}\langle 0|0\rangle_{f,h} &= \exp\left[-i\int_{-\infty}^{\infty}dt\hat{\mathrm{H}}_I\left(\frac{1}{i}\frac{\delta}{\delta h(t)},\frac{1}{i}\frac{\delta}{\delta f(t)}\right)\right] \\ &\quad\times\int \mathcal{D}x\,\mathcal{D}p\,\exp\left[i\int_{-\infty}^{\infty}dt\left(p(t)\dot{x}(t) - (1-i\epsilon)\hat{\mathrm{H}}_0(p(t),x(t)) + f(t)x(t) + h(t)p(t)\right)\right]\,.\end{aligned} \tag{2.65}$$

Finally, in case of $\hat{\mathrm{H}}_0$ being only quadratic in $p(t)$ the integral over $p(t)$ is Gaussian and can be evaluated. Furthermore, if the appearing terms, which are quadratic in $p(t)$, are independent of $x(t)$, the prefactors of the $p(t)$ integration can simply be absorbed into the normalization of the $\mathcal{D}x$ integral so that the path integral becomes

$$\langle 0|0\rangle_f = \exp\left[i\int_{-\infty}^{\infty}dtL_I\left(\frac{1}{i}\frac{\delta}{\delta f(t)}\right)\right]\int\mathcal{D}x\exp\left[i\int_{-\infty}^{\infty}dtL_0(\dot{x}(t),x(t)) + f(t)x(t)\right]\,, \tag{2.66}$$

where the ϵ factor is neglected to obtain the usual form[16].

2.4.2 Common Extension of the Path Integral in Quantum Field Theory

The path integral formalism can be generalized to QFTs where instead of position operators $\hat{x}$, field operators $\psi(x)$ are considered. Hence, the path integral in QFT integrates over all field configurations $\psi_c(x)$ fulfilling the boundary conditions. Besides, the function $f(t)$ becomes a function of spacetime and is usually named $J(x)$. Thus, the path integral of a QFT is

$$Z_0(J) = \langle 0|0\rangle_J = \int \mathcal{D}\psi_c \exp\left[i \int dx \left(\mathcal{L}(\psi_c(x)) + J(x)\psi_c(x)\right)\right] . \tag{2.67}$$

Excluding the interaction Lagrangian from the path integral by expressing it in terms of functional derivatives with respect to $J(x)$, the remaining path integral corresponds to a non-interacting theory including the *classical sources* $J(x)$. Consequently, for a scalar theory the relevant path integral is given by

$$Z_0(J) = \int \mathcal{D}\phi_c \exp\left[i \int dx \left(-\frac{1}{2}(\partial^\mu \phi_c(x))(\partial_\mu \phi_c(x)) - \frac{1}{2}(m^2 + i\epsilon)\phi_c(x)^2 + J(x)\phi_c(x)\right)\right] . \tag{2.68}$$

Next, $\phi_c(x)$ and $J(x)$ can be expressed in terms of their Fourier transformed

$$\phi_c(x) = \int \frac{dk}{(2\pi)^4} \phi_c(k) e^{-ikx} \qquad \text{and} \qquad J(x) = \int \frac{dk}{(2\pi)^4} J(k) e^{-ikx} , \tag{2.69}$$

allowing to rewrite the space integral into a momentum integral

$$\frac{1}{2} \int \frac{dk}{(2\pi)^4} \left[-\phi_c(k)(k^2 - m^2 + i\epsilon)\phi_c(-k) + J(k)\phi_c(-k) + J(-k)\phi_c(k)\right] . \tag{2.70}$$

By transforming $\phi(k) \to \phi(k) - J(k)/(k^2 - m^2 + i\epsilon)$, the mixed terms disappear. Thus, demanding $Z_0(0) = 1$ the path integral completely disappears:

$$Z_0(J) = \exp\left[\frac{i}{2} \int \frac{dk}{(2\pi)^4} \frac{J(k)J(-k)}{k^2 - m^2 + i\epsilon}\right] . \tag{2.71}$$

Finally, the integral can be transformed back into position space:

$$Z_0(J) = \exp\left[\frac{1}{2} \int dx\, dy\, J(x) D_\phi(x - y) J(y)\right] , \tag{2.72}$$

with $D_\phi(x - y)$ being the propagator of scalar bosons, cf. equation (A.60).
Using the path integral method, the propagators of fermions (A.61), massive vector bosons (A.62), and gauge bosons (A.63) can be evaluated in the same way. Furthermore, the well-known Feynman rules can be deduced.

However, as discussed in the previous section, loop corrections containing only massive vector boson propagators and derivatives of scalar boson propagators deviate from the naive expectation, cf. equation (2.55). Hence, the question arises whether subtleties of the path integral formalism have not been considered yet.

[16] Note that when considering a Hamiltonian which includes a mass term, the factor ϵ can be reintroduced by just exchanging $m^2 \to m^2 - i\epsilon$ fulfilling the same function and besides allowing to maintain the factor in the Lagrangian.

2.4.3 Subtleties of the Path Integral for Quantum Field Theory

In QM, in position space, all operators can be expressed in terms of the position and the momentum operator. For both of these operators, eigenstates can be found, fulfilling the relations (2.60) which was essential for the derivation of the path integral. In contrast, considering QFT, the state vector only contains information about the particle content and the relevant operators are the field operators containing creation and annihilation operators. As a consequence, the action of each field operator modifies the state vector by altering the particle content, implying that no eigenstates of the field operator exist[17]. This modification of the state vector by the action of field operators cannot be ignored because the creation and annihilation operators have a non-vanishing mass dimension, implying that the mass dimension of a state vector changes.
This can e.g. be seen considering the action of a single field operator on a full set of states, cf. equation (A.67),

$$\begin{aligned}\psi_i(x)\,|S\rangle\,\langle S| = &\left(\prod_i \sum_{n_i=0}^{\infty} \frac{1}{(n_i-1)!}\right)\left(\prod_i \prod_{j=1}^{n_i} \int d\tilde{k}_{i,j}\right) u_i(\vec{k}_{i,n_i}) e^{-ik_{i,n_i}x} \\ &\times \left(\prod_i \prod_{j=1}^{n_i-1} a_i(\vec{k}_{i,j})\right)^{\dagger} |0\rangle\,\langle 0| \left(\prod_i \prod_{j=1}^{n_i} a_i(\vec{k}_{i,j})\right) = |S\rangle\,\langle S|\,\psi_i(x)\,, \end{aligned} \tag{2.73}$$

where not only a prefactor is obtained but the full set of states becomes asymmetric. In addition, including a full set of states into an amplitude at any point is irrelevant because, according to equation (2.73), the operator commutes with it,

$$\big[\psi_i(x), |S\rangle\,\langle S|\,\big] = 0\,, \tag{2.74}$$

meaning that only the action on a distinct state vector is relevant.

To circumvent the issue that relation (2.60) cannot be counted on to replace the field operators by field configurations, instead, the action of a field operator on a state produced by another field operator can be investigated:

$$\begin{aligned}&\int dx\,\langle F'|J'(y)\psi_i(y)\psi_i^{\dagger}(x)J(x)|F\rangle \\ &\quad = \int dx \int d\tilde{k}_i \left(u_i(\vec{k})u_i^{\dagger}(\vec{k})e^{ik_i(x-y)} + v_i(\vec{k})v_i^{\dagger}(\vec{k})e^{-ik_i(x-y)}\right)\langle F'|J'(y)J(x)|F\rangle\ . \end{aligned} \tag{2.75}$$

Next, the momentum integral can be rewritten into a dk integral by making use of the residue theorem:

$$\int dx \int \frac{dk}{(2\pi)^4} \frac{i}{k^2 - m_i^2} u_i'(k)(u_i')^{\dagger}(k) e^{ik(x-y)}\,\langle F'|J'(y)J(x)|F\rangle\ . \tag{2.76}$$

Thus, the allowed field values at y are proportional to $u_i'(k)e^{iky}$, where k is determined by the external momenta. As a consequence, in the path integral, it can be integrated over all field configurations when $u_i'(k)$ represents a full basis in the field configuration space.

[17] In principle, for bosons, an infinite series of state vectors with increasing occupation number can be defined such that the action of the annihilation operator results in the same state but this state cannot be normalized.

However, as has been discussed in the previous section, this is not the case for vector bosons and derivatives of scalar boson field operators. Thus, focusing again on massive vector bosons, it makes sense to start with the investigation of the path integral in the Hamilton form where the path integral only integrates over $\vec{\Pi}_A(x)$ and $\vec{A}(x)$, cf. reference [68, pp. 389-395]. Starting with the investigation of a single non-self-interacting massive vector boson, one can in principle evaluate the path integral of $\vec{\Pi}_A(x)$. However, the obtained Lagrangian is not equivalent to the Lagrangian initially considered, cf. equation (2.38), but still includes the local interaction term, cf. equation (2.39).
In contrast, as shown in reference [68, p. 394], the auxiliary field can be reintroduced by subtracting

$$\Delta H = \frac{m_A^2}{2} \int d^3x \left(A^0(x) - \frac{1}{m_A^2} \left[\nabla \vec{\Pi}_A(x) + J_A^0(x) \right] \right)^2 \tag{2.77}$$

from the Hamiltonian, cf. equation (2.46) with $J^{\mu\nu}(x) = 0$, and, at the same time, including a path integral over $A^0(x)$[18]. Finally, evaluating the path integral over $\vec{\Pi}_A(x)$, the naively expected form of the path integral – where the action is determined by the initially considered Lagrangian and the path integral integrates over all field configurations – is obtained.

In contrast, considering the Hamiltonian of a theory including self-interacting massive vector bosons, cf. equations (2.47) and (2.48), this trick does not allow to rewrite the path integral into the naively expected form. However, rewriting the interaction Hamiltonian into the form given in equation (A.84), it seems that one can still use the trick to rewrite the path integral into a simpler form. For that,

$$\begin{aligned} \Delta H = {} & \frac{1}{2} \left(m_A^2 - \frac{1}{2m_B^2} \left[J^{00}(x) \right]^2 \right) \int d^3x \left(A^0(x) - \frac{1}{m_A^2} \left[\nabla \vec{\Pi}_A(x) + J_A^0(x) \right] \right)^2 \\ & + \frac{m_B^2}{2} \int d^3x \left(B^0(x) - \frac{1}{m_B^2} \left[\nabla \vec{\Pi}_B(x) + J_B^0(x) \right] \right)^2 \\ & + \int d^3x \, J^{i0}(x) A_i(x) \left(B^0(x) - \frac{1}{m_B^2} \left[\nabla \vec{\Pi}_B(x) + J_B^0(x) \right] \right) \end{aligned} \tag{2.78}$$

can be subtracted from the interaction Hamiltonian and, at the same time, include a path integral over $A^0(x)$ and $B^0(x)$. Even though this cannot be used to absorb all local interaction terms, it can be seen that a local interaction term of the form $[J^{00}(x)A_0(x)]^2$ occurs. Thus, it can be expected that this local interaction term guarantees the equivalence of the loop contribution calculated using the path integral formalism and time-dependent perturbation theory, respectively.

Note that loops contributions only containing massive vector boson propagators are only induced by the interaction term $\mathcal{L}_I(x) = -J_{\mu\nu}(x) A_H^\mu(x) B_H^\nu(x)$. Considering only these interaction term, the equations of motion for $A_H^0(x)$ and $B_H^0(x)$ in the Heisenberg picture for the two massive vector boson case become

$$A_H^0(x) = \frac{1}{m_A^2} \left(A^0(x) + J^{0\nu}(x) B_\nu(x) + \frac{J^{00}(x)}{m_B^2} \left(J^{\mu 0}(x) A_\mu(x) + \frac{J^{00}(x)}{m_A^2} \dots \right) \right), \tag{2.79a}$$

$$B_H^0(x) = \frac{1}{m_B^2} \left(B^0(x) + J^{\mu 0}(x) A_\mu(x) + \frac{J^{00}(x)}{m_A^2} \left(J^{0\nu}(x) B_\nu(x) + \frac{J^{00}(x)}{m_B^2} \dots \right) \right), \tag{2.79b}$$

[18] The introduction of the additional path integral is justified in reference [68, p. 394] with the argument that the integral over $A^0(x)$ only induces a field-independent prefactor because ΔH is quadratic in $A^0(x)$.

cf. equation (2.46), with $A^\mu(x)$ and $B^\mu(x)$ being the fields in the interaction picture with $A^0(x)$ and $B^0(x)$ being defined in equation (2.49). Hence, considering e.g. the loop from the previous section, cf. equation (2.54), $A^0_H(x)$ and $B^0_H(x)$ are both determined by the field operators $B_\nu(x)$ and $A_\mu(x)$, respectively, and the external current $J^{\mu\nu}(x) \sim e^{ipx}$. As a consequence, accounting for p^0, either $A^0_H(x)$ or $B^0_H(x)$ can become a field variable independent of the loop momenta integral but not both at once.

Note that for the same reason, the result from the path integral integrating over all field configurations for loops only containing massless gauge bosons differs from equation (2.58). However, instead of sticking to the physical field configurations for one of the gauge bosons in the loop, the problem can also be solved by the well-known gauge-fixing procedure being discussed in the context of gauge theories, cf. section 2.6.

2.5 Renormalization and Renormalization Group Equations

As was discussed in the previous sections, the perturbation series of an interacting QFT contains elements where the momentum of the exchanged particles is not fixed due to four-momentum conservation, cf. e.g. equation (2.30)[19]. In general, these loop contributions can be divergent. However, this contradicts the observation of finite transition amplitudes.
In principle, the divergence of a single matrix element could cancel when summing up all matrix elements contributing to a certain process, but for most of the considered models this is not the case. For this reason, methods have been developed to erase the unobserved divergences from the perturbation series.

For being able to erase the divergences, the momentum integral has to be regularized first, meaning that the divergence appears in the limit of some new parameter. The resulting loop contribution can then be divided into a finite part depending on the kinematics of the considered process and some remaining part which diverges. Subsequently, the fact that the masses and coupling strengths can be measured at least for one specific kinematic configuration is used, to redefine the Hamiltonian such that it already contains all loop corrections at this *renormalization scale*[20]. This procedure – known as *renormalization* – is essential for QFTs because the concept of a *bare* parameter, which does not contain loop corrections, is insufficient considering a theory where the divergences does not cancel out. In this case, bare parameters are not observable and all predictions have to be expressed in terms of measured quantities to obtain finite expressions. Note that especially for the mass terms which are part of the free Hamiltonian this redefinition of the Hamiltonian is essential: Particles are defined as eigenstates of the free Hamiltonian and are only described correctly when all corrections

[19] In detail, these loop corrections always appear when a matrix element defined in equation (2.22) – which can be visualized by a connected diagram – contains more than $2n-2$ field operators where n is the number of different spacetime interaction points.

[20] Note that the renormalization scale can be chosen at will because the division of the loop contribution into a finite and a divergent part is arbitrary. Furthermore, in the literature also other renormalization schemes which are independent of a renormalization scale are used. However, the resulting amplitudes are independent of the renormalization scale and the renormalization scheme.

to the free Hamiltonian are included.
For more details on regularization and renormalization, cf. appendix A.8.

A QFT is called renormalizable if all appearing loop divergences can be absorbed by redefining the bare parameters of a theory. The reason for this is that one cannot absorb the divergences of purely loop induced couplings by redefining the Hamiltonian. In detail, only theories in which all coupling constants have a vanishing or positive mass dimension are called renormalizable because otherwise an infinite series of bare parameters is needed to absorb all divergences. Consequently, only interaction terms with up to four bosons and with two fermions and one boson can appear in a renormalizable theory[21].

2.5.1 Renormalization Group Equations

Instead of considering a specific renormalization scale, typically, depending on the regularization method, only a specific part of the loop contribution is absorbed. Considering the commonly used dimensional regularization, cf. appendix A.8, one can e.g. only absorb the poles in ϵ (MS scheme) or also further universal factors as in the $\overline{\text{MS}}$ scheme, cf. e.g. reference [63]. With this, the running of the couplings depending on the choice of the arbitrary energy scale μ can be expressed in terms of a differential equation:

$$\frac{dg}{d\ln\mu} = \beta(g) = \sum_{n=1}^{\infty} \beta_n(g)\,, \tag{2.80}$$

where $\beta(g)$ is the so-called β-function being independent of μ and n is the loop order, meaning that $\beta_n(g)$ are the n^{th} order parts of the β-function. Note that in case of multiple considered coupling constants, in general, a coupled system of differential equations – known as renormalization group equations (RGEs) – is obtained[22].

For the SM, cf. section 2.8, only taking into account the gauge couplings, the dominant Yukawa interactions (top, bottom and tau), and the Higgs self coupling, the RGEs at one-loop order in the $\overline{\text{MS}}$ scheme are given in appendix A.9. The solution of these differential equations are shown in figure 2.1[23]. Considering the running of the couplings in the $\overline{\text{MS}}$ scheme, for a process at a kinematic scale Λ, the tree-level coupling can be approximated by the coupling strength at $\mu = \Lambda$. Doing so, the logarithms in the loop corrections remain small, meaning that higher order loop corrections to

[21] Interaction terms involving one fermion and two bosons are forbidden due to the conservation of the fermion number.

[22] Note that considering RGEs is useful when the kinematic scale of interest deviates significantly from the scale where the effective couplings are measured. In this case, simply choosing the renormalization scale to be the scale where the effective couplings are measured, the suppression of higher order loop corrections decreases for larger scale shifts, meaning that higher order loop corrections become more important. Considering the running of the couplings instead, this issue is shifted into the RGEs where it is addressed more properly. This can be understood from the fact that the RGEs consider the μ dependence of the parameters of the theory and not loop contributions to individual processes.

[23] Note that a negative value for λ is not directly a problem in light of perturbation theory. However, considering vacuum loop corrections to the effective Higgs potential, the Higgs potential becomes negative as well for large VEV implying the potential to become unstable. Note that a detailed analysis including higher order loop corrections shows that the SM Higgs potential is actually at least meta stable.

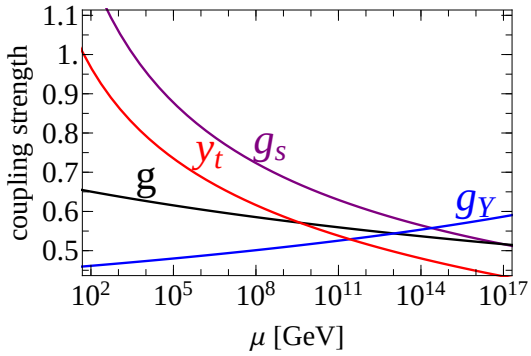

(a) Scale dependence of the gauge couplings (g' for $U(1)_Y$, g for $SU(2)_L$, and g_s for $SU(3)_c$) and the top Yukawa coupling (y_t).

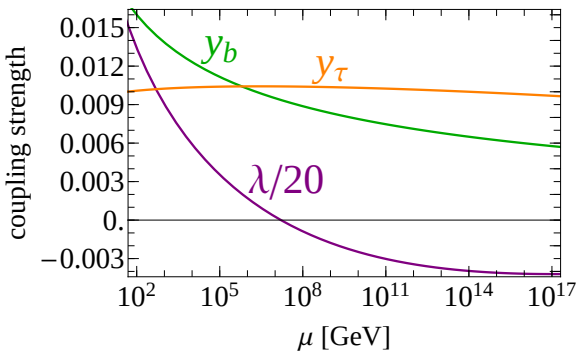

(b) Scale dependence of the Higgs self coupling (λ), the bottom Yukawa coupling (y_b), and the tau Yukawa coupling (y_τ).

Figure 2.1: Scale dependence of the dominant SM coupling constants in the $\overline{\text{MS}}$ scheme considering the RGEs of the SM at one-loop order.

the considered process are less important. For this reason, considering thermal systems at high temperatures, the couplings at $\mu \sim T$ are used for the calculation of transition amplitudes.

2.6 Introduction Into Gauge Theories

As preparation for the investigations following in the next section, in this section, at first, a short introduction into the essentials of gauge theories is presented to remind the reader of the basic concepts. Afterwards, the gauge fixing procedure – representing an elegant solution to the issues arising from loop corrections including gauge bosons – is introduced.

2.6.1 Essentials of Gauge Theories

In general, any given Lagrangian and therewith the equations of motion can be invariant under certain transformations. This invariance is of special interest because according to Noether's theorem, each of these symmetry transformations correspond to a conserved quantity. Following this, the system of equations of motion is over-determined. In quantum field theory, two different kinds of symmetries are distinguished, namely global symmetries, which can be discrete or continuous, and local symmetries which have to be differentiable and therefore continuous. Hence, local symmetries are associated with Lie groups.
The local symmetries of quantum field theories are called gauge symmetries and are defined by the invariance of the action of the Lagrangian on any given state under a local transformation which can be parameterized by a continuous and differentiable set of functions $\alpha^a(x)$:

$$\mathcal{L}(x)|_{\alpha^a(x)=0}\,|F\rangle = \mathcal{L}(x)|_{\alpha^a(x)=f^a(x)}\,|F\rangle\ , \tag{2.81}$$

where $f^a(x)$ are arbitrary continuous and differentiable functions and $|F\rangle$ is an arbitrary state vector.

To obtain the conserved quantity corresponding to the gauge invariance, an infinitesimal set of symmetry transformation $\delta\alpha^a(x)$ is considered:

$$\begin{aligned}\left(\mathcal{L}(x)|_{\alpha^a(x)=\delta\alpha^a(x)} - \mathcal{L}(x)|_{\alpha^a(x)=0}\right)|F\rangle &= \left(\left.\frac{d\mathcal{L}(x)}{d\alpha^a(x)}\right|_{\alpha^a(x)=0}\delta\alpha^a(x) + \mathcal{O}(\delta\alpha^a(x)^2)\right)|F\rangle \\ = \left(\sum_i\left(\frac{\partial\mathcal{L}(x)}{\partial\psi_i(x)}\frac{d\psi_i(x)}{d\alpha^a(x)} + \frac{\partial\mathcal{L}(x)}{\partial[\partial_\mu\psi_i(x)]}\frac{d(\partial_\mu\psi_i(x))}{d\alpha^a(x)}\right)\right|_{\alpha^a(x)=0}&\delta\alpha^a(x) + \mathcal{O}(\delta\alpha^a(x)^2)\Bigg)|F\rangle \stackrel{!}{=} 0\,. \quad (2.82)\end{aligned}$$

Considering only leading order terms in $\delta\alpha^a(x)$ and making use of the Euler–Lagrange equation,

$$\frac{\partial\mathcal{L}(x)}{\partial\psi_i(x)} = \partial_\mu\frac{\partial\mathcal{L}(x)}{\partial[\partial_\mu\psi_i(x)]}\,, \quad (2.83)$$

the well-known statement of *Noether's theorem*

$$\partial_\mu J^{a\,\mu}(x)\,|F\rangle = \partial_\mu\sum_i\left(\frac{\partial\mathcal{L}(x)}{\partial(\partial_\mu\psi_i(x))}\frac{d\psi_i(x)}{d\alpha^a(x)}\right)\Bigg|_{\alpha^a(x)=0}|F\rangle = 0\,, \quad (2.84)$$

is obtained, saying that for every differentiable continuous symmetry there is a conserved current $J^{a\,\mu}(x)$.

Consequently, fields have to transform non-trivially under a certain group transformation to obtain a non-vanishing conserved current. E.g. considering an invariance under a $U(n)$ (unitary group) transformation, the Lagrangian has to be invariant under the transformation

$$\psi_i(x) \to \psi_i'(x) = e^{i\alpha^a(x)t^a}\psi_i(x)\,, \quad (2.85)$$

with t^0 being a diagonal matrix and t^i being the generators of the $SU(n)$ (special unitary group) symmetry transformation defined in equation (A.24).
Considering a general Lagrangian of a QFT, mass terms are trivially invariant under a $U(n)$ group transformation while the kinetic terms are not:

$$m_i^2(\psi_i')^\dagger(x)\psi_i'(x) = m_i^2\psi_i^\dagger(x)\psi_i(x) \quad (2.86a)$$

$$\begin{aligned}|\partial_\mu\psi_i'(x)|^2 &= |\exp(i\alpha^a(x)t^a)(\partial_\mu + i(\partial_\mu\alpha(x)^a)t^a)\psi_i(x)|^2 \\ &\neq |\exp(i\alpha^a(x)t^a)\partial_\mu\psi_i(x)|^2 = |\partial_\mu\psi_i(x)|^2\,. \quad (2.86b)\end{aligned}$$

Consequently, to obtain a gauge invariant Lagrangian, the derivative of a field transforming non-trivially under a $U(n)$ transformation needs to be replaced by a covariant derivative

$$\partial_\mu \to D_\mu \qquad \text{with} \qquad D_\mu = \partial_\mu - igA_\mu(x)\,, \quad (2.87)$$

where $A_\mu(x) = A_\mu^a(x)t^a$ is an element of the Lie-Algebra which transforms as defined in equation (A.25).
Next, to make the interaction term induced by the covariant derivative physical and not completely arbitrary, the local field $A_\mu(x)$ has to be interpreted as a quantum field. Therefore, a kinetic term

for the gauge field is added to the Lagrangian which also needs to be invariant under the gauge transformation. This requirement lead to the Yang-Mills actions, defined in equation (A.20), which in case of considering a non-abelian gauge theory ($SU(n)$ with $n > 1$) give also rise to interaction terms among the gauge fields.

Because all derivatives of a field transforming non-trivially under a $U(n)$ transformation are replaced by covariant derivatives, the equation of motion of the gauge field can be expressed in terms of the conserved current defined in (2.84):

$$\partial_\mu \frac{\partial \mathcal{L}(x)}{\partial[\partial_\mu A^a_\nu(x)]} = \frac{\partial \mathcal{L}(x)}{\partial A^a_\nu(x)} = -g J^{a\,\nu}(x)\,. \tag{2.88}$$

Since $\partial_\mu J^{a\,\mu}(x) = 0$ holds, the k^μ polarization of the gauge field does not couple to $J^{a\,\nu}(x)$, which for tree-level processes means that the propagator can be rewritten into a Lorentz invariant form, cf. section 2.3.

2.6.2 The Gauge-Fixing Procedure

As was discussed in section 2.3, for non-abelian gauge theories, one cannot simply count on gauge invariance to rewrite the propagator into a Lorentz invariant form because non-vanishing loop contributions from unphysical polarizations are obtained. Moreover, it was investigated that the contribution of the unphysical polarizations vanishes when one of the gauge bosons in the loop is considered to be on-shell because in this case, the conservation of the gauge current guarantees that the unphysical polarizations do not contribute. However, another method to remove the unphysical loop contributions known as gauge fixing, which uses gauge invariance, is typically used in literature.

As can be seen in equation (A.25), the appearance of the k_μ polarization is a relic of gauge invariance. Consequently, one can get rid of the paths of the unphysical polarizations by introducing a Dirac delta function – fixing the gauge function – into the path integral:

$$\int \mathcal{D}A\; \delta(\alpha - f(x))\; e^{iS}\,. \tag{2.89}$$

Next, choosing the gauge function such that $\partial^\mu A_\mu$ is fixed to $\omega(x)$, the Dirac delta function is accompanied by a functional determinant:

$$\int \mathcal{D}A \det\left(\frac{\delta G}{\delta \alpha}\right)\; \delta(G(\alpha))\; e^{iS}\,, \tag{2.90}$$

with $G(\alpha(x)) = \partial^\mu A_\mu(x) - \omega(x)$. The functional determinant can be calculated by introducing Faddeev-Popov ghosts to the path integral:

$$\det\left(\frac{\delta G}{\delta \alpha}\right) \sim \int \mathcal{D}c\,\mathcal{D}\overline{c} \exp\left[i \int d^4x \left(-(\partial^\mu \overline{c}^a(x))(\partial_\mu c^a(x)) + g f^{abc}(\partial^\mu \overline{c}^a(x)) c^b(x) A^c_\mu(x)\right)\right]\,. \tag{2.91}$$

Consequently, additional Feynman rules for the anti-commuting ghost fields ($c^a(x)$) are obtained which precisely cancel the loop contributions from the unphysical polarizations. To obtain the

gauge boson propagator in a nice form only depending on $g^{\mu\nu}$ and $k^\mu k^\nu$, a proper superposition of different $\omega(x)$ can be used resulting in an additional gauge fixing term in the Lagrangian

$$\mathcal{L} = \mathcal{L}_0 - \frac{1}{2\xi}(\partial^\mu A^a_\mu(x))^2\,, \tag{2.92}$$

with the arbitrary gauge-fixing parameter ξ. The resulting propagator for the gauge bosons is given by equation (A.63).

2.7 Spontaneously Broken Symmetries

In this section, first of all, the concept of spontaneous symmetry breaking (SSB) is introduced. Furthermore, the equations of motion for fields after SSB are investigated and issues appearing when quantizing the resulting equations of motion are briefly discussed.

2.7.1 Essentials of Spontaneous Symmetry Breaking

Considering a theory containing a complex scalar field ϕ, the corresponding renormalizable Lagrangian ignoring interaction terms with other fields in the most general form is given by

$$\mathcal{L}_\phi(x) = [\partial_\mu\phi^\dagger(x)][\partial^\mu\phi(x)] - m_\phi^2\phi^\dagger(x)\phi(x) - \frac{\lambda}{2}\left(\phi^\dagger(x)\phi(x)\right)^2 := [\partial_\mu\phi^\dagger(x)][\partial^\mu\phi(x)] - V(x)\,. \tag{2.93}$$

This potential is invariant under a local $U(1)$ symmetry transformation: $\phi(x) \to e^{i\alpha(x)}\phi(x)$. To obtain a stable potential, $\lambda > 0$ is required while m_ϕ^2 can be negative resulting in a minimum of the potential for non-vanishing field values. As a consequence, the field takes on a non-vanishing vacuum expectation value (VEV)

$$|\,\langle 0|\phi|0\rangle\,| = v/\sqrt{2} \neq 0\,, \tag{2.94}$$

with $v^2 = -2m_\phi^2/\lambda$. Note that the absolute value appears because the scalar field is complex, implying that the minimum of the potential is not distinct but continuous. However, the VEV is observable and therefore distinct. Next, the complex scalar field can be globally rotated, $\phi(x) \to e^{i\alpha}\phi(x)$, such that only a certain component obtains a VEV, $\langle 0|\phi_i|0\rangle = \sqrt{2}v\delta_{i0}$, where ϕ_i are the real scalar field components of ϕ.
Defining

$$\phi(x) = \frac{1}{\sqrt{2}}\left(v + h(x) + i\,\varphi(x)\right)e_0\,, \tag{2.95}$$

where $e_0 = e^{i\phi_0}$ denotes the direction of symmetry breaking, it can be deduced that the fields φ, which are orthogonal to the VEV, become massless:

$$\begin{aligned}\mathcal{L}'_\phi(x) = {}& \frac{1}{2}[\partial_\mu h(x)][\partial^\mu h(x)] + \frac{1}{2}[\partial_\mu\varphi(x)][\partial^\mu\varphi(x)] - \left(\frac{m_\phi^2}{2} + \frac{\lambda}{4}v^2\right)\left[2vh(x) + h(x)^2 + \varphi(x)^2\right] \\ & - \frac{\lambda}{2}v^2h(x)^2 - \frac{\lambda}{2}vh(x)\left[h(x)^2 + \varphi(x)^2\right] - \frac{\lambda}{8}\left[h(x)^2 + \varphi(x)^2\right]^2\,,\end{aligned} \tag{2.96}$$

with $m_\phi^2 + \lambda/2v^2 = 0$ in the minimum of the potential. The fact that for each spontaneously broken symmetry a massless particle appears is known as the *Goldstone's theorem* and the corresponding particles are called *Goldstone bosons*.

Next, considering the case where the complex scalar field transforms non-trivially under an $U(1)$ gauge transformation, the corresponding gauge invariant Lagrangian is given by

$$\mathcal{L}(x) = -\frac{1}{4}F_{\mu\nu}(x)F^{\mu\nu}(x) + [(\partial_\mu - igA_\mu(x))\,\phi(x)]^\dagger[(\partial^\mu - igA^\mu(x))\,\phi(x)] - V(x)\,. \tag{2.97}$$

Defining ϕ again as in equation (2.95), it can be seen that the VEV does not only break the rotation invariance of ϕ' but the gauge invariance of the corresponding Lagrangian:

$$\begin{aligned}\mathcal{L}(x) = \mathcal{L}'_\phi(x) - \frac{1}{4}F_{\mu\nu}(x)F^{\mu\nu}(x) - gA_\mu(x)\big[(v + h(x))[\partial^\mu\varphi(x)] - [\partial^\mu h(x)]\varphi(x)\big] \\ + \frac{g^2}{2}\big[(v + h(x))^2 + \varphi(x)^2\big]A_\mu(x)A^\mu(x)\,,\end{aligned} \tag{2.98}$$

with $m_A^2 = g^2v^2$ being the mass of the gauge boson induced by SSB. Note that in case of spontaneously broken gauge symmetries, the corresponding Goldstone bosons become unphysically. This can be understood from the fact that they can be absorbed by an according gauge transformation.

2.7.2 Equations of Motion for Goldstone Bosons and Massive Vector Bosons

Considering the Lagrangian given in equation (2.98), due to the mixing term $(m_A A_\mu(x)[\partial^\mu\varphi(x)])$, the resulting free equations of motion for A_μ and φ are coupled. This becomes clear when considering the Euler-Lagrange equation for φ:

$$\begin{aligned}\partial^\mu\frac{\partial\mathcal{L}(x)}{\partial[\partial^\mu\varphi(x)]} = \partial^\mu\left[\partial_\mu\varphi(x) - g[v + h(x)]A_\mu(x)\right] = \frac{\partial\mathcal{L}(x)}{\partial\varphi(x)} \\ \Rightarrow\partial^\mu\left[\partial_\mu\varphi(x) - m_A A_\mu(x)\right] - \frac{\partial\mathcal{L}_0}{\partial\varphi(x)} = \frac{\partial\mathcal{L}_I(x)}{\partial\varphi(x)} - \partial^\mu\frac{\partial\mathcal{L}_I(x)}{\partial[\partial^\mu\varphi(x)]} =: -J_\varphi(x)\,,\end{aligned} \tag{2.99}$$

with

$$\begin{aligned}J_\varphi(x) = -g[\partial^\mu A_\mu(x)]h(x) - 2gA_\mu(x)[\partial^\mu h(x)] - g^2\varphi(x)A_\mu(x)A^\mu(x) \\ + \frac{\lambda}{2}[2vh(x) + h(x)^2 + \varphi(x)^2]\varphi(x)\end{aligned} \tag{2.100}$$

for the considered Lagrangian and $\mathcal{L}_0(x)$ being the free Lagrangian. Consequently, $\partial\mathcal{L}_0(x)/\partial\varphi(x) = 0$ is obtained in the minimum of the potential.
Next, the Euler-Lagrange equations for A_μ are given by

$$\partial^\nu\frac{\partial\mathcal{L}(x)}{\partial[\partial^\nu A^\mu(x)]} = -\partial^\nu F_{\nu\mu}(x) = \frac{\partial\mathcal{L}(x)}{\partial A^\mu(x)} = -J^1_{A,\mu}(x) - m_A[\partial_\mu\varphi(x)] + m_A^2 A_\mu(x)\,, \tag{2.101}$$

with

$$J^1_{A,\mu}(x) = -\frac{\partial\mathcal{L}_I(x)}{\partial A^\mu(x)} = g\left(h(x)[\partial_\mu\varphi(x)] - [\partial_\mu h(x)]\varphi(x)\right) - g^2\left[2vh(x) + h(x)^2 + \varphi(x)^2\right]A_\mu(x)\,. \tag{2.102}$$

Using this equation,

$$\partial^\mu \left(J_{A,\mu}(x) + m_A[\partial_\mu \varphi(x)] - m_A^2 A_\mu(x) \right) = 0 \tag{2.103}$$

can be derived with

$$\partial^\mu \partial^\nu F_{\nu\mu}(x) = \partial^\mu \partial^\nu \frac{\partial \mathcal{L}_I(x)}{\partial[\partial^\nu A^\mu(x)]} =: -\partial^\mu J^2_{A,\mu}(x)\,, \tag{2.104}$$

which vanishes for the considered Abelian case and $J_{A,\mu}(x) = J^1_{A,\mu}(x) + J^2_{A,\mu}(x)$. Putting this into equation (2.99),

$$\frac{\partial^\mu}{m_A} J_{A,\mu}(x) = J_\varphi(x) - \frac{\partial \mathcal{L}_0(x)}{\partial \varphi(x)} \tag{2.105}$$

is obtained. This important result states that in the minimum of the potential, the amplitude of coupling to a Goldstone boson with momentum k^μ is equivalent to the amplitude of coupling to a vector boson with momentum k^μ times k^μ/m_A. This fact is well-known as *Goldstone equivalence theorem.*

If one now tries to switch to the Hamilton formalism in order to quantize the theory, $A^0(x)$ is still an auxiliary field because $\Pi^0(x)$ vanishes, cf. equation (2.43) and following. However, replacing $A^0(x)$ by making use of equation (2.101),

$$A_0(x) = \frac{1}{m_A^2} \left(-\partial^i F_{i0}(x) + J_{A,0} + m_A \partial_0 \varphi(x) \right)\,, \tag{2.106}$$

the conjugated field of φ becomes independent of $\partial^0 \varphi(x)$:

$$\Pi_\varphi(x) = \partial_0 \varphi(x) - m_A A_0(x) = \frac{1}{m_A} \left(\partial^i F_{i0}(x) + J_{A,0}(x) \right). \tag{2.107}$$

Thus, $\partial^0 \varphi(x)$ cannot be expressed in terms of $\Pi_\varphi(x)$ but only in terms of $A^0(x)$ so that naively, it seems not possible to switch to the Hamilton formalism[24].

To overcome this issue, typically, the gauge invariance of the considered Lagrangian, cf. equation (2.97), is used to remove the Goldstone bosons from the theory – known as unitary gauge – or to derive in analogy to the gauge fixing procedure of massless vector bosons the well-known R_ξ gauge Feynman rules, cf. e.g. references [37, 69, 64].

2.8 The Standard Model of Particle Physics

The SM of particle physics summarizes the knowledge about observed particles and their interaction which can be put together into a consistent theory. Consequently, the SM does not contain any particle not observed but it includes interaction terms which are needed to obtain a consistent theory but have not been directly measured yet (e.g. the Yukawa interaction of the light quarks

[24] For switching to the Hamilton formalism, auxiliary fields as well as time derivatives of fields need to be replaced by fields and conjugated field.

or the Higgs self interaction). The fermionic particle content of the SM comes in three families which only differ by their Yukawa interaction. Each family consists of a right-chiral lepton ($\ell_{R,i}$), a left-chiral lepton doublet (ℓ_i), an up-type right-chiral quark (U_i), a down-type right-chiral quark (D_i) and a left-chiral quark doublet (Q_i). In addition, for each fermion there is an antiparticle with opposite charge ($\overline{\ell}_{R,i}$, $\overline{\ell}_i$, $\overline{U}_i$, $\overline{D}_i$, and $\overline{Q}_i$). This classification of the fermions is a consequence of the three gauge symmetries, cf. section 2.6, being part of the SM.

The Lagrangian of the SM is invariant under a $U(1)_Y \times SU(2)_L \times SU(3)_c$ gauge transformation. The gauge boson associated to the $U(1)_Y$ is $B_\mu(x)$. The fermionic degrees of freedom forming one class carry the same hypercharge (Y) determining their transformation behavior

$$\Psi_i(x) \to \Psi_i'(x) = \exp\left(iY_i\alpha(x)\right)\Psi_i(x)\,, \tag{2.108}$$

resulting in a different coupling strength to the corresponding gauge boson ($D_\mu = \partial_\mu - iY_i g' B_\mu(x)$). The $SU(2)_L$ symmetry has three gauge bosons $W_\mu^b(x)$ ($b \in \{1,2,3\}$). Left- and right-chiral particles are distinguished by their transformation behavior under the $SU(2)_L$. Right-chiral particles are uncharged and therefore singlets under the $SU(2)_L$ while left-chiral particles transform as doublets and contain two degrees of freedom. Furthermore, the strong interaction ($SU(3)_c$) has eight gauge bosons called gluons $G_\mu^a(x)$ ($a \in \{1,\ldots,8\}$) and differentiates between leptons which are singlets and quarks which are triplets under the $SU(3)_c$.

In contrast to $U(1)$ symmetries where the gauge bosons are uncharged under the corresponding symmetry, in $SU(n)$ symmetries the gauge bosons self interact. As a consequence of this self interaction, the energy which is needed to separate a bound state diverges. Consequently, fermions which are charged under an $SU(n)$ and the corresponding gauge bosons cannot be observed as free particles but only as uncharged bound states. Thus, this so-called confinement does not allow for distinguishing the single $SU(3)_c$ triplet components. For this reason, it is not distinguished between quarks of different color, and they are simply counted as three degrees of freedom. The same would also be true for the $SU(2)_L$ doublets without the last ingredient of the SM, the Higgs mechanism. Besides fermions and gauge bosons, the SM contains a complex scalar $SU(2)_L$ doublet $H(x)$. This doublet is also charged under the $U(1)_Y$ but not under the $SU(3)_c$. Consequently, besides self interactions and the coupling to the gauge bosons, an interaction term which involves right- and left-chiral leptons or quarks is allowed. As already mentioned, these Yukawa interaction terms distinguish the three families. The crucial point of the Higgs mechanism is that $H(x)$ is spontaneously broken, cf. section 2.7, meaning that the $H(x)$ takes on a non-vanishing VEV. As a consequence, the electroweak $SU(2)_L \times U(1)_Y$ symmetry (Glashow-Salam-Weinberg model [31, 65]) breaks down to the electromagnetic interaction $U(1)_{\text{em}}$ and the weak interaction which is no longer associated with a gauge symmetry. While the gauge boson of the $U(1)_{\text{em}}$ called photon ($A_\mu(x)$) remains massless, the three remaining bosons ($W^\pm(x)$ and $Z(x)$), which are the mediators of the weak interaction, become massive. Moreover, mass terms between right-chiral singlets and left-chiral doublet components are induced by electroweak symmetry breaking (EWSB). Furthermore, confinement is resolved, meaning that the single doublet components can be observed as free particles which can be distinguished by their masses.

Finally, the basis of three left-chiral quark doublets in which each component Q_i interacts with one of the right-chiral quarks (U_i or D_i) via the Yukawa interaction does not coincide with the

basis in which a $SU(2)_L$ transformation is diagonal. Consequently, in Yukawa basis conversions between the different quark families are allowed and can be described by the Cabibbo-Kobayashi-Maskawa (CKM) matrix, cf. equation (A.93). For the leptons – assuming neutrinos to be massless – the basis of the doublets is defined such that each doublet just couples to one of the right-chiral charged leptons.

Defining the direction of EWSB such that only the lower real component take on an VEV, the $SU(2)_L$ doublets are defined as

$$\Psi_{\ell_i}(x) = \begin{pmatrix} \Psi_{\nu_i}(x) \\ \Psi_{\ell^-}(x) \end{pmatrix}, \qquad \Psi_{Q_i}(x) = \begin{pmatrix} \Psi_{Q_i^1}(x) \\ \Psi_{Q_i^2}(x) \end{pmatrix}, \quad \text{and} \quad H(x) = \frac{1}{\sqrt{2}} \begin{pmatrix} 0 \\ v + h(x) \end{pmatrix}, \tag{2.109}$$

with the left-chiral neutrinos ν_i, the left-chiral charged leptons ℓ^-, the left-chiral up-type quarks Q_i^1, the left-chiral down-type quarks Q_i^2, the Higgs particle $h(x)$, and the VEV of the Higgs field v. Furthermore, the hypercharge of the different particles

$$Y_{\ell_i} = -\frac{1}{2}, \qquad Y_{Q_i} = \frac{1}{6}, \qquad Y_H = \frac{1}{2}, \qquad Y_{\ell_{R,i}} = -1, \qquad Y_{U_i} = \frac{2}{3}, \quad \text{and} \quad Y_{D_i} = -\frac{1}{3}, \tag{2.110}$$

is associated to the conserved electric charge (Q) by

$$Q = t_2^3 + Y = \frac{\sigma_3}{2} + Y, \tag{2.111}$$

with t_2^3 being a generator of $SU(2)_L$. After EWSB, the gauge bosons of the electroweak interaction are redefined:

$$A_\mu(x) = \frac{1}{\sqrt{g^2 + g'^2}} \left(g' W_\mu^3(x) + g B_\mu(x) \right), \tag{2.112a}$$

$$W_\mu^\pm(x) = \frac{1}{\sqrt{2}} \left(W_\mu^1(x) \mp W_\mu^2(x) \right), \tag{2.112b}$$

$$Z_\mu(x) = \frac{1}{\sqrt{g^2 + g'^2}} \left(-g W_\mu^3(x) + g' B_\mu(x) \right), \tag{2.112c}$$

such that the photon stays massless while the $W^\pm(x)$ and the $Z(x)$ bosons obtain a mass of

$$m_W = \frac{g}{2} v \qquad \text{and} \qquad m_Z = \frac{\sqrt{g^2 + g'^2}}{2} v, \tag{2.113}$$

with g' and g being the gauge couplings of the $U(1)_Y$ and $SU(2)_L$ symmetries, respectively. The gauge coupling constant of $SU(3)_c$ is in the following called g_s.

2.9 Flavor Oscillation

In section 2.2, transition probabilities among different state vectors induced by the interaction Hamiltonian are calculated. State vectors with a definite particle content (species and energy) are considered meaning that all particles are completely unlocalized. However, usually, the focus is set on transition probabilities for scattering processes of localized particles. Nevertheless, as long as the annihilation and production region of the initial and final states overlap, the result

from perturbation theory is a very good approximation because the size of the wave packets is so large that integrating over all spacetime differences is a reasonable approximation. This changes when two or more locally separated interaction regions become relevant. Such processes are usually treated as two independent interaction processes which is reasonable as long as a distinct particle is exchanged between the separated interaction regions. However, if instead a superposition of different particles is exchanged, interference effects – known as flavor oscillation (FO) – can be relevant. As a consequence, the squared amplitude for the whole process – production and measurement – and not for both individually has to be calculated.

Considering a process where an interaction eigenstate which does not correspond to an energy eigenstate $\psi_i(x)$ is produced with energy E or momentum $\vec{p}$ the corresponding wave function is

$$\psi(x) = \sum \alpha_i \psi_i(x) = \sum \alpha_i u_i e^{ip_i x} \,, \tag{2.114}$$

with $\Sigma\alpha_i^2 = 1$. Furthermore, considering the high energy limit $\mathbf{p}_i = \sqrt{E^2 - m_i^2} \approx E - m_i^2/(2E)$ or $E_i = \sqrt{\mathbf{p}^2 + m_i^2} \approx \mathbf{p} + m_i^2/(2\mathbf{p})$, the wave function becomes

$$\psi(x) = \sum \alpha_i u_i e^{iE(t-\mathbf{x}_p)} \exp\left(-i(E-\mathbf{p}_i)\mathbf{x}_p\right) \approx \sum \alpha_i u_i e^{iE(t-\mathbf{x}_p)} \exp\left(i\frac{m_i^2}{2E}\mathbf{x}_p\right) \qquad \text{or} \tag{2.115a}$$

$$\psi(x) = \sum \alpha_i u_i e^{i\mathbf{p}(t-\mathbf{x}_p)} \exp\left(i(E_i-\mathbf{p})t\right) \approx \sum \alpha_i u_i e^{i\mathbf{p}(t-\mathbf{x}_p)} \exp\left(i\frac{m_i^2}{2\mathbf{p}}t\right) \,, \tag{2.115b}$$

with $\mathbf{x}_p = \vec{x}\vec{p}/\mathbf{p}$. While the first exponential function is the same for all particle species – just giving rise to an overall phase factor – the second exponential function induces a particle dependent phase resulting in a spacetime dependent amplitude for interaction eigenstates which do not correspond to energy eigenstates.

However, for a realistic derivation of FO, wave packets, which are localized in space and consequently do not carry a distinct momentum, need to be considered. FO only occurs when the momentum uncertainty is comparable to or larger than the momentum differences of the energy eigenstates because otherwise the individual mass eigenstates can be distinguished. Consequently, for being able to observe FO involving larger mass squared differences, a larger momentum uncertainty is needed, requiring a more precise localization.
It is notable that this condition directly results from the uncertainty principle ($\sigma_x\sigma_p \geq 1/2$) because a localization which is roughly smaller than the oscillation length is required ($\sigma_x \lesssim 2E/(\Delta m_i^2)$) for FO to be relevant. Thus, the uncertainty principle requires $\sigma_p \gtrsim \Delta m_i^2/(2E)$.
Note that due to the momentum uncertainty the energy is not definite either, implying that the oscillation length is not distinct. In the case of $E \gg \sigma_E$, this effect is irrelevant at the scale of the oscillation length. However, for much larger distances, this effect leads to a damping of FO.

For two reasons, the phenomenon of FO is of special relevance for neutrinos. First of all, they only interact with other SM particles via the weak interaction, meaning that only eigenstates of this interaction can be observed. Secondly, their mass differences are very small ($<$ eV), implying that for relevant energies, the oscillation length is macroscopic and therefore observable. Considering e.g. neutrinos produced in nuclear reactions ($E \sim$ MeV), the oscillation length is of order $\sim km$ and $\sim 30km$ for Δm^2_{atm} and Δm^2_{sol}, respectively, cf. equation (C.4).

Besides, FO effects are also relevant for neutral mesons where the energy eigenstates do not correspond to a distinct quark content inducing particle-antiparticle oscillations, such as $K^0 - \overline{K}^0$, $D^0 - \overline{D}^0$, and $B^0 - \overline{B}^0$ oscillations.

It can be concluded that FO is relevant when both the production and detection uncertainties are small compared to the oscillation length or when the free propagation length is comparable to the oscillation length so that oscillation phenomena become relevant but do not average out.

2.10 Decaying Particles and CP violation

In this section, first of all, the effective time evolution of a particle whose amplitude is damped by an interaction rate is considered in detail. Afterwards, the amount of CP violation – being a key element of all baryogenesis models – induced by the interaction rate part of the effective time evolution is calculated.

2.10.1 Effective Free Equation of Motion of Decaying Particles

In section 2.2, time-dependent perturbation theory for QFT is introduced as a general method for the calculation of transition amplitudes between eigenstates of the time-independent undisturbed Hamiltonian. At that, the undisturbed Hamiltonian is assumed to be equivalent to the free Hamiltonian ($\hat{\mathrm{H}}_0$). This assumption is well motivated from the observation of approximately free particles. However, transition amplitudes have a pole at an exchanged four-momentum fulfilling the energy momentum relation of the mediator ($p^2 = m^2_{\mathrm{mediator}}$) resulting in a divergent transition amplitude. This issue can be understood from the fact that the interaction range diverges when the intermediate state is produced on-shell and, at the same time, at each spacetime point, the intermediate state has a non-vanishing probability to produce the final state. Actually, the non-vanishing interaction probability induces a damping of the mediator amplitude, implying that the amplitude of producing the final state should not diverge but is less or equal to one. Thus, this damping of the mediator, induced by a non-vanishing interaction rate, needs to be taken into account when mediators are produced close to their mass-shell. This can e.g. be done by defining an effective equation of motion including such a damping term.

In practice, divergent transition amplitudes often arise from s-channel diagrams, where the initial states produce the mediator which then decays into the final state. In this case, producing the mediator on-shell implies that the mediator can at least decay into the initial as well as the final state. This damping of the mediator amplitude, induced by a decay width, is not state dependent but only determined by the theory, meaning that it can be included into the effective equation of motion without difficulty. Using this, divergences arising from s-channel diagrams disappear and the resonant part of the cross section becomes the production probability of the intermediate state times the branching ratio of the decay into the final state of interest.

To derive the effective equation of motion, it is used that – similar to a measurement – the state changing interactions induce a damping of the amplitude squared[25]. In addition, the interaction amplitude of a state induced by a certain interaction I is determined by the scalar product of the wave function with the corresponding interaction eigenstate $|\psi_I\rangle$. As a consequence, the damping induced by the considered interaction can be written as

$$\frac{\frac{d}{dt}|\langle\psi_I|\psi(t)\rangle|^2}{|\langle\psi_I|\psi(t)\rangle|^2} = 2\frac{\frac{d}{dt}|\langle\psi_I|\psi(t)\rangle|}{|\langle\psi_I|\psi(t)\rangle|} = -\Gamma_I\,, \tag{2.116}$$

where Γ_I is the interaction rate of $|\psi_I\rangle$ and the time derivative does not act on $|\psi_I\rangle$. Furthermore, the interaction rate does not damp the whole state but only the part being proportional to the interaction eigenstate. Thus, the generalized equation of motion including the interaction rate induced by the interaction Hamiltonian is given by

$$i\frac{d}{dt}|\psi\rangle = \left(\hat{\mathrm{H}} - \frac{i}{2}\sum_I \Gamma_I |\psi_I\rangle\langle\psi_I|\right)|\psi\rangle := \left(\hat{\mathrm{H}} - \frac{i}{2}\hat{\Gamma}\right)|\psi\rangle := \hat{\mathbb{H}}|\psi\rangle\,, \tag{2.117}$$

where I runs over all relevant interactions and $\hat{\mathrm{H}}$ and $\hat{\Gamma}$ are both Hermitian operators meaning that $i\hat{\Gamma}$ is skew-Hermitian.

This form of the equation of motion is also reproduced considering self-energy corrections $\Pi(p^2)$ – loop corrections with only two external lines – in more detail. In the case where the decay into the loop particles is kinematically allowed, the self-energy correction becomes complex where, according to the optical theorem, the imaginary part is given by

$$\mathrm{Im}[\Pi_i(p^2)] = \frac{1}{2}\int |M_{i\to f_1\dots f_n}|^2(2\pi)^4\delta^4\left(p_i - \sum_l p_{f_l}\right)\prod_l d\tilde{p}_{f_l} = \sqrt{p^2}\Gamma_{i\to f_1\dots f_n}(p^2)\,, \tag{2.118}$$

with $f_1\dots f_n$ being all combinations of loop particles into which the particle i can decay and $\Gamma_{i\to f_1\dots f_n}(p^2)$ being the decay width of the considered particle in its rest frame, cf. equation (2.23). This imaginary part of the self-energy correction is non-Hermitian, implying that it cannot be absorbed into the Hamiltonian using renormalization. As a consequence, the effective free Lagrangian can be written as

$$\mathcal{L}_{\text{eff}} = \phi_i^\dagger(x)\partial^\mu\partial_\mu\phi_i(x) + \phi_j^\dagger(x)\left[-m_{ij}^2 - \mathrm{Re}[\Pi_{ij}(p^2)] - i\sqrt{p^2}\Gamma_{ij}(p^2)\right]\phi_i(x)\,, \tag{2.119}$$

so that the equation of motion becomes

$$\frac{d^2}{dt^2}\phi(x) = \left[\nabla^2 + m^2 + \mathrm{Re}[\Pi(p^2)] + i\sqrt{p^2}\Gamma(p^2)\right]\phi(x)\,. \tag{2.120}$$

Using again a Fourier ansatz for the field operators, cf. equation (A.39), the equation of motion in momentum space is obtained:

$$k_0^2\phi(x) = \left[\vec{k}^2 + m^2 + \mathrm{Re}[\Pi(k^2)] + i\sqrt{k^2}\Gamma(k^2)\right]\phi(x)\,. \tag{2.121}$$

[25] The wave function of the scattered particle typically does not interfere in a relevant way with the unscattered one anymore.

Approaching e.g. $k^2 = m_i^2 + im_i\Gamma_i$ with m_i and Γ_i being real, the eigenvalue equation becomes non-trivial:

$$\left[m_i^2 + im_i\Gamma_i\right]\phi(x) = \left[m^2 + \mathrm{Re}[\Pi(m_i^2 + im_i\Gamma_i)] + i\sqrt{m_i^2 + im_i\Gamma_i}\,\Gamma(m_i^2 + im_i\Gamma_i)\right]\phi(x)\,. \tag{2.122}$$

In case of $m_i^2 \gg im_i\Gamma_i$, this approximately simplifies to

$$im_i[\Gamma_i - \Gamma(m_i^2)] = \left[m^2 + \mathrm{Re}[\Pi(m_i^2)] - m_i^2\right]\,. \tag{2.123}$$

Furthermore, in the limit $\sqrt{\vec{k}^2 + m_i^2} \gg \sqrt{m_i\Gamma_i}$, the intuitive result

$$k_0 = \sqrt{\vec{k}^2 + m_i^2 + im_i\Gamma_i} \approx \sqrt{\vec{k}^2 + m_i^2} + i\frac{m_i}{2\sqrt{\vec{k}^2 + m_i^2}}\Gamma_i \tag{2.124}$$

is obtained, with $m_i\Gamma_i/\sqrt{\vec{k}^2 + m_i^2}$ being the Lorentz boosted decay width.

Note that the propagator resulting from the effective equation of motion modifies to

$$\frac{i}{k^2 - m_i^2 + im_i\Gamma_i}\,, \tag{2.125}$$

which is well-known as the *Breit-Wigner propagator*.

2.10.2 CP Violation

This paragraph focuses on the violation of the CP symmetry – in the following called CP *violation* – which is a key element for the generation of the observed B asymmetry, cf. chapter 4. At tree-level, neglecting the decay width in the generalized equation of motion discussed previously, the amplitude of processes are in general not CP invariant because couplings are replaced by their complex conjugate. However, each vertex and each propagator appears with a factor of i in the matrix element and, at tree level, the number of both vertices and propagators for interfering diagrams differ by the same number. Consequently, the CP-transformed matrix element is determined by the complex conjugate of the considered matrix element, implying that the transition probability is CP invariant.

Next, including the decay width of particles, a CP-invariant complex phase arises from the Breit-Wigner propagator. As a consequence, interfering diagrams can deviate by a complex phase which changes under a CP transformation[26], as well as a complex phase which is CP invariant:

$$CP\text{-odd phase:} \qquad e^{i\varphi^{CP}_{\mathrm{odd}}} \overset{CP}{\to} e^{-i\varphi^{CP}_{\mathrm{odd}}}\,, \tag{2.126a}$$

$$CP\text{-even phase:} \qquad e^{i\varphi^{CP}_{\mathrm{even}}} \overset{CP}{\to} e^{i\varphi^{CP}_{\mathrm{even}}}\,. \tag{2.126b}$$

Besides including the decay width, a CP-even phase also arises from vertex corrections when the decay into loop particles is kinematically allowed. In this case, the complex phase arises from the

[26] In the SM, a CP-odd phase naturally arises from Yukawa interactions which, in contrast to the gauge interactions, arise with complex coupling constants.

interference of the decay into the loop particles with a succeeding scattering process producing the final states. Thus, similar to producing the mediator on-shell, the considered process decomposes into two distinct scattering processes which each arises with a complex phase of i ($\mathcal{M} = i\mathcal{M}_1\mathcal{M}_2$). Nonetheless, in this thesis, the focus is mainly on the CP violation induced by particle decays which alter the eigensystem. As a consequence, the resulting CP violation can in principle be large compared to the CP violation induced by vertex corrections which are always suppressed by the additional scattering amplitude.

The CP violation induced by particle decays can be deduced from the eigenvalues of the effective equation of motion. To find a general analytic expression for the eigensystem, time-independent perturbation theory can be used when the time evolution can be divided accordingly. In many cases, it is e.g. reasonable to assume that the interaction rate is small compared to the differences of the energy eigenstates, meaning that $\hat{\Gamma}$ can be treated as a perturbation. Consequently, cf. appendix (A.3.3), the eigensystem is approximately given by

$$\lambda_i = E_i - \frac{i}{2}\langle\psi_i|\hat{\Gamma}|\psi_i\rangle - \frac{1}{4}\sum_{j\neq i}\frac{|\langle\psi_j|\hat{\Gamma}|\psi_i\rangle|^2}{E_i - E_j}\,, \tag{2.127a}$$

$$|\psi_i'\rangle = |\psi_i\rangle - \frac{i}{2}\sum_{j\neq i}\frac{\langle\psi_j|\hat{\Gamma}|\psi_i\rangle}{E_i - E_j}|\psi_j\rangle\,. \tag{2.127b}$$

At first sight, this does not seem to violate the CP symmetry because the eigenvalues of the equation of motion for particles and antiparticles are equivalent[27]. Note that the equivalence of the interaction rate of particles and antiparticles is a direct consequence of the CPT invariance and unitarity of the S-matrix, implying that, summing over all processes, the production and annihilation probabilities of a state are equivalent. However, considering only the damping induced by a particular interaction, CP violation becomes visible [53]:

$$\Gamma_{I,i}' = \langle\psi_i|\hat{\Gamma}_I|\psi_i\rangle + \frac{1}{2}\sum_{j\neq i}\mathrm{Im}\left[\frac{\langle\psi_i|\hat{\Gamma}_I|\psi_j\rangle\langle\psi_j|\hat{\Gamma}|\psi_i\rangle}{E_i - E_j}\right]. \tag{2.128}$$

Thus, the total interaction rate is CP invariant but the interaction rates for the individual processes are not when the involved couplings are complex and multiple processes, inducing non-vanishing $\langle\psi_i|\hat{\Gamma}_I|\psi_j\rangle$ with different complex phases, contribute. Furthermore, substantial CP asymmetry is only achieved when the mixing is not too small, implying that $\langle\psi_j|\hat{\Gamma}|\psi_i\rangle$ needs to be sizable compared to $E_i - E_j$.

Another case of interest, which allows using perturbation theory, is a time evolution operator which is dominantly diagonal in a certain basis:

$$\hat{\mathbb{H}} = \hat{\mathbb{H}}_0 + \hat{\mathbb{H}}_I\,, \qquad \text{with} \qquad |(\hat{\mathbb{H}}_0)_{ii} - (\hat{\mathbb{H}}_0)_{jj}| \gg |(\hat{\mathbb{H}}_I)_{ij}| \quad \text{for} \quad i \neq j\,, \tag{2.129}$$

$\hat{\mathbb{H}}_0$ being diagonal ($(\hat{\mathbb{H}}_0)_{ij} = (E_i - i\Gamma_i/2)\delta ij$), and $\hat{\mathbb{H}}_I$ being off-diagonal. In this case, the eigensystem

[27] $\langle\psi_i|\hat{\Gamma}|\psi_i\rangle$ is real because $\hat{\Gamma}$ is Hermitian

is approximately given by

$$\lambda_i = E_i - \frac{i}{2}\Gamma_i + 2\sum_{j\neq i} \frac{\langle\psi_i|\hat{\mathbb{H}}_I|\psi_j\rangle \langle\psi_j|\hat{\mathbb{H}}_I|\psi_i\rangle}{2(E_i - E_j) - i(\Gamma_i - \Gamma_j)}\,, \tag{2.130a}$$

$$|\psi_i'\rangle = |\psi_i\rangle + 2\sum_{j\neq i} \frac{\langle\psi_j|\hat{\mathbb{H}}_I|\psi_i\rangle}{2(E_i - E_j) - i(\Gamma_i - \Gamma_j)} |\psi_j\rangle\ . \tag{2.130b}$$

Consequently, the interaction rate, being the imaginary part of the eigenvalue, is[28]

$$\begin{aligned}\Gamma_i' &= \Gamma_i - 4\sum_{j\neq i} \frac{(\Gamma_i - \Gamma_j)\mathrm{Re}[\langle\psi_i|\hat{\mathbb{H}}_I|\psi_j\rangle \langle\psi_j|\hat{\mathbb{H}}_I|\psi_i\rangle] + 2(E_i - E_j)\mathrm{Im}[\langle\psi_i|\hat{\mathbb{H}}_I|\psi_j\rangle \langle\psi_j|\hat{\mathbb{H}}_I|\psi_i\rangle]}{4(E_i - E_j)^2 + (\Gamma_i - \Gamma_j)^2} \\ &= \Gamma_i - 4\sum_{j\neq i} \frac{(\Gamma_i - \Gamma_j)(|\hat{\mathrm{H}}_{ij}|^2 + |\Gamma_{ij}|^2/4) + (E_i - E_j)\mathrm{Re}[\Gamma_{ij}\hat{\mathrm{H}}_{ij}^*]}{4(E_i - E_j)^2 + (\Gamma_i - \Gamma_j)^2}\,,\end{aligned} \tag{2.131}$$

with $\hat{\mathrm{H}}_{ij} = \langle\psi_i|\hat{\mathrm{H}}_I|\psi_j\rangle$ and $\Gamma_{ij} = \langle\psi_i|\hat{\Gamma}_I|\psi_j\rangle$[29]. Thus, the total interaction rate is again CP invariant. However, considering a particular interaction process, in case of $\mathrm{Im}[\Gamma_{I,ij}\hat{\Gamma}_{ij}^*] \neq 0$, a CP-violating interaction rate is obtained:

$$\begin{aligned}\Gamma_{I,i}' &= \Gamma_{I,i} - 4\sum_{j\neq i} \frac{(\Gamma_{I,i} - \Gamma_{I,j})(|\hat{\mathrm{H}}_{ij}|^2 + |\Gamma_{ij}|^2/4) - (E_i - E_j)\mathrm{Re}[\langle\psi_i|\hat{\Gamma}_I|\psi_j\rangle \langle\psi_j|\hat{\mathbb{H}}_I|\psi_i\rangle]}{4(E_i - E_j)^2 + (\Gamma_i - \Gamma_j)^2} \\ &= \Gamma_{I,i} - 4\sum_{j\neq i} \frac{(\Gamma_{I,i} - \Gamma_{I,j})(|\hat{\mathrm{H}}_{ij}|^2 + |\Gamma_{ij}|^2/4) - (E_i - E_j)(\mathrm{Re}[\Gamma_{I,ij}\hat{\mathrm{H}}_{ij}^*] - \mathrm{Im}[\Gamma_{I,ij}\hat{\Gamma}_{ij}^*]/2)}{4(E_i - E_j)^2 + (\Gamma_i - \Gamma_j)^2}\,.\end{aligned} \tag{2.132}$$

Note that for $\Gamma_i - \Gamma_j \ll E_i - E_j$, the CP-violating term is equivalent to the one case considered before, cf. equation (2.128).

It can be concluded that substantial CP asymmetry can only be achieved when $|\hat{\Gamma}_{ij}|$ is not too small compared to $[4(E_i - E_j)^2 + (\Gamma_i - \Gamma_j)^2]/(E_i - E_j)$, requiring an interaction rate which is sizable compared to the energy difference and an interaction rate which is not dominantly diagonal. Consequently, either sizable couplings or small mass squared differences are needed.
Furthermore, it should be mentioned that in the used approximation where the eigensystem is mainly determined by $\hat{\mathbb{H}}_0$, FOs become irrelevant because either the off-diagonal interaction rate is small compared to the oscillation length, or the interaction rate is mainly diagonal in the eigenbasis of the free equation of motion, or the interaction rate dominates and the eigenbasis is determined by the interaction eigenbasis. Only in the non-perturbative case where the interaction rate induces large mixing between the eigenstates of the free equation of motion with energy differences of the order of the interaction rate, FO becomes relevant.

[28] A comparable result can be found e.g. in references [9, 24] for the production rate of sterile neutrinos.
[29] Note that the term proportional to $\Gamma_i - \Gamma_j$ is induced by the mixing of the undisturbed eigenstates while the term proportional to $E_i - E_j$ considers the damping induced by the off-diagonal elements of the interaction rate.

3 Description of Many-Particle Systems

In this chapter, the focus is shifted from considering the time evolution of a few single particles to the description of many-particle systems. In principle, also a many-particle system can be described by an exact state vector. However, considering many particles, an exact description is inconvenient. To find an effective description, the basic concepts of thermodynamics and thermal equilibrium are introduced in section 3.1. Afterwards, in section 3.2, the focus is turned to QFT again and the time evolution of the many-particle state vector induced by inelastic scattering processes is examined leading to the well-known Boltzmann equations. These equations are e.g. essential for the investigation of particle densities or particle-antiparticle asymmetries of the early universe. Because the focus in this thesis is on the latter, the Boltzmann equations for chemical potentials are derived in order to handle the different properties of bosons and fermions properly.

Besides "real" scattering processes changing the state of the system also *coherent forward scattering* occurs leaving the state vector unchanged. These processes give rise to an effective potential, implying that effective masses and couplings become dependent on the state of the system. In section 3.3, it is discussed how these corrections can be taken into account, leading to the well-known formalism of thermal quantum field theory (TFT). Subsequently, in section 3.4, details of the approximation of the thermal self-energy corrections are discussed. These thermal masses are e.g. of relevance to determine which decay processes, being of special interest in light of Boltzmann equations, are kinematically allowed at which temperature scale. Furthermore, both TFT and the resulting thermal masses are needed for the calculation of the effective Higgs potential in dependence of the temperature investigated in section 6.3

Afterwards, in section 3.5, the influence of thermal masses on FO is examined. Finally, in section 3.6, the validity of the thermal equilibrium assumption is discussed, allowing to simplify Boltzmann equations significantly. Moreover, the thermal rates for the dominant Yukawa interactions (top, bottom, and tau) and the scales at which they reach thermal equilibrium are calculated.

3.1 Introduction to the Basic Concepts of Thermodynamics and Thermal Equilibrium

In this section, the most relevant quantities describing a system in thermodynamic equilibrium are shortly motivated. Furthermore, the free energy density, which can be used to deduce equilibrium states, is introduced. For a more detailed derivation of the given equations and further explanations, cf. appendix B.1.

According to QFT, a system can be fully described as a set of particles i where each particle can be fully described by their momentum $\vec{p}_i$ and mass m_i. Knowing the corresponding state vector for

a time t_0 exactly, the time evolution of the full state vector can be calculated. But with increasing particle number and density – causing a larger number of scattering processes –, the necessary computation power increases rapidly, meaning that the description of systems with many particles by an exact state vector is unpractical. To find an effective description, one can use that, independent of the exact form of the initial state vector, many body systems tend to take on a distribution of states which can be described by only a few quantities.

Considering an isolated system first, due to elastic scattering processes, the probability of measuring the system in a certain state is – after many scattering processes (*equilibration*) – equally distributed over the entire allowed phase space. During equilibration, the allowed phase space is restricted by conserved quantities such as energy and momentum. To quantify the distance of a state from its equilibrium state, it is convenient to define the *entropy*

$$S = -\int \rho \ln(\rho)\,, \tag{3.1}$$

with the phase space density ρ. Using this definition, the entropy is minimal when a system is in a defined state. Moreover, when the entropy is maximal, a system is in its equilibrium state. Consequently, the phase space density in thermal equilibrium can be obtained by minimizing the entropy. Thus, demanding an expectation value for the energy as an additional condition,

$$\rho = \frac{1}{Z} e^{-\beta E} \tag{3.2}$$

is obtained, where $\beta = 1/T$ is the inverse of the temperature and the *canonical partition function* Z is determined by the normalization condition:

$$\int \rho = 1 \qquad \Rightarrow \qquad Z = \int e^{-\beta E}\,. \tag{3.3}$$

Furthermore, considering a system with variable particle content, additionally, an expectation value for the number of particles can be introduced, resulting in an equilibrium phase space density of the form

$$\rho = \frac{1}{\mathcal{Z}} e^{-\beta(E+\mu N)}\,, \tag{3.4}$$

where the *grand canonical partition function* $\mathcal{Z}$ is determined by

$$\mathcal{Z} = \int e^{-\beta(E+\mu N)}\,, \tag{3.5}$$

with the *chemical potential* μ.
In the context of this thesis, it is of special interest to assume an expectation value for particle number differences such as particle-antiparticle asymmetries instead:

$$\rho = \frac{1}{\mathcal{Z}} e^{-\beta(E+\mu[N_1-N_2])}\,, \tag{3.6}$$

with appropriate changes in the definition of $\mathcal{Z}$. As a consequence, the distribution functions for particles and antiparticles in the presence of a particle-antiparticle asymmetry differ by a sign in front of the chemical potentials while the absolute values are equivalent ($\mu_i = -\mu_{\bar{i}}$).

So far, particle configurations which are in agreement with external conditions have been considered. The resulting probability to measure a particle in a certain state is determined by the Maxwell-Boltzmann statistics (B.20). However, this does not take into account the properties of bosons and fermions properly. Considering the commutator relations for bosons and the anti-commutator relations for fermions, the distribution functions of bosons and fermions are determined by the Bose-Einstein statistics (B.18) and the Fermi-Dirac statistics (B.19), respectively.

Further quantities of relevance in this thesis are the *free energy* F and the *grand potential* Ω being defined as

$$\Omega = F - \mu N = -\frac{1}{\beta}\ln(\mathcal{Z}) \qquad \text{and} \tag{3.7}$$

$$F = \langle E\rangle - TS = \frac{1}{\beta}\left[\mu\frac{\partial}{\partial\mu}\ln(\mathcal{Z}) - \ln(\mathcal{Z})\right] = \Omega - \mu\frac{\partial}{\partial\mu}\Omega\,. \tag{3.8}$$

Considering a system with constant temperature (and constant chemical potential), the corresponding equilibrium state minimizes the free energy (grand potential).
Considering the partition functions for bosons and fermions, the grand potential density is given by[1]

$$\begin{aligned}\frac{\Omega}{V} &= -\frac{1}{\beta}\left[\sum_{b_i}\int\frac{d^3\vec{k}}{(2\pi)^3}\ln\left(\mathcal{Z}_{b_i}\right) + \sum_{f_i}\int\frac{d^3\vec{k}}{(2\pi)^3}\ln\left(\mathcal{Z}_{f_i}\right)\right] \\ &= \frac{1}{\beta}\left[\sum_{b_i}\int\frac{d^3\vec{k}}{(2\pi)^3}\ln\left(1-e^{-\beta(E_k+\mu_{b_i})}\right) - \sum_{f_i}\int\frac{d^3\vec{k}}{(2\pi)^3}\ln\left(1+e^{-\beta(E_k+\mu_{f_i})}\right)\right].\end{aligned} \tag{3.9}$$

According to equation (3.8), the corresponding free energy density in the limit of small asymmetries ($\mu_i \ll T$) becomes

$$\frac{1}{T^4}\frac{F}{V} = \sum_{b_i}\left[-\frac{\pi^2}{90} + \frac{1}{12}\frac{\mu_{b_i}^2}{T^2}\right] + \sum_{f_i}\left[-\frac{7\pi^2}{720} + \frac{1}{24}\frac{\mu_{f_i}^2}{T^2}\right] + \mathcal{O}\left(\frac{\mu_i}{T}\right)^3. \tag{3.10}$$

This free energy density is relevant when processes changing the chemical potentials are considered because their equilibrium condition can be obtained by minimizing the free energy[2]. Considering e.g. a process converting a set of bosons b_i and fermions f_i into a different set of bosons b_f and fermions f_f, according to equation (B.22), the chemical potential of fermions in the limit $\mu_i \ll T$ receive an additional factor two, compared to bosons. Thus, the values for the chemical potentials of the involved particles which can be reached by the considered process are given by

$$\mu_{b_i} = \mu_{b_i}^i + \Delta\,, \qquad \mu_{f_i} = \mu_{f_i}^i + 2\Delta\,, \qquad \mu_{b_f} = \mu_{b_f}^i - \Delta\,, \qquad \mu_{f_f} = \mu_{f_f}^i - 2\Delta\,. \tag{3.11}$$

[1] Note that in the literature, cf. e.g. reference [], the free energy density is sometimes defined similar to the grand potential, which is only valid as long as the chemical potentials vanish. However, considering particle-antiparticle asymmetries, terms which are odd in the chemical potentials cancel out so that assuming small asymmetries $\mu_i \ll T$, the grand potential and the free energy only differ by a minus sign in front of the dominant μ_i^2 dependence. As a consequence, setting the derivative of the free energy to zero, the same result is obtained but now with a maximum instead of a minimum.

[2] Note that only processes with interaction rates much larger than the changing rate of the temperature equilibrate to a state minimizing the free energy because otherwise, the assumption of a constant temperature is not valid.

Minimizing the resulting free energy density with respect to Δ, the well-known equilibrium condition

$$\sum \mu_{b_i} + \sum \mu_{f_i} = \sum \mu_{b_f} + \sum \mu_{f_f} \,, \tag{3.12}$$

is obtained.

3.2 Derivation of the Boltzmann Equations

In this section, the Boltzmann equations – describing the time evolution of the number density of each particle species in a thermal system – are derived using different approximations. These Boltzmann equations are e.g. used for the investigation of the time evolution of particle numbers and particle number asymmetries in the early universe.

At first, to be able to investigate the time evolution of a thermal system, it has to be described as a set of particles. Actually, as long as the time evolution of a system is clearly dominated by the effective free Hamiltonian – describing the time evolution of a state vector which leaves the particle content unchanged – the description of the state vector as a set of eigenstates of the effective free Hamiltonian is a good approximation. This is the case when the coupling strength is not too large so that the perturbation series converges and no bound states are formed. As can be deduced from the SM RGE, cf. equation (A.88), for $\mu \gtrsim 100$ MeV, all SM couplings are perturbative, implying that the basis of elementary particles can be used at high temperatures ($T \gtrsim$ GeV).
However, when the temperature is close to the binding energy, the interaction Hamiltonian becomes relevant and bound states begin to form. Consequently, the plasma has to be described in a mixed basis. When the temperature drops significantly below the binding energy, the particle densities of the corresponding elementary particles are irrelevant and it becomes sufficient to consider the distribution functions of bound states[3].

In general, many-particle systems can be described by the distribution functions of the single constituents (elementary particle and bound states) f_i. The time evolution of these distribution functions is determined by the probability of annihilating a state from the distribution function and the probability of creating a state. As discussed in section 2.2, these probabilities are determined by equation (2.22), implying that the time evolution of the distribution function of a particle species i can be written as:

$$\begin{aligned} 2E_i \frac{df_i}{dt} = &- \int (\Pi d\tilde{k}_{f_i})(\Pi d\tilde{k}_{b_i})(\Pi d\tilde{k}_{f_f})(\Pi d\tilde{k}_{b_f})(2\pi)^4 \delta(k_i + \Sigma k_{f_i} + \Sigma k_{b_i} - \Sigma k_{f_f} - \Sigma k_{b_f}) \\ &\times \Big[|\mathcal{M}_{i f_{i_1} \dots b_{i_1} \dots \to f_{f_1} \dots b_{f_1} \dots}|^2 f_i (\Pi f_{f_i})(\Pi f_{b_i})(\Pi[1 - f_{f_f}])(\Pi[1 + f_{b_f}]) \\ &\quad - |\mathcal{M}_{f_{f_1} \dots b_{f_1} \dots \to i f_{i_1} \dots b_{i_1} \dots}|^2 (\Pi f_{f_f})(\Pi f_{b_f})(1 \pm f_i)(\Pi[1 - f_{f_i}])(\Pi[1 + f_{b_i}]) \Big] := C[f_i] \,. \end{aligned} \tag{3.13}$$

[3]Note that for non-abelian gauge theories, things are more complicated because only uncharged bound states can exist. However, for temperatures above the binding energy, the particle density is larger than for bound states. As a consequence, there is a force ensuring that the plasma is uncharged on the bound state scale but the single particles are not bound together and can be assumed to be approximately free. The reason for that is that the energy of a bound state is determined by the mass and the kinetic energy of the particle content and the kinetic energy is – according to QM – determined by the size of the bound state.

Furthermore, the time evolution of a thermal plasma in the early universe is also affected by the expansion of the universe. Taking this into account, the time evolution of the distribution function is given by [47]:

$$\frac{df_i}{dt} = \mathsf{H}(t)\frac{\vec{k_i}^2}{E_i}\frac{\partial f_i}{\partial E} + \frac{1}{2E_i}C[f_i]\,, \tag{3.14}$$

where $\mathsf{H}(t)$ is the Hubble expansion rate being defined in equation (A.5). Next, assuming thermal equilibrium for elastic scattering processes, only particle densities become relevant. By further normalizing the number density to the *entropy density*, the time evolution simplifies to [47]

$$\frac{dY_i(t)}{dt} =: \frac{d}{dt}\frac{n_i(t)}{s(t)} = \frac{1}{s}\int d\tilde{k}_i\, C_{\text{inelastic}}[f_i]\,. \tag{3.15}$$

Considering particle densities which significantly differ from the equilibrium density at $\mu_i = 0$, $C_{\text{inelastic}}[f_i]$ is often further simplified by neglecting the influence of T violation:

$$|\mathcal{M}_{if_{i_1}\ldots b_{i_1}\cdots\to f_{f_1}\ldots b_{f_1}\ldots}|^2 \approx |\mathcal{M}_{f_{f_1}\ldots b_{f_1}\cdots\to if_{i_1}\ldots b_{i_1}\ldots}|^2\,. \tag{3.16}$$

Furthermore, both the Fermi-Dirac and the Bose-Einstein statistics are approximated by the Maxwell-Boltzmann distribution ($f_i = e^{-\beta(E_i+\mu_i)} =: e^{-\beta\mu_i} f_i^{\text{eq}}$), which – in case of small occupation numbers – is a good approximation. With this, the time evolution becomes

$$\begin{aligned}\frac{dY_i(t)}{dt} &= -\frac{1}{s}\left(e^{-\Sigma\beta\mu_{f_f}-\Sigma\beta\mu_{b_f}} - e^{-\beta\mu_i-\Sigma\beta\mu_{f_i}-\Sigma\beta\mu_{b_i}}\right)\int d\tilde{k}_i(\Pi d\tilde{k}_{f_i})(\Pi d\tilde{k}_{b_i})(\Pi d\tilde{k}_{f_f})(\Pi d\tilde{k}_{b_f})\\ &\quad\times(2\pi)^4\delta(k_i+\Sigma k_{f_i}+\Sigma k_{b_i}-\Sigma k_{f_f}-\Sigma k_{b_f})|\mathcal{M}_{if_{i_1}\ldots b_{i_1}\cdots\to f_{f_1}\ldots b_{f_1}\ldots}|^2 e^{-\beta k_0} &\text{(3.17a)}\\ &=: -\frac{1}{s}\left(e^{-\Sigma\beta\mu_{f_f}-\Sigma\beta\mu_{b_f}} - e^{-\beta\mu_i-\Sigma\beta\mu_{f_i}-\Sigma\beta\mu_{b_i}}\right)\gamma_{if_{i_1}\ldots b_{i_1}\cdots\to f_{f_1}\ldots b_{f_1}}\,, &\text{(3.17b)}\end{aligned}$$

with the spacetime density of scattering $\gamma_{if_{i_1}\ldots b_{i_1}\cdots\to f_{f_1}\ldots b_{f_1}}$ – in the following called *thermal rate*. For a more detailed derivation of the given equations, cf. appendix B.2.

It can be assumed that processes producing and annihilating particle-antiparticle pairs are also in thermal equilibrium. Consequently, only inelastic scattering processes changing particle-antiparticle asymmetries $C'_{\text{inelastic}}[f_i]$ have to be considered in detail:

$$\frac{dY_{\Delta i}(t)}{dt} =: \frac{dY_i(t)}{dt} - \frac{dY_{\bar{i}}(t)}{dt} = \frac{1}{s}\int d\tilde{k}_i\left(C'_{\text{inelastic}}[f_i] - C'_{\text{inelastic}}[f_{\bar{i}}]\right)\,. \tag{3.18}$$

Using the CPT invariance of the matrix element

$$|\mathcal{M}_{\bar{i}\bar{f}_{i_1}\ldots\bar{b}_{i_1}\cdots\to\bar{f}_{f_1}\ldots\bar{b}_{f_1}\ldots}|^2 = |\mathcal{M}_{f_{f_1}\ldots b_{f_1}\ldots i\to f_{i_1}\ldots b_{i_1}\ldots}|^2\,, \tag{3.19}$$

the relations (B.18b) and (B.19c), and $\mu_{\bar{i}} = -\mu_i$, cf. equation (3.6),

$$\begin{aligned}\frac{dY_{\Delta i}(t)}{dt} &= -\frac{1}{s}\int d\tilde{k}_i(\Pi d\tilde{k}_{f_i})(\Pi d\tilde{k}_{b_i})(\Pi d\tilde{k}_{f_f})(\Pi d\tilde{k}_{b_f})(2\pi)^4\delta(k_i+\Sigma k_{f_i}+\Sigma k_{b_i}-\Sigma k_{f_f}-\Sigma k_{b_f})\\ &\quad\times\Big[|\mathcal{M}_{if_{i_1}\ldots b_{i_1}\cdots\to f_{f_1}\ldots b_{f_1}\ldots}|^2\left(e^{\Sigma\beta\mu_{f_f}+\Sigma\beta\mu_{b_f}} + e^{\beta\mu_{\bar{i}}+\Sigma\beta\mu_{\overline{f_i}}+\Sigma\beta\mu_{\overline{b_i}}}\right)\\ &\qquad - |\mathcal{M}_{f_{f_1}\ldots b_{f_1}\cdots\to if_{i_1}\ldots b_{i_1}\ldots}|^2\left(e^{\beta\mu_i+\Sigma\beta\mu_{f_i}+\Sigma\beta\mu_{b_i}} + e^{\Sigma\beta\mu_{\overline{f_f}}+\Sigma\beta\mu_{\overline{b_f}}}\right)\Big]\\ &\quad\times e^{\beta K^0} f_i(\Pi f_{f_i})(\Pi f_{b_i})(\Pi f_{f_f})(\Pi f_{b_f})\end{aligned} \tag{3.20}$$

is obtained. Furthermore, defining

$$\delta_{CP} = \delta_T := \frac{|\mathcal{M}_{if_{i_1}\dots b_{i_1}\dots\to f_{f_1}\dots b_{f_1}\dots}|^2 - |\mathcal{M}_{f_{f_1}\dots b_{f_1}\dots\to if_{i_1}\dots b_{i_1}\dots}|^2}{|\mathcal{M}_{if_{i_1}\dots b_{i_1}\dots\to f_{f_1}\dots b_{f_1}\dots}|^2 + |\mathcal{M}_{f_{f_1}\dots b_{f_1}\dots\to if_{i_1}\dots b_{i_1}\dots}|^2}\,, \tag{3.21}$$

using $\mu_{\bar{i}} = -\mu_i$, cf. equation (3.6), and expanding the collision term up to first order in the chemical potentials ($\mu_i \ll T$) as well as CP violation ($\delta_{CP} \ll 1$), equation (3.20) simplifies to

$$\begin{aligned}\frac{dY_{\Delta i}(t)}{dt} = -\frac{1}{s}\int d\tilde{k}_i(\Pi d\tilde{k}_{f_i})(\Pi d\tilde{k}_{b_i})(\Pi d\tilde{k}_{f_f})(\Pi d\tilde{k}_{b_f})(2\pi)^4\delta(k_i + \Sigma k_{f_i} + \Sigma k_{b_i} - \Sigma k_{f_f} - \Sigma k_{b_f})\\ \times\left[|\mathcal{M}_{if_{i_1}\dots b_{i_1}\dots\to f_{f_1}\dots b_{f_1}\dots}|^2 + |\mathcal{M}_{f_{f_1}\dots b_{f_1}\dots\to if_{i_1}\dots b_{i_1}\dots}|^2\right] f_i^{\mathrm{eq}}(\Pi f_{f_i}^{\mathrm{eq}})(\Pi f_{b_i}^{\mathrm{eq}})(\Pi f_{f_f}^{\mathrm{eq}})(\Pi f_{b_f}^{\mathrm{eq}})\\ \times\left(\Sigma\beta\mu_{f_f} + \Sigma\beta\mu_{b_f} - \beta\mu_i - \Sigma\beta\mu_{f_i} - \Sigma\beta\mu_{b_i} + 2\delta_{CP}\right)e^{\beta K^0}\,,\end{aligned} \tag{3.22}$$

where the distribution functions f_i are evaluated at $\mu_i = 0$. Again, the evaluation of the momentum integrals can be simplified by approximating both the Fermi-Dirac and the Bose-Einstein statistics by the Maxwell-Boltzmann distribution[4]:

$$\begin{aligned}\frac{dY_{\Delta i}(t)}{dt} = -\left(\frac{1}{2}\right)\frac{d}{dt}\frac{\mu_i T^2}{3s} = -\frac{1}{s}\left(\Sigma\beta\mu_{f_f} + \Sigma\beta\mu_{b_f} - \beta\mu_i - \Sigma\beta\mu_{f_i} - \Sigma\beta\mu_{b_i} + 2\delta'_{CP}\right)\\ \times\left(\gamma_{if_{i_1}\dots b_{i_1}\dots\to f_{f_1}\dots b_{f_1}\dots} + \gamma_{f_{f_1}\dots b_{f_1}\dots\to if_{i_1}\dots b_{i_1}\dots}\right),\end{aligned} \tag{3.23}$$

with

$$\delta'_{CP} = \frac{\gamma_{if_{i_1}\dots b_{i_1}\dots\to f_{f_1}\dots b_{f_1}\dots} - \gamma_{f_{f_1}\dots b_{f_1}\dots\to if_{i_1}\dots b_{i_1}\dots}}{\gamma_{if_{i_1}\dots b_{i_1}\dots\to f_{f_1}\dots b_{f_1}\dots} + \gamma_{f_{f_1}\dots b_{f_1}\dots\to if_{i_1}\dots b_{i_1}\dots}}\,. \tag{3.24}$$

Note that equation (3.23) is valid for bosons as well as fermions for which the extra factor $1/2$ in parentheses is obtained.

The equilibrium condition of equation (3.23) is

$$\Sigma\beta\mu_{f_f} + \Sigma\beta\mu_{b_f} - \beta\mu_i - \Sigma\beta\mu_{f_i} - \Sigma\beta\mu_{b_i} + 2\delta'_{CP} = 0\,, \tag{3.25}$$

which, in case of vanishing CP violation, is equivalent to the well-known equilibrium condition derived previously, cf. equation (3.12). On the other hand, a non-vanishing CP violation induces non-vanishing chemical potentials in thermal equilibrium, even when their initial values vanish. However, this statement is based on the consideration of a single process. Considering all processes instead, as a consequence of the unitarity of the S-matrix, the total interaction rate of a state is T invariant, implying that in thermal equilibrium, the individual δ'_{CP} cancel out when summing over all processes[5]. Thus, the equilibrium condition resulting from the Boltzmann equations always coincides with the condition resulting from minimizing the free-energy.

[4] Note that in literature, the Boltzmann approximation is typically used earlier in the derivation so that an equation for the time evolution of particle-antiparticle number asymmetries instead of chemical potentials is obtained, cf. e.g. reference [30]. As a consequence, the fact that the same value of the chemical potential for bosons correspond to twice the amount of particle-antiparticle number asymmetry than for fermions is ignored.

[5] Often, the out-of-equilibrium condition is justified directly or indirectly (e.g. that only a deviation form thermal equilibrium defines a arrow of time) by the CPT invariance, cf. e.g. reference [21] or [6]. However, the unitarity of the S-matrix on its own is responsible for the vanishing asymmetries associated to non-conserved quantities in thermal equilibrium; cf. reference [48] for a detailed investigation.

Since in thermal equilibrium no asymmetry is produced, CP-violation and at least one particle involved in a process leaving its equilibrium density is required to generate a non-vanishing particle-antiparticle asymmetry. To obtain the time evolution of the asymmetry, the contribution from the other processes compensating δ'_{CP} need to be subtracted. Furthermore, when elastic scattering processes are efficient, the deviation from the equilibrium densities of the involved particles can be implemented by a chemical potential being equivalent for particles and antiparticles $\mu'_{\bar{i}} = \mu'_i$. Using this and the Boltzmann approximation ($f_i = e^{-\beta(E_i+\mu'_i)} = e^{-\beta\mu'_i} f_i^{\mathrm{eq}}$), equation (3.20) becomes

$$\begin{aligned}\frac{dY_{\Delta i}(t)}{dt} = -\frac{1}{s}\Big(\gamma_{i f_{i_1}\ldots b_{i_1}\cdots\to f_{f_1}\ldots b_{f_1}\ldots} + \gamma_{f_{f_1}\ldots b_{f_1}\cdots\to i f_{i_1}\ldots b_{i_1}\ldots}\Big)\Big[&-\beta\mu_i - \Sigma\beta\mu_{f_i} - \Sigma\beta\mu_{b_i} \\ &+ \Sigma\beta\mu_{f_f} + \Sigma\beta\mu_{b_f} + \delta'_{CP}\left(e^{-\Sigma\beta\mu'_{f_f}-\Sigma\beta\mu'_{b_f}} + e^{-\beta\mu'_i-\Sigma\beta\mu'_{f_i}-\Sigma\beta\mu'_{b_i}} - 2\right)\Big]\,. \end{aligned} \tag{3.26}$$

Considering this Boltzmann equation, it seems that deviation from thermal equilibrium of any particle involved in a process is sufficient to generate a particle-antiparticle asymmetry. However, the total interaction rate of the particle deviating from thermal equilibrium is CP invariant, cf. section 2.10, implying that for fermion-number conserving interactions, summing over all particle-antiparticle asymmetries induced by the deviation from thermal equilibrium of the considered particle, a vanishing total amount of particle-antiparticle asymmetry is obtained. Thus, only particles being involved in processes as well as their CP transformed processes (e.g. decaying into particles as well as their antiparticles) can produce a non-vanishing total amount of particle-antiparticle asymmetry, cf. reference [47, 48]. Consequently, a non-vanishing fermion-antifermion asymmetry can only be induced by deviation from thermal equilibrium of bosons coupling to fermion number violation currents (e.g. leptoquarks) or by Majorana fermions, cf. chapter 5, whose mass terms violate the fermion number (e.g. right-handed Majorana neutrinos).

Thus, considering e.g. the time evolution of the baryon number (B), CP-violation, a reaction out of thermal equilibrium, and obviously a reaction that violates B is required to produce the observed B asymmetry. Additionally, P violation is needed because otherwise, the asymmetry produced in the left-handed sector would be offset by the asymmetry produced in the right-handed sector. These conditions necessary for receiving a net B asymmetry are well-known as Sakharov conditions [62].

The most dominant contribution to the Boltzmann equations usually comes from particle decays and inverse decays as well as $2 \to 2$ processes. For the decays and inverse decays the thermal rate reduces to

$$\gamma_{i\to f_1\cdots f_n} = \gamma_{f_1\cdots f_n\to i} = \frac{m_i^4}{2\pi^2}\sqrt{a_{\Gamma_{i\to f_1\cdots f_n}}}\,\frac{K_1(z)}{z}\,, \tag{3.27}$$

cf. equation (D.12), with $K_\alpha(z)$ being the modified Bessel functions of the second kind.
For a $2 \to 2$ process, the thermal rate in the common form is derived using equation (2.24):

$$\gamma_{i_1 i_2\to f_1 f_2} = \frac{1}{8\pi}\int \frac{dk}{(2\pi)^4}\hat{\sigma}_{i_1 i_2\to f_1 f_2}(k) e^{-\beta k_0}\,, \tag{3.28}$$

cf. equation (D.13), which, in case of a cross section that only depends on the Mandelstam variable s, simplifies to

$$\gamma_{i_1 i_2\to f_1 f_2} = \frac{m_i^4}{64\pi^4}\int\limits_{u_{\min}}^{\infty} du\sqrt{u}\,\hat{\sigma}_{i_1 i_2\to f_1 f_2}(u)\frac{K_1\left(\sqrt{u}z\right)}{z}\,, \tag{3.29}$$

cf. equation (D.14), with $u_{min} = \max\{(\sqrt{a_{i_1}}+\sqrt{a_{i_2}})^2, (\sqrt{a_{f_1}}+\sqrt{a_{f_2}})^2\}$ and the reduced cross section being defined as

$$\hat{\sigma}(u) = 2u\,\lambda\left[1, \frac{a_{i_1}}{u}, \frac{a_{i_2}}{u}\right]^2 \sigma(u)\,. \tag{3.30}$$

The common abbreviations

$$z = \frac{m_i}{T}\,, \qquad u = \frac{s}{m_i^2}\,, \qquad a_j = \frac{m_j^2}{m_i^2}\,, \qquad \text{and} \qquad a_{\Gamma_j} = \frac{\Gamma_j^2}{m_i^2}\,, \tag{3.31}$$

are used, where m_i is some arbitrary mass scale which is typically chosen to be the largest particle mass involved in the process.
Note that rewriting the thermal rates in terms of z is useful when the expansion of the universe is dominated by radiation and no significant reheating occurs. Under these premises, the scale factor $a(t)$ is proportional to z, which – together with the Friedmann equation (A.5) – leads to the relation

$$\mathsf{H}(t) = \frac{1}{a(t)}\frac{da(t)}{dt} = \frac{1}{a(z)}\frac{da(z)}{dz}\frac{dz}{dt} = \frac{1}{z}\frac{dz}{dt}\,, \tag{3.32}$$

where $\mathsf{H}(t)$ is the Hubble expansion rate. This, together with the relations

$$\mathsf{H}(T) = \sqrt{\frac{8\pi^3}{90}g_{\text{eff}}}\frac{T^2}{m_P}\,, \tag{3.33a}$$

$$s = \frac{2\pi^2}{45}g_{\text{eff}}^S T^3\,, \tag{3.33b}$$

which are valid during the radiation-dominated epoch, allows to rewrite the time evolution completely in terms of z so that equations (3.17b) and (3.23) become

$$z\frac{dY_i(t)}{dz} = -\frac{1}{\mathsf{H}(T)s}\left(e^{\Sigma\beta\mu_{f_f}+\Sigma\beta\mu_{b_f}} - e^{\beta\mu_i+\Sigma\beta\mu_{f_i}+\Sigma\beta\mu_{b_i}}\right)\gamma_{if_{i_1}\ldots b_{i_1}\cdots\to f_{f_1}\ldots b_{f_1}}\,, \tag{3.34}$$

$$\begin{aligned} z\frac{d}{dz}\beta\mu_i = {} & \left(\Sigma\beta\mu_{f_f} + \Sigma\beta\mu_{b_f} - \beta\mu_i - \Sigma\beta\mu_{f_i} - \Sigma\beta\mu_{b_i} + 2\Delta_{CP}\right) \\ & \times \frac{(2)3}{\mathsf{H}(T)T^3}\left(\gamma_{if_{i_1}\ldots b_{i_1}\cdots\to f_{f_1}\ldots b_{f_1}\ldots} + \gamma_{f_{f_1}\ldots b_{f_1}\cdots\to if_{i_1}\ldots b_{i_1}\ldots}\right). \end{aligned} \tag{3.35}$$

$m_P = \sqrt{\hbar c/G} \approx 1.22\times10^{19}$ GeV is the Planck mass and the effective degrees of freedom are defined by

$$g_{\text{eff}} = \sum_{i=\text{bosons}}\left(\frac{T_i}{T}\right)^4 + \frac{7}{8}\sum_{j=\text{fermions}}\left(\frac{T_j}{T}\right)^4\,, \tag{3.36a}$$

$$g_{\text{eff}}^S = \sum_{i=\text{bosons}}\left(\frac{T_i}{T}\right)^3 + \frac{7}{8}\sum_{j=\text{fermions}}\left(\frac{T_j}{T}\right)^3\,, \tag{3.36b}$$

where T is the temperature of the entire system and T_i are the temperatures of the single particle species. Assuming all particles to be in thermal equilibrium, all T_i become equivalent to T so that

$g_{\text{eff}} = g_{\text{eff}}^S = 106.75$ is obtained for the SM. Furthermore, the Hubble expansion rate is simply proportional to T^2:

$$\mathsf{H}(T) = \sqrt{\frac{8\pi^3}{90} g_{\text{eff}}^{SM}} \frac{T^2}{m_P} =: A_{\mathsf{H}} T^2 \,, \tag{3.37}$$

with $A_{\mathsf{H}} \approx 1.405 \times 10^{-18}/\text{GeV}$ for the SM.
Note that in this thesis, the differential equation for $\beta\mu_i$ is considered for relativistic particles ($T \gg m_i$) because – following from previous assumptions – it is conserved by the expansion of the universe.

In light of equations (3.34) and (3.35), the relevant quantity to decide whether a reaction can be assumed to be in thermal equilibrium or not is $\gamma/(\mathsf{H}(T)T^3)$. For the decay process, assuming the masses of all involved particles to be constant or negligibly small,

$$\frac{\gamma_{i\to f_1\cdots f_n}}{\mathsf{H}(T)T^3} = \frac{1}{2\pi^2} \frac{\sqrt{a_{\Gamma_{i\to f_1\cdots f_n}}}}{A_{\mathsf{H}} m_i} K_1(z) z^4 \lesssim \frac{1}{6} \frac{\sqrt{a_{\Gamma_{i\to f_1\cdots f_n}}}}{A_{\mathsf{H}} m_i} \tag{3.38}$$

is obtained, with $\sqrt{a_{\Gamma_{i\to f_1\cdots f_n}}}$ being constant. Moreover, $K_1(z)z^4$ scales like z^3 for $z < 1$, reaches the upper bound at $z \sim 3.4$ and scales like $\sqrt{z}^7 e^{-z}$ for larger z with $z = m_i/T$. In contrast, assuming all masses to be proportional to the temperature, the relevant ratio becomes

$$\frac{\gamma_{i\to f_1\cdots f_n}}{\mathsf{H}(T)T^3} = \frac{1}{2\pi^2} \frac{\sqrt{a_{\Gamma_{i\to f_1\cdots f_n}}}}{A_{\mathsf{H}} T} K_1(z) z^3 \propto \frac{1}{T} \,, \tag{3.39}$$

where $\sqrt{a_{\Gamma_{i\to f_1\cdots f_n}}}$ and $z = m_i/T$ are constant.

For the $2 \to 2$ process, in the high temperature approximation, $\hat{\sigma}$ is basically constant[6] and

$$\frac{\gamma_{i_1 i_2\to f_1 f_2}}{\mathsf{H}(T)T^3} = \frac{1}{16\pi^4} \frac{1}{A_{\mathsf{H}} T} \hat{\sigma}_{i_1 i_2\to f_1 f_2} \propto \frac{1}{T} \tag{3.40}$$

is obtained. Furthermore, considering scattering processes involving fermions, $\hat{\sigma}(u)$ in case of a fermionic mediator scales as $u = s/m_M^2$ when the temperature falls significantly below the mediator mass m_M and the relevant ratio becomes

$$\frac{\gamma_{i_1 i_2\to f_1 f_2}}{\mathsf{H}(T)T^3} = \frac{1}{2\pi^4} \frac{T}{A_{\mathsf{H}} m_M^2} \frac{\hat{\sigma}_{i_1 i_2\to f_1 f_2}(u)}{u} \propto T \,. \tag{3.41}$$

Finally, considering pure bosonic scattering processes, $\hat{\sigma}(u)$ induced by quartic couplings is again constant. Thus, the relevant ratio for the pair annihilation and pair production rate of i assuming $m_i > m_{f_{1,2}}$ is given by

$$\frac{\gamma_{ii\to f_1 f_2}}{\mathsf{H}(T)T^3} = \frac{\gamma_{f_1 f_2\to ii}}{\mathsf{H}(T)T^3} = \frac{\hat{\sigma}_{ii\to f_1 f_2}}{64\pi^4 A_{\mathsf{H}} T} \int_4^\infty du \sqrt{u} \frac{K_1(z\sqrt{u})}{z} = \frac{\hat{\sigma}}{8\pi^4 A_{\mathsf{H}} m_i} \frac{K_2(2z)}{z} \,. \tag{3.42}$$

[6] Including thermal masses, $\hat{\sigma}(u)$ is usually not exactly constant but still independent of T.

3.3 Introduction to Thermal Field Theory

In this section, scattering processes which do not change the state of a system – known as coherent forward scattering processes – are investigated. Similar processes (self-energy corrections) were already encountered in vacuum QFT where renormalization is used to absorb these corrections into the free Hamiltonian (on-shell renormalization), cf. appendix A.8, meaning that the time evolution of a free non-decaying particle is completely determined by the free equation of motion. However, considering a set of particles, coherent forward scattering processes with the other particles give rise to an additional non-vanishing contribution to the effective free equation of motion. Consequently, it is reasonable to absorb this additional contribution into the free Hamiltonian by including an effective potential, causing that the interaction Hamiltonian still only induces state changing interactions[7]

thermal quantum field theory (TFT) was developed to formalize the contribution of coherent forward scattering processes, cf. e.g. reference [51], for an detailed introduction into TFT. In the previous chapter, the action of a pair of field operators on a vacuum state as an key element of the perturbation series was examined, cf. section 2.3. In analogy, considering many body systems, the action of a pair of field operators on a general state vector $|F\rangle$ becomes an essential part of the perturbation series. Consequently, for scalar bosons, the *thermal propagator* in the position space is defined as

$$\langle F|\, T\phi(x+y)^\dagger \phi(y)\,|F\rangle = \int d\tilde{k}\left[\big(\Theta(x_0)+f_b(E_k)\big)e^{-ikx} + \big(\Theta(-x_0)+f_{b^*}(E_k)\big)e^{ikx}\right]. \tag{3.43}$$

Using

$$f(E_p) = \int_{-\infty}^{\infty} dp_0\, f(p_0)\delta\left(p_0 - E_p\right) \tag{3.44}$$

and substituting $p^\mu \to -p^\mu$ for the term proportional to e^{ikx}, the thermal propagator can be written as

$$\begin{aligned}\langle F|\, T\phi(x+y)^\dagger \phi(y)\,|F\rangle = &\int d\tilde{k}\int dk_0\Big(f_b(k_0)\delta\left(k_0 - E_k\right) + f_{b^*}(-k_0)\delta\left(k_0 + E_k\right)\Big)e^{-ikx} \\ &+ \int d\tilde{k}\left[\Theta(x_0)e^{-ikx} + \Theta(-x_0)e^{ikx}\right].\end{aligned} \tag{3.45}$$

Like for the vacuum case, the part being independent of the distribution function can be rewritten by applying the residue theorem, while the density dependent part can be summarized using the relation

$$\delta(k^2 - m^2) = \frac{1}{2E_k}\Big(\delta\left(k_0 - E_k\right) + \delta\left(k_0 + E_k\right)\Big). \tag{3.46}$$

Thus, the thermal propagator for a scalar boson in the *real-time formalism* is given by

$$D_b^T(x) = \int \frac{d^4k}{(2\pi)^4}\left(\frac{i}{k^2 - m_b^2} + 2\pi\left(\Theta(k_0)f_b(k_0) + \Theta(-k_0)f_{b^*}(-k_0)\right)\delta(k^2 - m_b^2)\right)e^{-ikx}. \tag{3.47}$$

[7] Note that in contrast to vacuum QFT, the properties of the eigenstates of the effective free equation of motion of particles in a thermal environment are not known from experiment where approximately free particles are observed. Consequently, the thermal quantities (e.g. thermal masses) need to be calculated using perturbation theory.

For deriving the propagator in the *imaginary time formalism*, typically, the time component is continued to imaginary time arguments $0 \leq (x_0, y_0) \leq i\beta$ and the time ordered operator is assumed to order imaginary time [20]. However, this way of deriving the thermal propagator is only reasonable when the real part of x_0 vanishes. More generally, the propagator in the imaginary time formalism can also be derived by rewriting equation (3.45) as

$$\int \frac{d^4k}{(2\pi)^4} \frac{2\pi}{2E_k} \left[\left(\frac{1}{2} + f_b(E_k) \right) \delta(k_0 - E_k) + \left(\frac{1}{2} + f_{b^*}(E_k) \right) \delta(k_0 + E_k) \right] e^{-ikx} \,. \tag{3.48}$$

Assuming the particle to be in thermal equilibrium with vanishing chemical potential ($n_b(E_p) = n_{b^*}(E_p)$) and using

$$\frac{1}{2E_p}(1 + 2f_b(E_p)) = \frac{1}{\beta} \sum_{n=-\infty}^{\infty} \frac{1}{(2\pi n/\beta)^2 + E_p^2} \,, \tag{3.49}$$

the propagator in the imaginary time formalism is obtained[8] [55]:

$$D_b^T(x) = \int \frac{d^4k}{(2\pi)^4} \frac{\pi}{\beta} \sum_{n=-\infty}^{\infty} \frac{1}{(2\pi n/\beta)^2 + E_p^2} \big[\delta(k_0 - E_p) + \delta(k_0 + E_p) \big] e^{-ikx} \,. \tag{3.50}$$

In case of $x_0 = 0$, the k_0 integral results in a factor of two so that the well-known form is deduced:

$$D_b^T(0, \vec{x}) = \int \frac{d^3k}{(2\pi)^3} \frac{1}{\beta} \sum_{n=-\infty}^{\infty} \frac{1}{(2\pi n/\beta)^2 + E_p^2} e^{i\vec{k}\vec{x}} \,. \tag{3.51}$$

Similar to the vacuum propagator, the thermal propagator for vector bosons is simply given by the scalar boson propagator multiplied with the polarization sum over the physical polarizations. Furthermore, as discussed in section 2.3, the vacuum part of the propagator can be expressed in the common Lorentz invariant form when local interaction terms are included. However, the thermal part remains unaffected by local interaction terms.

Equivalently, for the thermal fermionic propagator

$$\begin{aligned} &\langle F | \, T\Psi(x+y)^\dagger \Psi(y) \, | F \rangle \\ &\quad = \int d\tilde{k} \left[\big(\Theta(x_0) - f_f(E_k) \big) (\not{k} + m) e^{-ikx} + \big(\Theta(-x_0) - f_{\bar{f}}(E_k) \big) (-\not{k} + m) e^{ikx} \right] , \end{aligned} \tag{3.52}$$

the real-time formalism result is

$$S_f^T(x) = \int \frac{d^4k}{(2\pi)^4} (\not{k} + m) \left[\frac{i}{k^2 - m_f^2} - 2\pi \left(\Theta(k_0) f_f(k_0) + \Theta(-k_0) f_{\bar{f}}(-k_0) \right) \delta(k^2 - m_f^2) \right] e^{-ikx} \,. \tag{3.53}$$

Using

$$\frac{1}{2E_p}(1 - 2f_f(E_p)) = \frac{1}{\beta} \sum_{n=-\infty}^{\infty} \frac{1}{(\pi(2n+1)/\beta)^2 + E_p^2} \,, \tag{3.54}$$

[8] Note that in the usual form of the propagator in the imaginary time formalism, the energy integral and the Dirac delta functions are absent with $k_0 = 2\pi n/\beta$. This does not coincide with the given result, but in case of considering loops, without external momentum flow – as for loop corrections to the Higgs potential – the result is equivalent.

the result in the imaginary time formalism is obtained:

$$S_f^T(x) = \int \frac{d^4k}{(2\pi)^4} \frac{\pi}{\beta} \sum_{n=-\infty}^{\infty} \frac{\not{k} + m}{(\pi(2n+1)/\beta)^2 + E_k^2} \big[\delta(k_0 - E_k) + \delta(k_0 + E_k)\big] e^{-ikx} \,. \tag{3.55}$$

Again, in case of $x_0 = 0$, the k_0 integral can be evaluated:

$$S_f^T(0, \vec{x}) = \int \frac{d^3k}{(2\pi)^3} \frac{1}{\beta} \sum_{n=-\infty}^{\infty} \frac{\not{k} + m}{(\pi(2n+1)/\beta)^2 + E_k^2} e^{i\vec{k}\vec{x}} \,, \tag{3.56}$$

with $k_0 = \pi(2n+1)/\beta$ and the relation

$$\sum_{n=-a}^{a-1} \frac{\pi(2n+1)/\beta}{(\pi(2n+1)/\beta)^2 + E_p^2} = 0 \qquad\qquad a \in \mathbb{N}^+ \,. \tag{3.57}$$

Using this formalism allows to calculate the matrix element of a process taking place inside a medium, cf. equation (2.22), by replacing the vacuum propagators in the vacuum matrix element by thermal propagators[9]. Note that during this replacement, the diagram should not be split into two isolated diagrams by the thermal part of the propagator as they are already taken into account by the Boltzmann equations. This means that each diagram has to be interconnected via vacuum propagators, implying that only one thermal contribution can appear for each loop momentum integral. However, considering self-energy corrections, diagrams being split by the thermal part of the propagators contribute to the imaginary part of the self-energy correction, cf. reference [71]. Consequently, similar to the imaginary part of vacuum loop corrections, cf. section 2.10, this considers the damping of mediator states induced by the particle decay and scattering processes with other particles.

3.4 Approximation of Thermal Masses

As mentioned in the previous section, thermal self-energy corrections give rise to an effective potential which alters the properties of particles inside a medium. Well-known examples for this effect are the altered speed of light and the altered neutrino masses in a medium resulting e.g. in dispersion of light and the Mikheyev–Smirnov–Wolfenstein (MSW) effect [73, 58] explaining the observed neutrino flavor flux from the sun. However, the implications of thermal masses on FO are investigated in detail in the next section while, in this section, the focus is set on the elaboration of the effective potential.

Using TFT, the thermal masses are determined by self-energy corrections ($\Pi(p^2)$) replacing all vacuum propagators by thermal propagators. At that, as discussed in the previous section, only

[9] Note that in general, considering multiple field operators of the same species, this replacement is non-trivial because the creation and annihilation operators alter the particle content, implying that the next creation or annihilation operator acts on a field with modified particle content. However, usually, this effect only leads to very small deviations so that it is reasonable to only use the derived thermal propagator.

the real part of the self-energy correction contribute to the thermal mass while the imaginary part considers the interaction rate. However, calculating the thermal self-energy correction $\Pi_T(p^2)$, usually one has to start from only knowing the mass eigenstates in the vacuum. This implies that the loop integrals have to be renormalized as in the vacuum case. Consequently, the eigenstates of the effective Hamiltonian differ from the ones used for the calculation leading to a couple of conceptional difficulties[10].

The main problem of not knowing the eigensystem of the effective equation of motion in advance is that the distribution functions assuming thermal equilibrium are unknown. As a consequence, the result is self dependent because the thermal self-energy corrections depend on the distribution functions which in turn depend on the effective thermal masses. However, in practice, considering some self dependent thermal self-energy correction, recalculating the thermal mass iteratively starting from the vacuum masses, the result typically converges rapidly. Thus, the perturbation series still converges and can be considered order by order[11]. However, at the same loop order, diagrams including corrections to the thermal masses of the propagating particles contribute significantly more than diagrams without these corrections. This means that using a better approximation for the distribution functions is for not very large coupling constants more relevant than an additional thermal loop, cf. appendix B.3.

For calculating $\Pi_T(p^2)$, it is useful to make some approximations. First of all, including thermal propagators breaks the Lorentz invariance because the distribution functions are not Lorentz invariant. Thus, $\Pi_T(p^2)$ is not only a function of p^μ but also of the four-velocity u^μ describing the motion relative to the rest frame of the plasma. However, in many cases, the dependence on u^μ in the rest frame of the plasma only gives rise to a small correction so that it is typically ignored and the distribution functions in the rest frame are used ($\Pi_T(p^\mu, u^\mu) \to \Pi_T(p^2)$), cf. reference [70]. Another approximation which can be made without changing the result significantly is to use $\Pi_T(p^2)$ to approximate the effective on-shell mass but to ignore the p^2 dependence for the further calculation[12].

A very simple approximation for the thermal mass, which is often used, is to consider only first order corrections ($\Pi_T^1(p^2)$) in the high temperature limit ($T \gg m$), meaning that $\Pi_T^1(p^2) \propto T^2$ is obtained. As can be seen from the results given in appendix B.3, this approximation ($m^2 \approx m_0^2 + \alpha T^2$) is reasonable if α is not too large.

[10] In the vacuum case it is typically insisted on renormalizing such that on-shell particles are eigenstates of H_0. Practically, this is done because the on-shell mass can be measured directly. (For quarks and gluons this is debatable but only because they do not exist as free particles. However, for their bound states (hadrons) the on-shell masses can be measured.) Moreover, the propagator contributes most if p^2 is close to the pole mass which is given by the mass of the mass eigenstates of H_0. Thus, on average, the perturbation series converges most rapidly if on-shell renormalization is used. In thermal field theory renormalizing on-shell becomes even more important because the forward scattering contribution comes always from on-shell particles whose distribution functions in thermal equilibrium depend on the on-shell masses.

[11] Note that self-energy corrections to a thermal propagator inside a diagram do not divide the thermal propagator into two parts but only change the masses the thermal propagators depend on.

[12] For the vacuum case where the effective on-shell mass is known, this would be pointless but at high temperatures, where the thermal loop contribution dominates and the on-shell mass is not known from measurement, this approximation is useful because the thermal contribution only comes form on-shell particles.

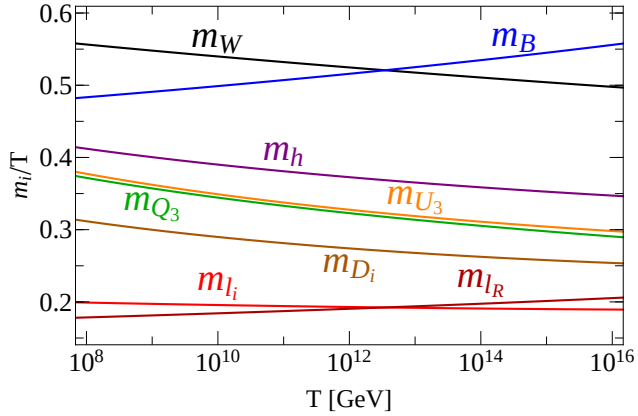

Figure 3.1: Leading order thermal masses of the SM particles being relevant for this thesis, cf. equation (B.40), normalized to the temperature in the high temperature region. The shown temperature dependence results form considering the one-loop running of the SM coupling constants.

Within the SM, the thermal masses induced by the gauge interactions, the Higgs self coupling, and the top Yukawa interaction before EWSB in this high temperature limit are given by equation (B.40). Taking into account the one-loop running of the SM coupling constants, cf. figure 2.1, and setting the Higgs self coupling $\lambda = 0$ for large μ for simplicity, the resulting thermal masses for the relevant SM particles in the region 10^8 GeV $\leq T \leq 10^{16}$ GeV are shown in figure 3.1

3.5 Matter Effects on Flavor Oscillation

Including thermal corrections, the mixing angles between interaction and mass eigenstates as well as the mass squared differences between mass eigenstates can change. As a consequence, the oscillation behavior, investigated in section 2.9, changes when the effective potential is non-diagonal because otherwise – if all relevant interaction eigenstates interact with the medium with the same strength – the matter effects just give rise to an overall phase factor. Such an altered oscillation behavior occurs e.g. considering neutrinos traveling through matter containing a surplus of electrons compared to muons and taus as it is the case for the earth or the sun.

In general, these matter effects and, for this reason, the effective potential are spacetime dependent, implying that it is not sufficient to simply decompose the interaction eigenstates into energy eigenstates with a trivial time evolution. Actually, the time dependence of the eigensystem induces transitions between the different energy eigenstates where the transition probability depends on how fast the eigensystem changes. To show this, it can be used that ignoring the state changing interactions, the time evolution operator (Hamiltonian) is Hermitian, implying that the normalized eigenvectors v_i build an orthonormal basis. Consequently, any state at any time can be expressed as a superposition of the time-dependent eigenstates

$$|\psi(t)\rangle = \sum_i a_i(t)\,|v_i(t)\rangle \ , \tag{3.58}$$

with

$$a_i(t) = \langle v_i(t)|\psi(t)\rangle \ . \tag{3.59}$$

Using this, the time evolution of $\psi(t)$ can be transferred to a differential equation for $a_i(t)$,

$$\begin{aligned}\frac{d}{dt}a_i(t) &= \left(\frac{d}{dt}\langle v_i(t)|\right)|\psi(t)\rangle + \langle v_i(t)|\frac{d}{dt}|\psi(t)\rangle \\ &= \sum_j a_j\left[\left(\frac{d}{dt}\langle v_i(t)|\right) - i\langle v_i(t)|\hat{\mathrm{H}}\right]|v_j\rangle \\ &= -iE_i a_i(t) + \sum_{j\neq i} a_j(t)\left(\frac{d}{dt}\langle v_i(t)|\right)|v_j\rangle := -i\sum_j \hat{\mathrm{H}}_{\mathrm{coff}}(t)a_j(t)\,,\end{aligned} \tag{3.60}$$

where it is used that an infinitesimal shift of a normalized vector is orthogonal to the normalized vector:

$$\left(\frac{d}{dt}\langle v_i(t)|\right)|v_i(t)\rangle = 0\,. \tag{3.61}$$

Consequently, transitions between energy eigenstates are suppressed as long as the time derivative of the eigenvectors is small compared to the mass squared differences. In contrast to this adiabatic transition, for rapidly changing eigenvectors, transitions between the energy eigenstates become important. Hence, considering a rapidly changing eigensystem – meaning that the time derivative of the eigenvectors are dominant – investigating the time evolution in the energy eigenbasis is not very useful anymore.

A phenomenon of special interest that can arise from spacetime dependent matter effect is a level crossing where the effective potential gives rise to an effective Hamiltonian with at least two diagonal elements which are in a certain fixed basis degenerated at a certain time t_{LC}. As a consequence, the mixing in the considered fixed basis is maximal at t_{LC} while, in case of constant off-diagonal elements of the Hamiltonian, the difference of the energy eigenvalues is minimal. Moreover, the mass hierarchy is inverted, meaning that the diagonal element which is larger for $t < t_{LC}$ becomes smaller for $t > t_{LC}$ and vice versa. In the simplest case of considering a two component state vector where the matter effects are purely diagonal in a certain basis, the corresponding Hamiltonian is given by

$$\hat{\mathrm{H}}_{\mathrm{eff}} = E_0 I_2 + \frac{\Delta E_0}{2}\begin{pmatrix}\cos 2\theta & \sin 2\theta \\ \sin 2\theta & -\cos 2\theta\end{pmatrix} + V(t)I_2 + V'(t)\sigma_3\,, \tag{3.62}$$

where $E_0 = (E_{1,0}+E_{2,0})/2$ is the mean of vacuum energy eigenvalues, $\Delta E = E_{1,0}-E_{2,0}$ the difference of the vacuum energy eigenvalues, and $V(t)$ and $V'(t)$ are effective potentials. Consequently, the mixing of the first and the second component is maximal when $V'(t)+\Delta E_0/2\cos 2\theta$ vanish ($t = t_{LC}$). During a level crossing, the flavor of a state not only oscillates into another flavor but the flavor composition of the energy eigenstates completely changes. This behavior can e.g. be seen considering neutrino oscillation inside of the sun. There, neutrinos within a certain energy range experience an adiabatic level crossing during their propagation from the core, where they are produced by nuclear reactions, to the surface, converting the electron neutrinos produced in nuclear reaction mainly into

a neutrino mass eigenstate which is dominated by the muon and tau neutrino flavor. This Mikheyev-Smirnov-Wolfenstein (MSW) effect [73, 58] explains the observed neutrino flavor flux from the sun.

Considering more generally a non-adiabatic level crossing, in many cases of interest, it can be assumed that in the resonance region, the off-diagonal elements of the Hamiltonian are approximately constant, cf. equation (3.62), and the difference of the diagonal elements changes approximately linearly, $\hat{\mathrm{H}}_1(t) - \hat{\mathrm{H}}_2(t) = \alpha t + \mathcal{O}(t^2)$. Within this approximation, the equation of motion in the resonance region can be rewritten into one second order differential equation, which can be solved analytically [75]. For this purpose, one defines

$$|\psi_i(t)\rangle = \exp\left[-i\int_0^t \hat{\mathrm{H}}_i(t')dt'\right] c_i(t) \tag{3.63}$$

to rewrite the equation of motion into

$$\begin{aligned}\frac{d}{dt}|\psi(t)\rangle &= -i\begin{pmatrix}\hat{\mathrm{H}}_1(t) & 0\\ 0 & \hat{\mathrm{H}}_2(t)\end{pmatrix}|\psi(t)\rangle + \begin{pmatrix}\exp\left[-i\int_0^t \hat{\mathrm{H}}_1(t')dt'\right]\frac{d}{dt}c_1(t)\\ \exp\left[-i\int_0^t \hat{\mathrm{H}}_2(t')dt'\right]\frac{d}{dt}c_2(t)\end{pmatrix}\\ &\stackrel{!}{=} -i\begin{pmatrix}\hat{\mathrm{H}}_1(t) & \hat{\mathrm{H}}_{12}(t)\\ \hat{\mathrm{H}}_{21}(t) & \hat{\mathrm{H}}_2(t)\end{pmatrix}|\psi(t)\rangle\ .\end{aligned} \tag{3.64}$$

Using $\hat{\mathrm{H}}_1(t) - \hat{\mathrm{H}}_2(t) = \alpha t$, the resulting equation of motion for $c_i(t)$ becomes

$$\frac{d}{dt}\begin{pmatrix}c_1(t)\\ c_2(t)\end{pmatrix} \approx -i\begin{pmatrix}\hat{\mathrm{H}}_{12}(0)e^{i\alpha/2t^2}c_2(t)\\ \hat{\mathrm{H}}_{21}(0)e^{-i\alpha/2t^2}c_1(t)\end{pmatrix}\ . \tag{3.65}$$

Next, defining $c_1'(t) = e^{-i\alpha/4t^2}c_1(t)$, the second order differential equation

$$\frac{d^2}{dt^2}c_1'(t) = -\left[\frac{\alpha^2t^2}{4} + \frac{i\alpha}{2} + \hat{\mathrm{H}}_{12}(0)\hat{\mathrm{H}}_{21}(0)\right]c_1'(t) \tag{3.66}$$

is obtained. Solving this differential equation, the transition probability in the flavor basis ($|\psi_1\rangle \to |\psi_2\rangle$ and $|\psi_2\rangle \to |\psi_1\rangle$, respectively) integrating over all times is given by [75]

$$P_{\text{transit}} = 1 - \exp\left[-2\pi\frac{\hat{\mathrm{H}}_{12}(0)\hat{\mathrm{H}}_{21}(0)}{|\alpha|}\right]\ . \tag{3.67}$$

Note that this result is in agreement with the statement that a sufficiently large mixing and a slow enough transition is needed for having an adiabatic level crossing.

3.6 Details on Thermal Equilibrium

In section 3.1, it was shown that a process in thermal equilibrium leads to a compensation of the involved chemical potentials, resulting in condition (3.12). In this section, this estimation will be

investigated in more detail. Subsequently, the thermal rates of processes inducing the equilibrium condition of the top, bottom, and tau Yukawa interaction are calculated.

Considering a single process with a reaction rate Γ_i, the involved chemical potentials μ_i approach their equilibrium value μ_i^{eq} being given by the equilibrium condition of the reaction as

$$\frac{\mu_i(t) - \mu_i^{\mathrm{eq}}}{\mu_i(t_0) - \mu_i^{\mathrm{eq}}} = \exp\left(- \int_{t_0}^{t} \Gamma_i(t) dt \right) . \tag{3.68}$$

Comparing this result with the cooling of the plasma due to the expansion of the universe,

$$\frac{T(t)}{T(t_0)} \propto \frac{a(t_0)}{a(t)} = \exp\left(- \int_{t_0}^{t} \mathsf{H}(t) dt \right) , \tag{3.69}$$

the assumption of thermal equilibrium is well motivated when a process is efficient ($\Gamma \gg \mathsf{H}$) for a sufficiently long period. In this case, the equilibrium condition can be used to simplify a system of coupled Boltzmann equations involving reactions which are in thermal equilibrium and ones that are not. In this case, the equilibrium conditions can be used for the reactions which are efficient to reduce the number of free parameters and rates that have to be taken into account.
However, considering a system of coupled Boltzmann equations involving rates which are efficient for only a short period or where the interplay of efficient and less efficient reactions is of special interest (e.g. for the production of small asymmetries such as the observed B asymmetry), it cannot be assumed that all processes whose rates are efficient to be in thermal equilibrium. Yet, the equilibrium condition can be used for those reactions which are much more efficient than the investigated ones and also when the time period of interest is still large compared to $1/\Gamma$. In addition, processes of no special interest whose rates are much smaller than the dominant rates of interest can be ignored even if they are efficient because on the time scale where the process or the interplay of interest is relevant, processes with much smaller rates do not shift the involved chemical potentials significantly.

3.6.1 Thermal Equilibrium of the Dominant Yukawa Interactions

Within the scope of this thesis, Boltzmann equations are used to calculate the time evolution of B and L asymmetries involving sphaleron transitions and L violating processes, cf. chapter 4. For the resulting Boltzmann equations, the transfer of asymmetry between $SU(2)_L$ charged and uncharged particles is relevant because sphaleron transitions and depending on the considered model also the L violation only act on asymmetries of $SU(2)_L$ charged particles. In addition, the transfer of asymmetry between different generations is relevant because the rate of L violation is not expected to be equivalent for all generations. Hence, to study the interplay of sphaleron transitions and L violation, the thermal rates for the dominant Yukawa interactions need to be calculated first.

Considering the thermal masses shown in figure 3.1, for 10^8 GeV $< T < 10^{16}$ GeV, the decay of H into quarks is kinematically forbidden and the decay into leptons is either kinematically forbidden or strongly kinematically suppressed. Consequently, the shift of asymmetries resulting in the equilibrium condition is dominated by $2 \to 2$ processes. Thus, to estimate the temperature where a

Yukawa interaction becomes efficient, $2 \to 2$ scattering processes involving the corresponding Yukawa couplings have to be considered. The dominant processes are given by the Yukawa interaction with an additionally emitted or absorbed gauge boson. The corresponding Feynman diagrams for the top Yukawa interaction are shown in figure 3.2[13].

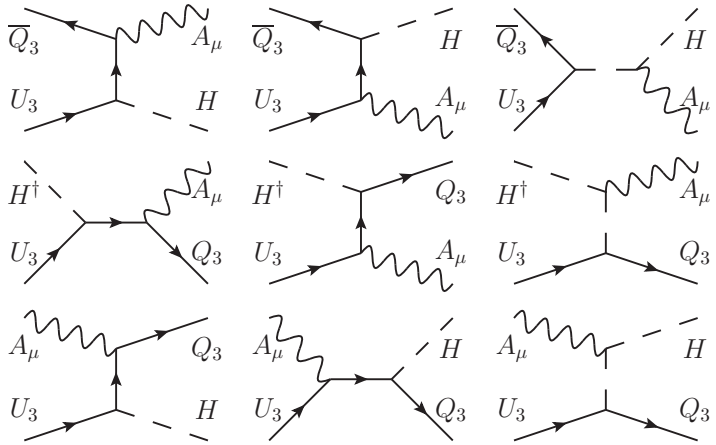

Figure 3.2: Dominant $2 \to 2$ scattering processes generating the equilibrium condition of the top Yukawa interaction: $U_3\overline{Q}_3 \to HA_\mu$ (top row), $U_3H^\dagger \to Q_3A_\mu$ (middle row), and $U_3A_\mu \to Q_3H$ (bottom row).

The corresponding matrix elements for the top Yukawa interaction before EWSB are given by

$$i\mathcal{M}_1(U_3\overline{Q}_3 \to HA_\mu) = y_t\epsilon_\mu^{(a)}\overline{v}_{Q_3}\left[\alpha_1^a\frac{\gamma^\mu \not{p}_t}{t-m_{Q_3}^2} + \alpha_2^a\frac{\not{p}_u\gamma^\mu}{u-m_{U_3}^2} + \alpha_3^a\frac{p_s^\mu + p_H^\mu}{s-m_H^2}\right]Ru_{U_3}\,, \tag{3.70a}$$

$$i\mathcal{M}_2(U_3H^\dagger \to Q_3A_\mu) = y_t\epsilon_\mu^{(a)}\overline{u}_{Q_3}\left[\alpha_1^a\frac{\gamma^\mu \not{p}_s}{s-m_{Q_3}^2} + \alpha_2^a\frac{\not{p}_u\gamma^\mu}{u-m_{U_3}^2} + \alpha_3^a\frac{p_t^\mu - p_H^\mu}{t-m_H^2}\right]Ru_{U_3}\,, \tag{3.70b}$$

$$i\mathcal{M}_3(U_3A_\mu \to Q_3H) = y_t\epsilon_\mu^{(a)}\overline{u}_{Q_3}\left[\alpha_1^a\frac{\gamma^\mu \not{p}_u}{u-m_{Q_3}^2} + \alpha_2^a\frac{\not{p}_s\gamma^\mu}{s-m_{U_3}^2} + \alpha_3^a\frac{p_t^\mu + p_H^\mu}{t-m_H^2}\right]Ru_{U_3}\,, \tag{3.70c}$$

where the kinematic variables defined in equation (D.1) are used. The index a runs over all group generators and α_i^a is determined by the coupling strength times the generator of the corresponding gauge group $(SU(3)_c/SU(2)_L/U(1)_Y)$:

$$\alpha_1^a = g_s t_3^a/gt_2^a/g'Y_{Q_3}\,, \qquad \alpha_2^a = g_s t_3^a/0/g'Y_{U_3}\,, \qquad \alpha_3^a = 0/gt_2^a/g'Y_H\,, \tag{3.71}$$

with the weak hypercharges $Y_{Q_3} = \frac{1}{6}$, $Y_{U_3} = \frac{2}{3}$, and $Y_H = \frac{1}{2}$.
Taking the average over the different colors of U_3, summing over all other external states, and using the limit of small masses (m_{U_3}, m_{Q_3}, m_H, $m_{A^\mu} \ll s, t, u$), cf. equation (D.3), the squared matrix

[13]Note that the scattering process involving twice the top Yukawa interaction does not change μ_{U_3} and the corresponding equilibrium condition is $\mu_{H^+} + \mu_{Q_3^1} = \mu_{H^0} + \mu_{Q_3^2}$ which is irrelevant for vanishing asymmetry among the doublet components.

elements averaged over the scattering angle, cf. equation (D.18), become

$$\overline{|\mathcal{M}_1|^2} \approx -2|y_t|^2\mathrm{Tr}\left[(\alpha_1^a)^2\ln\left(\frac{m_{Q_3}^2}{s}\right)+(\alpha_2^a)^2\ln\left(\frac{m_{U_3}^2}{s}\right)+(\alpha_1^a-\alpha_2^a)^2+(\alpha_1^a-\alpha_2^a+\alpha_3^a)\alpha_3^a\right], \tag{3.72a}$$

$$\overline{|\mathcal{M}_2|^2} \approx |y_t|^2\mathrm{Tr}\left[(\alpha_1^a)^2-2(\alpha_2^a)^2\ln\left(\frac{m_{U_3}^2}{s}\right)-4\alpha_1^a\alpha_2^a+2(\alpha_1^a-\alpha_2^a+\alpha_3^a)\alpha_3^a\right], \tag{3.72b}$$

$$\overline{|\mathcal{M}_3|^2} \approx |y_t|^2\mathrm{Tr}\left[-2(\alpha_1^a)^2\ln\left(\frac{m_{Q_3}^2}{s}\right)+(\alpha_2^a)^2-4\alpha_1^a\alpha_2^a+2(\alpha_1^a-\alpha_2^a+\alpha_3^a)\alpha_3^a\right]. \tag{3.72c}$$

Thus, the sum over all squared matrix elements is given by

$$\begin{aligned}\overline{|\mathcal{M}_{y_t}|^2} &= \overline{|\mathcal{M}_1|^2}+\overline{|\mathcal{M}_2|^2}+\overline{|\mathcal{M}_3|^2}\\ &\approx |y_t|^2\mathrm{Tr}\Big[-4(\alpha_1^a)^2\ln\left(\frac{m_{Q_3}^2}{s}\right)-4(\alpha_2^a)^2\ln\left(\frac{m_{U_3}^2}{s}\right)-(\alpha_1^a+\alpha_2^a)^2-2\alpha_1^a\alpha_2^a+2(\alpha_1^a-\alpha_2^a+\alpha_3^a)\alpha_3^a\Big].\end{aligned} \tag{3.73}$$

Plugging in α_i^a for the SM gauge interactions,

$$\overline{|\mathcal{M}_{y_t}|^2} \approx \begin{cases} -8|y_t|^2g_s^2\left[3+2\ln\left(\frac{m_{Q_3}^2}{s}\right)+2\ln\left(\frac{m_{U_3}^2}{s}\right)\right] & \text{for } SU(3)_c \\ \frac{3}{2}|y_t|^2g^2\left[3-4\ln\left(\frac{m_{Q_3}^2}{s}\right)\right] & \text{for } SU(2)_L \\ -|y_t|^2\frac{g'^2}{36}\left[33+4\ln\left(\frac{m_{Q_3}^2}{s}\right)+64\ln\left(\frac{m_{U_3}^2}{s}\right)\right] & \text{for } U(1)_Y \end{cases} \tag{3.74}$$

is obtained.
Furthermore, using $m_{Q_3} \approx m_{U_3} \sim m_h$, cf. figure 3.1, the thermal rate can be approximated as

$$\gamma_{U_3,y_t} \approx \frac{T^4}{16(2\pi)^5}\int\limits_{(m_h+m_A)^2/T^2}^{\infty} du\sqrt{u}\,|M_{y_t}|^2K_1(\sqrt{u}), \tag{3.75}$$

with $u = s/T^2$, cf. equation (3.29). The calculation of the squared matrix element can be repeated for the less efficient bottom Yukawa interaction:

$$\overline{|M_{y_b}|^2} \approx \begin{cases} -8|y_b|^2g_s^2\left[3+2\ln\left(\frac{m_{Q_3}^2}{s}\right)+2\ln\left(\frac{m_{D_i}^2}{s}\right)\right] & \text{for } SU(3)_c \\ \frac{3}{2}|y_b|^2g^2\left[3-4\ln\left(\frac{m_{Q_3}^2}{s}\right)\right] & \text{for } SU(2)_L \\ -|y_b|^2\frac{g'^2}{36}\left[3+4\ln\left(\frac{m_{Q_3}^2}{s}\right)+16\ln\left(\frac{m_{D_i}^2}{s}\right)\right] & \text{for } U(1)_Y \end{cases}, \tag{3.76}$$

and tau Yukawa interaction:

$$\overline{|M_{y_\tau}|^2} \approx \begin{cases} 0 & \text{for } SU(3)_c \\ \frac{3}{2}|y_\tau|^2g^2\left[3-4\ln\left(\frac{m_{\ell_i}^2}{s}\right)\right] & \text{for } SU(2)_L \\ -|y_\tau|^2\frac{g'^2}{4}\left[13+4\ln\left(\frac{m_{\ell_i}^2}{s}\right)+16\ln\left(\frac{m_{\ell_{R,i}}^2}{s}\right)\right] & \text{for } U(1)_Y \end{cases}. \tag{3.77}$$

However, in contrast to the top and the bottom Yukawa interaction, the Higgs decay for the tau Yukawa interaction is kinematically allowed for $T \lesssim 10^{11}$ GeV, cf. figure 3.1. Thus, the corresponding thermal rate – which is calculated for a similar process in section 5.1 – needs to be included. Hence, the thermal rates for the bottom and tau Yukawa interaction can be approximated by

$$\gamma_{D_3,y_b} \approx \frac{T^4}{16(2\pi)^5} \int\limits_{(m_h+m_A)^2/T^2}^{\infty} du\sqrt{u}\,|M_{y_b}|^2 K_1(\sqrt{u})\,, \tag{3.78}$$

$$\begin{aligned}\gamma_{\tau_R^-,y_\tau} \approx{}& \frac{T^4}{16(2\pi)^5} \int\limits_{(m_h+m_A)^2/T^2}^{\infty} du\sqrt{u}\,|M_{y_\tau}|^2 K_1(\sqrt{u}) \\ &+ \frac{m_H^3 T}{2\pi^2}\frac{|y_\tau|^2}{16\pi}\left(1-\frac{m_{\ell_i}^2}{m_H^2}-\frac{m_{\ell_{R,i}}^2}{m_H^2}\right)\lambda\left(1,\frac{m_{\ell_i}^2}{m_H^2},\frac{m_{\ell_{R,i}}^2}{m_H^2}\right)K_1\left(\frac{m_H}{T}\right)\,,\end{aligned} \tag{3.79}$$

where the contribution from the decay is ignored for the region where the decay is kinematically forbidden.
Note that especially for the tau Yukawa interaction, the approximation $m_{\ell_i} \approx m_{\ell_{R,i}} \sim m_h$ is not as good as before, but the expected deviation from the exact result is still small because the lower bound of the integral is only slightly shifted to lower values while the integrand is not significantly larger in this region. Taking into account the one-loop running of the gauge couplings and the top, bottom, and tau Yukawa couplings, the thermal rates in comparison to the rate of B violation induced by sphaleron transitions are shown in figure 4.1. In detail, $\Gamma_{U_3,y_t} = 6\gamma_{U_3,y_t}/T^3 > \mathsf{H}(T)$ is obtained for $T \lesssim 7.7 \times 10^{14}$ GeV, while $\Gamma_{D_3,y_b} > \mathsf{H}(T)$ and $\Gamma_{\tau_R^-,y_\tau} > \mathsf{H}(T)$ requires $T \lesssim 2.0 \times 10^{11}$ GeV and $T \lesssim 1.2 \times 10^{11}$ GeV, respectively.

3.6.2 Implication of the Equilibrium Condition

As discussed in section 3.1, the equilibrium condition of a process on its own is not sufficient to describe equilibration but only represents a relation of the involved chemical potentials after equilibration. However, to obtain the values of the individual chemical potentials, starting from some initial condition, also the relative change of the single chemical potentials mediated by the process becomes essential. If e.g. an extended Higgs sector with m scalar Higgs doublets is considered, where the reactions sharing the asymmetry among the different doublets are assumed to be in thermal equilibrium ($\hat{\mathcal{H}}_I(x) \sim (H_i^\dagger(x)H_j(x))^2 + (H_j^\dagger(x)H_i(x))^2$), the corresponding equilibrium condition is given by

$$\mu_{H_1} = \cdots = \mu_{H_m}\,. \tag{3.80}$$

Next, to obtain the individual resulting chemical potentials, it is used that a shift of the chemical potential of one doublet always shifts the chemical potential of another doublet by the opposite amount. Consequently, the sum over all μ_{H_i} is conserved by the interactions of interest. Thus, the individual chemical potentials after equilibration become

$$m\,\mu_{H_i} := \mu_H = \sum_{i=1}^{m} \mu_{H_i}^{\mathrm{ex}}\,, \tag{3.81}$$

where μ_α^{ex} are the chemical potentials given by the initial conditions $\mu_\alpha^{\text{initial}}$ and shifts induced by other reactions Δ_α:

$$\mu_\alpha^{\text{ex}} = \mu_\alpha^{\text{initial}} + \Delta_\alpha \,. \tag{3.82}$$

Taking e.g. also the top Yukawa interaction into account, the equilibrium condition

$$\mu_{H^{\text{SM}}} + \mu_{Q_3} - \mu_{U_3} = 0 \tag{3.83}$$

has to be fulfilled. In addition, the relative shifts of the involved chemical potentials are given by

$$4\Delta\mu_{H^{\text{SM}}} = 6\Delta\mu_{Q_3} = -3\Delta\mu_{U_3} \,, \tag{3.84}$$

where the prefactors count the number of degrees of freedom, where bosons obtain an additional factor 2, cf. equation (B.22).
Combining these conditions with the ones from the equilibration among the m Higgs doublets, cf. equation (3.81),

$$\frac{\mu_H}{m} + \mu_{Q_3} - \mu_{U_3} = 0 \,, \tag{3.85a}$$

$$4\Delta\mu_H = 6\Delta\mu_{Q_3} = -3\Delta\mu_{U_3} \,, \tag{3.85b}$$

is deduced. Accordingly, the chemical potentials after equilibration are given by

$$\mu_H = \frac{1}{1+2m}(2\mu_H^{\text{ex}} - \mu_{Q_3}^{\text{ex}} + \mu_{U_3}^{\text{ex}}) \,, \tag{3.86a}$$

$$\mu_{Q_3} = \frac{1}{3+6m}(-2\mu_H^{\text{ex}} + (3+4m)\mu_{Q_3}^{\text{ex}} + 2m\mu_{U_3}^{\text{ex}}) \,, \tag{3.86b}$$

$$\mu_{U_3} = \frac{1}{3+6m}(4\mu_H^{\text{ex}} + 4m\mu_{Q_3}^{\text{ex}} + (3+2m)\mu_{U_3}^{\text{ex}}) \,. \tag{3.86c}$$

4 Violation of Baryon and Lepton number

From cosmological observations, it is known that the baryonic content of the observable part of the universe mainly consists of matter and not of antimatter. The existence of a significant amount of antimatter would lead to measurable particle-antiparticle annihilation emitting a characteristic radiation signal. Furthermore, measurements of the abundance of light elements such as hydrogen, deuterium, helium-3, helium-4, and lithium-7 produced during the first minutes after the Big Bang ($T \gtrsim$ MeV) – a process known as BBN – are sensitive to the baryon abundance (Ω_B). An even stronger constraint baryon number (B) is determined from the measurements of the CMB. Considering the base-ΛCDM model, the obtained relic B abundance is given by [47, p.81]

$$\frac{1}{7.04}\frac{n_B}{n_\gamma} \simeq Y_B = 3.81 \times 10^{-9} \times (\Omega_B h^2) = (8.54 \pm 0.05) \times 10^{-11}\,, \tag{4.1}$$

where the recent Planck data for $\Omega_B h^2$ is used, cf. equation (C.8).

The origin of this observed B asymmetry is an open question in particle physics as it cannot be explained within the SM. For calculations on perturbation level this is obvious because the interaction terms in the SM, cf. section 2.8, conserve B as well as L. On the other hand, due to non-perturbative transitions being efficient before EWSB – known as sphaleron transitions –, violation of B and L occurs, cf. section 4.1. Since sphaleron transitions wash out $B-L$ conserving asymmetries in thermal equilibrium, they cannot individually explain the observed B asymmetry. A detailed investigation, cf. section 3.2, shows that three criteria – known as the Sakharov conditions – need to be fulfilled to obtain a final non-vanishing baryon asymmetry [62]:

1. Violation of B

2. Violation of the C-symmetry and CP-symmetry

3. Out-of-thermal-equilibrium interactions

Sphaleron transitions can only account for the first condition as well as P violation and they only erase B asymmetries as long as $B-L$ vanishes. Consequently, additional sources for B and/or L violation and CP violation are necessary to explain the observed B asymmetry. In section 4.2, three popular baryogenesis mechanisms are presented, two of which are of special interest in this thesis. Afterwards, in preparation for explicit investigations following in chapter 7 and chapter 8, the interplay of $B-L$ violation and sphaleron transitions is investigated and a general form of the time evolution of B and L including an additional source of L violation is deduced, in section 4.3.

4.1 Rate of B and L Violation Induced by Sphaleron Transitions

As was first shown by 't Hooft in 1976 [38], the electroweak field equations are broken by Adler-Bell-Jackiw anomalies, in the SM. As a consequence, the electroweak potential has distinct minima with different B and L while the difference of both, $B - L$, is conserved. However, in the vacuum only tunneling processes through the potential barriers separating the topologically different minima – called instantons – are possible. Thus, the rate of B and L violation is exponentially suppressed $\sim \exp(-4\pi/\alpha_W)$ and can be neglected to a good approximation.

Considering very hot thermal systems ($T \gtrsim 100$ GeV) thermal corrections to the Higgs potential shift the Higgs expectation value (EV) so that it becomes significantly smaller until it vanishes at a critical temperature (T_c) and the electroweak symmetry is restored, cf. section 6.3. In 1980, it was shown that the exponential suppression of the instanton transitions between the different vacua only holds after EWSB [52, 35]. For temperatures close to T_c or higher, non-perturbative transitions over the potential barrier are possible as well. These transitions – called sphalerons – were mathematically first described in 1984 [45]. The induced rate of B and L violation due to sphaleron transitions is only suppressed polynomially, $\sim \alpha_W^5$ [5].

In detail, each transition between different topological vacua converts three left-chiral quarks (anti-quarks) of each generation into one lepton (antilepton) of the same generation or vice versa. Thereby, each transition within one generation conserves all charges (color, weak isospin, and hypercharge). Consequently, $2Q_i^1 + Q_i^2 \leftrightarrow \ell_i^2$ ($2\overline{Q}_i^1 + \overline{Q}_i^2 \leftrightarrow \overline{\ell}_i^2$) and $Q_i^1 + 2Q_i^2 \leftrightarrow \ell_i^1$ ($\overline{Q}_i^1 + 2\overline{Q}_i^2 \leftrightarrow \overline{\ell}_i^1$) are the relevant processes, implying that summing over all generations there are $2 \times (2^{N_g})$ different allowed sphaleron transitions. As discussed in the previous chapter, cf. section 3.2, thermal equilibrium implies equivalence of the transition rates for the back and forth process. Consequently, the sum of all chemical potentials involved in each of the $2 \times (2^{N_g})$ different relevant transitions has to vanish in thermal equilibrium. For this condition to be fulfilled,

$$2\mu_{Q_i^1} + \mu_{Q_i^2} + \mu_{\ell_i^2} = \mu_{Q_i^1} + 2\mu_{Q_i^2} + \mu_{\ell_i^1} \tag{4.2}$$

is required, meaning that the equilibrium condition of all transitions is equivalent:

$$\sum_{i=1}^{N_g} (2\mu_{Q_i^1} + \mu_{Q_i^2} + \mu_{\ell_i^2}) = 0\,. \tag{4.3}$$

As has already been discussed in the previous chapter, cf. section 3.1, the equilibrium conditions can also be derived by minimizing the free energy F.
Furthermore, the exact form of the time evolution of B and L resulting from a detailed derivation is given by [44]

$$\frac{dn_B}{dt} = -N_g^2 \frac{\Gamma_{\text{diff}}}{VT} \frac{dF}{dn_B}\,, \tag{4.4}$$

with the volume V and the sphaleron diffusion constant Γ_{diff}, which is defined as [44]

$$\Gamma_{\text{diff}} = \lim_{V,t\to\infty} \frac{\left\langle [N_{\text{CS}}(t) - N_{\text{CS}}(0)]^2 \right\rangle}{Vt}\,. \tag{4.5}$$

The time evolution of the Chern-Simons number can be expressed as [38]

$$N_{\mathrm{CS}}(t) - N_{\mathrm{CS}}(0) = \frac{g^2}{32\pi^2} \int_0^t dt' \int d^3x \epsilon_{\mu\nu\rho\sigma} \mathrm{Tr}[W^{\mu\nu} W^{\rho\sigma}] \,, \tag{4.6}$$

where $W^{\mu\nu}$ is the field strength tensor of the $SU(2)_L$ gauge symmetry, cf. section 2.8. The sphaleron diffusion constant can e.g. be calculated using large-scale lattice simulations where for the SM [19],

$$\Gamma_{\mathrm{diff}} \approx (18 \pm 3)\alpha_W^5 T^4 \times \begin{cases} 1 & T \geq T_c \\ \exp\left((0.83 \pm 0.01)\frac{T-T_c}{\mathrm{GeV}}\right) & T < T_c \end{cases} \tag{4.7}$$

is obtained, meaning that sphaleron transitions become inefficient for $v^2 \gtrsim 1,5T^2$ [19].

Moreover, n_B is also diluted by the expansion of the universe, cf. equation (B.28). Thus, it is useful to rewrite the differential equation (4.4) in terms of the chemical potential normalized with respect to the temperature ($\beta = 1/T$) being conserved by the expansion of the universe as long as no reheating occurs:

$$\frac{d\beta\mu_B}{dt} = -\frac{36}{T^6} N_g^2 \frac{\Gamma_{\mathrm{diff}}}{VT} \frac{dF}{d\beta\mu_B} \,. \tag{4.8}$$

Next, to calculate the free energy as a function of $\beta\mu_B$, other reactions which are assumed to be in thermal equilibrium relate the individual chemical potentials with each other. Moreover, when not all relevant chemical potentials are related due to equilibrium conditions, additional assumptions (e.g. initial conditions) have to be made to obtain a definite free energy. Considering a SM-like theory with N_g generations and m $SU(2)_L$ Higgs doublets ($N_g = 3$ and $m = 1$ for the SM), assuming all reactions (gauge, Yukawa, and Higgs self-interactions) to be in thermal equilibrium and all charges to be conserved by the initial conditions, the free energy density in the small asymmetry limit ($\mu_i \ll T$), cf. equation (3.10), becomes [44, 36][1]

$$\frac{F}{V} = cT^4 + T^4 \frac{1}{48N_g} \frac{13m + 22N_g}{3m + 5N_g} \left(\beta\mu_B - \frac{4m + 8N_g}{13m + 22N_g} \beta\mu_{B-L}\right)^2 + \mathcal{O}(\beta\mu_B)^4 \,. \tag{4.9}$$

Thus, the resulting rate of B violation is given by

$$\frac{d\beta\mu_B}{dt} = -\frac{3N_g}{4} \frac{13m + 22N_g}{3m + 5N_g} \frac{\Gamma_{\mathrm{diff}}}{T^3} \left(\beta\mu_B - \frac{4m + 8N_g}{13m + 22N_g} \beta\mu_{B-L}\right) \,. \tag{4.10}$$

After EWSB, the rate of B violation is VEV-dependent

$$\frac{d\beta\mu_B}{dt} - N_g^2 \rho\left(\frac{v}{T}\right) \frac{\Gamma_{\mathrm{diff}}}{T^3} \left(\beta\mu_B - \frac{4m + 8N_g}{13m + 22N_g} \beta\mu_{B-L}\right) \,, \tag{4.11}$$

where $\rho(x)$ for $m = 1$ is given by [13]

$$\rho\,(x) = \frac{3}{2N_g} \frac{65 + 136N_g + 44N_g^2 + (117 + 72N_g)x^2}{30 + 62N_g + 20N_g^2 + (54 + 33N_g)x^2} \,. \tag{4.12}$$

[1] The free energy density with $m = 1$ was first calculated in reference [44] while n_B^{eq} with arbitrary m can be found in reference [36].

Ignoring all Yukawa interactions and assuming that the initial B and L asymmetry is completely stored in the left-chiral sector,

$$\mu_{U_i}^{\text{initial}} = \mu_{D_i}^{\text{initial}} = \mu_{\ell_{R,i}}^{\text{initial}} = 0\,, \tag{4.13a}$$

$$\mu_{Q_i^1}^{\text{initial}} = \mu_{Q_i^2}^{\text{initial}} := \mu_{Q_i}^{\text{initial}} = \frac{3}{N_g}\frac{n_B}{T^2} := \frac{\mu_B}{2N_g}\,, \tag{4.13b}$$

$$\mu_{\ell_i^1}^{\text{initial}} = \mu_{\ell_i^2}^{\text{initial}} := \mu_{\ell_i}^{\text{initial}} = 3\frac{n_{L_i}}{T^2} := \frac{\mu_{L_i}}{2}\,, \tag{4.13c}$$

$$\mu_H^{\text{initial}} = -\frac{3}{2m}\frac{n_{B-L}}{T^2} = -\frac{1}{4m}\left(\mu_B - \sum_{i=1}^{N_g}\mu_{L_i}\right) = -\frac{1}{4m}\mu_{B-L}\,, \tag{4.13d}$$

where the value of μ_H^{initial} results form conservation of hypercharge, the rate of B violation is determined by

$$\frac{d\beta\mu_B}{dt} = -6N_g\frac{\Gamma_{\text{diff}}}{T^3}\left(\beta\mu_B - \frac{1}{4}\beta\mu_{B-L}\right)\,. \tag{4.14}$$

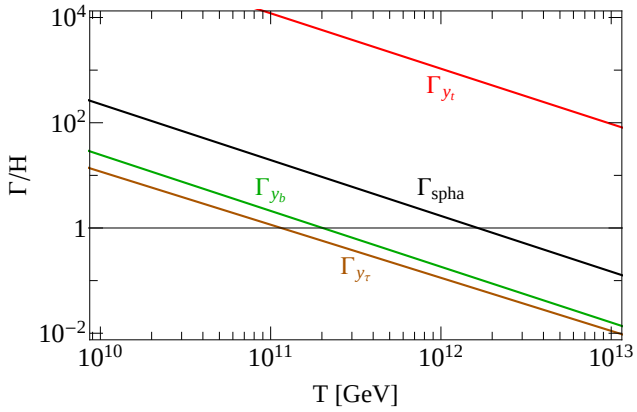

Figure 4.1: Comparison of the rate of $\beta\mu_B$ violation normalized to the Hubble expansion rate, cf. equation (4.15), induced by sphaleron transitions (black line) with the normalized rate of $\beta\mu_{U_3}$, $\beta\mu_{D_3}$, and $\beta\mu_{\tau_R^-}$ violation induced by the dominant top (red line), bottom (green line), and tau (dark orange line) Yukawa interaction respectively, cf. section 3.6.1.

Comparing the resulting rate of B violation with the rates generating the equilibrium condition of the dominant SM Yukawa interactions, cf. equations (3.75), (3.78), and (3.79), it can be deduced that before EWSB only the top Yukawa interaction is much more efficient than the rate of B violation induced by sphaleron transitions while all other SM Yukawa interactions are significantly less efficient, cf. figure 4.1. Thus, only the equilibrium condition of the top Yukawa interaction, cf. equation (3.86), can be used while the equilibrium condition of all other SM Yukawa interactions can be ignored when the rate of B violation induced by sphaleron transition itself and not only the equilibrium condition is relevant, cf. section 3.6. Using this together with the initial conditions given in equation (4.13), the rate of B violation becomes

$$\frac{d\beta\mu_B}{dt} = -3\left(2N_g - \frac{m}{2m+1}\right)\frac{\Gamma_{\text{diff}}}{T^3}\left(\beta\mu_B - \frac{mN_g}{m(4N_g-1)+2N_g}\beta\mu_{B-L}\right)\,. \tag{4.15}$$

4.2 Diversity of Baryogenesis Models

Sphaleron transitions on their own are insufficient to explain the observed B asymmetry. For this reason, physicists came up with a great number of models addressing this issue. Here, the basic mechanism of three popular categories of models are shortly explained to highlight their diversity. For a detailed, up-to-date investigation of diverse baryogenesis scenarios, cf. e.g. reference [6].

One category are electroweak baryogenesis models [49, 21], which only use sphaleron transitions as a source of B and L violation. However, to generate a non-vanishing B asymmetry by sphaleron transitions only, two more ingredients, CP violation and a strong first order electroweak phase transition (EWPT), are needed. In these models, the universe does not smoothly transit from the $SU(2)_L$ symmetric to the broken phase. Instead, the phase transition is of first order when the field value tunnels through the potential barrier separating two distinct minima – one with a vanishing and one with a non-vanishing EV of the Higgs field – at different spacetime points. Thus, rapidly expanding bubbles form, where the field inside of the bubbles is in the broken phase while outside, the state remains in the symmetric phase. Additionally, to have a **strong** first order phase transition, the EV inside the bubbles needs to be larger than the temperature, meaning that inside of the bubbles sphaleron transitions are inefficient. Furthermore, the masses of particles are different in the symmetric and broken phase, implying that the particles are partly reflected at the bubble wall – similar to light at the interface of media with different refraction indices.
Finally, CP violation implies that the reflection probabilities of particles and antiparticles are different, resulting in a net baryon flow through the bubble wall. The resulting surplus of antiparticles in front of the bubble wall is partly reduced by sphaleron transitions while the surplus of baryons inside the bubble is secured because sphaleron transitions are inefficient.
However, in the SM, there is no strong first order EWPT, meaning that an extended Higgs sector including multiple Higgs doublets is required. Furthermore, the CP violation within the SM is too small to produce the observed baryon asymmetry so that an additional source of CP-violation is needed as well.

Another category of special interest in the scope of this thesis are leptogenesis models where the observed B asymmetry has its origin in an asymmetry produced in the lepton sector which is then partly converted into a B asymmetry by sphaleron transitions. There are two main motivations to let the observed B asymmetry originate in the lepton sector. First of all, in contrast to B violating models, which are strongly restricted by the lower bound on the proton lifetime, L violation does not induce nucleon decays allowing for a larger parameter space – larger coupling constants and lower involved masses. Furthermore, right-chiral neutrinos – representing the simplest extension of the SM to explain the observed non-vanishing active neutrino masses – are uncharged under all SM gauge groups. As a consequence, they can have a Majorana mass naturally inducing L violation, cf. chapter 5.
In the original model suggested in 1986 by Fukugita and Yanagida [26] the necessary CP violation has its origin in the Yukawa couplings of the neutrino sector. The out-of-equilibrium condition is fulfilled if the right-handed neutrinos never reach thermal equilibrium or the production of right-handed neutrinos falls out of equilibrium when the temperature drops below their mass so that they

decay in a CP violating manner, cf. section 5.3. Note that also other mechanisms give rise to a Majorana mass for the left-chiral neutrinos inducing L violation.

Finally, another category which is of special interest in this thesis are Grand Unified Theory (GUT) baryogenesis models. GUTs aim at unifying the three SM gauge symmetries into one primal gauge symmetry. Similar to the unification of the electromagnetic ($U(1)_{em}$) and the weak force to the spontaneously broken electroweak force ($SU(2)_{\mathrm{L}} \times U(1)_Y$), the strong and the electroweak force are further unified to e.g. a spontaneously broken $SU(5)_{GUT}$ (Georgi–Glashow model [29]) or $SO(10)_{\mathrm{GUT}}$ [25] with $SU(3)_C \times SU(2)_L \times U(1)_Y \subset SU(5) \subset SO(10)$.
There are a couple of motivations for this unification. First of all, physicists strive to find a theory of everything with only one force and a minimal number of free parameters. Moreover, there are also practical reasons for assuming that the SM forces can be unified. One reason is that GUTs can explain the discrete values of the hypercharge of SM particles which in principle could have any value in $U(1)_Y$. Another hint at the existence of GUTs can be found by considering the running of the SM coupling constants g, g', and g_s since they have roughly the same value in the SM around 10^{15} GeV[2], cf. figure 2.1. Consequently, the scale where the unified theory breaks down into the three SM gauge symmetries is usually assumed to be roughly of this order. As for the breaking of $SU(2)_{\mathrm{L}} \times U(1)_{\mathrm{Y}} \to U(1)_{\mathrm{em}}$ where the masses of Higgs and gauge bosons are of the same order as the breaking scale ~ 100 GeV, it is expected that the masses of the particles given by the GUT breaking are also of the order of the GUT breaking scale. This assumption is also supported by the fact that the Georgi-Glashow model requires the existence of a scalar color triplet Higgs boson – also known as leptoquarks – inducing nucleon decays. Thus, their masses have to be greater than $\sim 10^{11}$ GeV [33] to be in agreement with the measured bound on the proton lifetime. However, particles with so large masses are way too heavy to be produced in current collider experiments, meaning that it is not expected to observe GUT particles inducing B violation in the near future.
Nevertheless, GUTs naturally lead to B violation and are therefore of interest for baryogenesis. However, in many GUT-baryogenesis models, an equivalent amount of L violation is induced, implying that the difference of both $(B - L)$ is conserved resulting in a complete washout of the produced asymmetry by sphaleron transitions if no further $B - L$ violating processes are active before sphalerons reach thermal equilibrium. The reason therefore is that in $SU(5)$, $B - L$ is a conserved quantity. Furthermore, GUTs of higher symmetry groups such as $SO(10)$ contain $U(1)_{B-L}$ as a subgroup which is unbroken above the GUT breaking scale. Consequently, before the GUT symmetry is broken, only many body decays can violate $B - L$. However, these many body decays are too inefficient to explain the observed asymmetry [27].

[2]Note that in the Minimal Supersymmetric Standard Model (MSSM), all SM coupling constants become equivalent at $\sim 10^{16}$ GeV, cf. e.g. review 94. in reference [76]

4.3 Interplay of Sphaleron Transitions and $B - L$ Violating Interactions

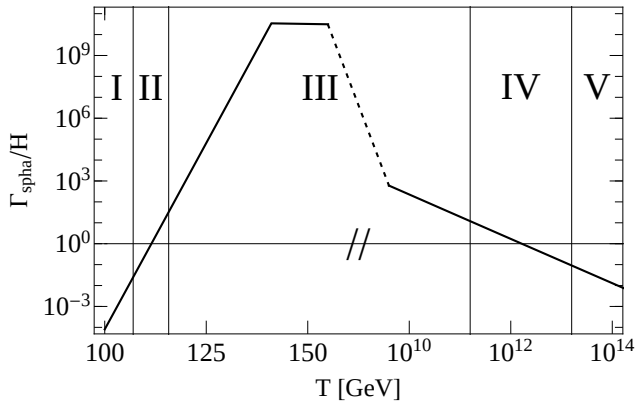

Figure 4.2: Rate of $\beta\mu_B$ violation induced by sphaleron transitions (Γ_{spha}) normalized to the Hubble expansion rate $\mathsf{H}(T)$ (black line), distinguishing five major regions of interest. In region I ($T \lesssim 110$ GeV) and region V ($T \gtrsim 10^{13}$ GeV), the violation of the baryon number is inefficient and sphaleron transitions are irrelevant. In region II ($T \sim 115$ GeV) and region IV (10^{11} GeV $\lesssim T \lesssim 10^{13}$ GeV), the rate of $\beta\mu_B$ violation is roughly of the same order as the Hubble expansion rate, implying that the interplay of sphaleron transitions and other processes become relevant. In region III (120 GeV $\lesssim T \lesssim 10^{11}$ GeV), the violation of the baryon number is very efficient, meaning that only the equilibrium condition is relevant.

After presenting the basic mechanism of various baryogenesis models, in this section the interplay between sphaleron transitions and other sources of B and/or L violation is investigated in more detail. Considering the rate of $\beta\mu_B$ violation induced by sphaleron transitions (Γ_{spha}), five major regions can be distinguished for the interplay with additional sources of B and/or L violation, cf. figure 4.2.
In the first region of interest ($T \gtrsim 10^{13}$ GeV), cf. region V in figure 4.2, Γ_{spha} is small compared to the Hubble expansion rate. Consequently, sphaleron transitions in this region can be ignored to a good approximation, meaning that only the rates of additional B- and/or L-violating processes are relevant for the time evolution of the B and L asymmetries. Thus, assuming the additional sources of B and/or L violation to only be relevant in this region, the resulting B asymmetry is determined by the $B - L$ asymmetry generated in this region, cf. the equilibrium condition of equation (4.10). The GUT baryogenesis scenarios mentioned in the previous section usually take place in this region.

Next, for 10^{11} GeV $\lesssim T \lesssim 10^{13}$ GeV, Γ_{spha} is comparable to the Hubble expansion rate, cf. region IV in figure 4.2. Consequently, the rate of B and L violation induced by sphaleron transitions has to be taken into account as a part of the Boltzmann equation requiring a more detailed analysis of the interplay of sphaleron transitions and additional B- and/or L-violating processes.
In the third region of interest (120 GeV $\lesssim T \lesssim 10^{11}$ GeV), cf. region III in figure 4.2, sphaleron transitions are in thermal equilibrium ($\Gamma_{\text{spha}} \gg \mathsf{H}(T)$). Hence, sphaleron transitions do not have to be taken into account as part of the Boltzmann equations. Instead, the equilibrium condition can be

used to simplify the Boltzmann equations. Leptogenesis scenarios are often assumed to take place in this region.

Moreover, after EWSB sphaleron transitions become exponentially suppressed so that for 110 GeV $\lesssim T \lesssim$ 120 GeV, Γ_{spha} is again comparable to the Hubble expansion rate, cf. region II in figure 4.2.

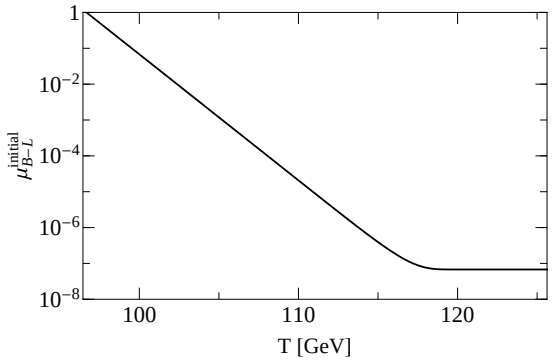

Figure 4.3: Required value of $\beta\mu_{B-L}$ in the SM depending on the generation scale necessary to obtain the observed B asymmetry of $\beta\mu_B^{\text{final}} = -2.4 \times 10^{-8}$, cf. equation (4.20). For the calculation of the critical temperature appearing in the sphaleron diffusion constant, only the leading thermal corrections to the effective Higgs potential have been taken into account, cf. equation (6.41).

The freeze out of sphaleron transitions can be visualized by calculating the initial $B-L$ asymmetry required to obtain the observed B asymmetry depending on the scale where the $B-L$ asymmetry is produced, cf. figure 4.3. As can be seen, an initial $B-L$ asymmetry of order $\beta\mu_{B-L}^{\text{initial}} \lesssim 10^{-7}$ being present at $T \sim 115$ GeV is sufficient to explain the observed B asymmetry if no further source of B violation is relevant at lower temperatures.

Finally, for $T \lesssim 110$ GeV the rate of B violation induced by sphaleron transitions is inefficient ($\Gamma_{\text{spha}} \ll \mathsf{H}(T)$), cf. region I in figure 4.2. Consequently, this last region is not very promising to account for the observed B asymmetry because an L asymmetry produced by additional sources of L violation cannot be converted into a sizable B asymmetry when sphaleron transitions are inefficient. Furthermore, additional B violating processes being efficient at such low temperatures naturally imply a decay width of the proton which exceeds the current limits.

In chapter 7, the focus is on the fourth region where the rate of B violation induced by sphaleron transitions is close to the Hubble expansion rate. Consequently, the interplay of both sphaleron transitions and B and/or L violation has to be studied in detail.
For simplicity, the initial conditions given in equation (4.13) are used and only an additional source of L violation is considered implying that B is only violated by sphaleron transitions. Furthermore, all other processes, which do not violate B and/or L but connect different chemical potentials, are assumed to be either in thermal equilibrium or negligible[3]. Within this set of conditions, the

[3] As discussed in section 4.1, this approximation is reasonable in the second and fourth region when only SM processes and additional sources of L violation are considered. In detail, in region IV, all SM gauge interactions and the top Yukawa interaction are way more efficient than sphaleron transitions, while all other Yukawa interactions are significantly less efficient so that they can be neglected. In region II, all SM interactions are in thermal equilibrium.

quantities being relevant for the time evolution of the B asymmetry reduce to the total amount of B asymmetry ($\beta\mu_B$) and the L asymmetry of each generation L_i ($\beta\mu_{L_i}$)[4], whose time evolution is determined by

$$\frac{d}{dt}\beta\mu_{L_i} = \Gamma_{\not{L},ij}\beta\mu_{L_j} + \Gamma_{\not{L},B}\beta\mu_B + \Gamma_{\text{spha}}\left(\beta\mu_{L_i} - \frac{c_s - 1}{2N_g}\beta\mu_{B-L}\right), \tag{4.16a}$$

$$\frac{d}{dt}\beta\mu_B = -\Gamma_{\text{spha}}\left(\beta\mu_B - c_s\beta\mu_{B-L}\right), \tag{4.16b}$$

with $\Gamma_{\not{L},ij}$ and $\Gamma_{\not{L},B}$ being rates induced by additional source of L violation.
However, the solution of the differential equations 4.16 can be numerically unstable because it strongly depends on $\mu_{B-L} = \mu_B - \mu_L$ being defined by the difference of two quantities, each of with can be large compared to their difference ($\mu_B, \mu_L \gg \mu_{B-L}$). To circumvent this problem, the time evolution of $\mu_{B-L_i} = \mu_B/N_g - \mu_{L_i}$ and μ_B can be considered instead:

$$\frac{d}{dt}\beta\mu_{B-L_i} = \Gamma_{\not{L},ij}\left(\beta\mu_{B-L_i} - \frac{\beta\mu_B}{N_g}\right) - \Gamma_{\not{L},2}\beta\mu_B\,, \tag{4.17a}$$

$$\frac{d}{dt}\beta\mu_B = -\Gamma_{\text{spha}}\left(\beta\mu_B - c_s\beta\mu_{B-L}\right), \tag{4.17b}$$

where the time evolution of μ_{B-L_i} is now independent of the rate of B violation induced by sphaleron transitions.

According to (4.17) and considering baryogenesis originating from a $B - L$ asymmetry produced above the scale where sphaleron transitions become inefficient ($T \gtrsim 115$ GeV), the final B asymmetry is given by

$$\beta\mu_B^{\text{final}} = c_s\beta\mu_{B-L}(T \sim 115\text{ GeV}) = 4\frac{m + 2N_g}{13m + 22N_g}\beta\mu_{B-L}(T \sim 115\text{ GeV})\,, \tag{4.18}$$

cf. equation (4.10). Based on observations,

$$\beta\mu_B^{\text{final}} = -\frac{6s}{T^3}Y_B^{\text{final}} = -\frac{4\pi^2}{15}g_{\text{eff}}^S \times (8.54 \pm 0.06) \times 10^{-11} \tag{4.19}$$

is required, which becomes

$$\beta\mu_B^{\text{final}} = -(2.40 \pm 0.01) \times 10^{-8} \tag{4.20}$$

for the SM ($N_g = 3$, $m = 1$, and $g_{\text{eff}}^S = 106.75$) and

$$\beta\mu_B^{\text{final}} = -(2.49 \pm 0.02) \times 10^{-8} \tag{4.21}$$

for an extended Higgs sector with two scalar Higgs doublets ($N_g = 3$, $m = 2$, and $g_{\text{eff}}^S = 110.75$).

[4]The chemical potentials of additional BSM particles inducing L violation are either irrelevant or can usually be expressed in terms of $\beta\mu_B$ and $\beta\mu_{L_i}$.

5 Introduction of Right-Handed Majorana Neutrinos

In the SM, the three left-chiral neutrinos (ν_e, ν_μ, and ν_τ) are massless but from the observation of neutrino oscillations, it is known that at least two of the three neutrinos have a non-vanishing mass, cf. equation (C.4). Consequently, an extension of the SM explaining these non-vanishing masses is needed. Because all other masses in the SM besides the Higgs mass are generated by the Higgs mechanism, it seems natural to introduce right-chiral neutrinos (ν^R) which are coupled to the left-chiral lepton doublet (ℓ) via Yukawa interactions:

$$\mathcal{L}_N = \sum_i \left[i\overline{\Psi}_{\nu_i^R} \partial\!\!\!/ \Psi_{\nu_i^R} - \sum_j \left(y_{ij} \overline{\Psi}_{\ell_j} H^c \Psi_{\nu_i^R} + y_{ij}^* \overline{\Psi}_{\nu_i^R} H^{c\dagger} \Psi_{\ell_j} \right) - \frac{M_{N_i}}{2} \left(\overline{\Psi^c}_{\nu_i^R} \Psi_{\nu_i^R} + \overline{\Psi}_{\nu_i^R} \Psi^c_{\nu_i^R} \right) \right], \tag{5.1}$$

with $H^c = i\sigma_2 H^*$ and the field operators in the charge-conjugated representation defined in equation (A.15).

First, forgetting about the Majorana mass terms ($M_{N_i} = 0$), as all other SM particles, neutrinos obtain a Dirac mass. This simple extension of the SM explains neutrino oscillations but it is difficult to confirm by experiments because the introduced Yukawa couplings have to be naturally very small ($\sum y_{ij} \lesssim 10^{-12}$) to be in agreement with the limit on the sum of the neutrino masses ($\sum m_\nu \lesssim 0.12$ eV [2]), meaning that the coupling of the dominantly right-chiral neutrino energy eigenstate to other SM particles is tiny. This can be understood from the fact that right-chiral neutrinos are uncharged under the SM gauge symmetries so that the dominantly right-chiral neutrino energy eigenstate only couple via weak interaction due to Dirac mass induced mixing. However, this mixing becomes very tiny for measurable neutrino energies ($E \gg y_{ij} v$).

On the other hand, the fact that right-chiral neutrinos are uncharged under the SM gauge symmetries allows the introduction of Majorana mass terms ($M_{N_i} \neq 0$), which for SM particles are forbidden by gauge symmetries. However, considering Majorana mass terms, the equations of motion resulting from $\mathcal{L}_N$ become more complicated because they also depend on field operators in the charge-conjugated representation. In the SM, the Lagrangian can be either written in terms of field operators or field operators in the charge-conjugated representation so that transition amplitudes can either be calculated in the usual or the charge-conjugated representation. But the Majorana mass terms switch between both representation, implying that the equations of motion of both representations do not decouple. Hence, the SM Lagrangian, cf. equation (A.92), and the additionally introduced Lagrangian including right-chiral neutrinos, cf. equation (5.1), in the charge-conjugated representation become relevant

$$\mathcal{L}_N^c = \sum_i \left[i\overline{\Psi^c}_{\nu_i^R} \partial\!\!\!/ \Psi^c_{\nu_i^R} - \sum_j \left(y_{ij}^* \overline{\Psi^c}_{\nu_j} H \Psi^c_{\nu_i^R} + y_{ij} \overline{\Psi^c}_{\nu_i^R} H^\dagger \Psi^c_{\nu_j} \right) - \frac{M_{N_i}}{2} \left(\overline{\Psi^c}_{\nu_i^R} \Psi_{\nu_i^R} + \overline{\Psi}_{\nu_i^R} \Psi^c_{\nu_i^R} \right) \right], \tag{5.2}$$

as well as equation A.95 for the SM Lagrangian in the charge-conjugated representation[1].

That both representations are needed to calculate a transition amplitude involving Majorana masses seem to be problematic because both representations contain the same creation and annihilation operators and – ignoring the Majorana masses – independently give rise to the same equations of motion. Nevertheless, fixing the used representation at one interaction point so that both representations become distinct at each interaction point, the equation of motion including both representations can be used as a simple method to calculate transition amplitudes involving Majorana masses. Because only Majorana masses switch between both representations, the propagators of all non-Majorana particles remain unchanged:

$$\langle 0|\mathcal{T}\psi_i^c(x+y)\overline{\psi}_i(y)|0\rangle = \langle 0|\mathcal{T}\psi_i(x+y)\overline{\psi^c}_i(y)|0\rangle = 0\,. \tag{5.3}$$

Only for the field operators of right-chiral Majorana neutrinos, representation changing propagators occur:

$$\langle 0|\mathcal{T}\Psi_{\nu_i^R}(x+y)\overline{\Psi}_{\nu_i^R}(y)|0\rangle = \langle 0|\mathcal{T}\Psi^c_{\nu_i^R}(x+y)\overline{\Psi^c}_{\nu_i^R}(y)|0\rangle = \int \frac{dk}{(2\pi)^4}\frac{i\not{k}}{k^2-M_{N_i}^2}e^{-ikx}\,, \tag{5.4a}$$

$$\langle 0|\mathcal{T}\Psi^c_{\nu_i^R}(x+y)\overline{\Psi}_{\nu_i^R}(y)|0\rangle = \langle 0|\mathcal{T}\Psi_{\nu_i^R}(x+y)\overline{\Psi^c}_{\nu_i^R}(y)|0\rangle = \int \frac{dk}{(2\pi)^4}\frac{iM_{N_i}}{k^2-M_{N_i}^2}e^{-ikx}\,, \tag{5.4b}$$

where all other contractions of field operators vanish (e.g. $\langle 0|\mathcal{T}\Psi_N^c(x+y)\Psi_N(y)|0\rangle = 0$). Furthermore, spin sums where the Majorana masses also change among the representations are given by

$$\langle 0|\Psi_{\nu_i^R}(x)\,|i,p\rangle\,\langle i,p|\,\overline{\Psi}_{\nu_i^R}(x)|0\rangle = \langle 0|\Psi^c_{\nu_i^R}(x)\,|i,p\rangle\,\langle i,p|\,\overline{\Psi^c}_{\nu_i^R}(x)|0\rangle = \sum u_{\nu_i^R}(\vec{p})\overline{u}_{\nu_i^R}(\vec{p}) = \not{p}\,, \tag{5.5a}$$

$$\langle 0|\Psi^c_{\nu_i^R}(x)\,|i,p\rangle\,\langle i,p|\,\overline{\Psi}_{\nu_i^R}(x)|0\rangle = \langle 0|\Psi_{\nu_i^R}(x)\,|i,p\rangle\,\langle i,p|\,\overline{\Psi^c}_{\nu_i^R}(x)|0\rangle = \sum v^c_{\nu_i^R}(\vec{p})\overline{u}_{\nu_i^R}(\vec{p}) = M_{N_i}\,, \tag{5.5b}$$

where the relations $v_s^c(\vec{p}) = u_s(\vec{p})$ and $u_s^c(\vec{p}) = v_s(\vec{p})$ are used. Note that, considering an antiparticle instead ($|i,p\rangle \to |\bar{i},p\rangle$ $u_{\nu_i^R} \leftrightarrow v_{\nu_i^R}$), a $-$ sign in front of M_{N_i} is obtained. In addition, $u_{\nu_i^R}$ are the positive and $v_{\nu_i^R}$ the negative energy eigenstates of the free equation of motion neglecting Dirac masses inducing mixing between left- and right-chiral components. Note that, due to the fixing of the representation at one interaction point, the second row of equation (5.5) can only become relevant when multiple Majorana field operators appear in the transition amplitude. Alike Feynman rules for Majorana fermions can be found in the literature, cf. e.g. reference [32], where the Majorana condition is used, meaning that calculations can be completely done in the usual representation. Nevertheless, charge-conjugated matrices have to be introduced and spinors have to be transposed meaning that the resulting amplitudes become equivalent.

However, using the derived formalism including both representations, the detailed investigation of eigenstates including both Majorana and Dirac masses become more obvious. Defining $\psi_{\nu_i^R} :=$

[1] Note that the equation of motion for the field operators in the charge-conjugated representation is related to the equation of motion of field operators by a complex conjugation of the Yukawa couplings and an additional minus sign in front of the gauge couplings. This is because the same state vector that describes a particle in the usual representation describes the corresponding antiparticle in the charge-conjugated representation.

$(\Psi_{\nu_i^R}, \Psi^c_{\nu_i^R})$ and $\psi_{\nu_j^L} := (\Psi_{\nu_j^L}, \Psi^c_{\nu_j^L})$, the time evolution can be written as

$$i\frac{d}{dt}\psi_{\nu_i^R} = \gamma^0(i\nabla\vec{\gamma} + M_{N_i})\psi_{\nu_i^R} + \sum_j m_{ij}^\dagger\, \psi_{\nu_j^L}\,, \tag{5.6a}$$

$$i\frac{d}{dt}\psi_{\nu_j^L} = -i\gamma^0\nabla\vec{\gamma}\,\psi_{\nu_j^L} + \sum_i m_{ij}\,\psi_{\nu_i^R}\,, \tag{5.6b}$$

with

$$m_{ij} = \frac{v}{\sqrt{2}}\begin{pmatrix} y_{ij}I_2 & 0 \\ 0 & y_{ij}^* I_2 \end{pmatrix}. \tag{5.7}$$

Note that one can always transform to a basis where $\vec{p} \parallel \vec{e}_z$ so that the time evolution of the first and third component decouples from the time evolution of the second and fourth component, which is important because each degree of freedom is considered twice. Next, considering the time evolution in the rest frame and defining $\psi' = (\psi_{\nu_1^L}, \ldots, \psi_{\nu_{N_g}^L}, \psi_{\nu_1^R}, \ldots, \psi_{\nu_{n_N}^R})$, the mass eigenstates are determined by

$$E\,\psi' = \begin{pmatrix} 0 & m_D \\ m_D^\dagger & M_N \end{pmatrix}\psi'\,, \tag{5.8}$$

where the Dirac and the Majorana mass matrices are given by

$$m_D = \begin{pmatrix} m_{11} & \cdots & m_{n_N 1} \\ \vdots & \ddots & \vdots \\ m_{1N_g} & \cdots & m_{n_N N_g} \end{pmatrix} \qquad \text{with} \qquad m_{ij} = \frac{v}{\sqrt{2}}\begin{pmatrix} y_{ij} & 0 \\ 0 & y_{ij}^* \end{pmatrix}, \tag{5.9a}$$

$$M_N = \begin{pmatrix} M_1 & 0 & 0 \\ 0 & \ddots & 0 \\ 0 & 0 & M_{n_N} \end{pmatrix} \qquad \text{with} \qquad M_i = \begin{pmatrix} 0 & M_{N_i} \\ M_{N_i} & 0 \end{pmatrix}. \tag{5.9b}$$

Furthermore, it can be shown that the eigenvalues of the given mass matrix are equivalent to the eigenvalues obtained by using $m_{ij} = \frac{v}{\sqrt{2}}y_{ij}$ and $M_i = M_{N_i}$ instead. Assuming $M_{N_i} \gg m_{ij}$, the eigenvalues of the mass matrix at first non-vanishing order are given by the Majorana masses (M_{N_i}) and the eigenvalues of the light mass matrix

$$(m_\nu^I)_{jk} := \sum_i \frac{y_{ij}^* y_{ik}}{2M_{N_i}}v^2 =: \sum_i (m_\nu^I)_{jk}^i\,, \tag{5.10}$$

which is known as the type-I seesaw mechanism [59]. This mechanism makes it possible to explain the smallness of the observed neutrino masses compared to all other Dirac masses which are present in the SM without requiring extremely small Yukawa couplings. Assuming e.g. $y_{ij} \sim 1$ and $M_{N_i} \sim 10^{15}$ GeV results in light neutrino masses of order 0.1 eV.

Note that the heavy-mass eigenstates (N_i), which are dominantly right-chiral, are usually named *right-handed neutrinos* while the light mass eigenstates (ν), which are observed in experiments, are dominantly left-chiral and are usually named *active neutrinos*. Before EWSB – when the Dirac masses were zero – chirality and helicity become equivalent ($\nu_i^R = N_i$ and $\nu_j^L = \nu_j$). Furthermore, in

contrast to only introducing Dirac mass terms, the resulting mass matrix for the active neutrinos, cf. equation (5.10), is also a Majorana mass matrix:

$$\mathcal{L}_0 = \sum_i \left(i\overline{\Psi}_{N_i} \not{\partial} \Psi_{N_i} - \frac{M_{N_i}}{2} \left(\overline{\Psi^c}_{N_i} \Psi_{N_i} + \overline{\Psi}_{N_i} \Psi^c_{N_i} \right) \right) + \sum_j \left(i\overline{\Psi}_{\nu_j} \not{\partial} \Psi_{\nu_j} - \sum_k \left(\frac{m_{jk}}{2} \overline{\Psi^c}_{\nu_k} \Psi_{\nu_j} + \frac{m^*_{jk}}{2} \overline{\Psi}_{\nu_k} \Psi^c_{\nu_j} \right) \right) . \tag{5.11}$$

Thus, neutrino-antineutrino oscillations are induced, resulting in the prediction of neutrinoless double beta decay, cf. e.g. reference [61]. The measurement of such a decay would manifest the Majorana type of the active neutrino masses. The type-I is the simplest and most popular model inducing Majorana masses for active neutrinos but there are also other models such as the type-II and type-III seesaw mechanisms or radiative seesaw models like the scotogenic model, cf. section 6.2, accomplishing this task.

Note that the active neutrino mass matrix, cf. equation (5.10), is not diagonal in the flavor basis so that similar to the CKM matrix in the quark sector, also a mixing matrix called Pontecorvo-Maki-Nakagawa-Sakata (PMNS) matrix occurs in the lepton sector. Defining the PMNS matrix similar to the CKM matrix, cf. equation (A.93), the corresponding angles are constrained by measurement, cf. equation (C.6).

In the following, first of all, the thermal rate of the two-body decay involving Majorana neutrinos, cf. section 5.1, and afterwards, the thermal rates of $2 \to 2$ scattering processes mediated by a Majorana neutrino, cf. section 5.2, are calculated. Both of them contribute to the time evolution of the L asymmetry and therefore are relevant for the investigations following in chapter 7. Finally, in section 5.3, CP violation in the context of the two-body decay of Majorana fermions is investigated and thermal leptogenesis is briefly discussed.

5.1 Thermal Rate of Two-Body Decays Involving Majorana Fermions

Considering the generalized interaction Lagrangian

$$\mathcal{L} \supset -y' \overline{\Psi}_\chi(x) \phi^\dagger(x) R \Psi_N(x) - y'^* \overline{\Psi}_N(x) L \phi(x) \Psi_\chi(x) \,, \tag{5.12a}$$

$$\mathcal{L}^c \supset -y'^* \overline{\Psi^c}_\chi(x) \phi^{c\dagger}(x) L \Psi^c_N(x) - y' \overline{\Psi^c}_N(x) R \phi^c(x) \Psi^c_\chi(x) \,, \tag{5.12b}$$

with a scalar field ϕ, a Dirac fermion χ, and a right-chiral Majorana fermion N, in case of $M_N > m_\chi + m_\phi$, $m_\chi > M_N + m_\phi$, or $m_\phi > M_N + m_\chi$, a decay of the heaviest particles is induced. The corresponding matrix elements are given by

$$i\mathcal{M} = \begin{cases} -iy' \overline{u}_\chi R u_N & \text{for } N \to \chi\phi \\ -iy'^* \overline{u}_N L u_\chi & \text{for } \chi \to N\phi^\dagger \\ -iy'^* \overline{u}_N L v_\chi & \text{for } \phi \to N\overline{\chi} \end{cases} , \tag{5.13a}$$

$$\begin{aligned} \Rightarrow \overline{|\mathcal{M}|^2} &= |y'_i|^2 \mathrm{Tr}\left[(\not{p}_\chi \pm m_\chi) R \not{p}_{N_i} \right] \\ &= 2|y'_i|^2 p_\chi p_{N_i} \,. \end{aligned} \tag{5.13b}$$

In case of $M_N > m_\chi + m_\phi$, in the rest frame of the decaying particle the decay width, cf. equation (2.25), is

$$\begin{aligned}\Gamma_{N\to\chi\phi} &= \frac{2|y_i'|^2 E_\chi M_N}{8\pi}\frac{|\vec{p}_\chi|}{M_N^2} = \frac{|y_i'|^2 M_N}{16\pi}\left(1+\frac{m_\chi^2}{M_N^2}-\frac{m_\phi^2}{M_N^2}\right)\lambda\left(1,\frac{m_\chi^2}{M_N^2},\frac{m_\phi^2}{M_N^2}\right)\\ &= \frac{|y_i'|^2 m_N}{16\pi}\left(1+a_\chi-a_\phi\right)\lambda\left(1,a_\chi,a_\phi\right)\,, \end{aligned} \tag{5.14}$$

where the abbreviations defined in equation (3.31) with $m_i = M_N$ are used. The decay width for $m_\chi > M_N + m_\phi$ is obtained by interchanging N and χ:

$$\begin{aligned}\Gamma_{\chi\to N\phi^\dagger} &= \frac{|y_i'|^2 m_\chi}{16\pi}\left(1+\frac{M_N^2}{m_\chi^2}-\frac{m_\phi^2}{m_\chi^2}\right)\lambda\left(1,\frac{M_N^2}{m_\chi^2},\frac{m_\phi^2}{m_\chi^2}\right)\\ &= \frac{|y_i'|^2 M_N}{16\pi}\sqrt{a_\chi}\left(1+\frac{1}{a_\chi}-\frac{a_\phi}{a_\chi}\right)\lambda\left(1,\frac{a}{a_\chi},\frac{a_\phi}{a_\chi}\right)\,. \end{aligned} \tag{5.15}$$

Finally, for $m_\phi > M_N + m_\chi$, the resulting decay width is given by

$$\begin{aligned}\Gamma_{\phi\to N\overline{\chi}} &= \frac{2|y_i'|^2(E_\chi E_N + |\vec{p}_N|^2)}{8\pi}\frac{|\vec{p}_N|}{m_\phi^2} = \frac{|y_i'|^2 m_\phi}{16\pi}\left(1-\frac{M_N^2}{m_\phi^2}-\frac{m_\chi^2}{m_\phi^2}\right)\lambda\left(1,\frac{M_N^2}{m_\phi^2},\frac{m_\chi^2}{m_\phi^2}\right)\\ &= \frac{|y_i'|^2 M_N}{16\pi}\sqrt{a_\phi}\left(1-\frac{1}{a_\phi}-\frac{a_\chi}{a_\phi}\right)\lambda\left(1,\frac{1}{a_\phi},\frac{a_\chi}{a_\phi}\right)\,. \end{aligned} \tag{5.16}$$

In the limit where the mass of the decaying particle is much larger than the masses of the decay products, the decay width simplifies to

$$\left(\Gamma_{N\to\chi\phi}/\Gamma_{\chi\to N\phi^\dagger}/\Gamma_{\phi\to N\overline{\chi}}\right) = \frac{|y_i'|^2 M_N}{16\pi}\left(1/\sqrt{a_\chi}/\sqrt{a_\phi}\right)\,. \tag{5.17}$$

According to equation (3.27), the corresponding thermal rate in case of $M_N > m_\chi + m_\phi$ is given by

$$\gamma_{N\to\chi\phi} = \frac{M_N^4}{2\pi^2}\sqrt{a_{\Gamma_{N\to\chi\phi}}}\,\frac{K_1(z)}{z}\,, \tag{5.18}$$

with $z = M_N/T$, while in case of $m_\phi > M_N + m_\chi$, it becomes

$$\gamma_{\phi\to N\overline{\chi}} = \frac{m_\phi^4}{2\pi^2}\frac{\Gamma_{\phi\to N\overline{\chi}}}{m_\phi}\frac{K_1(z')}{z'} = \frac{M_N^4}{2\pi^2}\sqrt{a_{\Gamma_{\phi\to N\overline{\chi}}}}\,a_\phi\frac{K_1(\sqrt{a_\phi}\,z)}{z}\,, \tag{5.19}$$

with $z' = m_\phi/T = \sqrt{a_\phi}z$. Since the thermal rate of the (inverse) decay at $T \sim m$ often dominates the Boltzmann equations, it makes sense to improve the used approximation by using the Fermi-Dirac and Bose-Einstein statistics instead of Boltzmann statistics [30]:

$$\frac{K_1(\sqrt{a_i}\,z)}{z} \to \frac{1}{2}\int\limits_{\sqrt{a_i}}^{\infty} dE_i'\sqrt{(E_i')^2-a_i}\,\frac{e^{zE_i'}}{e^{zE_i'}\pm 1}\int\limits_{-1}^{1} dx\frac{1}{e^{zE_{f_1}'}\pm 1}\frac{1}{e^{zE_{f_2}'}\pm 1}\,, \tag{5.20}$$

with $E_i' = E_i/M_N$. Note that the decay width can be excluded from the integral because it is independent of x.

5.2 Thermal Rate of Majorana Fermion Mediated Fermion Number Violating $2 \to 2$ Scattering Processes

Considering the interaction term given in equation (5.12), besides the (inverse) decay, also scattering processes violating the particle-antiparticle asymmetry of χ and ϕ ($\chi\phi \to \chi^c\phi^c$ and $\chi\chi \to \phi^c\phi^c$) are induced.
The matrix element of the process $\chi\phi \to \chi^c\phi^c$ mediated by N_i (s- and t-channel process) is given by

$$\mathcal{M} = -i\overline{u^c}_{\chi,r}(-iy_i'^*)\frac{iM_{N_i}}{q^2 - M_{N_i}^2 + iM_{N_i}\Gamma_{N_i}}(-iy_i'^*)Lu_{\chi,s}\,. \tag{5.21}$$

Evaluating the spin sum

$$\sum_{r,s}\mathrm{Tr}\big[Ru^c_{\chi,r}\overline{u^c}_{\chi,r}Lu_{\chi,s}\overline{u}_{\chi,s}\big] = \mathrm{Tr}\big[R(\not{p}_3 - m_3)L(\not{p}_1 + m_1)\big] = 2(p_1p_3)\,, \tag{5.22}$$

the squared matrix element summed over all spins is given by

$$\sum_{r,s}|\mathcal{M}|^2 = |y_i'|^4\frac{M_{N_i}^2(-t+2m_\chi^2)\left[\left(s+t-2M_{N_i}^2\right)^2 + 4M_{N_i}^2\Gamma_{N_i}^2\right]}{\left[st - M_{N_i}^2\left(s+t-M_{N_i}^2+\Gamma_{N_i}^2\right)\right]^2 + M_{N_i}^2\Gamma_{N_i}^2\left(s+t-2M_{N_i}^2\right)^2}\,. \tag{5.23}$$

Using equation (D.8), the reduced cross section, cf. equation (3.30), is obtained:

$$\begin{aligned}\hat{\sigma}_{N,s}(u) &:= \int_0^2 dx\,\hat{\sigma}_{Ns}(u,x) = \int_0^2 dx\frac{|y_i'|^4}{32\pi}\left(\lambda[u,a_\chi,a_\phi]^2\frac{x}{u} + 4a_\chi\right)\frac{\lambda[u,a_\chi,a_\phi]^2}{u^2}\\ &\times\frac{\left(2u - \lambda[u,a_\chi,a_\phi]^2\frac{x}{u} - 4\right)^2 + 16a_{\Gamma_{N_i}}}{\left[\lambda[u,a_\chi,a_\phi]^2 x + \left(2u - \lambda[u,a_\chi,a_\phi]^2\frac{x}{u} - 2 + a_{\Gamma_{N_i}}\right)\right]^2 + a_{\Gamma_{N_i}}\left(2u - \lambda[u,a_\chi,a_\phi]^2\frac{x}{u} - 4\right)^2}\,.\end{aligned} \tag{5.24}$$

The corresponding thermal rate γ_{Ns} can be evaluated using equation (3.29) with $m_i = M_{N_i}$ and $u_{\min} = (\sqrt{a_\phi} + \sqrt{a_\chi})^2$.
However, the resulting thermal rate has to be calculated numerically, which can be difficult when the decay $N \to \chi\phi$ is kinematically allowed because in this case the s-channel propagator hits the resonance. Furthermore, as discussed in section 2.10, this resonant contribution is already taken into account by the thermal rate of the (inverse) decay $\gamma_{N\to\chi\phi}$ calculated in the previous section, cf. equation (5.18). Thus, γ_{Ns} includes $\gamma_{N\to\chi\phi}/2$ [30], where the factor $1/2$ appears because N can decay into both χ and χ^c. To obtain a numerically stable formula for the subtracted thermal rate ($\gamma_{Ns}^{\mathrm{sub}} = \gamma_{Ns} - \gamma_{N\to\chi\phi}/2$), $\gamma_{N\to\chi\phi}$ can be rewritten using equation (D.19):

$$\frac{\gamma_{N\to\chi\phi}}{2} = \frac{M_{N_i}^4}{4\pi^3}a_{\Gamma_{N_i}}\frac{K_1(z)}{z}\int_{-\infty}^{\infty}du\,\frac{1}{(u-1)^2 - a_{\Gamma_{N_i}}} := \frac{M_{N_i}^4}{64\pi^4}\int_{-\infty}^{\infty}du\,\frac{K_1(z)}{z}\int_0^2 dx\,\hat{\sigma}_N(u,x)\,, \tag{5.25}$$

with

$$\hat{\sigma}_N(u,x) = \frac{|y_i'|^4}{32\pi}\left(\lambda[1,a_\chi,a_\phi]^2 x + 4a_\chi\right)\lambda[1,a_\chi,a_\phi]^2\frac{1}{(u-1)^2 - a_{\Gamma_{N_i}}}\,. \tag{5.26}$$

Consequently, the subtracted thermal rate can be expressed as

$$\gamma_{N,s}^{\text{sub}} = \frac{M_{N_i}^4}{64\pi^4} \int_0^2 dx \Bigg[- \int_{-\infty}^{(\sqrt{a_\phi}+\sqrt{a_\chi})^2} du\, \hat{\sigma}_N(u,x) \frac{K_1(z)}{z} + \int_{(\sqrt{a_\phi}+\sqrt{a_\chi})^2}^{\infty} du \left(\sqrt{u}\, \hat{\sigma}_{Ns}(u,x) \frac{K_1(\sqrt{u}z)}{z} - \hat{\sigma}_N(u,x) \frac{K_1(z)}{z} \right) \Bigg] \overset{M_{N_i} \gg T}{\approx} \frac{|y_i|^4 T^6}{8\pi^5 M_{N_i}^2}\,, \tag{5.27}$$

where the resonance is erased from the integral.
Moreover, the relation

$$\int_{u_{\min}}^{2-u_{\min}} f(u) du = \int_{u_{\min}}^{1} \big[f(u) + f(2-u) \big] du\,, \tag{5.28}$$

can be used to subtract terms which are linear in $u-1$. This simple trick can further suppress the maximal value of the integrand by orders of magnitudes because terms which are linear in $u-1$ multiplied with the resonance can be very large while terms of higher order in $u-1$ are unimportant. This can be understood from the fact that the resonance scales with $1/(u-1)^2$ for $(u-1)^2 \gtrsim a_{\Gamma_{N_i}}$. Finally, the integral up to $u_{\min}$ can be solved analytically, cf. equation (D.19):

$$-\int_0^2 dx \int_{-\infty}^{(\sqrt{a_\phi}+\sqrt{a_\chi})^2} du\, \hat{\sigma}_N(u,x) \frac{K_1(z)}{z} = -4\pi \sqrt{a_{\Gamma_{N_i}}} \frac{K_1(z)}{z} \left[2 \arctan\left(\frac{(\sqrt{a_\phi}+\sqrt{a_\chi})^2 - 1}{\sqrt{a_{\Gamma_{N_i}}}} \right) + \pi \right]. \tag{5.29}$$

For the process $\chi\chi \to \phi^c\phi^c$, the matrix element ($t$- and u-channel process) is equivalent to the matrix element of $\chi\phi \to \chi^c\phi^c$, cf. equation (5.21). Hence, the squared matrix element summed over all spins becomes

$$\sum_{r,s} |\mathcal{M}|^2 = |y_i'|^4 \frac{4M_{N_i}^2 (s-2m_\chi^2) \left[(m_\phi^2 + m_\chi^2 - s/2 - M_{N_i}^2)^2 + M_{N_i}^2 \Gamma_{N_i}^2 \right]}{\lambda[(m_\phi^2 + m_\chi^2 - s/2 - M_{N_i}^2)^2, (s-4m_\phi^2)(s-4m_\chi^2)x^2/4, -M_{N_i}^2\Gamma_{N_i}^2]^2}\,. \tag{5.30}$$

Using equation (D.7), the reduced cross section can be written as

$$\hat{\sigma}_{N,t}(u) = \int_{-1}^{1} dx \frac{|y_i'|^4}{4\pi} (u - 2a_\chi) \left(1 - 4\frac{a_\phi}{u} \right) \frac{\sqrt{u} - 2\sqrt{a_\chi}}{\sqrt{u} - 2\sqrt{a_\phi}} \times \frac{(a_\phi + a_\chi - 1 - u/2)^2 + a_{\Gamma_{N_i}}}{\lambda[(a_\phi + a_\chi - 1 - u/2)^2, (u-4a_\phi)(u-4a_\chi)x^2/4, -a_{\Gamma_{N_i}}]^2}\,, \tag{5.31}$$

so that the induced thermal rate is given by

$$\gamma_{N,t} = \frac{M_{N_i}^4}{64\pi^4} \int_{\max[4a_\phi, 4a_\chi]}^{\infty} du\, \sqrt{u}\, \hat{\sigma}_{Nt}(u) \frac{K_1(\sqrt{u}z)}{z} \overset{M_{N_i} \gg T}{\approx} \frac{|y_i|^4 T^6}{4\pi^5 M_{N_i}^2}\,. \tag{5.32}$$

5.3 CP Violation in the Two-Body Decay of Majorana Fermions and Thermal Leptogenesis

In section 5.1, the two-body decay width of a Majorana fermion N into ϕ and χ is calculated. The corresponding thermal rate for not too large coupling constants ($y' \lesssim 1$) clearly dominates the interaction rate involving the Majorana fermion for the temperature region where it becomes Boltzmann suppressed ($M_N/10 \lesssim T \lesssim M_N$). Furthermore, the interaction rate involving the Majorana fermion is most efficient in the same temperature region ($\Gamma/\mathsf{H}(T)$ becomes maximal). Cf. figure 7.1 for an exemplary plot of the dominant thermal rates. Consequently, for most leptogenesis scenarios, the CP violation induced by the two-body decay is the essential ingredient for the generation of an L asymmetry. As was discussed in section 3.2, the relevant quantity for the generation of an asymmetry, cf. equation 3.21, is

$$\delta_{CP,N\to\chi\phi} = \frac{|\mathcal{M}_{N\to\chi\phi}|^2 - |\mathcal{M}_{\overline{N}\to\overline{\chi}\phi^\dagger}|^2}{|\mathcal{M}_{N\to\chi\phi}|^2 + |\mathcal{M}_{\overline{N}\to\overline{\chi}\phi^\dagger}|^2} = \frac{\Gamma_{N\to\chi\phi} - \Gamma_{\overline{N}\to\overline{\chi}\phi^\dagger}}{\Gamma_{N\to\chi\phi} + \Gamma_{\overline{N}\to\overline{\chi}\phi^\dagger}}\,. \tag{5.33}$$

As can be deduced from equation 2.132, at least two Majorana fermions decaying both into at least two different final states, where at least two of the decay products for both Majorana fermions must be equivalent, are required to obtain a non-vanishing CP violation[2]. For this reason, in the following, a model with multiple Majorana fermions N_i decaying into a scalar boson $\phi(x)$ and non-Majorana fermions χ_j is considered. In principle also multiple scalar bosons can be considered. However, this only induces an extra sum over all scalar bosons and does not change the given results relevantly.

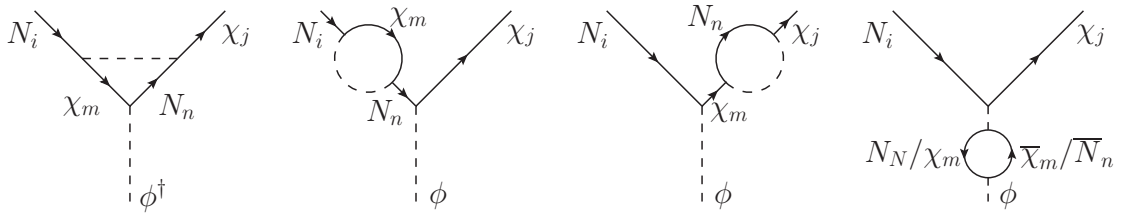

Figure 5.1: One-loop corrections to the Yukawa interaction term $y'_{ij}\overline{\Psi}_\chi(x)\phi^\dagger(x)\Psi_N(x)$, where the left diagram with $\phi^\dagger(x)$ as final state only contributes when $\phi(x)$ is a real scalar field.

As discussed in section 3.2, due to the unitarity of the S-matrix, only CP violation of processes involving fermion number violation can induce a non-vanishing particle-antiparticle asymmetry. Such a source of fermion number violation are Majorana fermions where the energy eigenstates can decay into both, particles and antiparticles. This can be seen by considering one-loop corrections to the Yukawa interaction term $y'_{ij}\overline{\Psi}_\chi(x)\phi^\dagger(x)\Psi_N(x)$, cf. figure 5.1, which are all proportional to $y'_{im}y'^*_{nm}y'_{nj}$ so that the induced CP violation becomes[3]

$$\delta_{CP} \propto \sum_{m,n} f(M_{N_i}, M_{N_n})\,\mathrm{Im}[y'_{im}y'^*_{nm}y'_{nj}y'^*_{ij}]\,, \tag{5.34}$$

[2]Note that this statement is also valid for CP violation induced by vertex loop corrections which is not considered in section 2.10

[3]Note that all other complex phases arising e.g. from including the decay widths of M_{N_i} and M_{N_n} are CP-even phases.

implying that summing over all non-Majorana fermions (j) the total amount of particle-antiparticle asymmetry produced by the decay of N_i vanishes. Note that this statement is only valid at one-loop order. In contrast, e.g. considering two-loop corrections, the CP violation becomes

$$\delta_{CP} \propto \sum_{m_1,m_2,n_1,n_2} f_2(M_{N_i}, M_{N_{n_1}}, M_{N_{n_2}}) \operatorname{Im}[y'_{im_2} y'^{*}_{n_2 m_2} y'_{n_2 m_1} y'^{*}_{n_1 m_1} y'_{n_2 j} y'^{*}_{ij}] \,, \tag{5.35}$$

which in case of considering at least three different right-handed Majorana neutrinos does not vanish when summing over all j.

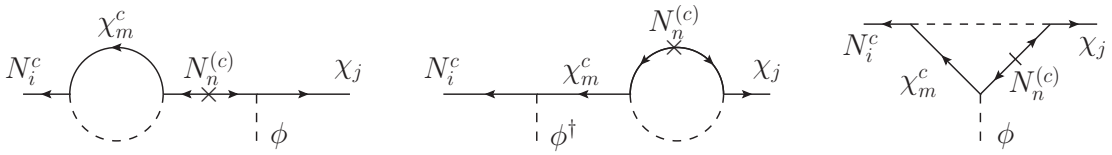

Figure 5.2: One-loop corrections to the Yukawa-like interaction term $\sim \overline{\Psi}_\chi(x)\phi^\dagger(x)\Psi^c_N(x)$. The left diagram considers N_i-N_n mixing at first order, the center diagram considers ν_j-ν_m mixing at first order, and the right diagram shows the one-loop vertex correction. The center-loop correction with $\phi^\dagger(x)$ as final state only contributes when $\phi(x)$ is a real scalar field.

Thus, to obtain a total amount of CP violation at one-loop order interference with a Yukawa-like interaction term $\sim \overline{\Psi}_\chi(x)\phi^\dagger(x)\Psi^c_N(x)$, being allowed due to the Majorana mass, need to be considered, cf. figure 5.2. In this case, all loop contributions are proportional to $y'^{*}_{im} y'_{nm} y'_{nj}$ so that the induced CP violation becomes

$$\delta_{CP} \propto \sum_{m,n} g(M_{N_i}, M_{N_n}) \operatorname{Im}[y'^{*}_{im} y'_{nm} y'_{nj} y'^{*}_{ij}] \,, \tag{5.36}$$

which does not vanish when summing over all final states.

Consequently, to obtain the particle-antiparticle asymmetry induced by the decay of the Majorana fermion, the interference of the tree-level decay with the loop induced decays shown in figure 5.2 have to be considered. Because here leptogenesis is studied, from now on right-handed Majorana fermions N_i decaying into a Higgs doublet H and lepton doublets ℓ_j are considered. In this case, H only corresponds to a real scalar field after EWPT, implying that the center diagram shown in figure 5.2 does not induce CP violation before EWSB.

In the case of not very strongly degenerate masses for the Majorana fermions ($E_i - E_j \gg \Gamma_i - \Gamma_j$), the amount of CP violation originating from the decay width induced mixing between right-handed neutrinos can be calculated perturbatively in orders of N_i-N_n mixing. At first order in the mixing, cf. left diagram in figure 5.2, the resulting CP violation ignoring thermal corrections is given by [17]

$$\delta^{\text{wave}}_{CP,N_i\to\ell_j H} = -\frac{1}{8\pi} \sum_{m,n\neq i} \frac{M_{N_i} M_{N_n}}{M^2_{N_n} - M^2_{N_i}} \frac{\operatorname{Im}\left[y^*_{nm} y_{im} y^*_{nj} y_{ij}\right]}{|y_{ij}|^2} \,, \tag{5.37}$$

where $M_{N_i}, M_{N_n} \gg m_{\ell_j} + m_H$ is assumed, n sums over all other Majorana fermions, and m over all decay products. Furthermore, using the same approximation, the CP violation originating from

the vertex loop correction, cf. the right diagram in figure 5.2, is determined by [17]

$$\delta^{\text{vertex}}_{CP,N_i\to\ell_j H} = \frac{1}{8\pi}\sum_{m,n\neq i}\frac{M_{N_n}}{M_{N_i}}\frac{\text{Im}\left[y^*_{nm}y_{im}y^*_{nj}y_{ij}\right]}{|y_{ij}|^2}\left[1-\left(\frac{M^2_{N_i}+M^2_{N_n}}{M^2_{N_i}}\right)\ln\left(\frac{M^2_{N_i}+M^2_{N_n}}{M^2_{N_n}}\right)\right]$$
$$\overset{M_{N_n}\gg M_{N_i}}{\approx} -\frac{1}{16\pi}\sum_{m,n\neq i}\frac{M_{N_i}}{M_{N_n}}\frac{\text{Im}\left[y^*_{nm}y_{im}y^*_{nj}y_{ij}\right]}{|y_{ij}|^2}\,. \tag{5.38}$$

As expected, in case of closely degenerated masses ($|M_{N_i}-M_{N_n}|\ll M_{N_i}$), the CP violation is mainly determined by the wave contribution and can in principle be sizable even when small couplings are considered. However, in the typically considered case of hierarchical masses $M_{N_n}\gg M_{N_i}$, both contributions are relevant and the total amount of CP violation becomes

$$\epsilon_{N_i} := \frac{\sum_j(\Gamma_{N_i\to\ell_j H}-\Gamma_{\overline{N}_i\to\bar{\ell}_j H^\dagger})}{\sum_j(\Gamma_{N_i\to\ell_j H}+\Gamma_{\overline{N}_i\to\bar{\ell}_j H^\dagger})} = -\frac{3}{16\pi}\sum_{m,j,n\neq i}\frac{M_{N_i}}{M_{N_n}}\frac{\text{Im}\left[y^*_{nm}y_{im}y^*_{nj}y_{ij}\right]}{\sum_k|y'_{ik}|^2}\,, \tag{5.39}$$

$$\Rightarrow |\epsilon_{N_i}| \leq \frac{3M_{N_i}}{16\pi}\sum_{m,j,n\neq i}\frac{1}{M_{N_n}}\frac{|y^*_{nm}y^*_{nj}y_{im}y_{ij}|}{\sum_k|y_{ik}|^2} \leq \frac{3M_{N_i}}{16\pi}\sum_{m,j,n\neq i}\frac{|y_{nm}||y_{nj}|}{M_{N_n}}\frac{|y_{im}||y_{ij}|}{\sum_k|y_{ik}|^2}\,. \tag{5.40}$$

Next, using

$$\sum_{j,m}|y_{nj}||y_{nm}||y_{ij}||y_{im}| \leq \sum_{j,m}|y_{nm}|^2|y_{ij}|^2\,, \tag{5.41}$$

and equation (5.10), the upper bound on the CP violation can be written as

$$|\epsilon_{N_i}| \leq \frac{3M_{N_i}}{16\pi}\sum_{m,n\neq i}\frac{|y_{nm}|^2}{M_{N_n}} \leq \frac{3M_{N_i}}{16\pi v^2}\sum_j(m^I_\nu)_{jj}\,. \tag{5.42}$$

Finally, using

$$0.12\text{ eV} \geq \sum_j(m^I_\nu)_{jj} \geq \sqrt{\Delta m^2_{\text{atm}}}+\sqrt{\Delta m^2_{\text{sol}}} \sim 0.06\text{ eV}\,, \tag{5.43}$$

cf. equations C.7 and C.4, the upper bound on the CP violation becomes[4]

$$|\epsilon_{N_i}| \lesssim \frac{M_{N_i}}{\text{GeV}}\times 10^{-16}\,. \tag{5.44}$$

Considering for simplicity only the thermal rate induced by the two body decay ($\gamma^D_{N_i}$), the Boltzmann equations describing the time evolution of the number density of N_i, cf. equation (3.17), is given by

$$z\frac{dY_{N_i}}{dz} = -\frac{\gamma^D_{N_i}}{\mathsf{H}(T)s}\left(\frac{Y_{N_i}}{Y^{\text{eq}}_{N_i}}-1\right)\,, \tag{5.45}$$

[4]This upper bound coincides with the value given in the current literature, cf. e.g. reference [6]

while for the $B-L$ asymmetry, cf. equation (3.26),

$$z\frac{d\mu_{B-L}}{dz} = \frac{6\gamma^D_{N_i}}{\mathsf{H}(T)T^3}\left[-\alpha\beta\mu_{B-L} - \epsilon_{N_i}\left(\frac{Y_{N_i}}{Y^{\text{eq}}_{N_i}} - 1\right)\right] \qquad \text{with} \quad \alpha \geq 0 \tag{5.46}$$

is obtained, where the number densities of the decay products (ℓ_j and H) are assumed to be in thermal equilibrium and the non-trivial prefactor α considers the shift of the produced $B-L$ between different degrees of freedom induced by SM processes. A detailed analysis of the obtained Boltzmann equations shows that the produced $B-L$ asymmetry generated by the CP violating decay of N_i is at least roughly one order of magnitudes smaller than $|\epsilon_{N_i}|$, cf. e.g. reference [11]. Thus, $|\epsilon_{N_i}| \sim 10^{-6}$ and, consequently, $M_{N_i} \gtrsim 10^{10}$ GeV are required to generate a B asymmetry of the observed size, cf. equations (4.18) and (4.20).

Note that this statement is only true if a vanishing initial abundance for N_i is assumed. In contrast, considering a thermal initial abundance, the decay width of N_i can be chosen to be so small that the corresponding thermal rate remains significantly below the Hubble expansion rate for all temperatures. As a consequence, N_i simply decays when the temperature falls significantly below M_{N_i} i.e. the age of the universe becomes comparable to the inverse of the decay width. Using this initial condition, $|\mu_{B-L}/\epsilon_{N_i}| \sim 1$ can be achieved, cf. e.g. reference [11], and, consequently, $M_{N_i} \gtrsim 10^9\ GeV$ is required to generate a B asymmetry of the observed size. However, other processes producing the thermal abundance of N_i at higher temperatures are needed.

Note that in order to fulfill the out-of-equilibrium condition, while still maintaining a sufficiently efficient thermal rate resulting in a maximal ratio for $|\mu_{B-L}/\epsilon_{N_i}|$, the decay rate should at maximum be of the order of the Hubble expansion rate, cf. reference [11]. Using equations (3.38) and (5.17), this leads to the condition

$$\sum_j \frac{6\gamma_{N_i\to\ell_j H}}{\mathsf{H}(T)T^3} \lesssim \sum_j \frac{|y_{ij}|^2}{8\pi A_{\mathsf{H}} M_{N_i}} = \frac{1}{4\pi A_{\mathsf{H}} v^2}\sum_j (m^I_\nu)^i_{jj} \approx \frac{100}{0.12\text{eV}}\sum_j (m^I_\nu)^i_{jj} \overset{!}{\approx} 1\,, \tag{5.47}$$

where $(m^I_\nu)^i_{jk}$ are the active neutrino masses induced by N_i by the type-I seesaw mechanism, cf. equation (5.10), and an additional factor of two arises in the decay width since the decay into doublets is considered here. Thus, the contribution of N_i to the active neutrino mass can still be sizable ($\sim 10^{-3}$ eV). Furthermore, the contribution to the active neutrino mass can be larger if M_{N_i} significantly above 10^{10} GeV are considered. In this case, larger values for $|\epsilon_{N_i}|$ are possible and, for this reason, a less efficient asymmetry generation (smaller $|\mu_{B-L}/\epsilon_{N_i}|$) is sufficient to explain the observed B asymmetry.

6 Investigation of an Extended Higgs Sector With Focus on the Inert Higgs Model

In section 2.7, the Higgs mechanism basing on the concept of SSB was introduced. There, only the most simple case of having one scalar field transforming non-trivially under a certain gauge transformation was discussed. However, in general, also multiple scalar fields can be introduced, resulting in an extended parameter space. This extended parameter space e.g. allows for an altered dynamic of the EWPT and additional sources of CP violation, which are both required for electroweak baryogenesis, cf. section 4.2. Moreover, the additionally introduced scalar particles may include a DM candidate. Because in this thesis, the focus is on DM, a simple extension known as inert Higgs model is investigated in more detail. This extension is of special interest because it not only includes a DM candidate but in combination with right-handed neutrinos – known as scotogenic model – also allows for a radiative generation of the active neutrino masses which are suppressed compared to the active neutrino masses induced by the type-I seesaw mechanism. As a consequence, larger Yukawa couplings of the neutrino sector are allowed without being in conflict with the Planck bound on the sum of the active neutrino masses, cf. equation (C.7).

Considering e.g. an extended Higgs sector with m complex $SU(2)_L$ Higgs doublets $(\phi_i, \dots \phi_m)$ which all carry the same hypercharge ($Y_{\phi_i} = Y_H = 1/2$), the corresponding Lagrangian is given by

$$\mathcal{L} \supset \sum_{i=1}^{m} \left[\left(D_\mu \phi_i\right)^\dagger \left(D^\mu \phi_i\right) - y_{i,ff'} \bar{\Psi}_f \phi_i \Psi_{f'} - y^*_{i,ff'} \bar{\Psi}_{f'} \phi_i^\dagger \Psi_f \right] - V_m(x)\,, \tag{6.1}$$

where the m Higgs doublet potential in the most general form can be written as

$$\begin{aligned} V_m(x) = \sum_{i=1}^{m} \Bigg[& m_i^2 (\phi_i^\dagger \phi_i) + \frac{\lambda_i}{2} (\phi_i^\dagger \phi_i)^2 + \sum_{j=1}^{i-1} \Bigg(\lambda_{3,ij} (\phi_i^\dagger \phi_i)(\phi_j^\dagger \phi_j) + \lambda_{4,ij} (\phi_i^\dagger \phi_j)(\phi_j^\dagger \phi_i) \\ & + \frac{\lambda_{5,ij}}{2} \left[(\phi_i^\dagger \phi_j)^2 + (\phi_j^\dagger \phi_i)^2 \right] + \Big(m_{ij}^2 + \lambda_{6,ij} (\phi_i^\dagger \phi_i) + \lambda_{7,ij} (\phi_j^\dagger \phi_j) \Big) (\phi_i^\dagger \phi_j + \phi_j^\dagger \phi_i) \Bigg) \Bigg]\,. \end{aligned} \tag{6.2}$$

If the potential has a minimum at $\langle \phi_i \rangle \neq 0$, once again the $SU(2)_L \times U(1)_Y$ symmetry of the SM is broken and three of the four gauge bosons become massive:

$$m_{W^\pm}^2 = \frac{g^2}{4} v^2\,, \qquad m_Z^2 = \frac{g^2 + g'^2}{4} v^2\,, \qquad \text{and} \qquad m_A = 0\,, \tag{6.3}$$

with the VEV $v^2 = \sum \langle \phi_i \rangle^2$. Furthermore, three degrees of freedom of the Higgs sector corresponding to the Goldstone bosons become unphysical.

In following, the inert Higgs model is investigated and experimental constraints are discussed, cf. section 6.1. Afterwards, in section 6.2, the scotogenic model – an extension of the inert Higgs model

including right-chiral Majorana neutrinos – where the active neutrino masses become loop induced is introduced. Finally, in section 6.3, thermal corrections to the effective Higgs potential leading to a restoration of the $SU(2)_L \times U(1)_Y$ symmetry are discussed and the temperature dependence of the inert Higgs potential is investigated in detail.

6.1 The Inert Higgs Model

The inert Higgs model is a 2HDM ($m = 2$) where the additional Higgs doublet ϕ transforms non-trivially under an imposed Z_2 symmetry ($\phi(x) \to -\phi(x)$, *odd* transformation), while all SM particles including the SM Higgs doublet H transform trivially ($H(x) \to H(x)$, *even* transformation). Consequently, the Yukawa interaction involving only SM particles and ϕ vanishes, implying that the masses of the SM fermions are determined by

$$m_f^2 = y_f^2 \langle H \rangle^2 \,. \tag{6.4}$$

Furthermore, the imposed Z_2 symmetry simplifies the Higgs potential to

$$\begin{aligned} V_{\text{inert}}(x) = {} & m_H^2 H^\dagger(x) H(x) + m_\phi^2 \phi^\dagger(x)\phi(x) + \frac{\lambda_1}{2}[H^\dagger(x)H(x)]^2 + \frac{\lambda_2}{2}[\phi^\dagger(x)\phi(x)]^2 \\ & + \lambda_3 [H^\dagger(x)H(x)][\phi^\dagger(x)\phi(x)] + \lambda_4 [H^\dagger(x)\phi(x)][\phi^\dagger(x)H(x)] \\ & + \frac{\lambda_5}{2}\left([H^\dagger(x)\phi(x)]^2 + [\phi^\dagger(x)H(x)]^2\right) . \end{aligned} \tag{6.5}$$

For the vacuum to be stable, a finite VEV has to globally minimize this Higgs potential, which, at tree level, leading to the three conditions

$$\lambda_1 > 0\,, \qquad \lambda_2 > 0\,, \quad \text{and} \quad \lambda_1 + \lambda_2 y^2 + 2\lambda_3 |y| + 2(\lambda_4 + \lambda_5) y > 0 \quad \forall\, y \in \mathbb{R}\,. \tag{6.6a}$$

To constrain λ_3, λ_4, and λ_5, the left side of the third condition has to be minimized in y, whereas the boundary conditions ($y \to 0$ and $y \to \pm\infty$) are satisfied by the first two conditions. Because of the absolute value appearing in the third condition, all cases ($\lambda_3 > 0 \;\vee\; \lambda_3 < 0$ and $\lambda_4 + \lambda_5 > 0 \;\vee\; \lambda_4 + \lambda_5 < 0$) have to be considered individually which all lead to the condition

$$|\lambda_4 + \lambda_5| < \sqrt{\lambda_1 \lambda_2} + \lambda_3\,. \tag{6.7}$$

Thus, to obtain a potential that is stable at tree level, λ_3 is not allowed to take on negative values smaller than $\sqrt{\lambda_1\lambda_2}$. Moreover, λ_4 and λ_5 can be further constrained by demanding the conservation of the same charge for both VEVs, leading to the conditions $\lambda_5 < 0$ and $\lambda_4 + \lambda_5 < 0$.

Next, to calculate the VEVs of $\langle H \rangle = v_H$ and $\langle \phi \rangle = v_\phi$, the inert Higgs potential has to be minimized, leading to the conditions

$$\left(m_{11} + \frac{\lambda_1}{2} v_H^2 + \frac{\lambda_{345}}{2} v_\phi^2\right) v_H = 0\,, \tag{6.8a}$$

$$\left(m_{22} + \frac{\lambda_2}{2} v_\phi^2 + \frac{\lambda_{345}}{2} v_H^2\right) v_\phi = 0\,, \tag{6.8b}$$

with $\lambda_{345} = \lambda_3 + \lambda_4 + \lambda_5$. For non-vanishing VEVs, it is useful to rotate the fields:

$$\phi_1(x) = H(x)\cos\beta + \phi(x)\sin\beta\,, \tag{6.9a}$$
$$\phi_2(x) = -H(x)\sin\beta + \phi(x)\cos\beta\,, \tag{6.9b}$$

with

$$\tan\beta = \frac{v_\phi}{v_H}\,. \tag{6.10}$$

Using this redefinition, only ϕ_1 obtains a VEV. Next, to obtain the mass eigenstates, it is useful to start from

$$\phi_1(x) = \frac{1}{\sqrt{2}}\begin{pmatrix} \varphi_1(x) + i\varphi_2(x) \\ i\varphi_3(x) + H_0(x)c_\beta + \phi_0(x)s_\beta + v \end{pmatrix}, \tag{6.11a}$$
$$\phi_2(x) = \frac{1}{\sqrt{2}}\begin{pmatrix} \eta_1(x) + i\eta_2(x) \\ i\eta_3(x) - H_0(x)s_\beta + \phi_0(x)c_\beta \end{pmatrix}, \tag{6.11b}$$

where the abbreviations $v = \sqrt{v_H^2 + v_\phi^2}$, $c_\beta = \cos\beta$, and $s_\beta = \sin\beta$ are used.
Evaluating the mass matrices for (φ_i, η_i) and making use of the conditions 6.8a and (6.8b), it can be seen that the masses of the Goldstone bosons φ_1, φ_2, and φ_3 vanish while the masses of η_1, η_2, and η_3 are given by

$$m^2_{\eta_{1,2}} = m^2_\phi + \frac{\lambda_3}{2}v^2 \qquad \text{and} \qquad m^2_{\eta_3} = m^2_\phi + \frac{\lambda_3+\lambda_4-\lambda_5}{2}v^2 \qquad \text{for } v_H \neq 0 \wedge v_\phi = 0\,, \tag{6.12a}$$
$$m^2_{\eta_{1,2}} = m^2_H + \frac{\lambda_3}{2}v^2 \qquad \text{and} \qquad m^2_{\eta_3} = m^2_H + \frac{\lambda_3+\lambda_4-\lambda_5}{2}v^2 \qquad \text{for } v_H = 0 \wedge v_\phi \neq 0\,, \tag{6.12b}$$
$$m^2_{\eta_{1,2}} = -\frac{\lambda_4+\lambda_5}{2}v^2 \qquad \text{and} \qquad m^2_{\eta_3} = -\lambda_5 v^2 \qquad \text{for } v_H \neq 0 \wedge v_\phi \neq 0\,. \tag{6.12c}$$

Moreover, the mass matrix of H_0 and ϕ_0 is only diagonal if either v_H or v_ϕ vanishes:

$$m^2_{H_0} = \lambda_1 v^2 \qquad m^2_{\phi_0} = m^2_\phi + \frac{\lambda_3+\lambda_4+\lambda_5}{2}v^2 \qquad \text{for } v_H \neq 0\,, \tag{6.13a}$$
$$m^2_{\phi_0} = \lambda_2 v^2 \qquad m^2_{H_0} = m^2_H + \frac{\lambda_3+\lambda_4+\lambda_5}{2}v^2 \qquad \text{for } v_\phi \neq 0\,. \tag{6.13b}$$

If both v_H and v_ϕ are non-zero the eigenvalues of the mass matrix are given by

$$\frac{v^2}{2}\left(\lambda_1 c_\beta^2 + \lambda_2 s_\beta^2 \pm \sqrt{\left(\lambda_1 c_\beta^2 - \lambda_2 s_\beta^2\right)^2 + 4\left(\lambda_3+\lambda_4+\lambda_5\right)^2 c_\beta^2 s_\beta^2}\right), \tag{6.14}$$

where the particle with a larger mass is called $\tilde{H}$ and the lighter one h. It is further common to define

$$\tan(\alpha) = 2c_\beta s_\beta\left(\lambda_3+\lambda_4+\lambda_5\right) \Big/ \left(\lambda_1 c_\beta^2 - \lambda_2 s_\beta^2\right), \tag{6.15}$$

so one can write $H_0 = h\cos\alpha - \tilde{H}\sin\alpha$ and $\phi_0 = h\sin\alpha + \tilde{H}\cos\alpha$. Note that using this convention, in the case of $v_H = 0$ or $v_\phi = 0$, h corresponds to the remaining physical component of the broken

field, while $\tilde{H}$ corresponds to the real electrical neutral component of the unbroken field.
For a more detailed discussion of the 2HDM, the interested reader is referred to e.g. reference [10].

Considering the case where only H takes on a non-vanishing VEV, the inert Higgs model contains the DM candidate $\phi_0 = \tilde{H}$. For that, $\tilde{H}$ has to be the lightest component of ϕ:

$$m_{\tilde{H}}^2 = m_\phi^2 + \frac{\lambda_3+\lambda_4+\lambda_5}{2}v^2 < m_{\eta^\pm}^2 = m_{\eta_{1,2}}^2 = m_\phi^2 + \frac{\lambda_3}{2}v^2\,, \tag{6.16a}$$

$$m_{\tilde{H}}^2 = m_\phi^2 + \frac{\lambda_3+\lambda_4+\lambda_5}{2}v^2 < m_{\eta_3}^2 = m_\phi^2 + \frac{\lambda_3+\lambda_4-\lambda_5}{2}v^2\,, \tag{6.16b}$$

requiring $\lambda_5 < 0$ and $\lambda_4 + \lambda_5 < 0$.
Demanding that $\tilde{H}$ individually is responsible for the observed relic DM density, cf. equation (C.8), the parameter space can be constrained further. Due to the imposed Z_2 symmetry, the decay of all components of ϕ is forbidden as long as ϕ remains unbroken ($v_\phi = 0$). Consequently, only pairwise annihilation processes can change the total number of $\tilde{H}$, meaning that the corresponding Boltzmann equation can be in general written as

$$z\frac{dY_{\tilde{H}}}{dz} = -\frac{1}{\mathsf{H}(T)s}\left(\gamma_{\tilde{H}\tilde{H}\to\dots}\left[\left(\frac{Y_{\tilde{H}}}{Y_{\tilde{H}}^{\mathrm{eq}}}\right)^2 - 1\right] + \sum_i \gamma_{\tilde{H}\eta_i\to\dots}\left[\frac{Y_{\tilde{H}}}{Y_{\tilde{H}}^{\mathrm{eq}}}\frac{Y_{\eta_i}}{Y_{\eta_i}^{\mathrm{eq}}} - 1\right]\right)\,. \tag{6.17}$$

Similarly, Boltzmann equations for η_i are obtained. However, the masses of $\tilde{H}$ and η_i are degenerate before and almost degenerate after EWSB, meaning that their distribution functions can be assumed to be equivalent. Thus, four equivalent Boltzmann equations are obtained:

$$z\frac{dY_{\tilde{H}}}{dz} = -\frac{\gamma_{\mathrm{annihilation}}}{\mathsf{H}(T)s}\left[\left(\frac{Y_{\tilde{H}}}{Y_{\tilde{H}}^{\mathrm{eq}}}\right)^2 - 1\right]\,, \tag{6.18}$$

with $Y_{\tilde{H}}^{\mathrm{eq}} = 45/(4\pi^4 g_{\mathrm{eff}}^S) z^2 K_2(z)$. The thermal annihilation rate ($\gamma_{\mathrm{annihilation}}$) has been calculated in equation (3.42) and the appearing reduced cross section is taken from reference [28]:

$$\hat{\sigma}_{\mathrm{annihilation}} = \frac{1}{32\pi}\left[\frac{3}{2}g^2 + 3g^2g'^2 + \frac{1}{2}g'^4 + (2\lambda_3+\lambda_4)^2 + 3\lambda_4^2 + 6\lambda_5^2\right]\,, \tag{6.19}$$

where only annihilation processes into lighter particles are considered.

According to reference [42], the relic density resulting from a time evolution of the considered form is given by

$$\Omega_{\tilde{H}}h^2 \approx \frac{3\times10^{-27}\ \mathrm{cm}^3/\mathrm{s}}{\langle\sigma v\rangle}\,, \tag{6.20}$$

with the thermally-averaged annihilation cross section multiplied by the relative DM velocity $\langle\sigma v\rangle$. In the considered case, $\langle\sigma v\rangle$ can be approximated by [28]

$$\langle\sigma v\rangle \approx \frac{\hat{\sigma}_{\mathrm{annihilation}}}{8m_{\tilde{H}}^2} \approx \frac{\hat{\sigma}_{\mathrm{annihilation}}}{(m_{\tilde{H}}/\mathrm{TeV})^2}\times 1.5\times10^{-24}\mathrm{cm}^3/\mathrm{s}\,. \tag{6.21}$$

Consequently, the resulting condition

$$\left(\frac{m_{\tilde{H}}}{\mathrm{TeV}}\right)^2 \approx 500\,\hat{\sigma}_{\mathrm{annihilation}}\,\Omega_{\tilde{H}}h^2\,, \tag{6.22}$$

allows to express $m_{\tilde{H}}$ as a function of λ_3, λ_4, and λ_5 by demanding that the observed relic DM density, cf. equation (C.8), completely consist of $\tilde{H}$. Furthermore, assuming $\lambda_3 = \lambda_4 = \lambda_5 = 0$, this sets a lower bound of (560 ± 50) GeV on $m_{\tilde{H}}$[1].

Besides the observed relic DM density, the parameter space of the inert Higgs model is further constrained by various experiments. Independent of $\tilde{H}$ being a DM candidate, collider experiments constrain $m_{\tilde{H}} + m_{\eta_3} > m_Z$ and $m_{\tilde{H}} + m_{\eta^\pm} > m_W$ from measuring the decay width of the Z boson and the $W^\pm$ boson. Furthermore, for $m_{\tilde{H}} < m_h/2$, $\lambda_3 + \lambda_4 + \lambda_5$ can be constrained from invisible decays of the SM Higgs boson. However, considering larger values of $m_{\tilde{H}}$, in collider experiments, $\tilde{H}$ can only be observed as missing transverse momentum where the current measurements do not put any further constraints on the parameter space of the inert Higgs model.

On the other side, assuming $\tilde{H}$ to be responsible for the observed relic DM density, direct detection experiments set limits on the DM-nucleon cross section. For the inert Higgs model, $\tilde{H}$ at tree level only scatters with nucleons via exchange of a Higgs boson. The corresponding spin-independent cross section is given by [15]

$$\sigma_{SI} = (\lambda_3 + \lambda_4 + \lambda_5)^2 \frac{f_N^2}{4\pi m_h^4} \frac{m_N^4}{(m_N + m_{\tilde{H}})^2}\,, \tag{6.23}$$

where m_N is the nucleon mass ($m_N \approx m_p \approx m_n \approx 940$ MeV) and f_N the Higgs-nucleon coupling which can be estimated by $f_N \approx 0.30$ [15] so that

$$\sigma_{SI,n} \approx \frac{(\lambda_3 + \lambda_4 + \lambda_5)^2}{(1 + m_{\tilde{H}}/m_n)^2} \times 10^{-38}\mathrm{cm}^2 \overset{m_{\tilde{H}} \gg m_n}{\approx} (\lambda_3 + \lambda_4 + \lambda_5)^2 \frac{\mathrm{TeV}^2}{m_{\tilde{H}}^2} \times 10^{-44}\mathrm{cm}^2 \tag{6.24}$$

is obtained. Comparing this with the constraint from XENON1T's direct search at 90% CL [4],

$$\sigma_{SI} \lesssim 10^{-45} \frac{m_{\tilde{H}}}{\mathrm{TeV}} \mathrm{cm}^2 \qquad \text{for} \qquad m_{\tilde{H}} \gtrsim 50 \text{ GeV}\,, \tag{6.25}$$

the condition

$$(\lambda_3 + \lambda_4 + \lambda_5)^2 \lesssim \frac{1}{10} \left(\frac{m_{\tilde{H}}}{\mathrm{TeV}}\right)^2\,, \tag{6.26}$$

is deduced. Combining this limit with the condition arising from requiring the production of the observed relic DM density, cf. equation (6.22), the allowed parameter space for λ_3, λ_4, and λ_5 becomes restricted.

Moreover, $\tilde{H}$ can also scatter inelastically via Z boson exchange with nucleons when the mass difference to η_3 is sufficiently small. In reference [43], a lower bound for the mass difference of roughly 200 keV is found[2], resulting in a lower bound on λ_5:

$$m_{\eta_3} - m_{\tilde{H}} \approx -\frac{\lambda_5 v^2}{m_{\tilde{H}}} \gtrsim 200 \text{ keV} \qquad \Rightarrow \qquad |\lambda_5| \gtrsim 3.3 \times \frac{m_{\tilde{H}}}{\mathrm{TeV}} \times 10^{-6} \gtrsim 2 \times 10^{-6}\,, \tag{6.27}$$

[1] In reference [28] a lower bound of 530 GeV is found but it seems that the gauge coupling dependence of $\hat{\sigma}_{\text{annihilation}}$ has not be considered correctly in the given form of $\langle \sigma v \rangle$, cf. equations (C8) - (C14) in reference [28]

[2] In reference [43] considers data from XENON100's direct search. However, the given lower bound on the mass difference does change significantly when considering e.g. the current data from XENON1T's direct search because it is not limited by experimental sensitivity but the maximal kinetic energy of the DM particle

where $m_{\tilde{H}} \gtrsim 560$ GeV is used. In principle, a similar lower bound on $|\lambda_4 + \lambda_5|$ can be found from the requirement of not too small mass difference between $\tilde{H}$ and $\eta^{\pm}$. However, considering the one-loop RGE of the Higgs self couplings of the inert Higgs model, cf. equation A.89, a lower bound on λ_4 is not very relevant because it can only become so small in a very narrow energy scale region. In contrast, the RGE for λ_5 is always proportional to λ_5, implying that λ_5 cannot only be chosen to be small at one specific energy scale and the limit becomes relevant.

6.2 The Scotogenic Model

In 2006, Ma suggested an extension of the SM called scotogenic model [54] including the inert Higgs model and right-chiral Majorana neutrinos which also transform oddly under the imposed Z_2 symmetry. The Lagrangian is given by

$$\begin{aligned}\mathcal{L}(x) = \mathcal{L}_{\mathrm{SM}}|_{m_H=\lambda=0}(x) + (D^{\mu}\phi(x))^{\dagger}(D_{\mu}\phi(x)) - V_{\mathrm{inert}}(x) \\ + \sum_i \Big[i\overline{\Psi}_{\nu_i^R}(x)\partial\!\!\!/\Psi_{\nu_i^R}(x) - \sum_j \Big(y'_{ij}\overline{\Psi}_{\ell_j}(x)\phi^c(x)\Psi_{\nu_i^R}(x) + (y'_{ij})^*\overline{\Psi}_{\nu_i^R}(x)\phi^{c\dagger}(x)\Psi_{\ell_j}(x)\Big) \\ - \frac{M_{N_i}}{2}\left(\overline{\Psi^c}_{\nu_i^R}(x)\Psi_{\nu_i^R}(x) + \overline{\Psi}_{\nu_i^R}(x)\Psi^c_{\nu_i^R}(x)\right)\Big]\,, \end{aligned} \tag{6.28}$$

with $\mathcal{L}_{SM}$ being defined in equation (A.92) and $V_{\mathrm{inert}}(x)$ being defined in equation (6.5). Furthermore, demanding that only the SM Higgs doublet obtains a VEV while the new Higgs doublet remains unbroken ($\langle H\rangle = v$ and $\langle\phi\rangle = 0$), the two Higgs doublets become

$$H(x) = \frac{1}{\sqrt{2}}\begin{pmatrix}0\\ h(x)+v\end{pmatrix} \qquad \text{and} \tag{6.29a}$$

$$\phi(x) = \frac{1}{\sqrt{2}}\begin{pmatrix}\eta_1(x)+i\eta_2(x)\\ \tilde{H}(x)+i\eta_3(x)\end{pmatrix} = \frac{1}{\sqrt{2}}\begin{pmatrix}\sqrt{2}\eta^+(x)\\ \tilde{H}(x)+i\eta_3(x)\end{pmatrix}\,, \tag{6.29b}$$

where Goldstone bosons are ignored. The masses of the single components of ϕ have been calculated in the previous section[3]:

$$m_{\eta^{\pm}} = m_{\phi}^2 + \frac{\lambda_3}{2}v^2\,, \tag{6.30a}$$

$$m_{\eta_3} = m_{\phi}^2 + \frac{\lambda_3+\lambda_4-\lambda_5}{2}v^2\,, \tag{6.30b}$$

$$m_{\tilde{H}} = m_{\phi}^2 + \frac{\lambda_3+\lambda_4+\lambda_5}{2}v^2\,. \tag{6.30c}$$

Since ϕ remains unbroken, the active neutrino masses in the scotogenic model are not produced by the type-I seesaw mechanism but become only loop induced. Thus, the resulting Majorana masses

[3] Note that the VEV is defined differently in reference [54], so that v^2 has to be replaced by $v^2/2$ to match the definition used in this thesis.

for the active neutrinos are now determined by [54][4]

$$(m_\nu^S)_{jk} = \sum_i (m_\nu^S)_{jk}^i := \sum_i \frac{(y'_{ij})^* y'_{ik} M_{N_i}}{32\pi^2} \left(\frac{m_{\tilde{H}}^2}{m_{\tilde{H}}^2 - M_{N_i}^2} \ln \frac{m_{\tilde{H}}^2}{M_{N_i}^2} - \frac{m_{\eta_3}^2}{m_{\eta_3}^2 - M_{N_i}^2} \ln \frac{m_{\eta_3}^2}{M_{N_i}^2} \right)$$
$$= \sum_i \frac{(m_\nu^I)_{jk}^i M_{N_i}^2}{16\pi^2 v^2} \left(\frac{m_{\tilde{H}}^2}{m_{\tilde{H}}^2 - M_{N_i}^2} \ln \frac{m_{\tilde{H}}^2}{M_{N_i}^2} - \frac{m_{\eta_3}^2}{m_{\eta_3}^2 - M_{N_i}^2} \ln \frac{m_{\eta_3}^2}{M_{N_i}^2} \right) =: \sum_i \alpha_S^i (m_\nu^I)_{jk}^i \,, \quad (6.31)$$

with $(m_\nu^I)_{jk}^i$ being the type-I seesaw mass induced by N_i, cf. equation (5.10). In case of

$$m_{\tilde{H}}^2 - m_{\eta_3}^2 = \lambda_5 v^2 \ll m_0^2 = \frac{m_{\tilde{H}}^2 + m_{\eta_3}^2}{2} = m_\phi^2 + \frac{\lambda_3 + \lambda_4}{2} v^2 \,, \quad (6.32)$$

this expression simplifies to

$$\alpha_S^i := \frac{\lambda_5}{16\pi^2} \frac{M_{N_i}^2}{m_0^2 - M_{N_i}^2} \left(1 - \frac{M_{N_i}^2}{m_0^2 - M_{N_i}^2} \ln \frac{m_0^2}{M_{N_i}^2} \right) \quad (6.33a)$$
$$\overset{M_{N_i} \gg m_0}{\approx} \sum_i \frac{\lambda_5}{16\pi^2} \left(2 \ln \frac{M_{N_i}}{m_0} - 1 \right) . \quad (6.33b)$$

As a consequence, considering e.g. $m_0 \sim$ TeV and $M_{N_i} \sim 10^{12}$ GeV, $(m_\nu^S)_{jk}^i$ is suppressed by $\alpha_S^i \sim \lambda_5/4$ compared to $(m_\nu^I)_{jk}^i$, cf. figure 6.1.

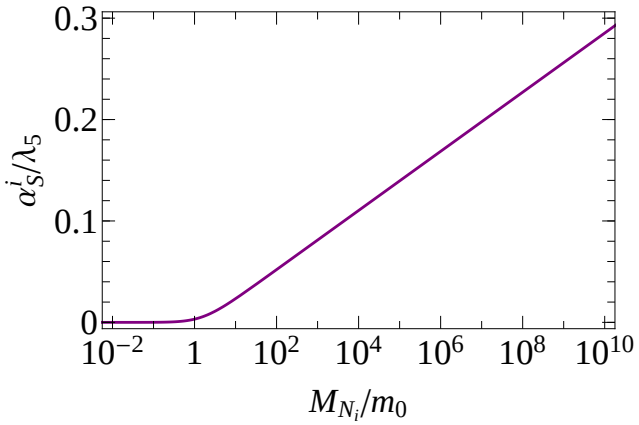

Figure 6.1: Suppression of the active neutrino mass generated in the scotogenic model compared to the active neutrino masses generated by the type-I seesaw mechanism. The suppression is shown normalized with respect to proportionality factor λ_5 and in dependence of the determining mass ratio M_{N_i}/m_0.

6.3 Thermal Corrections to the Effective Higgs Potential

In this section, the influence of a matter density ρ_{mat} on the EV of the Higgs field is investigated. Like in classical mechanics, a quantum field ϕ takes on an EV $\langle\phi\rangle$ that minimize the energy density

[4] Note that there is a missing factor 1/2 in the original paper – see e.g. version 1 of reference [56].

in the state of equilibrium:

$$\rho_E = \frac{1}{V} \langle F|\hat{\mathrm{H}}|F\rangle \ , \tag{6.34}$$

with $\hat{\mathrm{H}}$ being the Hamiltonian. Assuming that the mass eigenstates in dependence of the EV and the temperature are known ($E_i(\vec{k})^2 = \vec{k^2} + m^2_{\mathrm{eff},i}$), cf. section 3.4, the contribution of the effective free Hamiltonian is given by[5]

$$\frac{1}{V} \langle \hat{\mathrm{H}}_{\,\mathrm{eff,free}} \rangle = V_{\text{tree-level}} + \sum_i^{N_{\mathrm{dof}}} \int \frac{d^3k}{(2\pi)^3} E_i(\vec{k}) \left(f_i(\vec{p}) \pm \frac{1}{2} \right) , \tag{6.35}$$

where i runs up all degrees of freedom and is $+1/2$ for bosons and $-1/2$ for fermions.

The divergent contributions are absorbed by renormalization. However, this subtraction is non-trivial because thermal loop corrections to the divergent loop corrections need to be considered as well to cancel the divergences in equation (6.35). Thus, the part of equation (6.35) which is already considered by the renormalized potential is dimensional regularization ($d = 4 - \epsilon$) given by

$$\pm \frac{m^4_{\mathrm{eff},i}}{64\pi^2} \frac{A_0(m^2_{0,i})}{m^2_{0,i}} = \pm \frac{m^4_{\mathrm{eff},i}}{64\pi^2} \left(\frac{2}{\epsilon} - \gamma + \ln 4\pi + 1 - \ln \frac{m^2_{0,i}}{\mu^2} \right) , \tag{6.36}$$

with the Euler-Mascheroni constant $\gamma \approx 0.577$ and $m^2_{0,i}$ is the mass of the particle i in the vacuum, implying that the effective potential in the vacuum in the minimum of the potential is equivalent to the tree-level potential. Subtracting this, the effective Higgs potential becomes

$$V_{\mathrm{eff}} = V^R_{\text{tree-level}} + \sum_i^{N_{\mathrm{dof}}} \left[\int \frac{d^3k}{(2\pi)^3} E_i(\vec{k}) f_i(\vec{k}) \pm \frac{m^4_{\mathrm{eff},i}}{64\pi^2} \ln \left(\frac{m^2_{\mathrm{eff},i}}{m^2_{0,i}} \right) \right] . \tag{6.37}$$

Next, when considering thermalized systems, the distribution functions are not independent of the particle masses. However, the EV takes on the value that minimizes the energy density for constant distribution functions. To circumvent this issue, e.g. the derivative of the effective potential with respect to the EV can be considered instead:

$$\frac{dV_{\mathrm{eff}}}{dv} = \frac{dV^R_{\text{tree-level}}}{dv} + \sum_i \int \frac{d^3k}{(2\pi)^3} \frac{dE_i(\vec{k})}{dv} f_i(\vec{k}) \pm \frac{d}{dv} \frac{m^4_{\mathrm{eff},i}}{64\pi^2} \ln \left(\frac{m^2_{\mathrm{eff},i}}{m^2_{0,i}} \right) . \tag{6.38}$$

[5] Note that an EV being constant in space is assumed for deriving the potential in this form. However, during EWPT, the field breaks in different directions at different spacetime points. Consequently, an additional energy density from the non-vanishing field gradient is obtained. However, this energy density does not change the shape of the potential. For this reason, only the dynamic of symmetry breaking changes slightly because the energy stored in the field gradient has to be smaller than the energy gained by the shift of the field EV to the minimum of the potential. Hence, the symmetry breaking process is slightly delayed because a smaller field gradient implies a larger correlation among field values in space. Moreover, it should be mentioned that the field gradient for spontaneously broken continuous symmetries flattens with time so that it is observed to be constant on very large scales. The reason for that is that, in contrast to a discrete symmetry where there are distinct minima separated by potential barriers, the field value at each spacetime point is in the minimum of the potential. Only the direction of symmetry breaking varies, implying that flattening the gradient gains energy.

With this, the EV minimizing the effective potential can also be calculated for thermalized systems without difficulty by setting the derivative of the effective potential equal to zero. However, to ascertain whether the obtained minima of V_{eff} are stable or not, V_{eff} has to be calculated using the distribution functions thermalized in the minimum. Furthermore, for unstable minima, the effective potential calculated in this way can be used to determine the tunneling probability to a another minimum[6].

Thus, either considering an effective potential with only one minimum or an initial state in a minimum that is stable on the considered time scales, equation (6.38) can be used to investigate the temperature dependence of the EV (e.g. for the expanding universe). Furthermore, to obtain the typically investigated well-known form of the effective Higgs potential, equation (6.38) is integrated over v, including the thermalized distribution functions[7] [16, 67, 20, 66]:

$$\int_0^v dv' \, \frac{dV_{\text{eff}}}{dv'} \propto V^R_{\text{tree-level}} + \sum_i^{N_{\text{dof}}} \pm \left[T \int \frac{d^3k}{(2\pi)^3} \ln\left[1 \mp \exp\left(-E_i(\vec{k})/T\right)\right] + \frac{m^4_{\text{eff},i}}{64\pi^2} \ln\left(\frac{m^2_{\text{eff},i}}{m^2_{0,i}}\right)\right] , \quad (6.39)$$

where the solution of the remaining momentum integrals are usually series expanded in powers of $m_{\text{eff},i}/T$, cf. equation (D.10).

Note that for the Higgs boson, here, the full EV induced mass term ($m_h^2 = 3\lambda/2v^2 + m_H^2$) needs to be considered. However, this causes problems considering an EV corresponding to a negative mass of the Higgs boson. To circumvent this problem, at least in the minimum potential, thermal corrections to the Higgs boson mass need to be considered, cf. e.g. reference [14]. However, these thermal corrections are basically equivalent to the corrections to the effective Higgs potential, implying that the Higgs mass in the minimum of the potential is still determined by λv^2. Thus, the issue of negative Higgs masses can be circumvented by using $m_h^2 = \lambda v^2$ for the evaluation of the distribution functions in equation (6.38). To compensate the altered v^2 dependence when using $m_h^2 = \lambda v^2$ for the calculation of the effective potential in the common form, cf. equation (6.39), the Higgs boson has to be counted as 3/2 degrees of freedom.

Finally, to calculate the effective Higgs potential, it has to be decided which degrees of freedom are to be summed over. The intuitive answer would be all observable ones especially relating to the thermal contributions because only these degrees of freedom are present in the state vector of a thermal system. However, in references [20, 66], it is argued that also unphysical degrees of freedom such as unphysical gauge boson polarizations, Goldstone bosons, and ghosts need to be considered as part of the sum. Intuitively, one would expect that the contributions from unphysical degrees of freedom cancel out when they are considered properly. However, comparing the effective potential calculated in R_ξ gauge with the result form unitary gauge, the altered mass of the Goldstone boson outside the minimum of the potential ($m_\varphi^2 = \xi m_A^2 + \lambda(v^2 - v^2_{\text{min}})$) give rise to extra terms – even in the limit $\xi \to \infty$ – which on the other hand are absent in unitary gauge.

[6] One should keep in mind that the resulting EV after the tunneling process slightly differs from the value given by the calculated V_{eff} because the distribution functions change when the system thermalizes again.

[7] Note that the density-dependent part of the given effective potential coincides with the grand potential density, cf. equation (3.9), being minimized by the equilibrium state for constant temperature and constant chemical potentials.

The argument for trusting the R_ξ gauge result given in reference [20] is that the unitary gauge Lagrangian does not correspond to a renormalizable theory and that for this reason higher-order loop corrections are expected to remove the discrepancy. A similar argument can also be found in reference [66], where it is stated that only the effective potential in the renormalizable gauge can be used to study symmetry breaking.

Considering the SM Higgs sector, the matter density needed to substantially change the effective potential is so large that the effects are mainly of interest in the very early universe ($T \gtrsim$ GeV). As discussed before, at this stage of the universe, all SM particles are in thermal equilibrium. Furthermore, for calculating the effective Higgs potential, it is convenient to only consider degrees of freedom which couple strongest to the EV. This means that for the SM, photons, gluons, and light fermions can be neglected to a very good approximation. Thus, in case of only considering physical degrees of freedom, one is left with three degrees of freedom for each the massive gauge bosons ($W^\pm$ and Z^0), the Higgs particle, and the twelve degrees of freedom for the top quark:

$$V_{\text{eff}} \sim V_0 + \left(\frac{3\lambda}{2} + \frac{9g^2 + 3g'^2}{4} + 3y_t^2 \right) \frac{T^2}{24} v^2 \,. \tag{6.40}$$

Moreover, also taking into account the contribution from the three Goldstone bosons, the R_ξ-gauge result, which is used to approximate the temperature dependence of the EV in this thesis, is obtained:

$$V_{\text{eff}} \sim V_0 + \left(3\lambda + \frac{9g^2 + 3g'^2}{4} + 3y_t^2 \right) \frac{T^2}{24} v^2 \,. \tag{6.41}$$

7 L Violation Assisted GUT Baryogenesis

As was discussed in the section 4.2, many GUT baryogenesis models have the problem that the produced B asymmetry conserves $B - L$, meaning that the produced B asymmetry is completely washed out by sphaleron transitions. Consequently, these models need an additional source of $B - L$ violation, securing a part of the produced B asymmetry before sphaleron transitions become efficient.

A simple extension of the SM, inducing $B - L$ violation in the region of interest 10^{11} GeV $\lesssim T \lesssim 10^{15}$ GeV[1], are right-handed Majorana neutrinos (N), cf. chapter 5. In light of GUTs, right-handed Majorana neutrinos can be introduced as singlets under $SU(5)_{\mathrm{GUT}}$ or embedded into the 16-dimensional representation of $SO(10)_{\mathrm{GUT}}$. This interplay of GUT baryogenesis, L violation – induced by right-handed Majorana neutrinos –, and sphaleron transitions was first suggested in 2002 by Yanagida und Fukugita [27] but no detailed analyses were made. In my master thesis [74], this idea was further investigated and the Boltzmann equations for a simplified model including one right-handed Majorana neutrino were solved, but L-violating processes were only partly taken into account. In the following, this analysis is significantly improved and the model is extended to a more realistic case involving two right-handed Majorana neutrinos to be able to explain the phenomenology of neutrino oscillation. Furthermore, additional L-violating processes, which become relevant when the decay involving right-handed Majorana neutrinos is kinematically forbidden, are included in the Boltzmann equations. This work has been published in collaboration with Wei-Chih Huang and Heinrich Päs, cf. reference [40]. Subsequently, an extended Higgs sector is investigated for being able to explain both the observed B asymmetry and the observed DM relic density. The results are published in reference [39].

However, before starting with the detailed discussion, it should be mentioned that the calculation methods used in references [40, 39] have been significantly improved after publication and some conceptual mistakes have been corrected. The most important differences will be discussed at the respective places.

In the following, in section 7.1, the Boltzmann equations for the time evolution of the B and L asymmetry involving sphaleron transitions and L violating processes induced by right-handed Majorana neutrinos are derived. Afterwards, in section 7.2, the general setup and methods which are used to solve the Boltzmann equations are discussed. Finally, in sections 7.3 - 7.5, three different scenarios are investigated in detail and numerical results for parameter scans are shown.

[1] The region of interest w.r.t. the temperature lies above the scale where sphaleron transitions become very efficient, cf. region IV and V in figure 4.2, but below the scale where the GUT symmetry is expected to break down to the SM.

7.1 Interplay of Sphaleron Transitions and L Violation Induced by Right-Handed Majorana Neutrinos

As discussed in chapter 4, the essential ingredients for the Boltzmann equations of B and L are the rate of B violation induced by sphaleron transitions and the thermal rates of additional B- and/or L-violating processes. The details of sphaleron transitions have already been investigated in section 4.1. For the rate of L violation induced by right-handed Majorana neutrinos, different processes which are efficient at different temperatures need to be considered. First of all, there are two-body (inverse) decays involving a right-handed Majorana neutrino, a lepton doublet, and a Higgs doublet, cf. section 5.1. These processes are expected to dominate the rate of L violation within the temperature range where the (inverse) decay is kinematically allowed, the mass of the decaying particle is sizable compared to the temperature, and the density of all involved particles is still sizable ($M_N \gtrsim T \gtrsim M_N/10$). The corresponding thermal rate is given by

$$\gamma_D = \begin{cases} \gamma_{N\to\ell_i H} = 2\gamma_{N\to\chi\phi}\big|_{m_N\to M_{N_i}, m_\chi\to m_{\ell_i}, m_\phi\to m_H} & M_{N_i} > m_{\ell_i} + m_H \\ \gamma_{H\to N\bar{\ell}_i} = 2\gamma_{\phi\to N\overline{\chi}}\big|_{m_N\to M_{N_i}, m_\chi\to m_{\ell_i}, m_\phi\to m_H} & m_H > M_{N_i} + m_{\ell_i} \end{cases}, \tag{7.1}$$

with $\gamma_{N\to\chi\phi}$ and $\gamma_{\phi\to N\overline{\chi}}$ being calculated in equations (5.18) and (5.19). Note that the additional factor of 2 for the thermal rates appears because the decay into doublets is considered. Furthermore, the calculation of the thermal decay rate – being dominant in the most relevant region ($M_N/10 \lesssim T \lesssim M_N$) – is improved by using the Fermi-Dirac and Bose-Einstein statistics instead of Boltzmann statistics, cf. equation (5.20). Note that, at least in the SM, the case $m_{\ell_i} > M_{N_i} + m_H$ is not fulfilled for the temperatures of interest, cf. figure 3.1.

However, for temperatures where the number density of the right-handed neutrino is already strongly Boltzmann suppressed ($T \lesssim M_N/10$), the dominant L violation comes from the scattering processes exchanging a right-handed Majorana neutrino: $\ell_i H \leftrightarrow \bar{\ell}_i H^\dagger$ and $\ell_i\ell_i \leftrightarrow H^\dagger H^\dagger / \bar{\ell}_i\bar{\ell}_i \leftrightarrow HH$. In case of $M_N > m_{\ell_i} + m_H$, the resonant contribution from the s-channel diagram has to be subtracted because it is already taken into account by $\gamma_{N\to\ell_i H}$, cf. section 5.2. The corresponding thermal equilibrium rates $\gamma^{\text{sub}}_{N,s} = \gamma_{N,s} - \gamma_{N\to\ell_i H}/8$ and $\gamma_{N,t}$ of these processes violating L by two units have been calculated in section 5.2, cf. equations (5.27) and (5.32). Note that here, $\gamma_{N\to\ell_i H}/8$ instead of $\gamma_{N\to\ell_i H}/2$ is subtracted because of the additional factor of 2 in the decay width.

Finally, in the region where the temperature become large compared to the Majorana mass and especially in the region where the decay is kinematically forbidden – neither $M_{N_i} > m_{\ell_i} + m_H$ nor $m_H > M_N + m_{\ell_i}$ is fulfilled – also $2 \to 2$ scattering processes with a right-handed Majorana neutrino and a lepton doublet as external particles become relevant. Accordingly, the relevant processes are given by $\ell_i N \leftrightarrow Q_3\bar{U}_3$ ($\gamma_{H,s}$), $\ell_i\overline{Q}_3 \leftrightarrow N\bar{U}_3$ (γ_{H,t_1}), $\ell_i U_3 \leftrightarrow NQ_3$ (γ_{H,t_2}), $\ell_i N \leftrightarrow H^* A$ ($\gamma_{A,s}$), $\ell_i H \leftrightarrow NA$ (γ_{A,t_1}), and $\ell_i A \leftrightarrow NH^*$ (γ_{A,t_2}). For the corresponding reduced cross sections, the results from reference [30] are used[2], where the small mass difference between the thermal masses of m_{U_3} and m_{Q_3}, cf. figure 3.1, is neglected to approximate $\gamma_{H,t_1} = \gamma_{H,t_2} := \gamma_{H,t}$. Note that all other $2 \to 2$ processes with a right-handed Majorana neutrino as external particle involve subleading Yukawa

[2] In the reference, the other relevant thermal rates are given as well but the result for $\gamma^{\text{sub}}_{N,s}$ slightly differs from the exact result calculated in this thesis. For all other thermal rates, the results from the paper were confirmed.

interactions. Hence, their thermal rates are strongly suppressed ($y_b^2, y_\tau^2 \ll g^2, g'^2, y_t^2$) as long as the processes considered before are not kinematically suppressed, which is only the case after EWPT when the temperature drops below the top quark mass.

Thus, using equation (3.35), where the thermal rates for the back and forth processes are assumed to be equivalent, the time evolution induced by the mentioned L-violating processes is given by[3]

$$\begin{aligned} z\frac{d}{dz}\beta\mu_{\ell_i} = -\frac{12}{\mathsf{H}(z)T^3}\Bigg[&\left(\frac{\gamma_D}{2} + 4\gamma_{N,s}^{\text{sub}} + 4\gamma_{N,t}\right)(\beta\mu_{\ell_i} + \beta\mu_H) + \gamma_{H,s}\left(\frac{n_N}{n_N^{\text{eq}}}\beta\mu_{\ell_i} - \beta\mu_{Q_3} + \mu_{U_3}\right) \\ &+ \gamma_{H,t_1}\left(\beta\mu_{\ell_i} - \beta\mu_{Q_3} + \beta\mu_{U_3}\frac{n_N}{n_N^{\text{eq}}}\right) + \gamma_{H,t_2}\left(+\beta\mu_{\ell_i} - \beta\mu_{Q_3}\frac{n_N}{n_N^{\text{eq}}} + \beta\mu_{U_3}\right) \\ &+ \gamma_{A,s}\left(\frac{n_N}{n_N^{\text{eq}}}\beta\mu_{\ell_i} + \beta\mu_H\right) + \gamma_{A,t_1}(\beta\mu_{\ell_i} + \beta\mu_H) + \gamma_{A,t_2}\left(\beta\mu_{\ell_i} + \frac{n_N}{n_N^{\text{eq}}}\beta\mu_H\right)\Bigg], \end{aligned} \tag{7.2}$$

with $\mu_{\ell_i^1} = \mu_{\ell_i^2} = \mu_{\ell_i} = \mu_{L_i}/2$.

Next, in general, as discussed in section 3.2, a system of coupled Boltzmann equations is obtained involving all particle densities which directly or indirectly influence the time evolution of the quantity of interest. Consequently, as discussed in section 3.6, it is useful to simplify the Boltzmann equations by neglecting reactions whose influence on the quantity of interest is negligible and assuming thermal equilibrium for all reactions which are in thermal equilibrium $\Gamma > \mathsf{H}$ and are significantly more efficient than the reactions of interest.
In detail, as discussed in section 4.1, this means that in the region of interest, cf. region IV in figure 4.2, where the focus is set of the rate of B violation induced by sphaleron transitions, only gauge interactions and the top Yukawa interaction can be assumed to be in thermal equilibrium, while all other SM processes can be neglected to a good approximation. Thus, the time evolution given in equation (7.2) can be simplified using the equilibrium of the top Yukawa interaction, cf. equation (3.86), and the initial conditions given in equation (4.13) allowing to express all involved chemical potentials in terms of μ_B and μ_{L_i}. Note that both sphaleron transitions and the considered L-violating processes do not alter the form of the initial conditions ($\mu_H^{\text{ex}} = -\mu_{B-L}/(4m)$ and $\mu_{Q_3}^{\text{ex}} = \mu_B/(2N_g)$) but only shift μ_B and μ_{L_i}. Consequently,

$$\mu_H = \frac{1}{1+2m}\left(-\frac{\mu_{B-L}}{2m} - \frac{\mu_B}{2N_g}\right), \tag{7.3a}$$

$$\mu_{Q_3} = \frac{1}{3+6m}\left(\frac{\mu_{B-L}}{2m} + (3+4m)\frac{\mu_B}{2N_g}\right), \tag{7.3b}$$

$$\mu_{U_3} = \frac{1}{3+6m}\left(-\frac{\mu_{B-L}}{m} + 2m\frac{\mu_B}{N_g}\right), \tag{7.3c}$$

is obtained as long as only gauge interactions, top Yukawa interactions, sphaleron transitions, and L violation acting only one left-chiral leptons are considered.

Furthermore, including B violation induced by sphaleron transitions according to equation (4.17),

[3] Note that for $\gamma_{N,s}^{\text{sub}}$ and $\gamma_{N,t}$, a factor of 2 appears because all external particles are doublets and another factor of 2 because both chemical potential – μ_{ℓ_i} and μ_H – contribute twice.

the time evolution including all relevant processes can be expressed as[4]

$$z\frac{d}{dz}\beta\mu_{B-L_i} = -\frac{6}{\mathsf{H}(z)T^3}\left[2\gamma_{L_i}\left(\beta\mu_{B-L_i}-\frac{\mu_B}{N_g}\right)+4\gamma_{B-L}\frac{\beta\mu_{B-L}}{2m(1+2m)}+4\gamma_B\frac{\beta\mu_B}{2N_g(1+2m)}\right], \tag{7.4a}$$

$$z\frac{d}{dz}\beta\mu_B = -\frac{\Gamma_{\text{spha}}}{\mathsf{H}(z)}\left(\beta\mu_B - c_s\beta\mu_{B-L}\right), \tag{7.4b}$$

with

$$\gamma_{L_i} = \frac{\gamma_D}{2}+4\gamma_{N,s}^{\text{sub}}+4\gamma_{N,t}+\gamma_{H,s}\frac{n_N}{n_N^{\text{eq}}}+\gamma_{H,t_1}+\gamma_{H,t_2}+\gamma_{A,s}\frac{n_N}{n_N^{\text{eq}}}+\gamma_{A,t_1}+\gamma_{A,t_2}, \tag{7.5a}$$

$$\begin{aligned}\gamma_{B-L} = {}& \frac{\gamma_D}{2}+4\gamma_{N,s}^{\text{sub}}+4\gamma_{N,t}+\gamma_{H,s}+\gamma_{H,t_1}\left(\frac{1}{3}+\frac{2}{3}\frac{n_N}{n_N^{\text{eq}}}\right)\\ &+\gamma_{H,t_2}\left(\frac{1}{3}\frac{n_N}{n_N^{\text{eq}}}+\frac{2}{3}\right)+\gamma_{A,s}+\gamma_{A,t_1}+\gamma_{A,t_2}\frac{n_N}{n_N^{\text{eq}}},\end{aligned} \tag{7.5b}$$

$$\begin{aligned}\gamma_B = {}& \frac{\gamma_D}{2}+4\gamma_{N,s}^{\text{sub}}+4\gamma_{N,t}+\gamma_{H,s}+\gamma_{H,t_1}\left(\frac{3+4m}{3}-\frac{4m}{3}\frac{n_N}{n_N^{\text{eq}}}\right)\\ &+\gamma_{H,t_2}\left(\frac{3+4m}{3}\frac{n_N}{n_N^{\text{eq}}}-\frac{4m}{3}\right)+\gamma_{A,s}+\gamma_{A,t_1}+\gamma_{A,t_2}\frac{n_N}{n_N^{\text{eq}}},\end{aligned} \tag{7.5c}$$

and

$$\Gamma_{\text{spha}} = 3\left(2N_g-\frac{m}{2m+1}\right)(18\pm3)\alpha_W^5\frac{M_N}{z}, \tag{7.6a}$$

$$c_s = \frac{mN_g}{m(4N_g-1)+2N_g}, \tag{7.6b}$$

cf. equation (4.15).
Finally, using the approximation $\gamma_{H,t_1}=\gamma_{H,t_2}:=\gamma_{H,t}$, equation (7.5) simplifies to

$$\gamma_{L_i} = \frac{\gamma_D}{2}+4\gamma_{N,s}^{\text{sub}}+4\gamma_{N,t}+\gamma_{H,s}\frac{n_N}{n_N^{\text{eq}}}+2\gamma_{H,t}+\gamma_{A,s}\frac{n_N}{n_N^{\text{eq}}}+\gamma_{A,t_1}+\gamma_{A,t_2}, \tag{7.7a}$$

$$\gamma_{B-L}=\gamma_B = \frac{\gamma_D}{2}+4\gamma_{N,s}^{\text{sub}}+4\gamma_{N,t}+\gamma_{H,s}+\gamma_{H,t}\left(1+\frac{n_N}{n_N^{\text{eq}}}\right)+\gamma_{A,s}+\gamma_{A,t_1}+\gamma_{A,t_2}\frac{n_N}{n_N^{\text{eq}}}. \tag{7.7b}$$

Note that the derived Boltzmann equations are linear in the chemical potentials, implying that the ratios $\mu_{B-L}/\mu_B^{\text{initial}}$ and $\mu_B/\mu_B^{\text{initial}}$ are independent of μ_B^{initial}.

For the time evolution of right-handed Majorana neutrinos, number densities and not asymmetries are considered because asymmetries between N and N^c are erased by the Majorana mass when the

[4] There are three major differences between this time evolution and the time evolution considered in references [40, 39]. First of all, the time evolution of chemical potentials instead of differences of number densities in the Maxwell-Boltzmann approximation are considered. Thus, it is taken into account that for the same value of the chemical potential, each bosonic degree of freedom stores the double amount of particle number asymmetry as each fermionic degree of freedom. Furthermore, the interplay of sphaleron transitions and Yukawa interactions have been investigated properly, meaning that the bottom and tau Yukawa interactions are irrelevant and the rate of B violation induced by sphaleron transitions is determined by equation (4.17). In references [40, 39], the bottom interaction is assumed to be in thermal equilibrium for $T \lesssim 10^{12}$ GeV while the tau Yukawa interaction is ignored for simplicity. Moreover, the rate of B violation induced by sphaleron transitions is not calculated in detail but only roughly estimated.

mass becomes sizable ($M_N \gtrsim T$). Furthermore, right-handed Majorana neutrinos are not necessarily in thermal equilibrium, implying that the ration n_N/n_N^{eq} becomes relevant. For the calculation of this factor, the small asymmetries of the other involved particles are irrelevant so that the Boltzmann equation for N can be considered independently, cf. equation (3.34):

$$z\frac{dY_N}{dz} = -\frac{\gamma_N}{\mathsf{H}(z)s}\left(\frac{Y_N}{Y_N^{eq}} - 1\right) , \tag{7.8}$$

with [30]

$$\begin{aligned}\gamma_N &= 2\left(\gamma_D + 2\gamma_{H,s} + 2\gamma_{H,t_1} + 2\gamma_{H,t_2} + 2\gamma_{As} + 2\gamma_{A,t_1} + 2\gamma_{A,t_2}\right) \\ &\simeq 2\left(\gamma_D + 2\gamma_{H,s} + 4\gamma_{H,t} + 2\gamma_{As} + 2\gamma_{A,t_1} + 2\gamma_{A,t_2}\right) .\end{aligned} \tag{7.9}$$

Hence, when the reactions involving right-handed Majorana neutrinos as external particles are efficient, n_N becomes equivalent to n_N^{eq} and all rates defined in equation (7.7) become equivalent ($\gamma_{L_i} = \gamma_{B-L} = \gamma_B$). Consequently, the Boltzmann equation (7.4) simplifies to

$$z\frac{d}{dz}\beta\mu_{B-L_i} = -\frac{12}{\mathsf{H}(z)T^3}\gamma_{L_i}\left[\beta\mu_{B-L_i} + \frac{\beta\mu_{B-L}}{m(1+2m)} + \frac{1}{N_g}\left(\frac{1}{(1+2m)} - 1\right)\beta\mu_B\right] , \tag{7.10a}$$

$$z\frac{d}{dz}\beta\mu_B = -\frac{\Gamma_{\text{spha}}}{\mathsf{H}(z)}\left(\beta\mu_B - c_s\beta\mu_{B-L}\right) , \tag{7.10b}$$

resulting in the equilibrium condition

$$(1+2m)\beta\mu_{B-L_i} + \frac{\beta\mu_{B-L}}{m} = \frac{2m}{N_g}\beta\mu_B . \tag{7.11}$$

7.2 Approximation of the Thermal Rates of L Violation Induced by Right-Handed Majorana Neutrinos

Before solving the Boltzmann equations (7.4) and (7.8) numerically, all contributing thermal rates in the temperature range of interest have to be calculated. For the occurring masses, the leading contribution from the thermal one-loop correction are used, cf. equation (B.40) for the SM and equation (B.42) considering an extended Higgs sector. For simplicity, the thermal contribution induced by the new Yukawa couplings (y) – coupling left- and right-chiral neutrinos –, cf. equation (B.41), is ignored. This may not seem to be a reasonable approximation because y up to a value of 10 are investigated. However, for $T \lesssim M_N$, the thermal masses become suppressed by powers of T/M_N and, as can be seen from the numerical results, for $M_N \lesssim 10^{13}$ GeV, only $y \lesssim 0.3$ are relevant. Consequently, for the region where the interplay with sphaleron transitions becomes relevant, the thermal contributions involving y are either sub-dominant or kinematically suppressed. Furthermore, the neglected thermal corrections do not change the thermal rates by a lot but mainly shift the region where both decays $N \to \ell_i H$ and $H \to N\bar{\ell}_i$ are kinematically forbidden. For the main part, the region where the decay $H \to N\bar{\ell}_i$ is kinematically forbidden enlarges, meaning that the resonant behavior in the most important region $1 \lesssim z \lesssim 10$ does not change significantly.

Additionally, the one-loop running of the relevant SM coupling constants within the SM, cf. equation (A.88), is taken into account[5]while the running of y and its influence on the running of the other couplings is neglected. As for the thermal corrections, this represents a reasonable approximation as long as y is small or the considered energy scale is roughly below M_N and in the remaining region, the altered running of the relevant couplings does not influence the presented results significantly.
At one-loop order, only the RGE of λ depends on λ so that the problem of negative values of λ for $\mu \gtrsim 10^7$ GeV, cf. figure 2.1, is circumvented by setting $\lambda = 0$ at the energy scale of interest. Moreover, considering an extended Higgs sector, the added couplings do not alter the one-loop RGEs of the SM gauge and Yukawa couplings, cf. equation (A.88), so that their one-loop running can be considered separately, cf. equation (A.89)[6].
Notice that for the thermal rates only depending on y (γ_D, γ_{Ns}^{sub} and γ_{Nt}), the running of the SM couplings only alters the thermal masses which in case of $M_N \gg m_{\ell_i}, m_H$ does not change the thermal rates significantly. Only for the $\Delta L = 1$ processes, the thermal rates directly depend on the SM coupling constants, meaning that the running for these rates is more important. In detail, for the thermal rates, the couplings at the scale $\mu = \sqrt{s}$ are used while for the calculation of the thermal masses, the couplings at the average particle energy ($\mu = \rho_E/n \sim 3T$) are chosen, for the SM, cf. figure 3.1.

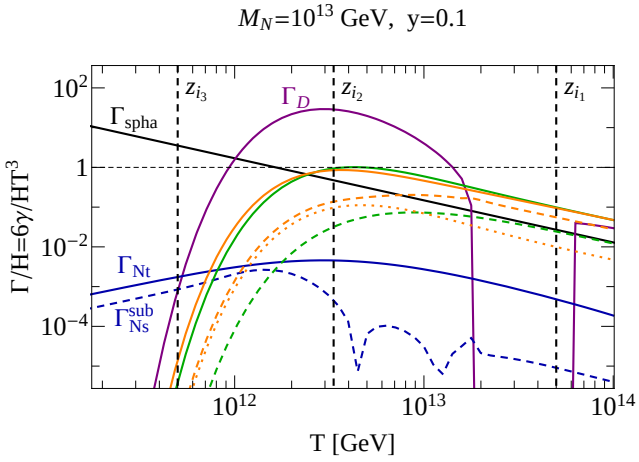

Figure 7.1: Rate of μ_B violation induced sphaleron transitions (straight black line) and L violation (γ_D purple line, $\gamma_{N,s}^{\text{sub}}$ dashed blue line, $\gamma_{N,t}$ blue line, $\gamma_{H,s}$ dashed green line, $\gamma_{H,t}$ green line, $\gamma_{A,s}$ dashed orange line, γ_{A,t_1} orange line, and γ_{A,t_2} dotted orange line) induced by a right-handed neutrino with a Majorana mass of $M_N = 10^{13}$ GeV and a Yukawa coupling of $y = 0.1$. All rates are normalized with respect to the Hubble expansion rate. The three dashed vertical lines correspond to three different initial B-generation scales of interest: $z_{i_1} = M_N/T_{i_1} = 0.2$, $z_{i_2} = M_N/T_{i_2} = 3$, and $z_{i_3} = M_N/T_{i_3} = 20$.

[5]The largest impact on the considered equations of motion when considering the one-loop running of the SM coupling constants is the g dependence of the sphaleron diffusion constant ($\Gamma_{\text{diff}} \propto g^{10}$), cf. equation (4.7). Because this effect was not taken into account in references [40, 39], the used rate of B violation induced by sphaleron transition is roughly three times smaller than the rate used in references [40, 39].

[6]In reference [39], the one-loop running of the Higgs self couplings is ignored. However, taking this one-loop running into account, the benchmark point investigated in reference [39] is disfavored because the coupling strength becomes non-perturbative at $\mu \gtrsim 10^6$ GeV which is way below the temperature range of interest.

An investigation of the thermal rates calculated using the given approximation, cf. figure 7.1 for a benchmark point, shows that, as expected for large z ($z \gtrsim 20$), even for small y, the thermal rates γ_{Ns}^{sub} and γ_{Nt} together dominate the time evolution, while γ_D is dominant for $10 \gtrsim z \gtrsim 1$. For $z \lesssim 1$, γ_D, the remaining $2 \to 2$ processes, and – for large Yukawa couplings – also $\gamma_{N,s}^{\text{sub}}$ and $\gamma_{N,t}$ are relevant. Thus, for small Yukawa couplings, in the window where the decay is kinematically forbidden, the remaining $2 \to 2$ processes with a right-handed Majorana neutrino as external particle dominate the rate of L violation.
Note that in the region where the decay $H \to N\bar{\ell}_i$ is kinematically allowed, no resonant contribution has to be subtracted from $\gamma_{H,s}$ and $\gamma_{A,s}$ because the decays $H \to HA$ and $H \to \overline{Q}_3 U_3$ are still kinematically forbidden, implying that s does not hit the resonance.

Finally, for solving the Boltzmann equations (7.4), initial conditions have to be considered. However, the temperature of the universe after inflation and therewith also the injection scale of the $B - L$ conserving B asymmetry (z_i) resulting from the decay of GUT particles is unknown. It might be argued that the temperature after inflation has to be at least of the order of the GUT breaking scale for being able to produce the bosons responsible for the generation of the B asymmetry. However, as has been shown in reference [46], heavy GUT bosons can also be produced non-thermally due to the decay of the inflaton field. Thus, in principle, the Boltzmann equations need to be solved starting from all reasonable initial temperatures. For this, three different regions of interest can be distinguished. First of all, for $z_i \ll 3$, the injection of the B asymmetry takes place before L violation becomes most efficient, implying that in case of $M_N \lesssim 10^{12}$ GeV sphaleron transitions can erase a significant mount of the B asymmetry before L violation becomes most efficient. For simplicity, this region is represented by choosing $z_{i_1} = 0.2$. For another region of interest, z_i is of the scale where L violation is most efficient, implying that the rate of L violation is only very efficient for a short period before it is Boltzmann suppressed ($z_{i_2} = 3$). Finally, the injection of the B asymmetry can be chosen to occur after L violation is most efficient so that larger Yukawa couplings are needed to obtain efficient rates of L violation. This region is represented by choosing z_i right below the resonance ($z_{i_3} = 20$)[7].

In the following, first of all, the simplest case with only one additional right-handed Majorana neutrino giving rise to a relevant amount of L-violation is investigated, cf. section 7.3. This case occurs when either the other right-handed Majorana neutrinos couple so weakly that the induced amount of L violation is negligible or the induced L violation is only relevant at scales above z_i, or after sphaleron transitions become inefficient ($T \lesssim 100$ GeV). Subsequently, in section 7.4, a simplified model including two right-handed Majorana neutrinos, which are responsible for the generation of the observed Δm^2 in normal and inverted hierarchy, is considered. Finally, in section 7.5, the simplified case with only one relevant right-handed Majorana neutrino is investigated within the scotogenic model, cf. section 6.2, allowing also for the generation of DM.

[7] In references [40, 39], for simplicity, only $z_i = 3$ and $z_i = 10$ are investigated to avoid the region where the decay $H \to N\bar{\ell}_i$ is kinematically allowed. The calculation method of γ_{Ns}^{sub} has been improved, cf. section 5.2, because the numerical integration used before is unstable for z much smaller than 3

7.3 L Violation Induced by One Right-Handed Majorana Neutrino

In the most simple case where it is sufficient to only investigate the SM extended by a single relevant right-handed Majorana neutrino, the basis of lepton doublets can be chosen such that only one of them couples to the right-handed Majorana neutrino of interest. In this basis, the Yukawa interactions involving right-handed charged leptons in general induce transitions between the lepton generations. However, as discussed in section 4.1, the corresponding thermal rates are small compared to the rate of B violation induced by sphaleron transitions meaning that they can be ignored to a good approximation. Thus, only the time evolution of one μ_{B-L_i}, cf. equation (7.4), becomes non-trivial and a coupled differential equation involving two relevant chemical potentials ($\mu_{B-L} = \mu_{B-L_i}$ and μ_B) is obtained. In this case, the equilibrium condition (7.11) simplifies to

$$\mu_{B-L} = \frac{1}{6}\mu_B \,, \tag{7.12}$$

where $m = 1$ and $N_g = 3$ are considered. Using the initial conditions $\mu_{B-L}(z_i) = 0$ and $\mu_B(z_i) = \mu_B^{\text{initial}}$ implies $|\mu_{B-L}(z_i)| \leq |\mu_B^{\text{initial}}|/6$. Furthermore, the equation of motion for μ_B determined by sphaleron transitions implies that $|\mu_B(z)| > c_s(z)|\mu_{B-L}(z)|$, where $c_s(z)$ for solving the Boltzmann equation is given by $c_s = 3/17$, cf. equation (7.6). However, the final value for the B asymmetry (μ_B^{final}) is determined by

$$\mu_B^{\text{final}} = c_s(T_c)\mu_{B-L}^{\text{final}} = \frac{28}{79}\mu_{B-L}^{\text{final}} \leq \frac{28}{79}\frac{1}{6}\mu_B^{\text{initial}} = \frac{14}{237}\mu_B^{\text{initial}} \simeq 0.059\mu_B^{\text{initial}} \,, \tag{7.13}$$

where $\beta\mu_B^{\text{final}} = (2.40 \pm 0.01) \times 10^{-8}$ is needed to produce the observed B asymmetry, cf. equations (4.18) and (4.20).

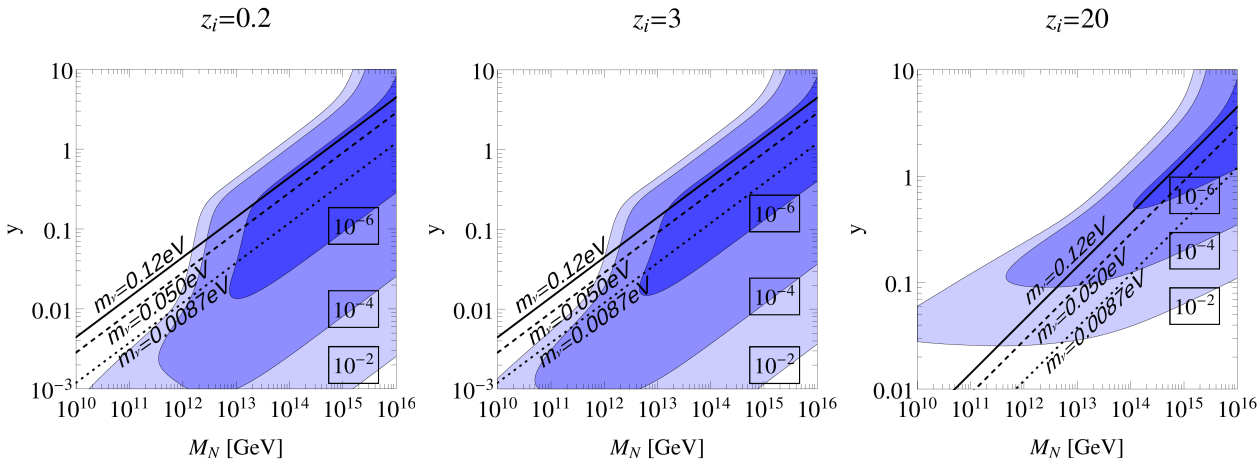

Figure 7.2: Contour plots of the necessary initial $B-L$ conserving B asymmetry ($\beta\mu_B^{\text{initial}}$) to produce the observed final B asymmetry as a function of the Yukawa coupling (y) and the Majorana mass of the right-handed neutrino (M_N). The initial B generation is assumed to occur at $z_{i_1} = M_N/T_{i_1} = 0.2$ (left panel), $z_{i_2} = M_N/T_{i_2} = 3$ (middle panel), and $z_{i_3} = M_N/T_{i_3} = 20$ (right panel). The three diagonal lines in each plot correspond to three different active neutrino masses resulting from the type-I seesaw mechanism. In the dark blue region $\beta\mu_B^{\text{initial}} < 10^{-6}$, in the middle blue region $\beta\mu_B^{\text{initial}} < 10^{-4}$, in the light blue region $\beta\mu_B^{\text{initial}} < 10^{-2}$, and in the remaining region $\beta\mu_B^{\text{initial}} > 10^{-2}$ are required.

Using this setup, the resulting Boltzmann equation can be solved numerically. The result for the required initial $B-L$ conserving B asymmetry $\beta\mu_B^{\text{initial}}$ to produce the observed final B asymmetry for the three different injection scales of interest ($z_{i_1}=0.2$, $z_{i_2}=3$, and $z_{i_3}=20$) as a function of M_N and y is shown in figure 7.2. For all considered injection scales, the necessary value of $\beta\mu_B^{\text{initial}}$ becomes large when y is either so large ($y \gtrsim \sqrt{M_N}\times 10^{-7}$) that the non-resonant L violation induced by $\gamma_{N,s}^{sub}$ and $\gamma_{N,t}$ efficiently coexists with sphaleron transitions or so small that L-violation is never efficient ($y \lesssim 2\sqrt{M_N}\times 10^{-10}$). Because the injection scale in the left panel of figure 7.2 ($z_{i_1}=0.2$) is assumed to be larger than to the scale where L violation is most efficient, the required $\beta\mu_B^{\text{initial}}$ becomes strongly suppressed for $M_N \lesssim 10^{13}$ GeV. If, the injection scale is assumed to be roughly at the scale where L violation is most efficient (middle panel, $z_{i_2}=3$) the necessary $\beta\mu_B^{\text{initial}}$ for $M_N \gtrsim 10^{13}$ GeV is close to the case of considering a higher injection scale. However, for $M_N \lesssim 10^{13}$ GeV, a slightly larger value for y is sufficient to explain the observed B asymmetry. The right panel in figure 7.2 ($z_{i_3}=20$) can be explained by the same argument but here, significantly larger values of y are allowed in the region $M_N \lesssim 10^{13}$ GeV because for the same value of y, the L violation is significantly less efficient, cf. figure 7.1. This can also be seen from the fact that the region where L violation is never efficient is significantly enlarged so that for $y \lesssim 0.1$, $\beta\mu_B^{\text{initial}} > 10^{-4}$ is required while for $z_i=3$ and $z_i=0.2$, $y\sim 0.01$ is still in the region of maximal washout requiring $\beta\mu_B^{\text{initial}} < 10^{-68}$.

The black lines in figure 7.2 correspond to different active neutrino masses of special interest resulting from the type-I seesaw mechanism, cf. equation (5.10): the black solid line represents an active neutrino mass of 0.12 eV which is the Planck bound, cf. equation (C.7), on the sum of the active neutrino masses, while the dashed and dotted black lines denote $m_\nu = \sqrt{\Delta m^2_{\text{atm}}} \simeq 5.0\times 10^{-2}$ eV and $m_\nu = \sqrt{\Delta m^2_{\text{sol}}} \simeq 8.7\times 10^{-3}$ eV, respectively, cf. equation (C.4). Thus, for the considered right-handed Majorana neutrino to contribute significantly to the active neutrino masses, y has to be in the region between the solid and the dotted black lines. Note that this region, without tuning the model in this direction, falls right into the region where the necessary initial B asymmetry is minimal. Thus, it can be concluded that a right-handed Majorana neutrino with $M_N \gtrsim 10^{13}$ GeV can naturally explain both the observed active neutrino masses and the observed B asymmetry when a $B-L$ conserving B asymmetry of the order $\beta\mu_B^{\text{initial}} \sim 10^{-6}$ is injected at $T \gtrsim M_N/3$.

To highlight the interplay of L violation and sphaleron transitions in more detail, three different regions of interest are investigated in more detail, cf. figure 7.3. First of all, choosing $M_N = 10^{15}$ GeV and $y=1$, the corresponding rate of L violation is very efficient before sphaleron transitions are efficient but become inefficient when sphaleron transitions reach equilibrium, cf. the top left panel in figure 7.3. Thus, the generated $B-L$ asymmetry is sizable for all considered z_i ($\mu_B^{\text{final}}/\mu_B^{\text{initial}} > 0.1$), cf. the bottom left panel in figure 7.3. In comparison, considering $M_N = 10^{15}$ GeV and $y=0.01$, the induced rate of L violation is never efficient, resulting in a small generated $B-L$ asymmetry, cf. the middle panels in figure 7.3. Finally, choosing $M_N = 2\times 10^{12}$ GeV and $y=0.1$, the corresponding rate of L violation coexists with sphaleron transitions, resulting in a small final $B-L$ asymmetry for $z_i=0.2$ and $z_i=3$ but for $z_i=20$ – where the rate of L violation is never too efficient – still

[8] Note that the deviation of the upper boundary of the blue regions from the linear behavior for $y \gtrsim 5$ is not a numerical mis-modulation but the decay width of N becomes comparable to M_N. Consequently, the Γ_N dependence of $\gamma_{N,s}^{\text{sub}}$ and $\gamma_{N,t}$ in the limit $s \ll M_N^2$ is relevant.

$\mu_B^{\text{final}}/\mu_B^{\text{initial}} \sim 10^{-3}$ is obtained, cf. the right panels in figure 7.3.

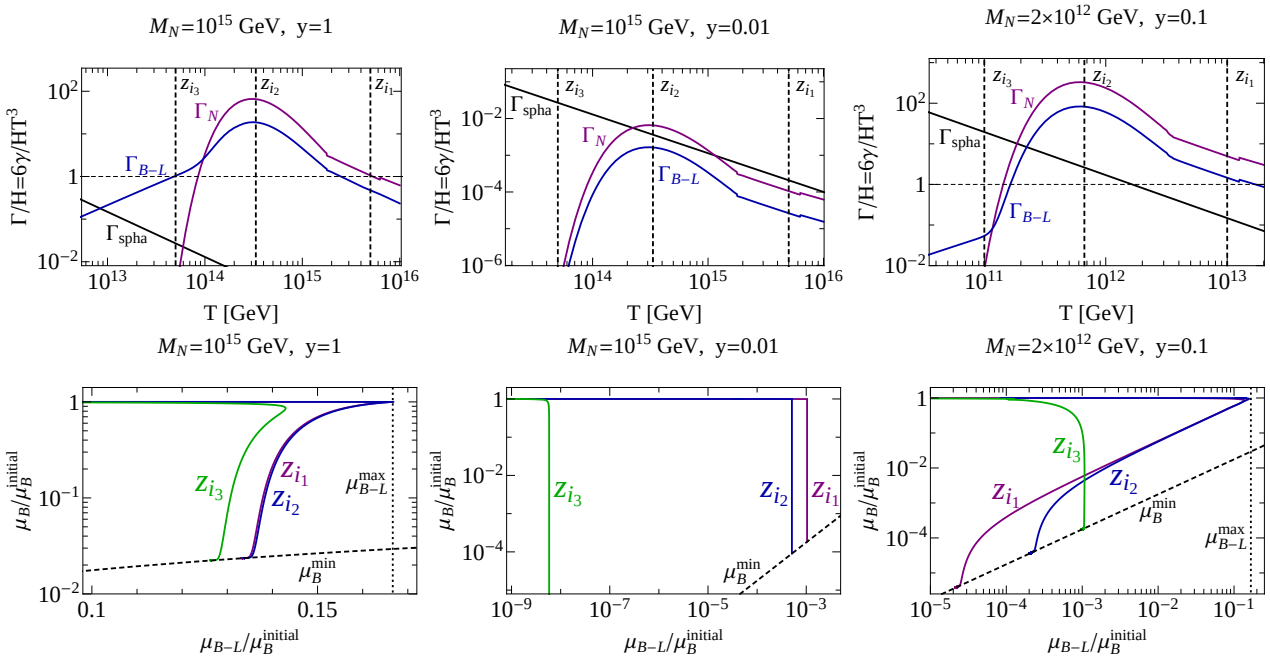

Figure 7.3: Top row: Rate of μ_B violation induced by sphaleron transitions (straight black line), L violation (blue line), and N interaction (purple line) for three benchmark points (columns) with different Yukawa couplings (y) and right-handed neutrino masses (M_N). All rates are normalized with respect to the Hubble expansion rate.
Bottom row: Time evolution trajectory in the μ_B-μ_{B-L} plane starting from an initial $B-L$ conserving B asymmetry (μ_B^{initial}) for the three benchmark points. The initial B generation is assumed to occur at $z_{i_1} = 0.2$ (right vertical dashed line in the rate plots and purple line in the bottom row plots), $z_{i_1} = 3$ (middle vertical dashed line in the rate plots and blue line in the bottom row plots), and $z_{i_1} = 20$ (left vertical dashed line in the rate plots and green line in the bottom row plots).

Finally, it should be mentioned that the statement given in reference [27] saying that for $M_N \sim 10^{16}$ GeV and $y \sim 1$, the observed B asymmetry can be reproduced, agrees with the results from the detailed analysis where this benchmark point falls into the region of minimal required $\beta\mu_B^{\text{initial}}$, cf. figure 7.2.

In preparation of explaining the numerical results shown in the next section, the required initial $B-L$ conserving B asymmetry ($\beta\mu_B^{\text{initial}}$) to produce the observed final B asymmetry when assuming the initial B generation to occur at $z_i = 6$ and $z_i = 10$ is shown in figure 7.4. As can be seen, assuming the initial B generation to occur in this region ($6 \lesssim z_i \lesssim 10$) is of special interest because, for the active neutrino masses of interest generated by the type-I seesaw mechanism, it allows to secure a sizable amount of the initial $B-L$ conserving B asymmetry ($\beta\mu_B^{\text{initial}} < 10^{-4}$) even for Majorana masses of a few 10^{10} GeV. The reason for that is that for $6 \lesssim z_i \lesssim 10$, L violation in the parameter space of interest is efficient a z_i but rapidly becomes inefficient. Thus, efficient L violation occurs before all asymmetry is washed out by sphaleron transitions but it becomes inefficient when the sphaleron equilibrium condition is reached.

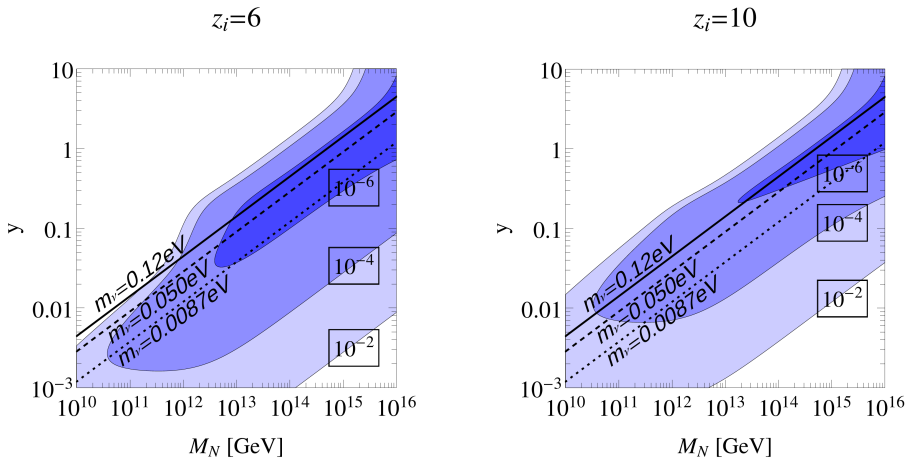

Figure 7.4: Contour plots of the needed initial $B-L$ conserving B asymmetry ($\beta\mu_B^{\text{initial}}$) to produce the observed final B asymmetry as a function of the Yukawa coupling (y) and the Majorana mass of the right-handed neutrino (M_N). The initial B generation is assumed to occur at $z_{i_1} = M_N/T_{i_1} = 6$ (left panel) and $z_{i_3} = M_N/T_{i_3} = 10$ (right panel). The three diagonal lines in each plot correspond to three different active neutrino masses of special interest resulting from the type-I seesaw mechanism, cf. equation (5.10). In the dark blue region $\beta\mu_B^{\text{initial}} < 10^{-6}$, in the middle blue region $\beta\mu_B^{\text{initial}} < 10^{-4}$, in the light blue region $\beta\mu_B^{\text{initial}} < 10^{-2}$, and in the remaining region $\beta\mu_B^{\text{initial}} > 10^{-2}$ are required.

7.4 L Violation Induced by Two Right-Handed Majorana Neutrinos

Next, a more general case involving two relevant right-handed Majorana neutrinos – N_1 and N_2, which are both mass eigenstates – is investigated. Again, it is assumed that the L violation induced by these two right-handed Majorana neutrinos is the only relevant source of L violation and that the Yukawa interaction involving right-handed charged leptons are irrelevant. In this case, the lepton doublets can be rotated into a basis in which only two of the three lepton doublets couple to the right-handed Majorana neutrinos while the third decouples. For simplicity, it is assumed that the lepton doublets can be further rotated such that only one of them couples to one of the right-handed Majorana neutrinos while the other couples to the other right-handed Majorana neutrino.
Thus, the relevant part of the Lagrangian in this rotated basis is given by

$$\mathcal{L} \supset \sum_{i=1}^{2} \left(i\overline{\Psi}_{N_i}\partial\!\!\!/\Psi_{N_i} - y_i\overline{\Psi}_{\ell_i}H^\dagger\Psi_{N_i} - \frac{M_{N_i}}{2}\left(\overline{\Psi^c}_{N_i}\Psi_{N_i} + \overline{\Psi}_{N_i}\Psi^c_{N_i}\right)\right) , \tag{7.14}$$

where the neutrinos after EWSB obtain masses of $m_1 = y_1^2v^2/(2M_{N_1})$ and $m_2 = y_2^2v^2/(2M_{N_2})$ from the type-I seesaw mechanism, cf. equation (5.10). Furthermore, to reduce the parameter space, it is assumed that there is no additional source of neutrino masses requiring either

$$\begin{aligned} m_1 &= \sqrt{\Delta m^2_{\text{sol}}} \simeq 8.7 \times 10^{-3}\ \text{eV} \\ m_2 &= \sqrt{\Delta m^2_{\text{atm}} + \Delta m^2_{\text{sol}}} \simeq 5.0 \times 10^{-2}\ \text{eV} \end{aligned} , \tag{7.15}$$

in normal order or

$$\begin{aligned} m_1 &= \sqrt{\left|\Delta m^2_{\text{sol}} + \Delta m^2_{\text{atm}}\right|} \simeq 4.9 \times 10^{-2}\ \text{eV} \\ m_2 &= \sqrt{\left|\Delta m^2_{\text{atm}}\right|} \simeq 5.0 \times 10^{-2}\ \text{eV} \end{aligned} \quad , \tag{7.16}$$

in inverted order to be in agreement with the observations from neutrino oscillation experiment, cf. equation (C.4).

Using these assumptions, the necessary initial $B-L$ conserving B asymmetry can again be calculated solving the Boltzmann equations (7.4) taking into account the L violation induced by N_1 and N_2. To examine the interplay of both $B-L$ violating rates, the injection scale of the GUT B asymmetry is assumed to be $z_i = M_{\text{min}}/T = 0.2$ with $M_{\text{min}} = \min\{M_{N_1}, M_{N_2}\}$ so that both rates can coexist efficiently – as long as their Majorana masses differ by less then one order of magnitude. Furthermore, the result can be compared with the result from the 3+1 case choosing $z_i = 0.2$ discussed in the previous section, cf. the left panel in figure 7.2.

Now the time evolution of two μ_{B-L_i} become non-trivial so that a coupled differential equation involving three relevant chemical potentials (μ_{B-L_1}, μ_{B-L_2}, and μ_B) is obtained. Consequently, the equilibrium condition (7.11) simplifies to

$$\mu_{B-L} = \frac{4}{15}\mu_B\,, \tag{7.17}$$

where $m = 1$ and $N_g = 3$ are considered. Using the initial conditions $\mu_{B-L_i}(z_i) = 0$ and $\mu_B(z_i) = \mu_B^{\text{initial}}$, this – similar to equation (7.13) – leads to the condition

$$\mu_B^{\text{final}} = c_s(T_c)\mu_{B-L}^{\text{final}} = \frac{28}{79}\mu_{B-L}^{\text{final}} \leq \frac{28}{79}\frac{4}{15}\mu_B^{\text{initial}} = \frac{112}{1185}\mu_B^{\text{initial}} \simeq 0.095\mu_B^{\text{initial}}\,. \tag{7.18}$$

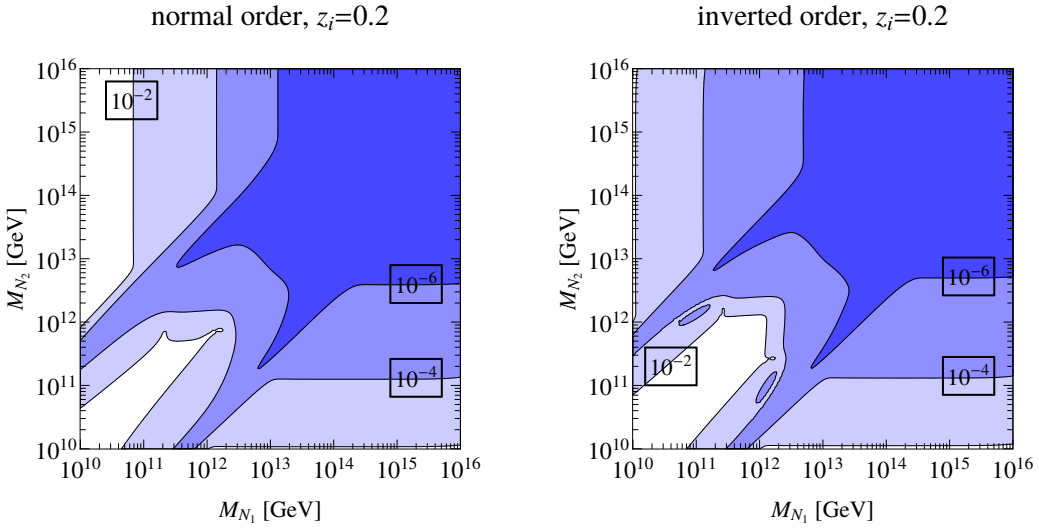

Figure 7.5: Contour plots of the necessary initial $B-L$ conserving B asymmetry μ_B^{initial} to produce the observed final B asymmetry as a function of the two right-handed neutrino mass, where M_{N_1} and M_{N_2} (horizontal and vertical axis) is responsible for the generation of m_1 and m_2, respectively, in normal order (left panel) or inverted order (right panel). It is assumed that the generation of initial B asymmetry occurs at $z_i = \min\{M_{N_1}, M_{N_2}\}/T = 0.2$.

The resulting required value for $\beta\mu_B^{\text{initial}}$ to produce the observed final B asymmetry for $z_i = 0.2$ in normal and inverted order as a function of both Majorana masses M_{N_1} and M_{N_2} is shown in figure 7.5. Contrary to the naive expectation, assuming one Majorana mass to be much larger than the other ones, the result from the previous section is not simply reproduced. For $M_{N_1}, M_{N_2} \gtrsim 10^{13}$ GeV, corresponding to the region of maximal washout, the result is indeed identical to the 3+1 result with $m_\nu = 8.7 \times 10^{-3}$ eV ($m_\nu = 5.0 \times 10^{-2}$ eV) corresponding to the dotted (dashed) line in the left panel of figure 7.2. Nevertheless, as can be seen in figure 7.5, considering another right-handed Majorana neutrino with much larger mass, in this region, still a sizable amount of B violation is secured.

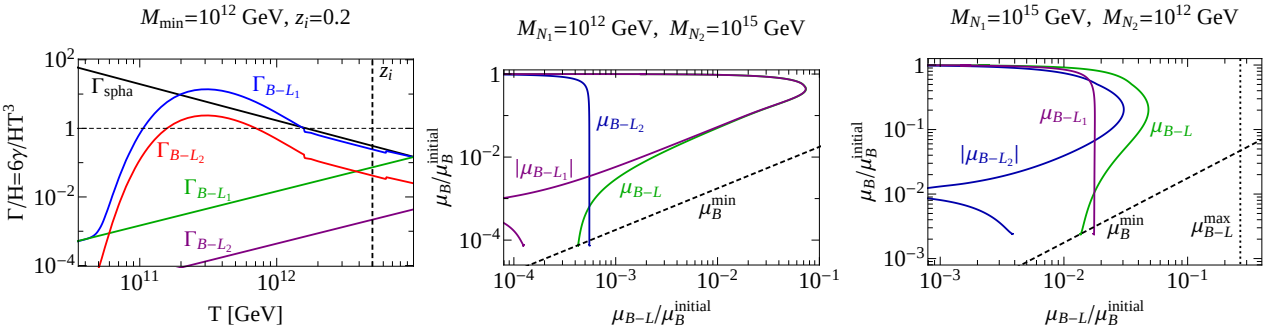

Figure 7.6: Right panel: Rate of μ_B violation induced by sphaleron transitions (straight black line), $B-L_1$ violation (blue and green line), and $B-L_2$ violation (red and purple line) where the blue (red) and the green (purple) lines correspond to two different Majorana masses of a right-handed neutrino ($M_{N_1}(M_{N_2}) = 10^{12}$ GeV for the blue (red) line and $M_{N_1}(M_{N_2}) = 10^{15}$ GeV for the green (purple) line) generating m_1 (m_2) defined in equation (7.15) by the type-I seesaw mechanism in normal hierarchy. All rates are normalized with respect to the Hubble expansion rate.
Middle and left panel: Time evolution trajectory in the μ_B-μ_{B-L} plane with $B - L$ corresponding to $B-L_1$ (purple line), $B-L_2$ (blue line), and the sum of both, $B-L$ (green line) for two benchmark points in the M_{N_1}-M_{N_2} plane. For both benchmark points, the initial B generation is assumed to occur at $T = 5 \times \min\{M_{N_1}, M_{N_2}\} = 5 \times 10^{12}$ GeV.

As can be seen in figure 7.6, the reason for that is that the rate of L violation induced by $\gamma_{N,s}^{\text{sub}}$ and $\gamma_{N,t}$ of the much heavier right-handed Majorana neutrino is still sizable enough to partly keep the initial B asymmetry from being washed out. Moreover, this result does not depend on the exact value of the heavier Majorana mass because the rate of L violation induced by a right-handed Majorana neutrino for $T \ll M_N$ is equivalent when the active neutrino mass generated by the type-I seesaw mechanism is equivalent and $y \lesssim 5$ holds so that Γ_N is negligibly small.

To understand the shape of the region where the interplay of both Majorana masses is relevant shown in figure 7.5, three benchmark points with a fixed initial B asymmetry injection scale ($M_{\text{min}}/z_i = 5 \times 10^{11}$ GeV) are investigated in more detail, cf. figure (7.7). First of all, considering degenerated Majorana masses $M_{N_2} = M_{N_1} = 10^{11}$ GeV, the L violation induced by both right-handed Majorana neutrinos efficiently coexists with sphaleron transitions for a long period, implying that only a tiny fraction of the initial B asymmetry survives, cf. the right panel in the top row of figure 7.7. However, considering $M_{N_2} = 2 \times 10^{12}$ GeV, L violation induced by N_2 is only efficient for a short period and then falls out of equilibrium rapidly, cf. the left panel in the top row of figure 7.7, meaning

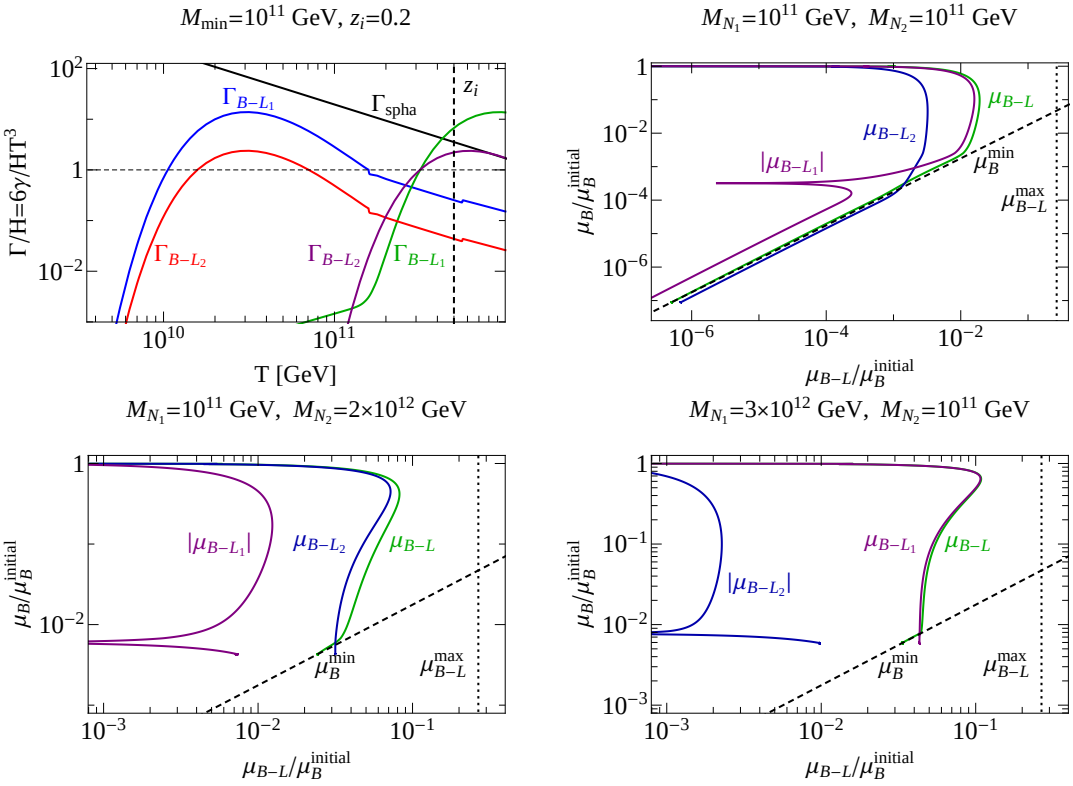

Figure 7.7: Top left panel: Rate of μ_B violation induced by sphaleron transitions (straight black line), $B-L_1$ violation (blue and green line), and $B-L_2$ violation (red and purple line) where the blue (red) and the green (purple) lines correspond to two different Majorana masses of a right-handed neutrino ($M_{N_1}(M_{N_2}) = 10^{11}$ GeV for the blue (red) line and $M_{N_1} = 3\times10^{12}$ GeV($M_{N_1} = 2\times10^{12}$ GeV) for the green (purple) line) generating m_1 (m_2) defined in equation (7.15) in normal hierarchy by the type-I seesaw mechanism. All rates are normalized with respect to the Hubble expansion rate.
Top right panel and bottom row: Time evolution trajectory in the μ_B-μ_{B-L} plane with $B-L$ corresponding to $B-L_1$ (purple line), $B-L_2$ (blue line), and the sum of both, $B-L$ (green line) for three benchmark points in the M_{N_1}-M_{N_2} plane. For all three benchmark points the initial B generation is assumed to occur at $T = 5\times\min\{M_{N_1}, M_{N_2}\} = 5\times10^{11}$ GeV.

that $B-L_2$ violation is only efficient before sphaleron transitions equilibrate, producing a sizable amount of $B-L_2$ asymmetry, cf. the left panel in the bottom row of figure 7.7. The same is also true considering $M_{N_1} = 3\times10^{12}$ GeV where the L violation induced by N_1 is only efficient for a short period, cf. the right panel in the bottom row of figure 7.7. Consequently, the peaks in the shapes shown in figure 7.5 correspond to the region $6 \lesssim z_i \lesssim 10$ with one of the right-handed Majorana neutrinos allowing to secure a sizable amount of the initial $B-L$ conserving B asymmetry even for small Majorana masses, cf. figure 7.4.

Note that both effects highlighted in figures 7.6 and 7.7 only occur in the approximation where each right-handed Majorana neutrino couples to one of the active neutrino mass eigenstates and

that mixing ($y_{12} \neq 0$ and $y_{21} \neq 0$) would reduce the amount of $B-L$ asymmetry produced in one of the lepton generations. Furthermore, the approximation of ignoring all Yukawa interactions besides the top Yukawa interaction can still be used for calculating the amount of $B-L$ asymmetry produced in one of the lepton generations. However, when the other right-handed Majorana neutrino coexists efficiently with sphaleron transitions so that both equilibrate, the sub-dominant tau Yukawa interaction transferring the produced $B-L$ asymmetry in one lepton generation with an inefficient rate of L violation into the other lepton generation with an efficient L violation leads to a washout of the secured B asymmetry.

Thus, it can be concluded that – independent of the other Majorana mass – having one of the Majorana masses in the region of minimal required initial B asymmetry ($M_N \gtrsim 10^{13}$ GeV, cf. figure 7.2) and assuming the B asymmetry injection to take place before this Majorana neutrino falls out of equilibrium, a sizable amount of $B-L$ asymmetry is produced, meaning that $\beta\mu_B^{\text{initial}} \lesssim 10^{-6}$ is sufficient to explain the observed B asymmetry. However, this statement is only valid as long as the influence of flavor mixing – inducing lepton asymmetry transitions between the different generations – can be neglected to a good approximation.

7.5 L Violation Induced by One Right-Handed Majorana Neutrino Within the Scotogenic Model

In the scotogenic model, cf. section 6.2, the masses of the active neutrinos are loop induced and in the limit $\lambda_5 v^2 \ll m_0^2 = m_\phi^2 + (\lambda_3+\lambda_4)v^2/2 \ll M_{N_i}$ given by equation (6.33b). Furthermore, the Yukawa interaction term $y_{ij}\overline{\Psi}_{\ell_j}(x)H^c(x)\Psi_{N_i}(x)$ is absent but instead the Yukawa interaction term $y'_{ij}\overline{\Psi}_{\ell_j}(x)\phi^c(x)\Psi_{N_i}(x)$ involving the additional Higgs doublet ϕ is present. Hence, the SM Higgs doublet H in all relevant L violating interactions has to be replaced by ϕ. Consequently, the processes inducing the thermal rates $\gamma_{H,s}$, γ_{H,t_1}, and γ_{H,t_2} are forbidden because of the imposed Z_2 symmetry. Thus, all relevant thermal rates are given by γ_D, $\gamma_{A,s}$, γ_{A,t_1}, γ_{A,t_2}, $\gamma_{N,s}^{\text{sub}}$, and $\gamma_{N,t}$ where the Yukawa coupling involving H is replaced by the Yukawa coupling involving ϕ ($y \to y'$) and m_H is replaced by m_ϕ.

Additionally, the reaction transferring a particle-antiparticle asymmetry between both Higgs doublets ($\phi^{(*)}\phi^{(*)} \leftrightarrow H^{(*)}H^{(*)}$) become relevant. The corresponding thermal rate is approximately given by

$$\gamma_{\phi\phi\to HH} \approx \frac{T^4}{64\pi^4}\int\limits_0^\infty dx\sqrt{x}\,\hat{\sigma}_{\phi\phi\to HH}(T^2x)K_1(\sqrt{x}) = \frac{T^4\lambda_5^2}{512\pi^5}\,, \tag{7.19}$$

with

$$\hat{\sigma}_{\phi\phi\to HH}(s) \approx 2s\sigma_{\phi\phi\to HH}(s) = \frac{8\pi s}{64\pi^2 s}\left(\frac{\lambda_5}{2}\right)^2 = \frac{\lambda_5^2}{32\pi}\,, \tag{7.20}$$

meaning that it enters the Boltzmann equations as[9]

$$z\frac{d}{dz}\beta\mu_\phi = -z\frac{d}{dz}\beta\mu_H = \frac{12\gamma_{\phi\phi\to HH}}{T^3\mathsf{H}(T)}(\beta\mu_H - \beta\mu_\phi) := \Gamma_{\lambda_5}(\beta\mu_H - \beta\mu_\phi)$$
$$\approx \frac{3T\lambda_5^2}{128\pi^5\mathsf{H}(T)}(\beta\mu_H - \beta\mu_\phi) \approx \frac{\lambda_5^2}{T}(\beta\mu_H - \beta\mu_\phi) \times 5.35 \times 10^{13}\ \text{GeV}\,. \tag{7.21}$$

Consequently, in the region of interest, $\lambda_5^2 \gtrsim 1/30$ is necessary to obtain a rate larger than the rate of B violation induced by sphaleron transitions.
Moreover, the time evolution considering the inert Higgs model is not expected to significantly differ from the SM case, cf. figure 7.2, but the generated active neutrino masses are suppressed by $\sim \lambda_5/4$ in the region of interest. Consequently, it can be estimated that $|\lambda_5| \gtrsim 0.2$ is needed to generate active neutrino masses within the observed rage and to secure a sizable amount of B asymmetry ($10^{-6} \lesssim \mu_B^{\text{initial}} \lesssim 10^{-4}$) from being washed out by sphaleron transitions.

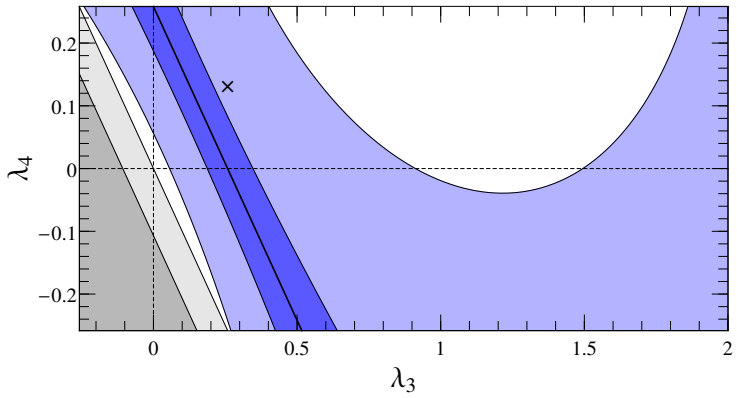

Figure 7.8: Contour plot of the region in the λ_3-λ_4 plane being not excluded at 90% CL by the XENON1T experiment (blue region) choosing $\lambda_5(m_{\tilde{H}}) = -\lambda_{\text{SM}}(m_h) \approx -0.258$. $\tilde{H}$ is assumed to be responsible for the observed relic DM density, implying that $m_{\tilde{H}}$ is determined by the required annihilation cross section. The darker blue region is more than one order of magnitude below the 90% CL bound of XENON1T and the straight black line corresponds to a vanishing DM-nucleon cross section at tree level. The light and dark gray region correspond to a potential which is unstable at tree level assuming $\lambda_2(m_{\tilde{H}}) = \lambda_{\text{SM}}(m_h)$ and $\lambda_2(m_{\tilde{H}}) = 2\lambda_{\text{SM}}(m_h)$, respectively.

For this reason, in the following $\lambda_5(m_H) = -\lambda_{\text{SM}}(m_h) \approx -0.258$ is chosen. Using this, the allowed values of $\lambda_4(m_{\tilde{H}})$ and $\lambda_3(m_{\tilde{H}})$ which generate the observed relic DM density, cf. equation (6.22), and, at the same time, are not in conflict with direct detection experiments, cf. equation (6.25), are shown in figure 7.8. The shown straight black line corresponds to $\lambda_3 + \lambda_4 + \lambda_5 = 0$ yielding – at tree-level – a vanishing DM-nucleon cross section. Note that the parameter space with $\lambda_4(m_{\tilde{H}}) > \lambda_{\text{SM}}(m_h)$ is excluded by requiring $\tilde{H}$ to be a DM candidate and demanding $m_{\tilde{H}}$ to be the lightest component of ϕ.

[9] The factor 12 is composed of a factor of 3 from equation (3.35), a factor of 2 arising from two contributing initial states, and a factor of 2 from having two initial ϕ and two final H.

Furthermore, the region with $\lambda_3 > 2$ not shown is completely unconstrained by direct detection[10].

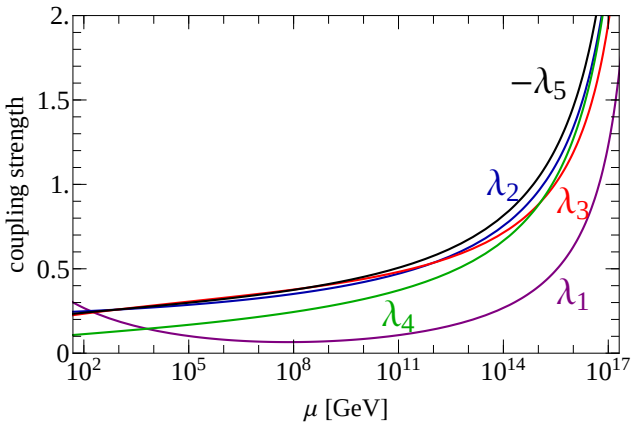

Figure 7.9: One-loop running of the Higgs self couplings for the benchmark point $\lambda_1(m_h) = \lambda_2(m_{\tilde{H}}) = \lambda_3(m_{\tilde{H}}) = -\lambda_5(m_{\tilde{H}}) = \lambda_{\text{SM}}(m_h) \approx 0.258$ and $\lambda_4(m_{\tilde{H}}) = \lambda_{\text{SM}}(m_h)/2 \approx 0.129$ represented by the cross mark in figure 7.8.

However, considering the one-loop running of the Higgs self couplings, cf. equation (A.89), the Higgs self couplings usually become non-perturbative in the region of interest ($\mu \lesssim 10^{15}$ GeV) when at least one of them is chosen to be approximately of the order 1 at $\mu \sim$ TeV without assuming unnatural cancellation. But having non-perturbative coupling constants does not allow the investigation of scattering processes involving ϕ in the temperature range of interest. To avoid this problem, the benchmark point with $\lambda_1(m_h) = \lambda_2(m_{\tilde{H}}) = \lambda_3(m_{\tilde{H}}) = -\lambda_5(m_{\tilde{H}}) = \lambda_{\text{SM}}(m_h) \approx 0.258$ and $\lambda_4(m_{\tilde{H}}) = \lambda_{\text{SM}}(m_h)/2 \approx 0.129$, cf. cross mark in figure 7.8, is investigated in more detail. These values for the Higgs self couplings fulfill all requirements and – considering the one-loop running – correspond to perturbative coupling constants for $T \lesssim 10^{17}$ GeV, cf. figure 7.9. Moreover, in the region of interest ($T \gtrsim 10^{10}$ GeV), $\lambda_5^2 \gtrsim 0.25$ holds, meaning that the conversion of the particle-antiparticle asymmetry among both Higgs doublets is roughly one order of magnitude more efficient than sphaleron transitions. Consequently, it can to a good approximation be assumed that the chemical potentials of H and ϕ are in thermal equilibrium, meaning that the time evolution of the relevant chemical potentials is still determined by equation (7.4) with $m = 2$.
Finally, to obtain the observed relic DM density, cf. equation (6.22), for this benchmark point, $m_{\tilde{H}} \approx 878$ GeV is required. Consequently, the benchmark point is also not excluded by other experiments such as collider experiments.

The thermal rates for the benchmark point choosing $M_N = 10^{13}$ GeV and $y' = 0.1$ are shown in figure 7.10. Because of the significantly larger thermal mass of ϕ compared to H, the region where the decay is kinematically forbidden ($\gamma_D = 0$) moves to larger values of z, cf. figure 7.1. The other thermal rates change slightly as well. However, the general picture is still the same so that no huge

[10] In reference [39], only the DM annihilation cross section induced by λ_3 and not the contribution form λ_4, λ_5 and the gauge couplings was considered. As a consequence, the parameter space with $\lambda_3 \lesssim 2$ was found to be excluded by direct detection. Furthermore, $\lambda_5 \sim 1$ was assumed. However, taking into account the one-loop running, this parameter region is disfavored because the coupling constants becomes non-perturbative at scales below the temperature range of interest.

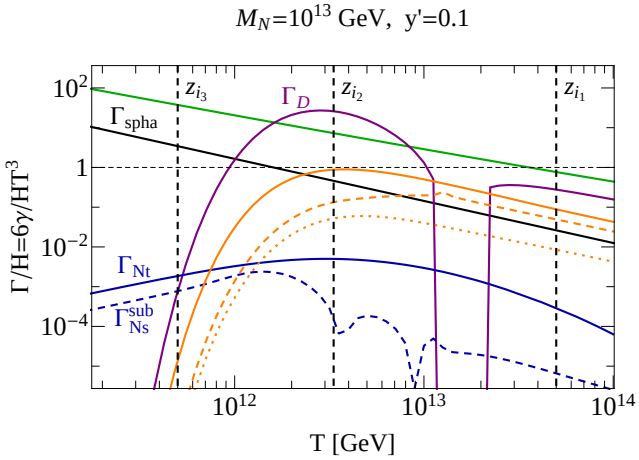

Figure 7.10: Rate of μ_B violation induced by sphaleron transitions (straight black line), μ_H-μ_ϕ equilibration (Γ_{λ_5} straight green line), and L violation (γ_D purple line, $\gamma^{\rm sub}_{N,s}$ dashed blue line, $\gamma_{N,t}$ blue line, $\gamma_{A,s}$ dashed orange line, γ_{A,t_1} orange line, and γ_{A,t_2} dotted orange line) induced by a right-handed neutrino with a Majorana mass of $M_N = 10^{13}$ GeV and a Yukawa coupling of $y = 0.1$. All rates are normalized with respect to the Hubble expansion rate. The three dashed vertical lines correspond to three different initial B generation scales of interest: $z_{i_1} = M_N/T_{i_1} = 0.2$, $z_{i_2} = M_N/T_{i_2} = 3$, and $z_{i_3} = M_N/T_{i_3} = 20$.

difference to the results from section 7.3 are expected.
Moreover, the equilibrium condition (7.11) becomes

$$\mu_{B-L} = \frac{8}{33}\mu_B\,, \tag{7.22}$$

leading to the condition

$$\mu_B^{\rm final} = c_s(T_c)\mu_{B-L}^{\rm final} = \frac{8}{23}\mu_{B-L}^{\rm final} \leq \frac{8}{23}\frac{8}{33}\mu_B^{\rm initial} = \frac{64}{759}\mu_B^{\rm initial} \simeq 0.084\mu_B^{\rm initial}\,, \tag{7.23}$$

where now $\beta\mu_B^{\rm final} = (2.49\pm0.01)\times10^{-8}$ is needed to produce the observed B asymmetry, cf. equation (4.21).

As expected, the numerical results from solving the Boltzmann equations, cf. figure 7.11, only slightly differ from the results shown in section 7.3. It can be seen that the different region shown in figure 7.11 are slightly enlarged to higher Yukawa couplings. The reason for that is that for the investigated benchmark point, m_ϕ is larger than m_H in the SM, resulting in a slightly smaller decay width and a shift of the region where the decay is kinematically forbidden, cf. figures 7.1 and 7.10. Furthermore, the Hubble expansion rate and the rate of μ_B violation induced by sphaleron transitions slightly change because two Higgs doublets are considered. Hence, the main difference between figure 7.2 and figure 7.11 is that the black lines – corresponding to three neutrino masses of special interest – move upwards as they are here determined by equation (6.33b) which is suppressed by approximately $|\lambda_5|/4$. As desired, for the chosen value of λ_5, the necessary initial B asymmetry in the region of special interest ($\Delta m^2_{\rm sol} \lesssim m^2_\nu \lesssim \Delta m^2_{\rm atm}$) is still reachable. But when choosing λ_5 significantly smaller

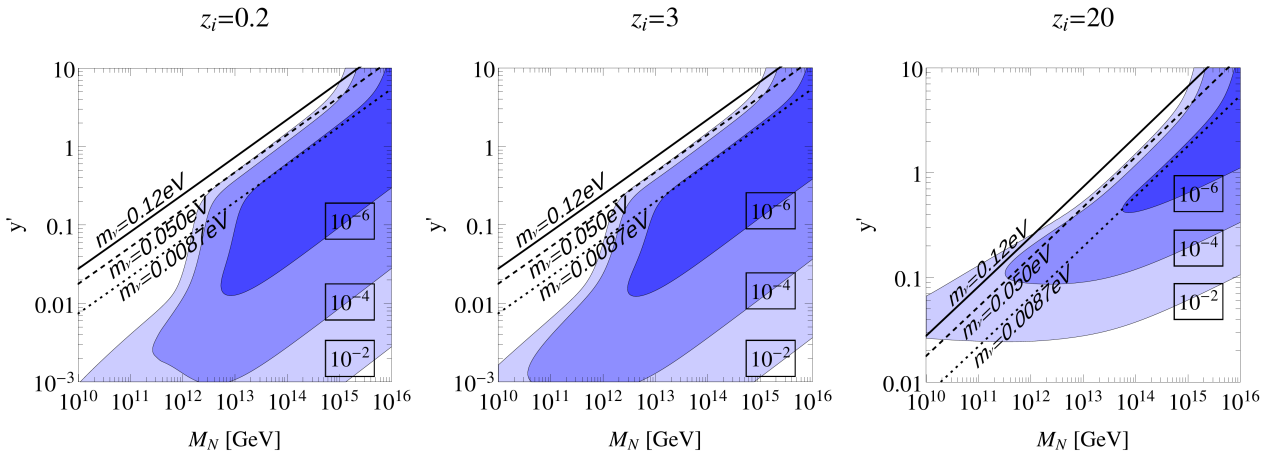

Figure 7.11: Contour plots of the necessary initial $B - L$ conserving B asymmetry ($\beta\mu_B^{\text{initial}}$) to produce the observed final B asymmetry as a function of the Yukawa coupling (y) and the Majorana mass of the right-handed neutrino (M_N). The initial B generation is assumed to occur at $z_{i_1} = M_N/T_{i_1} = 0.2$ (left panel), $z_{i_2} = M_N/T_{i_2} = 3$ (middle panel), and $z_{i_3} = M_N/T_{i_3} = 20$ (right panel). The three diagonal lines in each plot correspond to three different active neutrino masses resulting from the scotogenic model choosing $\lambda_5(m_H) \approx 0.258$ and $m_0 \approx 883$ GeV. In the dark blue region $\beta\mu_B^{\text{initial}} < 10^{-6}$, in the middle blue region $\beta\mu_B^{\text{initial}} < 10^{-4}$, in the light blue region $\beta\mu_B^{\text{initial}} < 10^{-2}$, and in the remaining region $\beta\mu_B^{\text{initial}} > 10^{-2}$ are required.

($\lambda_5 \lesssim 0.05$), even for a generated active neutrino mass of $m_\nu^2 = \Delta m_{\text{sol}}^2$, no significant amount of B asymmetry survives.

8 Thermal Aspects of Leptogenesis

In section 4.2, the idea of putting the origin of the observed B asymmetry into the lepton sector (leptogenesis) is motivated. Right-handed Majorana neutrinos, introduced to explain the small observed active neutrino masses, are a natural source of L violation and, for this reason, are the essential ingredient for most leptogenesis models. The first and simplest case of a leptogenesis induced by right-handed neutrinos is investigated in section 5.3. There, it is found that in the simplest extension of the SM, where the active neutrino masses are induced by the type-I seesaw mechanism, Majorana masses larger than 10^{10} GeV are required for being able to produce the observed B asymmetry. Thus, it is not expected to produce the particles being responsible for the generation of the observed B asymmetry in experiments in the near future so that proving or disproving this simple leptogenesis model is difficult.

However, this lower bound on the Majorana mass is deduced from considering non-degenerate but hierarchical Majorana masses. In contrast, considering nearly degenerate masses ($M_{N_i} - M_{N_n} \ll M_{N_i} + M_{N_n}$), according to equation (5.37), the CP asymmetry is enhanced, meaning that in principle, much smaller Yukawa couplings are sufficient to generate the required δ_{CP} violation of order 10^{-6}. Consequently, the Majorana mass of the right-handed neutrino, being responsible for the generation of the L asymmetry, can in principle be much smaller than 10^{10} GeV, cf. reference [23]. However, taking the Majorana masses, which are typically assumed to be independent quantities, to be nearly degenerate, seems unnatural.

Thus, to naturally explain the observed B asymmetry with Majorana neutrino masses significantly smaller than 10^{10} GeV, one can consider other active neutrino mass generation models such as the scotogenic model, cf. section 8.1. In this case, larger Yukawa couplings are allowed without being in conflict with the Planck bound on the sum of the active neutrino masses, allowing for larger CP violation. Thermal leptogenesis in the context of the scotogenic model is investigated in detail in reference [41]. Thus, even though the shown investigation was made independently, the given results coincide with the results given in this reference.
Instead of considering models with enlarged Yukawa couplings, one can also use thermal mass corrections to naturally obtain degenerate masses at a specific temperature scale, cf. section 8.2. The idea of using thermal degeneracy of right-chiral neutrino masses has been introduced in reference [3]. Moreover, here, also the idea of using thermal degeneracy of left-chiral neutrino masses and thermal degeneracy of left- and right-chiral neutrino masses are discussed. However, both of them do not allow for new possibilities of leptogenesis and are – probably for this reason – not presently discussed in literature.

8.1 Thermal Leptogenesis With Enlarged Yukawa Couplings

Considering models, such as the scotogenic model, where the masses of the active neutrinos are suppressed by a α_S^i compared to the masses generated by the type-I seesaw mechanism, cf. equation (6.31), significantly larger Yukawa couplings than in the type-I seesaw mechanism are allowed by the Planck bound on the sum of the active neutrino masses. Consequently, the upper bound on the CP violation is shifted, cf. equation (5.44):

$$|\epsilon_{N_i}| \lesssim \frac{\alpha_\nu^n}{\alpha_S^n} \frac{M_{N_i}}{\text{GeV}} \times 10^{-16}\,, \tag{8.1}$$

with $\alpha_\nu^n = \sum_j (m_\nu^I)_{jj}^n/(0.12\text{ eV}) \leq 1$ being the sum of the active neutrino masses induced by N_n in the type-I seesaw mechanism, cf. equation (5.10), normalized to the Planck bound on the sum of the active neutrino masses, cf. equation (C.7). Thus, $M_{N_i} \gtrsim \alpha_S^n \times 10^{10}$ GeV is required for being able to generate a B asymmetry of the observed size.

However, this idea has several weaknesses. First, the out-of-equilibrium condition, cf. equation (5.47), which now becomes

$$\frac{100}{0.12\text{ eV}} \frac{1}{\alpha_S^i} \sum_j (m_\nu)_{jj}^i \overset{!}{\sim} 1\,, \tag{8.2}$$

still needs to be satisfied, implying that the contribution of N_i to the active neutrino masses decreases as the lower bound on M_{N_i} gets smaller. Note that this statement is based on the natural assumption that the suppression of the seesaw mass is comparable for all right-handed Majorana neutrinos ($\alpha_S^i \sim \alpha_S^n$).

Moreover, the shifting of the lower bound on M_{N_i} is limited by the requirement that the rate of L violation induced by N_n needs to be inefficient at $T \sim M_{N_i}$. The rate of L violation induced by N_n for $T \lesssim M_{N_n}/10$ is given by

$$\begin{aligned} \frac{6}{\mathsf{H}(T)T^3}\left(\gamma_{N_n,s}^{\text{sub}} + \gamma_{N_n,t}\right) &\approx \sum_j \frac{9|y'_{nj}|^4 T}{4\pi^5 A_{\mathsf{H}} M_{N_n}^2} = \frac{9T}{\pi^5 A_{\mathsf{H}} v^4} \sum_j \left[(m_\nu^I)_{jj}^i\right]^2 \\ &> \frac{9T\Delta m_{\text{atm}}^2}{\pi^5 A_{\mathsf{H}} v^4}\left(\frac{\alpha_\nu^n}{\alpha_S^n}\right)^2 \approx \left(\frac{\alpha_\nu^n}{\alpha_S^n}\right)^2 \frac{T}{\text{GeV}} \times 10^{-14}\,, \end{aligned} \tag{8.3}$$

cf. equations (5.27) and (5.32). Thus, to fulfill both conditions,

$$\frac{\alpha_\nu^n}{\alpha_S^n}\frac{M_{N_i}}{\text{GeV}} \times 10^{-10} \gtrsim 1 \qquad \text{and} \qquad \left(\frac{\alpha_\nu^n}{\alpha_S^n}\right)^2 \times 10^{-14}\frac{M_{N_i}}{\text{GeV}} \lesssim 1\,, \tag{8.4}$$

$\alpha_\nu^n/\alpha_S^n \lesssim 10^4$ and, consequently, $M_{N_i} \gtrsim 10^6$ GeV are required[1]. Note that this lower bound is only valid when assuming a vanishing initial number density for N_i. In contrast, considering a thermal initial abundance for N_i, the decay width of N_i can be chosen smaller, implying that the production of the $B-L$ asymmetry can be shifted to lower temperatures where L violation induced

[1] Note that equivalently to the introduction of a suppression factor for the active neutrino masses, ignoring the upper bound on the sum of the active neutrino masses leads to the same lower bound for M_{N_i} [12].

by N_n is inefficient. However, the generation of the $B-L$ asymmetry has to proceed before sphaleron transitions become inefficient because otherwise, only an L but no B asymmetry is produced. Hence, it can be estimated that L violation induced by N_n should be inefficient at $T_c \sim \mathcal{O}(100)$ GeV, meaning that $\alpha_\nu^n/\alpha_S^n \lesssim 10^6$, and, consequently, $M_{N_i} \gtrsim 10^4$ GeV are required, cf. reference [41].

Considering the scotogenic model, cf. section 6.2, the suppression of the active neutrino masses compared to the type-I seesaw mass depends on the Higgs coupling λ_5 and the ratio M_{N_i}/m_0, cf. equation (6.33) and figure 6.1. As discussed in section 6.1, $\lambda_5 \gtrsim 2 \times 10^{-6}$, cf. equation (6.27), is required from direct detection experiments, implying that the suppression factors α_S^i and α_S^n are larger than $\sim 10^{-8}$ and 10^{-7} for $M_N \gtrsim 1$ TeV and $M_N \gtrsim 10^3$ TeV, respectively, cf. figure 6.1. Comparing this to the bound $\alpha_\nu^n/\alpha_S^n \lesssim 10^6$ with $\alpha_\nu^n \leq 1$ for not having efficient L violation at the scale where sphaleron transitions become inefficient, there is no significant restriction of the lower bound on λ_5.

Besides the suppression of the active neutrino masses, the scotogenic model also contains a DM candidate: the lightest component of ϕ, cf. section 6.1. Hence, one could get the idea that the out-of-equilibrium condition can be naturally fulfilled, cf. reference [8], because the density of a DM candidate has to fall out of equilibrium at the latest when the temperature falls significantly below the DM mass, to obtain a relic DM abundance. This idea is of special interest in the scotogenic model, where N_i decays into a left-chiral lepton doublet ℓ_i and ϕ, meaning that the decay product of N_i deviates from thermal equilibrium. Thus, for Majorana masses not much larger than the DM mass ($M_{N_i} \gtrsim m_{\tilde{H}}$), for temperatures not much smaller than M_{N_i}, the number density of ϕ naturally falls out of equilibrium when pair annihilation becomes inefficient.

However, there are two caveats to this idea. First, significant deviation from thermal equilibrium of the DM density occurs only when the density is close to the relic density, implying that also the corresponding right-handed neutrino density is strongly Boltzmann suppressed. Furthermore, the relic DM density is suppressed by at least two orders of magnitudes compared to the B asymmetry to be in agreement with the observation, cf. equation (C.8), because $m_{\tilde{H}} \gtrsim 560$ GeV is required, cf. section 6.1. Consequently, the DM density is already smaller than the required $B-L$ asymmetry when it significantly deviates from the equilibrium density, meaning that it is doubtful that within this scenario a sufficiently large B asymmetry is generated to explain observations.
Moreover, as discussed in section 3.2, an L asymmetry can only be generated when the particle inducing L violation fulfills the out-of-equilibrium condition because otherwise the CPT invariance and unitarity of the S matrix imply that no asymmetry is generated but only washed out. Thus, in the scotogenic model, no L asymmetry can be generated by the deviation of ϕ from thermal equilibrium because the only source of L violation are the Majorana fermions[2][3].

[2] Nevertheless, reference [8] claims that this idea is capable to explain the observed B asymmetry as well as the observed DM relic abundance. However, in the Boltzmann equation for the L asymmetry given in reference [8], an L asymmetry can be generated only from DM being out of equilibrium. Furthermore, the shown numerical result for the L violation does not seem to agree with the given Boltzmann equations because an L asymmetry is generated at temperatures where the considered right-handed Majorana neutrinos as well as all components of ϕ are not expected to relevantly deviate from their equilibrium densities.

[3] Note that considering models where pair annihilation itself induces B/L violation, a net B/L asymmetry can be generated, cf. reference [18]

8.2 Leptogenesis With Degenerated Masses Induced by Thermal Corrections

As has been discussed in section 2.10, small mass squared differences can induce large CP violation even for small coupling constants. However, it seems unnatural to assume strongly degenerate Majorana masses for the right-handed neutrinos. Consequently, the question arises whether thermal mass corrections, which can induce degenerated masses more naturally, are capable of significantly enhancing CP violation, leading to an enlarged parameter space for leptogenesis.
There are basically three different cases of interest which are investigated in the following: Degenerate masses of right-chiral neutrinos, degenerate masses of left-chiral lepton doublets, and degenerate masses of left- and right-chiral neutrinos. Note that also temperatures below T_c are investigated. For this reason, here, the distinction between chiral eigenstates and energy eigenstates is of special relevance.

8.2.1 Thermal Degeneracy of Right-Chiral Neutrino Masses

The idea of naturally increasing CP violation due to a mass degeneracy of right-chiral neutrinos induced by thermal mass corrections is investigated in reference [3]. In the following, the basic mechanism behind this idea is presented and the current bound on the sum of the active neutrino masses is applied. Note that the shown investigation is based on previous parts of this thesis and, for this reason, differs from the investigation presented in reference [3]. However, the given results coincides with the results from reference [3].
Considering right-chiral Majorana neutrinos, which only couple via Yukawa interactions to left-chiral neutrinos, their thermal mass correction is given by, cf. equation (B.41) or reference [3],

$$m_{in}^2 = \sum_j \frac{y_{ij} y_{nj}^*}{8} T^2 \tag{8.5}$$

$$\Rightarrow m_{ii}^2 = \sum_j \frac{(m_\nu^I)_{jj}^i}{4v^2} M_{N_i} T^2 \approx 4 \frac{\alpha_\nu^i}{\alpha_S^i} \frac{M_{N_i}}{\text{GeV}} T^2 \times 10^{-16} \,. \tag{8.6}$$

When the focus is on non-degenerate Majorana masses ($|M_{N_n} - M_{N_i}| \sim \max\{M_{N_i}, M_{N_n}\}$), in the region where thermal leptogenesis is not capable to generate the observed B asymmetry, the masses of the right-chiral neutrinos only become degenerate for temperatures much larger than the Majorana masses of interest. To be more precise, to obtain degenerate masses, for the lighter Majorana neutrino at least thermal corrections of the order of the heavier Majorana masses are required:

$$m_{ii}^2 \sim M_{N_n}^2 \qquad \Rightarrow \qquad T_{LC} \sim \sqrt{\frac{\alpha_S^i}{\alpha_\nu^i}} \sqrt{\frac{M_{N_n}^2}{M_{N_i}} \text{GeV}} \times 10^8 \,, \tag{8.7}$$

where $M_{N_i} < M_{N_n}$ is assumed and T_{LC} is the temperature where the energy difference between the energy eigenvalues is minimal.

Furthermore, as discussed in the previous chapter, the relevant processes for the production of right-handed neutrinos are the Higgs boson decay and the $2 \to 2$ scattering processes mediated via Higgs

boson exchange. For both of these processes, the interaction rate normalized with respect to the Hubble expansion rate scales as, cf. equations (3.39) and (3.40),

$$\frac{\Gamma_{N_i}}{\mathsf{H}(T)} \propto \sum_j \frac{|y_{ij}|^2}{T} \propto \frac{\alpha_\nu^i}{\alpha_S^i}\frac{M_{N_i}}{T} \tag{8.8}$$

for $T \gtrsim M_{N_i}$, where the exact proportionality factor depends on the thermal masses. As can be seen from figures 7.1 and 7.10, for the SM and the scotogenic model with not too large Higgs self couplings this proportionality factor is approximately one[4]:

$$\frac{\Gamma_{N_i}}{\mathsf{H}(T)} \sim \frac{\alpha_\nu^i}{\alpha_S^i}\frac{M_{N_i}}{T} \qquad \text{for} \quad T \gtrsim M_{N_i}\,. \tag{8.9}$$

Next, in order to fulfill the out-of-equilibrium condition, the interaction rate has to be inefficient ($\Gamma/\mathsf{H}(T_{LC}) \lesssim 1$). On the other hand, the interaction rate has to be large enough to significantly alter the time evolution during the period when the mixing is enhanced by mass degeneracy. To determine the temperature range of enhanced mixing, the interaction rate has to be compared to the energy difference of N_i and N_n:

$$\hat{\mathrm{H}}_{ii} - \hat{\mathrm{H}}_{nn} \approx \frac{M_{N_i}^2 - M_{N_n}^2}{6T} + 50\,\mathsf{H}(T)\left(\frac{\alpha_\nu^i}{\alpha_S^i}\frac{M_{N_i}}{T} - \frac{\alpha_\nu^n}{\alpha_S^n}\frac{M_{N_n}}{T}\right), \tag{8.10}$$

with $E \sim 3T$ and

$$\hat{\mathrm{H}}_{ii} \approx \frac{M_{N_i}^2 + m_{ii}^2}{2E} \approx \frac{M_{N_i}^2}{6T} + \frac{4}{6}\frac{\alpha_\nu^i}{\alpha_S^i}\frac{M_{N_i}}{\mathrm{GeV}}\,T\times 10^{-16} \approx \frac{M_{N_i}^2}{6T} + 50\,\mathsf{H}(T)\frac{\alpha_\nu^i}{\alpha_S^i}\frac{M_{N_i}}{T}\,. \tag{8.11}$$

Close to the level-crossing temperature, the energy difference can be approximated as

$$\begin{aligned}\hat{\mathrm{H}}_{ii} - \hat{\mathrm{H}}_{nn} &\approx \left[-\frac{M_{N_i}^2 - M_{N_n}^2}{6T_{LC}^2} + 50\frac{\mathsf{H}(T_{LC})}{T_{LC}}\left(\frac{\alpha_\nu^i}{\alpha_S^i}\frac{M_{N_i}}{T_{LC}} - \frac{\alpha_\nu^n}{\alpha_S^n}\frac{M_{N_n}}{T_{LC}}\right)\right](T - T_{LC}) \\ &\sim 100\,\mathsf{H}(T_{LC})\frac{\alpha_\nu^i}{\alpha_S^i}\frac{M_{N_i}}{T_{LC}}\frac{T - T_{LC}}{T_{LC}} =: \mathsf{H}(T_{LC})\,\alpha_{in}\frac{T - T_{LC}}{T_{LC}}\,,\end{aligned} \tag{8.12}$$

where again $M_{N_n} > M_{N_i}$ with non-degenerate masses is assumed, requiring $\alpha_\nu^i/\alpha_S^i \times M_{N_i}$ to be significantly larger than $\alpha_\nu^n/\alpha_S^n \times M_{N_n}$), and equation (8.7) is used to replace $M_{N_n}^2$. Thus, $\Gamma_i/(\hat{\mathrm{H}}_{ii} - \hat{\mathrm{H}}_{nn}) \sim T_{LC}^2/[100T(T - T_{LC})]$ is enlarged within a sizable region.

Since only mass squared differences are relevant in the investigated time evolution ($\hat{\mathrm{H}}_{ij} \approx m_{ij}^2/(2E)$), the induced mixing between right-chiral neutrinos does not violate the fermion number[5], meaning that no overall asymmetry is generated but only asymmetries between the different generations[6]. Consequently, a net B asymmetry can only be produced when at least one but not all right-handed neutrinos transfer their asymmetry to the active neutrino sector before sphaleron transitions become inefficient. Because the Majorana masses mix particle and antiparticle states, the transition of the

[4] In figures 7.1 and 7.10, the thermal rate for $M_N = 10^{13}$ GeV and $y = 0.1$ corresponding to $\alpha_\nu^i/\alpha_S^i \sim 1$ are shown.

[5] Fermion number violating amplitudes are always odd in powers of the Majorana masses.

[6] This statement can also be deduced from the fact that the eigenvalues of the effective equation of motion are CP invariant, cf. section 2.10

asymmetry needs to take place at temperatures before fermion number violation becomes efficient ($T \gtrsim M_N$). Furthermore, the rate of L violation has to be inefficient for $T > T_{Sph}$ so that the generated asymmetry is not washed out. Thus, to fulfill both conditions, at least one of the Majorana masses needs to be roughly smaller than T_{Sph} with its thermal rate being in thermal equilibrium. On the other hand, in order to avoid efficient L violation the rate cannot be too large either, where this upper bound on the thermal rate becomes weaker when the Majorana mass gets smaller.
The other neutrinos, whose asymmetries do not contribute effectively to the generation of the final B asymmetry, can either shift their asymmetries to the active sector and then wash it out by efficient L violation which becomes inefficient before the other right-handed neutrinos share their asymmetry with the active sector, or their thermal rate only reaches equilibrium for $T < T_{Sph}$.

Next, to calculate the $B - L$ asymmetry generated by this mechanism, the time evolution of the particle-antiparticle asymmetries for the right-handed neutrinos has to be investigated in detail. In light of section 2.10, the number density of N_i at a certain time t can be expressed as [3]

$$\frac{Y_{N_i}(t)}{Y_{N_i}^{\mathrm{eq}}(t)} = \sum_j \int_{t_0}^{t} dt' \, \Gamma_j(t') \Big| \langle \psi_{N_i}| \exp\Big[-i \int_{t'}^{t} dt'' \, \hat{\mathbb{H}}(t'') \Big] |\psi_j\rangle \Big|^2 , \tag{8.13}$$

where $\Gamma_j(t)$ is the production rate of the interaction eigenstate $|\psi_j\rangle$ at t and $\hat{\mathbb{H}}(t)$ is the generalized time evolution operator defined in equation (2.117). Considering this time evolution, as discussed in section 5.3, CP violation in the production rate of right-handed neutrinos only occurs when either interference with N_i-N_n mixing in the charged conjugated picture or multi-loop mixing including at least three different Majorana neutrinos is considered. First, including mixing between the pictures, an additional suppression factor of M_{N_n}/E appears, implying that the region of resonant enhanced mixing becomes much smaller. Consequently, in the investigated mechanism only mixing between multiple right-handed neutrinos can be capable of producing a sizable amount of particle-antiparticle asymmetry for each N_i.
However, only the masses of two mass eigenstates are expected to become degenerate at a specific temperature scale. As a consequence, two level crossings are required to induce sizable CP violation, cf. equation (5.35): The first level crossing enhances mixing between N_{n_1} and N_{n_2} at $T \sim T_{LC,1}$ and the second induces increased mixing between N_{n_2} and N_i at $T = T_{LC,2}$. Furthermore, to obtain a non-vanishing CP asymmetry, in addition to the CP-odd phase also a CP-even phase is required, implying that the action of the damping term in the generalized time evolution operator is essential.

Because

$$\frac{\hat{\mathrm{H}}_{ij}}{\mathsf{H}(T)} \lesssim 50 \frac{\alpha_\nu^i}{\alpha_S^i} \frac{M_{N_i}}{T} \qquad \text{and} \qquad \frac{\Gamma_{ij}}{\mathsf{H}(T)} \lesssim \frac{\alpha_\nu^i}{\alpha_S^i} \frac{M_{N_i}}{T} \tag{8.14}$$

are both expected to be small at the region of the level crossings ($T \gg M_{N_i}$) both are treated perturbatively. Thus, the dominant CP violating contribution includes one mixing between the right-handed neutrinos induced by $\hat{\mathrm{H}}_{ij}$ (larger and CP-odd phase) and another by Γ_{ij} (CP-odd and CP-even phase). According to equation (3.67), the conversion probability between two states

considering small mixing is given by

$$P_{n\to i} \approx \frac{2\pi|\hat{\mathrm{H}}_{in}(t_{LC})|^2}{\left|\frac{d}{dt}(\hat{\mathrm{H}}_{ii}-\hat{\mathrm{H}}_{nn})\big|_{t=t_{LC}}\right|} = \frac{2\pi|\hat{\mathrm{H}}_{in}(T_{LC})|^2}{\mathsf{H}(T_{LC})T_{LC}\left|\frac{d}{dT}(\hat{\mathrm{H}}_{ii}-\hat{\mathrm{H}}_{nn})\big|_{T=T_{LC}}\right|} = \frac{|\hat{\mathrm{H}}_{in}(T_{LC})|^2}{\mathsf{H}(T_{LC})^2}\frac{2\pi}{|\alpha_{in}|}\,, \quad (8.15)$$

with α_{in} being defined in equation (8.12)[7]. As a consequence, the transition amplitude can be approximated as

$$A_{n\to i} \approx \frac{\hat{\mathrm{H}}_{in}(T_{LC})}{\mathsf{H}(T_{LC})}\sqrt{\frac{2\pi}{|\alpha_{in}|}}\,. \quad (8.16)$$

Moreover, the result can equivalently be applied to the mixing induced by Γ_{ij}, implying that the produced particle-antiparticle asymmetry for the individual right-handed neutrinos after both level crossings can be approximated as

$$\begin{aligned}\frac{Y_{\Delta N_i}}{Y_{N_i}^{\mathrm{eq}}} &\approx \frac{2\pi}{\sqrt{\alpha_{n_2n_1}\alpha_{in_2}}}\left(\frac{\hat{\mathrm{H}}_{n_2n_1}}{\mathsf{H}(T_{LC,1})}\frac{\Gamma_{in_2}}{\mathsf{H}(T_{LC,2})}+\frac{\Gamma_{n_2n_1}}{\mathsf{H}(T_{LC,1})}\frac{\hat{\mathrm{H}}_{in_2}}{\mathsf{H}(T_{LC,2})}\right)\int\limits_{T_{\max}}^{\infty} dT'\,\frac{\Gamma_{n_1i}(T')}{\mathsf{H}(T')}\\ &\approx \frac{2\pi}{\sqrt{\alpha_{n_2n_1}\alpha_{in_2}}}\left(\frac{\hat{\mathrm{H}}_{n_2n_1}}{\mathsf{H}(T_{LC,1})}\frac{\Gamma_{in_2}}{\mathsf{H}(T_{LC,2})}+\frac{\Gamma_{n_2n_1}}{\mathsf{H}(T_{LC,1})}\frac{\hat{\mathrm{H}}_{in_2}}{\mathsf{H}(T_{LC,2})}\right)\frac{\Gamma_{n_1i}(T_{\max})}{\mathsf{H}(T_{\max})}\,,\end{aligned} \quad (8.17)$$

with $T_{\max} = \max\{T_{LC,1}, T_{LC,2}\}$ and $Y_{N_i}^{\mathrm{eq}} \approx 0.002$. Next, the fact that Γ_{in} and $\hat{\mathrm{H}}_{in}$ only differ by a proportionality factor, cf. equation (8.14), and that $\alpha_{in} \gtrsim \hat{\mathrm{H}}_{in}/\mathsf{H}(T)$ holds can be used to approximate[8]

$$\frac{Y_{\Delta N_i}}{Y_{N_i}^{\mathrm{eq}}} \lesssim 4\pi\sqrt{\frac{\Gamma_{n_2n_1}}{\mathsf{H}(T_{LC,1})}\frac{\Gamma_{in_2}}{\mathsf{H}(T_{LC,2})}}\frac{\Gamma_{n_1i}}{\mathsf{H}(T_{\max})}\,. \quad (8.18)$$

Considering $\alpha_\nu^i/\alpha_S^i \sim 1$, $M_{N_i} \sim 100$ GeV is required to at least partly shift the asymmetry to the active sector, cf. equation (8.9). Consequently, the natural – assuming no mass degeneracy of the Majorana masses – level-crossing temperature is of the order 10^9 GeV, cf. equation (8.7), implying that the interaction rate of the right-handed neutrinos is suppressed by $\Gamma_{in}/\mathsf{H}(T_{LC}) \lesssim 10^{-7}$ during the level crossing, cf. equation (8.9). Thus, only $Y_{\Delta N_i}/Y_{N_i}^{\mathrm{eq}} \lesssim 10^{-13}$ can be achieved which is too small to generate Y_{B-L} of order 10^{-10}, cf. equation (4.1).
In contrast, for $\alpha_S^i/\alpha_\nu^i \sim 0.01$, $M_{N_i} \lesssim 10$ GeV can be chosen, requiring $T_{LC} \lesssim 3\times10^6$ GeV. Consequently, the interaction rate at T_{LC} is only suppressed by $\Gamma_{in}/\mathsf{H}(T_{LC}) \lesssim 10^{-4}$ so that it seems possible to generate a sufficiently large B asymmetry to explain observations ($Y_{\Delta N_i} \lesssim 2\times10^{-10}$) without degenerate Majorana masses[9].

[7] Note that the proportionality of the results can directly be understood from the fact that $|\hat{\mathrm{H}}_{in}|/\mathsf{H}(T)$ is the mixing efficiency while $|\hat{\mathrm{H}}_{in}|/(\mathsf{H}(T)|\alpha_{in}|)$ is the time scale of enlarged mixing.

[8] Note that $Y_{\Delta N_i}$ scales as $\Gamma^2/\mathsf{H}(T_{LC})^2 \propto y^4 m_P^2/T_{LC}^2 \propto y^6 m_P^2/M_N^2$, which is equivalent to the proportionality given in reference [3].

[9] Note that the original considered case, cf. reference [3], is reobtained for $\alpha_S^i/\alpha_\nu^i \sim 0.01$ because the bound on the sum of the active neutrino masses was roughly two orders of magnitudes larger at the time when the paper was published.

8.2.2 Thermal Degeneracy of Left-Handed Neutrino Masses

Next, considering left-handed lepton doublets, their thermal masses and also their interaction rates are naturally degenerate because they only differ by their Yukawa interaction. Thus, according to equation (2.130), sizable mixing between the eigenstates of the effective free equation of motion and e.g. the eigenstates of the weak interaction can be expected. However, as has been discussed in section 5.3, at one-loop order only particle-antiparticle mixing induces CP violation which allows to produce a non-vanishing L asymmetry. Because particle-antiparticle mixing for left-chiral leptons is forbidden by charge conservation before EWSB, degenerate masses for the left-chiral neutrino at one-loop order can only induce relevant enhanced CP violation in a narrow region between the EWPT and the scale where sphaleron transitions become inefficient ($T_{LC} < T < T_c$).

Moreover, the interaction rate induced by the weak interaction, cf. equation (B.47), is large compared to the rate of particle-antiparticle mixing, implying that the free propagation length of active neutrinos is very small compared to the oscillation length. Thus, even though it seems that sizable mixing can emerge, in fact, neutrinos produced e.g. via Yukawa interactions interact so fast via weak interactions that no relevant neutrino-antineutrino oscillation occurs in the meantime[10]. Note that a similar effect can be observed considering e.g. active neutrino oscillations where the mixing between energy eigenstates and eigenstates of the weak interaction is sizable: When measuring neutrinos at a distance from the production region which is much smaller than the oscillation length, no sizable mixing is observed.

8.2.3 Thermal Degeneracy of Left- and Right-Chiral Neutrino Masses

An idea initially investigated in my master thesis, cf. reference [74], is to use mass degeneracy of left- and right-chiral neutrinos to convert part of the active neutrinos into right-handed neutrinos. In case of a non-adiabatic level crossing, cf. section 3.5, meaning that the conversion probability, cf. equation (3.67), is not close to one, the out-of-equilibrium condition can be fulfilled when the thermal rates are inefficient. Moreover, similar to the case of degenerate right-chiral neutrino masses, it was assumed that including CP violation, the conversion probability for particles and antiparticles is different. Consequently, a net L asymmetry would be shifted to at least one right-handed Majorana neutrino which is not in thermal equilibrium[11].

As was figured out in my master thesis, such a level crossing requires a Dirac mass term in order to have a non-vanishing conversion probability – neither mass mixing nor off-diagonal interaction rates are present for a vanishing VEV – implying that the level crossing has to take place in the region between the EWPT and the scale where sphaleron transitions become inefficient ($T_{Sph} < T_{LC} < T_c$). Consequently, to have degenerate masses in this region, 25 GeV $\lesssim M_{N_i} \lesssim$ 30 GeV is required, cf. equation (B.41). Furthermore, to have a non-adiabatic level crossing which still converts a sizable amount of particles ($P_{\text{transit}} \sim \mathcal{O}(0.1)$), depending on the EV at T_{LC}, a Yukawa coupling of

[10] Note that this statement is also valid considering multi-loop neutrino mixing.
[11] This idea was investigated in detail in collaboration with Tim Brune.

order $|y| \gtrsim 10^{-9}$ is needed, cf. equations (3.67) and (B.41):

$$\frac{\pi|y|^2v^2}{\left|\frac{d}{dt}\frac{m_{\ell_i}^2}{2E}\big|_{t=t_{LC}}\right|} = \frac{\pi|y|^2v^2}{\mathsf{H}(T)T\frac{d}{dT}\frac{m_{\ell_i}^2}{2E}\big|_{T=T_{LC}}} \approx 1.4 \times \frac{|y|^2v^2}{T^3} \times 10^{20}\ \text{GeV} \lesssim |y|^2 \times 10^{18} \overset{!}{\sim} 1\,, \tag{8.19}$$

where $v \lesssim T$ for $T > T_{Sph}$ and $T_{LC} \sim 100$ GeV are used. Consequently, for $v(T_{LC}) \sim T_{LC}$, the thermal rate of N_i is inefficient at T_{LC} ($\Gamma/\mathsf{H}(T) \sim 10^{-6}$) and the contribution to the active neutrino masses induced by the type-I seesaw mechanism is of order 10^{-6} eV.

When this idea was investigated in detail, multiple issues arose. First, CP violation being capable of producing a sizable amount of L asymmetry is required. Considering the relevant loop corrections shown in figure 5.2, the contribution of the left diagram is only enhanced when degenerate right-chiral neutrino masses are considered. Furthermore, as discussed previously, the center diagram never contributes significantly. However, assuming mass degeneracy for left- and right-chiral neutrinos, one might think that the right diagram shown in figure 5.2 can induce enlarged CP violation when the external Higgs in the diagram is replaced by the EV. The resulting diagram considers ν_m-N_n mixing in the loop at first order and interferes with the Dirac mass term. Thus, considering degenerate masses for N_n and ν_m, the contribution of the loop correction can in principle be enhanced in comparison to the Dirac mass term. However, even for sizable mixing, the loop correction is still suppressed quadratically in the Yukawa couplings while the Dirac mass is only suppressed linearly. Moreover, due to the fact that left-chiral neutrinos interact via weak interaction and the right-chiral neutrinos do not, the mixing between both is still suppressed by yv/Γ_ν, cf. equation (2.130), with $\Gamma_\nu \sim T \times 10^{-3}$, cf. equation (B.47), even for exactly degenerate masses. Thus, degeneracy of left- and right-chiral neutrino masses does not lead to strongly enhanced CP violation. Consequently, for Majorana masses in the region of interest ($25\ \text{GeV} \lesssim M_{N_i} \lesssim 30\ \text{GeV}$), either L violation is efficient at T_{Sph} or the CP violation is too small to generate a sizable amount of L asymmetry. The only way to circumvent this issue is to assume degenerate Majorana masses. However, in this case, also thermal leptogenesis is capable of generating a B asymmetry of the observed size.

Furthermore, the initial idea of considering ν_j-N_i conversion via a level-crossing does not work because a resonant particle conversion does not take place. This can also be understood from the fact that the interaction rate of left-chiral neutrinos is so large that, for a level crossing with a sizable conversion probability, their free propagation time is small compared to the time scale where the mixing induced by Dirac masses is large. Thus, the conversion probability becomes very small or left-chiral neutrinos basically stay left-chiral during their lifetime. Consequently, only the interaction strength for the dominantly right-chiral eigenstate of the effective free equation of motion becomes larger during the level crossing due to the increased mixing. Thus, the main influence of ν_j-N_i mixing is an altered interaction rate of the right-handed neutrino which at maximum is $\Gamma_N + 2y^2v^2/\Gamma_\nu$, cf. equation (2.132), and not, as naively expected, proportional to Γ_ν.

9 Conclusion

In the first part of this thesis, the time evolution of a theory including massive vector bosons interacting with each other was considered in time-dependent perturbation theory. It was shown that the corresponding interaction Hamiltonian includes an infinite series of local interaction terms. Considering these local interaction terms properly, at tree level, transition amplitudes of the naively expected form are obtained. However, for loop contributions, a proper consideration of local interaction terms results in Lorentz invariant S-matrix deviating from the naive expectation. Furthermore, it was shown that this deviation from the naive expectation is essential for proving that the degree of divergence in the S-matrix is equivalent to what is expected from R_ξ gauge.
Originally this investigation was made to understand the discrepancy between the R_ξ gauge and the unitary gauge result for the calculation of the effective Higgs potential. However, no intuitive explanation for the origin of thermal contribution of the Goldstone bosons appearing in R_ξ gauge was found.

Following this, relevant elements for the investigation of baryogenesis with a focus on right-handed Majorana neutrinos were introduced in a general way. Boltzmann equations in terms of chemical potentials were derived taking into account that in thermal equilibrium, due to the different statistics, bosonic degrees of freedom store twice the amount of number density asymmetry as fermionic degrees of freedom. Moreover, the rate of B violation induced by sphaleron transitions in the temperature range where sphaleron transitions reach thermal equilibrium ($T \sim 10^{12}$ GeV) was calculated. In particular, only reactions which are significantly more efficient than the rate of B violation induced by sphaleron transitions (e.g. the top Yukawa interaction) were assumed to be in thermal equilibrium while significantly less efficient reactions (e.g. the bottom and tau Yukawa interactions) were ignored.

In the main part of this thesis, the interplay of GUT baryogenesis, sphaleron transitions, and L violation induced by right-handed Majorana neutrinos was investigated. For this, L violation represents an essential ingredient because the $B-L$ conserving sphaleron transitions would completely wash out the initial $B-L$ conserving B asymmetry without having an additional source of $B-L$ violation. In particular, it was shown that right-handed Majorana neutrinos in the mass range $M_N \gtrsim 10^{12}$ GeV, which generate active neutrino masses within the observed mass range via the type-I seesaw mechanism, naturally secures a sizable amount of $B-L$ conserving B asymmetry from being washed out by sphaleron transitions. Thus, in light of this investigation, GUT baryogenesis scenarios, which typically have the issue of conserving $B-L$, are still a possible source for the observed B asymmetry.
Moreover, this investigation was extended to the scotogenic model, which is a two-Higgs-doublet model with an imposed Z_2 symmetry extended by right-handed Majorana neutrinos. The scotogenic model is considered here as a simple extension which includes a DM candidate and allows for larger Yukawa couplings of the neutrino sector without being in conflict with the Planck bound on the sum

of the active neutrino masses. It was shown that for the scotogenic model, a natural parameter space is left where a sizable amount of a $B - L$ conserving B asymmetry is secured from being washed out by sphaleron transitions, active neutrino masses within the observed rage are generated, and the dark matter relic density can be explained without being in conflict with the current experimental limits. However, for that, the active neutrino masses generated in the scotogenic model are not allowed to be suppressed by more than one order of magnitude compared to the active neutrino masses generated by the type-I seesaw mechanism.

These results can be understood intuitively when demanding that active neutrino masses in the observed range are induced by the type-I seesaw mechanism. This requires Yukawa couplings of a size that induces interaction rates for the right-handed Majorana neutrino which are efficient for temperatures close to the Majorana mass ($\Gamma_N/\mathsf{H} \lesssim \mathcal{O}(10)$) and become inefficient when the temperature drops significantly below the Majorana mass. Because of this, Majorana neutrinos, which generate the observed active neutrino masses via the type-I seesaw mechanism, represent a natural source of $B - L$ violation with a thermal interaction rate of the form required for thermal leptogenesis.

Addressing this, in the last part of this thesis, general options for leptogenesis with the Majorana masses of right-chiral neutrinos being the only source of fermion number violation were examined. It was discussed that for thermal leptogenesis, at least Majorana masses larger than roughly 10^6 GeV are required when neither degenerate Majorana masses nor an initial thermal abundance of the right-handed Majorana neutrinos is assumed.
Moreover, the idea of naturally enhancing CP violation by thermally degenerate neutrino masses was investigated. It was found that only mass degeneracy of right-chiral neutrino masses can significantly increase CP violation at a specific temperature scale. However, to be able to produce a B asymmetry of the observed size without considering degenerate Majorana masses, the bound on the sum of the active neutrino masses requires a suppression of the active neutrino masses by roughly two orders of magnitudes compared to the active neutrino masses induced by the type-I seesaw mechanism.
Finally, it was discussed that neither degenerated masses of left-chiral neutrinos nor mass degeneracy of left- and right-chiral neutrinos can enhance CP violation significantly because the interaction rate of left-chiral neutrinos via weak interaction in the region of interest is very large compared to the interaction rate via Yukawa interactions. This can be understood from the fact that CP violation enhanced by mass degeneracy originates from CP violating mixing in the generalized time evolution. This time evolution includes both the free time evolution determined by the Hamiltonian and a damping factor induced by the interaction rate. As a consequence, even for degenerate masses, the CP violating mixing is strongly suppressed when the interaction rate is dominantly diagonal.

Acknowledgment

First of all, I want to thank all the members of the TIII and TIV department for supporting me, especially during the final stage of writing my Ph.D. thesis. Unfortunately, due to my paternal obligation and, later on, due to the COVID-19 pandemic, we did not see each other that often. Nevertheless, the contact with you was always both friendly and enriching.
In particular, I want to thank my long-term study and office mates Mathias Becker and Kevin Moch for many helpful discussions, especially those about gauge fixing and spontaneous symmetry breaking.
My thanks also goes to my colleagues Wei-Chih Huang, supporting me in the project about neutrino assisted GUT baryogenesis, and Tim Brune, supporting me in the project about using thermal degeneracy of left- and right-chiral neutrino masses for leptogenesis.
Furthermore, I thank my wife for her mental and linguistic support and my little daughter for keeping me from work so that I could spend time doing arguably more beautiful and important things such as playing duplo, reading children's books, and going to the playground.
I thank Emmanuel Stamou for supporting me with the projects related to the investigation of self-interacting massive vector bosons during the final stage of writing this thesis and my supervisor Heinrich Päs for giving me the opportunity to doctorate and also for the fact that I was very free in my work.
Finally, I thank the Studienstiftung des Deutschen Volkes for the ideal and financial support since July 2017. It gave me the opportunity to move to Geneva for seven months and, more importantly, to make having a child and a doctorate work.

A Supplementary Details to Quantum Field Theory in the Vacuum

A.1 Spacetime Geometry

For the signature of the Minkowski space, the particle physics convention is used, where the Minkowski metric is defined as

$$ds^2 = g_{\mu\nu}dx^\mu dx^\nu = dx_0^2 - dx_1^2 - dx_2^2 - dx_3^2 = dx_0^2 - d\vec{x}^{\,2}\,, \tag{A.1}$$

with $g_{\mu\nu} = \eta_{\mu\nu} = \mathrm{diag}(+---)$, $x_0 = t$ being the time component, and $\vec{x}$ the space components. In this convention, the Lorentz transformation, which transforms a Lorentz vector from one inertial frame of reference A to another A' moving with speed $\vec{v}$ relative to A, is given by

$$x_0' = \gamma\,(x_0 - \vec{v}\vec{x}) \qquad \text{and} \qquad \vec{x}\,' = \gamma\,(\vec{x} - \vec{v}x_0)\,, \tag{A.2}$$

with $\gamma = (\sqrt{1-\vec{v}^{\,2}})^{-1}$.

The Einstein field equations are

$$G_{\mu\nu} - \Lambda g_{\mu\nu} = R_{\mu\nu} - \frac{1}{2}Rg_{\mu\nu} - \Lambda g_{\mu\nu} = 8\pi T_{\mu\nu}\,, \tag{A.3}$$

where the Ricci curvature tensor $R_{\mu\nu}$ and the scalar curvature $R = g^{\mu\nu}R_{\mu\nu}$ can be calculated from the metric and contain information about the curvature of the space. $T_{\mu\nu}$ is the energy-momentum tensor describing the energy density and its motion.
Assuming the universe to be homogeneous and isotropic (cosmological principle), the Friedmann-Lemaître-Robertson-Walker metric is obtained:

$$ds^2 = dt^2 - a(t)^2\left(\frac{dr^2}{1-kr^2} + r^2 d\Omega^2\right)\,, \tag{A.4}$$

with $a(t)$ being the scale factor. Considering this metric, Einstein's field equations simplify to the Friedmann equations [47]:

$$\left(\frac{1}{a(t)}\frac{da(t)}{dt}\right)^2 + \frac{k}{a(t)^2} = \frac{8\pi\rho(t)+\Lambda}{3} =: \mathsf{H}(t)^2 + \frac{k}{a(t)^2}\,, \tag{A.5a}$$

$$\frac{1}{a(t)}\frac{d^2a(t)}{dt^2} = \frac{-4\pi(\rho(t)+3p(t))+\Lambda}{3}\,, \tag{A.5b}$$

with ρ and p being the energy density and the pressure, respectively, both being part of the energy-momentum tensor and $\mathsf{H}(t)$ being the Hubble expansion rate.

A.2 Details on Relativistic Quantum Mechanics

Basing on the non-relativistic energy momentum relation the Schrödinger equation

$$i\frac{\partial}{\partial t}\psi(x) = \left(-\frac{1}{2m}\vec{\nabla}^2 + V(x)\right)\psi(x)\,, \tag{A.6}$$

is obtained, where constant terms such as the mass are ignored because physical observables in QM are always given by the expectation value of operators not depending on an overall phase of the wave function.
Relativistic invariant generalizations are the Klein-Gordon equation

$$(i^2\partial^\mu\partial_\mu - m^2)\phi(x) = -(\partial^\mu\partial_\mu + m^2)\phi(x) = 0\,, \tag{A.7}$$

applying to Lorentz scalar fields (spin-0), the Dirac equation

$$(i\partial\!\!\!/ - mI_4)\Psi(x) = 0\,, \tag{A.8}$$

describing the time evolution of spin-1/2 fermionic fields and the Proca equation

$$(i^2\partial^\mu\partial_\mu - m^2)A^\nu(x) - i^2\partial^\nu\partial_\mu A^\mu(x) = -(\partial^\mu\partial_\mu + m^2)A^\nu(x) + \partial^\nu\partial_\mu A^\mu(x) = 0\,, \tag{A.9}$$

being a generalization of the Klein-Gordon equation for Lorentz vector fields (spin-1). For the Dirac equation, the abbreviations $\overline{\Psi} = \Psi^\dagger\gamma_0$ and $\partial\!\!\!/ = \partial^\mu\gamma_\mu$ are used where the gamma matrices satisfy the anticommutator relation

$$\{\gamma^\mu, \gamma^\nu\} = 2g^{\mu\nu}I_4\,, \tag{A.10}$$

with I_n being the $n \times n$ identity matrix. In this thesis, the Weyl basis is used, in which the gamma matrices are given by

$$\gamma^0 = \begin{pmatrix} 0 & I_2 \\ I_2 & 0 \end{pmatrix}, \qquad \gamma^i = \begin{pmatrix} 0 & \sigma_i \\ -\sigma_i & 0 \end{pmatrix}, \qquad \text{and} \qquad \gamma^5 := i\gamma^0\gamma^1\gamma^2\gamma^3 = \begin{pmatrix} -I_2 & 0 \\ 0 & I_2 \end{pmatrix}, \tag{A.11}$$

with the Pauli matrices

$$\sigma_1 = \begin{pmatrix} 0 & 1 \\ 1 & 0 \end{pmatrix}, \qquad \sigma_2 = \begin{pmatrix} 0 & -i \\ i & 0 \end{pmatrix}, \qquad \text{and} \qquad \sigma_3 = \begin{pmatrix} 1 & 0 \\ 0 & -1 \end{pmatrix}. \tag{A.12a}$$

There are a couple of useful relations for the Pauli matrices:

$$\sigma_i^2 = I_2\,, \qquad [\sigma_a, \sigma_b] = 2i\epsilon_{abc}\sigma_c\,, \qquad \text{and} \qquad \{\sigma_a, \sigma_b\} = 2\delta_{ab}I_2\,. \tag{A.13}$$

Moreover, the gamma matrices fulfill the relations:

$$\gamma_0^2 = -\gamma_i^2 = I_4\,, \tag{A.14a}$$
$$(\gamma^\mu)^\dagger = \gamma^0\gamma^\mu\gamma^0\,, \tag{A.14b}$$
$$(\gamma^\mu)^* = \gamma^2\gamma^\mu\gamma^2\,, \tag{A.14c}$$
$$(\gamma^\mu)^T = \gamma^0\gamma^2\gamma^\mu\gamma^2\gamma^0\,, \tag{A.14d}$$
$$\mathrm{tr}[\gamma^\mu\gamma^\nu] = 4g^{\mu\nu}\,, \tag{A.14e}$$
$$\mathrm{tr}[\gamma^\mu\gamma^\nu\gamma^\rho\gamma^\sigma] = 4(g^{\mu\nu}g^{\rho\sigma} - g^{\mu\rho}g^{\nu\sigma} + g^{\mu\sigma}g^{\rho\nu})\,. \tag{A.14f}$$

Moreover, the wave function in the charge-conjugated representation is defined as

$$\Psi^c = \mathcal{C}(\Psi) = C\overline{\Psi}^T = C\gamma^0\Psi^* \qquad \Rightarrow \qquad \overline{\Psi^c} = \Psi^T\gamma^0 C^\dagger\gamma^0 = \Psi^T C\,, \tag{A.15}$$

with the charge-conjugation matrix

$$C = i\gamma^2\gamma^0 \qquad \Rightarrow \qquad C^{-1} = C^\dagger = C^T = -C\,. \tag{A.16}$$

The Lorentz transformation of Dirac spinors is given by

$$\Psi(x') = \exp\left[-\frac{i}{2}\vec{\theta}\gamma^5\gamma^0\vec{\gamma} + \frac{1}{2}\vec{\eta}\gamma^0\vec{\gamma}\right]\Psi(x)\,, \tag{A.17}$$

where $\vec{\theta}$ are rotation angles and $\tanh(\vec{\eta}) = \vec{v}$ are rapidities.

For all previously given relativistic equation of motions a corresponding Lagrangian density can be defined:

$$\mathcal{L}_{\text{Klein}-\text{Gordon}}(x) = (\partial^\mu\phi^\dagger(x))(\partial_\mu\phi(x)) - m^2\phi^\dagger(x)\phi(x)\,, \tag{A.18a}$$

$$\mathcal{L}_{\text{Dirac}}(x) = \overline{\Psi}(x)(i\partial\!\!\!/ - mI_4)\Psi(x)\,, \tag{A.18b}$$

$$\mathcal{L}_{\text{Proca}}(x) = -\frac{1}{4}F_{\mu\nu}(x)F^{\mu\nu}(x) + \frac{m^2}{2}A_\mu(x)A^\mu(x)\,, \tag{A.18c}$$

with the field strength tensor being defined as

$$F^{\mu\nu}(x) = \partial^\mu A^\nu(x) - \partial^\nu A^\mu(x)\,. \tag{A.19}$$

Furthermore, referring to the Proca Lagrangian for massless vector bosons, the Lagrangian density of Yang-Mills theories can be defined as

$$\mathcal{L}(x) = -\frac{1}{2}\text{Tr}[F_{\mu\nu}(x)F^{\mu\nu}(x)] = -\frac{1}{4}F^a_{\mu\nu}(x)F^{a\,\mu\nu}(x)\,, \tag{A.20}$$

with the generalized field strength tensor

$$F_{\mu\nu}(x) = D_\mu A_\nu(x) - D_\nu A_\mu(x) = \left[\partial_\mu A^a_\nu(x) - \partial_\nu A^a_\mu(x) + gf^{abc}A^b_\mu(x)A^c_\nu(x)\right]t^a = F^a_{\mu\nu}(x)t^a \tag{A.21a}$$

and the structure constants

$$[t^a, t^b] = if^{abc}t^c\,. \tag{A.22}$$

The covariant derivative D_μ is defined as

$$D_\mu = \partial_\mu - igA_\mu(x) = \partial_\mu - igA^a_\mu(x)t^a\,, \tag{A.23}$$

and t^a are the generators of the symmetry transformation. Considering an $SU(n)$ symmetry transformation, the n^2-1 generators are defined by the conditions

$$\text{Tr}[t^a] = 0\,, \qquad (t^a)^\dagger = t^a\,, \qquad \text{and} \qquad t^a t^b = \frac{1}{2n}\delta^{ab}I_n + \frac{1}{2}\sum_{c=1}^{n^2-1}\left(if^{abc} + d^{abc}\right)t^c\,. \tag{A.24}$$

The Lagrangian density of Yang-Mills theories is invariant under the transformation

$$A'_\mu(x) = G(\alpha(x))A_\mu(x)G^{-1}(\alpha(x)) - \frac{i}{g}(\partial_\mu G(\alpha(x)))G^{-1}(\alpha(x))\,, \tag{A.25}$$

with

$$G(\alpha(x)) = e^{i\alpha^a(x)t^a}\,. \tag{A.26}$$

This, according to Noether's theorem, implies that the current

$$J^{b\,\mu}(x) = \frac{\partial\mathcal{L}(x)}{\partial[\partial_\mu A_\nu(x)]}\frac{dA_\nu(x)}{d\alpha^b(x)} = -2\mathrm{Tr}[F^{\mu\nu}(x)f^{abc}A^a_\nu(x)t^c] = -f^{abc}A^a_\nu(x)F^{c\,\mu\nu}(x) \tag{A.27}$$

is conserved ($\partial_\mu J^{b\,\mu}(x) = 0$).

A.3 Perturbation Theory for Quantum Mechanics

The time evolution of a quantum mechanical system can in general be expressed as given in equation (2.9), implying that it can be fully described by the wave function $\psi(t_0, \vec{x})$ at an arbitrary time t_0 and the Hamiltonian $\hat{\mathrm{H}}$. Thus, to evaluate $\psi(x)$, the equation of motion has to be solved, which is simple as long as the eigenbasis of $\hat{\mathrm{H}}$ is time independent:

$$\hat{\mathrm{H}}\,|\psi_j\rangle = E_j\,|\psi_j\rangle\,. \tag{A.28}$$

In this case, $|\psi(t_0)\rangle$ can be decomposed into the eigenstates with a trivial time evolution:

$$|\psi(t)\rangle = \sum_j a_j\, e^{-iE_j(t-t_0)}\,|\psi_j\rangle\,, \tag{A.29}$$

with $a_j = \langle\psi(t_0)|\psi_j\rangle$.

A.3.1 Time-Dependent Perturbation Theory

On the other hand, solving the time evolution for a system with a time-dependent Hamiltonian can be challenging. Depending on the considered system, different ways of solving the equation of motion have been established. One often-used method is perturbation theory. In general, the Hamiltonian can be decomposed into a time-dependent $\hat{\mathrm{H}}_I$ and a time-independent part $\hat{\mathrm{H}}_0$. Using that the equation of motion for $\hat{\mathrm{H}}_0$ can be solved analytically, cf. equation (A.29). The interaction picture (D) – also known as the Dirac picture – can be defined:

$$|\psi_D(t)\rangle = e^{i\hat{\mathrm{H}}_0 t}\,|\psi_S(t)\rangle\,, \tag{A.30a}$$

$$\hat{O}_D(t) = e^{i\hat{\mathrm{H}}_0 t}\hat{O}_S(t)e^{-i\hat{\mathrm{H}}_0 t}\,, \tag{A.30b}$$

where the subscript S highlights the Schrödinger picture in which only the state vector evolves in time. In the interaction picture, the equation of motion becomes

$$\begin{aligned} i\frac{\partial}{\partial t}\left|\psi_D(t)\right\rangle &= -\hat{\mathrm{H}}_0 e^{i\hat{\mathrm{H}}_0 t}\left|\psi_S(t)\right\rangle + e^{i\hat{\mathrm{H}}_0 t} i\frac{\partial}{\partial t}\left|\psi_S(t)\right\rangle \\ &= -\hat{\mathrm{H}}_0 e^{i\hat{\mathrm{H}}_0 t}\left|\psi_S(t)\right\rangle + e^{i\hat{\mathrm{H}}_0 t}(\hat{\mathrm{H}}_0 + \hat{\mathrm{H}}_I(t))\left|\psi(t)\right\rangle = (\hat{\mathrm{H}}_I)_D(t)\left|\psi_D(t)\right\rangle \,, \end{aligned} \tag{A.31}$$

where (2.9) and $[\hat{\mathrm{H}}_0, \hat{\mathrm{H}}_0] = 0$ are used. Consequently, the time evolution of a state vector in the interaction picture can be written as

$$\left|\psi_D(t)\right\rangle = \mathcal{T}\exp\left[-i\int_{t_0}^{t} dt'(\hat{\mathrm{H}}_I)_D(t')\right]\left|\psi_D(t_0)\right\rangle \,, \tag{A.32}$$

where the time-ordered product $\mathcal{T}$ ensures that the product of multiple $(\hat{\mathrm{H}}_I)_D(t_i)$ is ordered such that the single $(\hat{\mathrm{H}}_I)_D(t_i)$ acts on the state vector in the correct time order:

$$\mathcal{T}\prod_i (\hat{\mathrm{H}}_I)_D(t_i) = (\hat{\mathrm{H}}_I)_D(t'_n)\ldots(\hat{\mathrm{H}}_I)_D(t'_2)(\hat{\mathrm{H}}_I)_D(t'_1)\,, \tag{A.33}$$

with $t'_1 < t'_2 < \cdots < t'_n$ and $\{t_1, t_2 \ldots t_n\} = \{t'_1, t'_2 \ldots t'_n\}$.
Considering

$$\int_{t_0}^{t} dt'(\hat{\mathrm{H}}_I)_D(t') \ll 1\,, \tag{A.34}$$

writing down the time evolution in the interaction picture is very useful because the series expansion of the exponential function converges. Thus, the time evolution can be approximated by only taking into account contributions up to a certain order in $(\hat{\mathrm{H}}_I)_D(t)$.

A.3.2 Diagrammatic Visualization of the Perturbation Series in QFT

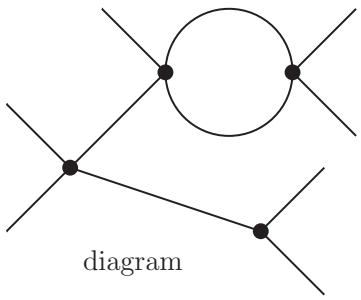

Figure A.1: Representation of some element of the perturbation series in a diagram.

It is convenient to visualize the elements of the QFT perturbation series which diagrams, as for example shown in figure A.1. For that, each spacetime interaction point called vertex is represented as a point from which lines originate, each line illustrating a field operator, cf. figure A.2. Each of these lines have to be connected to an external particle or to another line from another vertex.

Figure A.2: Diagrams are build of vertices and propagators.

Therefore, only field operators which can create or annihilate the external particles, respectively, can be connected to the corresponding external line and two vertices can only be connected when outgoing lines correspond to the same particle: one to create the state and the other to annihilate. As a consequence, diagrams only represent non-vanishing elements of the perturbation series.

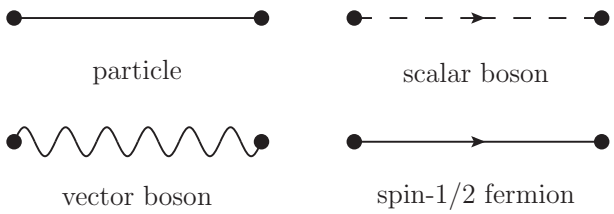

Figure A.3: Representation of different particle species in diagrams.

To write down the contribution of a single diagram to the considered matrix element, it also makes sense to indicate the particle species by labeling the line with the particle acronym. In addition, it is convenient to highlight the Lorentz structure of the corresponding particle (spin-0, spin-1/2, or spin-1) separately. For that, particles without requirements on their Lorentz structure are illustrated by solid lines while scalar and vector bosons are represented as dashed and waves lines, respectively (with an arrow when particles and antiparticles are distinguishable) and solid lines with an arrow correspond to spin-1/2 fermions, cf. figure A.3.

A.3.3 Time-Independent Perturbation Theory

Another interesting case is to consider a time-independent Hamiltonian $\hat{\mathrm{H}}$ which can be divided into a part which dominantly determines the eigenbasis $\hat{\mathrm{H}}_0$ and a remaining part $\hat{\mathrm{H}}_I$ being considered as a perturbation. Consequently, at zeroth order in perturbation theory, the eigensystem is only determined by $\hat{\mathrm{H}}_0$, whose eigensystem is assumed to be known:

$$\hat{\mathrm{H}}_0 \, |\psi_i^0\rangle = E_i^0 \, |\psi_i^0\rangle \ . \tag{A.35}$$

Next, treating $\hat{\mathrm{H}}_I$ as a perturbation, the eigensystem can be calculated order by order. At first order, the eigensystem is given by

$$E_i^1 = E_i^0 + \langle \psi_i^0 | \hat{\mathrm{H}}_I | \psi_i^0 \rangle \ , \tag{A.36a}$$

$$|\psi_i^1\rangle = |\psi_i^0\rangle + \sum_{j \neq i} |\psi_j\rangle \, \frac{\langle \psi_j^0 | \hat{\mathrm{H}}_I | \psi_i^0 \rangle}{E_i^0 - E_j^0} \ , \tag{A.36b}$$

while at second order, the energy eigenvalue becomes

$$E_i^2 = E_i^0 + \langle \psi_i^0 | \hat{\mathrm{H}}_I | \psi_i^0 \rangle + \sum_{j \neq i} \frac{| \langle \psi_j^0 | \hat{\mathrm{H}}_I | \psi_i^0 \rangle |^2}{E_i^0 - E_j^0} \,. \tag{A.37}$$

A.4 Detailed Introduction of Quantum Field Operators

To be able to apply the quantum mechanical equations of motion on a state vector $|F\rangle$ which only contains information about the particle content, quantum field operators convert the state vector into the corresponding set of quantum mechanical wave functions. In general, the wave function corresponding to $|F\rangle$ can be expressed in terms of eigenstates of the free Hamiltonian

$$\hat{\mathrm{H}}\, u_i(\vec{k}) = E_i(\vec{k})\, u_i(\vec{k}) \,, \tag{A.38}$$

where i denotes the particle species. Because all momenta are allowed in an infinite large space, it is reasonable to use a Fourier ansatz for the quantum field operators:

$$\psi_i(x) = \int d\tilde{k}_i \, \psi_i(\vec{k})\, e^{-ikx} \,, \tag{A.39}$$

with the Lorentz invariant phase space integral

$$\int \frac{dk}{(2\pi)^3}\, \delta(k^2 - m_i^2) = \int \frac{d^3k}{(2\pi)^3} \frac{1}{2E_i(\vec{k})} := \int d\tilde{k}_i \tag{A.40}$$

and the quantum field operator in momentum space

$$\psi_i(\vec{k}) = u_i(\vec{k})\, a_i(\vec{k}) \,. \tag{A.41}$$

Moreover, $a_i(\vec{k})$ is the *annihilation operator* whose action on the state vector $|F\rangle$ is defined such that it erases the corresponding state from the state vector if it is present or erases the entire state when it is not present:

$$a_i(\vec{k})\, |F\rangle = N\, |F'\rangle \,, \tag{A.42a}$$

$$a_i(\vec{k})\, |0\rangle = 0 \,, \tag{A.42b}$$

with N being a normalization factor[1] and $|F'\rangle$ being the state vector with the same particle content as $|F\rangle$ but with one fewer particle of species i and momentum $\vec{k}$. The conjugated of the annihilation operator ($a_i^\dagger(\vec{k})$) appearing in the conjugated quantum field operator is the *creation operator* adding the corresponding state to the state vector.

[1] Considering normalized state vectors ($\langle F|F\rangle = 1$), it is difficult to determine N. However, in textbooks, cf. e.g. reference [68], the state vector is often normalized such that the delta distribution appearing in equation (A.48) is part of the normalization. Using such a normalization for the state vector, a trivial normalization factor can be assumed ($N = 1$).

Requiring that an unnormalized one-particle state vector can be generated by just applying the creation operator on the vacuum state ($|0\rangle$) and that the action of the quantum field operator on this state results in the wave function of the corresponding state,

$$\int d\tilde{k}_i \, u_i(\vec{k}) \, a_i(\vec{k}) \, e^{-ikx} \, a_i^\dagger(\vec{p}) \, |0\rangle \stackrel{!}{=} u_i(\vec{p}) \, e^{-ipx} \, |0\rangle =: \tilde{\psi}_{i,\vec{k}}(x) \, |0\rangle \ , \tag{A.43}$$

the relation

$$a_i(\vec{k}) a_i^\dagger(\vec{p}) = 2E_i(\vec{k})(2\pi)^3 \delta^3 \left(\vec{p} - \vec{k}\right) \tag{A.44}$$

is obtained. Together with equation (A.42b) and the fact that the action of the creation operator increases the corresponding occupation number by one, the well-known commutator relation

$$[a_i(\vec{k}), a_i^\dagger(\vec{p})] = a_i(\vec{k}) a_i^\dagger(\vec{p}) - a_i^\dagger(\vec{p}) a_i(\vec{k}) = 2E_i(\vec{k})(2\pi)^3 \delta^3 \left(\vec{p} - \vec{k}\right) \ , \tag{A.45}$$

is obtained.
At this point, in contrast to QM, the Pauli exclusion principle can be implemented easily by demanding that the action of the creation operator on an occupied state vanishes:

$$a_i^\dagger(\vec{p}) a_i^\dagger(\vec{p}) \, |0\rangle = 0 \, . \tag{A.46}$$

This additional condition leads to the well-known anti-commutator relation

$$\{a_i(\vec{p}), a_i^\dagger(\vec{k})\} = a_i(\vec{k}) a_i^\dagger(\vec{p}) + a_i^\dagger(\vec{p}) a_i(\vec{k}) = 2E_i(\vec{k})(2\pi)^3 \delta^3 \left(\vec{p} - \vec{k}\right) \ . \tag{A.47}$$

Using this definition of the creation and annihilation operator, the normalization factor in equation (A.42a) is non-trivial and therefore, defining a normalized state with a certain particle content by the action of creation operators is difficult. However, using that an unnormalized state can be created by the action of creation operators, the relation

$$\langle F | a_i^\dagger(\vec{q}) a_i(\vec{k}) | F \rangle = f_i(\vec{k}) \, 2E_i(\vec{k})(2\pi)^3 \delta^3 \left(\vec{p} - \vec{k}\right) \ , \tag{A.48}$$

can be derived, with $f_i(\vec{k})$ being the occupation number of the annihilated state.

The normalization condition for the energy eigenstates can be obtained by demanding that the expectation value of the Hamiltonian is equal to the energy of the state,

$$\begin{aligned} \int d^3x \, \langle F | \psi^\dagger(x) \hat{\mathrm{H}} \psi(x) | F \rangle &= \int d^3x \int d\tilde{k}_i \int d\tilde{k}_i' \, u_i^\dagger(\vec{k}') \hat{\mathrm{H}} u_i(\vec{k}) e^{-i(k-k')x} \, \langle F | a_i^\dagger(\vec{k}') a_i(\vec{k}) | F \rangle \\ &= \int d\tilde{k}_i \, E_i(\vec{k}) u_i^\dagger(\vec{k}) u_i(\vec{k}) f_i(\vec{k}) \stackrel{!}{=} \int \frac{d^3k}{(2\pi)^3} E_i(\vec{k}) f_i(\vec{k}) \, , \qquad \text{(A.49a)} \\ \Rightarrow u_i^\dagger(\vec{k}) u_i(\vec{k}) &= 2E_i(\vec{k}) \, , \qquad \text{(A.49b)} \end{aligned}$$

where equation (A.38), equation (A.48), and

$$\int d^3x \, e^{-i(k-k')x} = \exp\left[-i\left(E_i(\vec{k}) - E_i(\vec{k}')\right)t\right] \delta^3\left(\vec{k} - \vec{k}'\right) \ , \tag{A.50}$$

are used.

Considering the relativistic equations of motion obtained at the beginning of this section, only the Hamiltonian for spin-1/2 fermions can be determined directly from the Dirac equation. For the Klein-Gordon and the Proca equation, the Hamiltonian can be derived from the Lagrange density instead. Hence, the Hamiltonian corresponding to the Klein-Gordon equation is given by

$$\begin{aligned}\hat{\mathrm{H}} &= \int d^3x\, \hat{\mathcal{H}}(x) = \int d^3x\, [\pi(x)\dot{\phi}(x) - \mathcal{L}(x)] \\ &= \int d^3x\, [\pi(x)\pi^\dagger(x) + (\nabla\phi(x))^\dagger(\nabla\phi(x)) + m^2\phi^\dagger(x)\phi(x)]\,, \end{aligned} \tag{A.51}$$

with

$$\pi(x) = \frac{\partial}{\partial\dot{\phi}(x)}\mathcal{L}(x)\,. \tag{A.52}$$

Replacing the wave functions by quantum field operators

$$\pi(x) = \int \frac{d^3k}{(2\pi)^3}\frac{i}{2}u_i^\dagger(\vec{k})a_i^\dagger(\vec{k})e^{ikx}\,, \tag{A.53}$$

the energy of a state is determined by

$$\int d^3x\, \langle F|\hat{\mathcal{H}}(x)|F\rangle = \int d\tilde{k}_i\, 2(E_i(\vec{k}))^2 u^\dagger(\vec{k})u_i(\vec{k})f_i(\vec{k}) \stackrel{!}{=} \int \frac{d^3k}{(2\pi)^3}E_i(\vec{k})f_i(\vec{k})\,, \tag{A.54a}$$

$$\Rightarrow u_i^\dagger(\vec{k})u_i(\vec{k}) = 1\,. \tag{A.54b}$$

For massive vector bosons, a similar condition is obtained. However, in the four-vector representation, where $u_i(\vec{k})$ is given by the polarization vectors defined in equation (A.59), $u_i^\dagger(\vec{k})u_i(\vec{k})$ is normalized to -1 instead.

Next, interpreting the negative energy eigenvalues of the relativistic equations of motion as anti-particles, the quantum field operators are modified such that they either annihilate a particle state or create an antiparticle state,

$$\psi(x) = \int d\tilde{k}_i \left(u_i(\vec{k})a_i(\vec{k})e^{-ikx} + v_i(\vec{k})b_i^\dagger(\vec{k})e^{ikx}\right)\,, \tag{A.55}$$

where the $v_i(\vec{k})$ are the eigenvectors corresponding to the negative energy eigenvalues

$$\hat{\mathrm{H}}\, v_i(\vec{k}) = -E_i(\vec{k})\, v_i(\vec{k})\,, \tag{A.56}$$

and $b_i^\dagger$ are the creation operators of the antiparticles. Considering quantum fields without charge under gauge symmetries, particles and antiparticles are indistinguishable, implying that they only correspond to one degree of freedom[2] ($b_i^\dagger = a_i^\dagger$).

[2] This is also true for particles of the adjoin representation because they carry both charge and anticharge so that the conjugated of a full set of these particles is equivalent to the full set.

Thus, the quantum field operators for scalar bosons, spin-1/2 fermions, and massive vector bosons can be defined as

$$\phi(x) = \int d\tilde{k} \left(a(\vec{k})\, e^{-ikx} + b^\dagger(\vec{k})\, e^{ikx} \right) , \tag{A.57a}$$

$$\Psi(x) = \int d\tilde{k} \sum_s \left(a(\vec{k})\, u_s(\vec{k})\, e^{-ikx} + b^\dagger(\vec{k})\, v_s(\vec{k})\, e^{ikx} \right) , \tag{A.57b}$$

$$A^\mu(x) = \int d\tilde{k} \sum_\lambda \left(a(\vec{k})\, \epsilon^\mu_\lambda(\vec{k})\, e^{-ikx} + a^\dagger(\vec{k}) \left(\epsilon^\mu_\lambda(\vec{k}) \right)^* e^{ikx} \right) . \tag{A.57c}$$

For spin-1/2 fermions, the eigenstates are defined by the conditions

$$(\not{k} + m)\, u_s(\vec{k}) = 0 \,, \tag{A.58a}$$

$$(\not{k} - m)\, v_s(\vec{k}) = 0 \,, \tag{A.58b}$$

with the spin index i, and for vector bosons, they are given by

$$\varepsilon^\dagger_\lambda\, \varepsilon_{\lambda'} = -\delta_{\lambda\lambda'} \,, \tag{A.59a}$$

$$\varepsilon_\lambda\, p = 0 \,, \tag{A.59b}$$

with the polarization index λ.

A.5 Propagators and Full Set of States

The propagators in vacuum QFT – resulting e.g. from the path integral formalism –, ignoring the difficulties arising from self-interacting massive vector bosons discussed in sections 2.3 and 2.4, are given by

$$G(x) = \lim_{\epsilon \to 0^+} \int \frac{dk}{(2\pi)^4} \frac{i}{k^2 - m^2 + i\epsilon} e^{-ikx} \tag{A.60}$$

for scalar bosons,

$$S_F(x) = \lim_{\epsilon \to 0^+} \int \frac{dk}{(2\pi)^4} \frac{i(\not{k} + m)}{k^2 - m^2 + i\epsilon} e^{-ikx} \tag{A.61}$$

for spin-1/2 fermions,

$$G_{\mu\nu}(x) = \lim_{\epsilon \to 0^+} \int \frac{dk}{(2\pi)^4} \left(g_{\mu\nu} - \frac{k_\mu k_\nu}{m^2} \right) \frac{-i}{k^2 - m^2 + i\epsilon} e^{-ikx} \tag{A.62}$$

for massive vector bosons, and

$$G^{ab}_{\mu\nu}(x) = \lim_{\epsilon \to 0^+} \int \frac{dk}{(2\pi)^4} \left(g_{\mu\nu} - (1 - \xi) \frac{k_\mu k_\nu}{k^2} \right) \frac{-i\delta^{ab}}{k^2 + i\epsilon} e^{-ikx} \tag{A.63}$$

for gauge bosons where ξ is an arbitrary constant which the time evolution does not depend on.

In contrast, in R_ξ gauge, the propagators of Goldstone bosons and the massive vector bosons are given by

$$G(x) = \lim_{\epsilon\to 0^+} \int \frac{dk}{(2\pi)^4} \frac{i}{k^2 - \xi m^2 + i\epsilon} e^{-ikx}\,, \tag{A.64a}$$

$$\begin{aligned} G_{\mu\nu}(x) &= \lim_{\epsilon\to 0^+} \int \frac{dk}{(2\pi)^4} i \left(\frac{-g_{\mu\nu} + k_\mu k_\nu/m^2}{k^2 - m^2 + i\epsilon} - \frac{k_\mu k_\nu/m^2}{k^2 - \xi m^2 + i\epsilon} \right) e^{-ikx} \\ &= \lim_{\epsilon\to 0^+} \int \frac{dk}{(2\pi)^4} \left(g_{\mu\nu} - (1-\xi)\frac{k_\mu k_\nu}{k^2 - \xi m^2} \right) \frac{-i}{k^2 - m^2 + i\epsilon} e^{-ikx}\,. \end{aligned} \tag{A.64b}$$

In QFT a full set of states for one particle species i can be defined as

$$|S\rangle \langle S|_i = \left(\sum_{n=0}^{\infty} \frac{1}{n!} \right) \left(\prod_{j=1}^{n} \int d\tilde{k}_{i,j} \right) \left(\prod_{j=1}^{n} a_i(\vec{k}_j) \right)^\dagger |0\rangle \langle 0| \left(\prod_{j=1}^{n} a_i(\vec{k}_j) \right)\,, \tag{A.65}$$

fulfilling the relation

$$\begin{aligned} |S'\rangle \langle S'|S\rangle \langle S|_i &= \left(\sum_{m=0}^{\infty} \frac{1}{m!} \right) \left(\sum_{n=0}^{\infty} \frac{1}{n!} \right) \left(\prod_{l=1}^{m} \int d\tilde{k}_{i,l} \right) \left(\prod_{j=1}^{n} \int d\tilde{k}_{i,j} \right) \\ &\quad \times \left(\prod_{l=1}^{m} a_i(\vec{k}_l) \right)^\dagger |0\rangle \langle 0| \left(\prod_{l=1}^{m} a_i(\vec{k}_l) \right) \left(\prod_{j=1}^{n} a_i(\vec{k}_j) \right)^\dagger |0\rangle \langle 0| \left(\prod_{j=1}^{n} a_i(\vec{k}_j) \right) \\ &= \left(\sum_{m=0}^{\infty} \frac{1}{m!} \right) \left(\sum_{n=0}^{\infty} \frac{1}{n!} \right) \left(\prod_{l=1}^{m} \int d\tilde{k}_{i,l} \right) \left(\prod_{j=1}^{n} \int d\tilde{k}_{i,j} \right) \left(\prod_{l=1}^{m} \prod_{j=1}^{n} 2E_i(\vec{k}_l) \delta^3(\vec{k}_l - \vec{k}_j) \right) \\ &\quad \times \delta_{nm} \left(\prod_{l=1}^{m} a_i(\vec{k}_l) \right)^\dagger |0\rangle \langle 0| \left(\prod_{j=1}^{n} a_i(\vec{k}_j) \right) = |S\rangle \langle S|_i\,. \end{aligned} \tag{A.66}$$

Moreover, considering multiple particle species, the full set of particles contains another product over all particle species:

$$|S\rangle \langle S| = \left(\prod_i \sum_{n_i=0}^{\infty} \frac{1}{n_i!} \right) \left(\prod_i \prod_{j=1}^{n_i} \int d\tilde{k}_{i,j} \right) \left(\prod_i \prod_{j=1}^{n_i} a_i(\vec{k}_{i,j}) \right)^\dagger |0\rangle \langle 0| \left(\prod_i \prod_{j=1}^{n_i} a_i(\vec{k}_{i,j}) \right)\,. \tag{A.67}$$

A.6 Calculation of Matrix Elements Without Using the Residue Theorem

The vacuum matrix-element including the action of two quantum field operators is proportional to the propagator in momentum space:

$$\mathcal{M} \propto \int dx \, \langle 0| \mathcal{T} \psi_i(x+y) \psi_i^\dagger(y) |0\rangle \, e^{ipx}\,, \tag{A.68}$$

with p being the sum over the incoming and outgoing external momenta, respectively. Using the commutation or anticommutation relation given in equation (A.45) and (A.47), respectively, and the normalization of the vacuum ($\langle 0|0\rangle = 1$),

$$\langle 0|\,\mathcal{T}\psi(x+y)\psi^\dagger(y)\,|0\rangle = \int d\tilde{k}\left(\big[f_1(\vec{k})+f_2(\vec{k})\big]\Theta(t)e^{-ikx} + \big[f_1(\vec{k})-f_2(\vec{k})\big]\Theta(-t)e^{ikx}\right) \tag{A.69}$$

is obtained with $\Theta(x)$ being the Heaviside step function defined in equation (D.9). Moreover, $f_1(\vec{k})$ and $f_2(\vec{k})$ are functions depending on the particle species: $f_1(\vec{k}) = 1$ and $f_2(\vec{k}) = 0$ for scalar bosons, cf. equation (2.27), $f_1(\vec{k}) = m - \vec{k}\vec{\gamma}$ and $f_2(\vec{k}) = E_k\gamma^0$ for spin-1/2 fermions, cf. equation (2.31), and $f_1(\vec{k}) = -g^{\mu\nu} + k_A^\mu k_A^\nu/m_A^2$ and $f_2(\vec{k}) = 0$ for massive vector bosons, cf. equation (2.34). Next, instead of using the residue theorem, the spacetime integral in equation (A.68) can also be evaluated:

$$\begin{aligned}
&\int dx \int d\tilde{k}\, e^{i(\vec{p}-\vec{k})\vec{x}}\Big(\big[f_1(\vec{k})+f_2(\vec{k})\big]\Theta(t)e^{-i(E_k-p_0)t} + \big[f_1(\vec{k})-f_2(\vec{k})\big]\Theta(-t)e^{i(E_k+p_0)t}\Big)\\
&= \frac{1}{2E_p}\int dt\left(\big[f_1(\vec{p})+f_2(\vec{p})\big]\Theta(t)e^{-i(E_p-p_0)t} + \Theta(-t)\big[f_1(\vec{p})-f_2(\vec{p})\big]e^{i(E_p+p_0)t}\right)\\
&= \frac{-i}{2E_p}\left(\frac{f_1(\vec{p})+f_2(\vec{p})}{E_p-p_0} + \frac{f_1(\vec{p})-f_2(\vec{p})}{E_p+p_0}\right) = \frac{i}{p_0^2-E_p^2}\left(f_1(\vec{p}) + f_2(\vec{p})\frac{p_0}{E_p}\right),
\end{aligned} \tag{A.70}$$

where the well-known replacement $E_p \to E_p - i\epsilon$ is used to evaluate the time integral and the limit $\epsilon \to 0^+$ is evaluated after time integration. Hence, the introduction of ϵ enforces the integrand to vanish at $t \to \pm\infty$[3].

Solving the time integral instead of simply making use the residue theorem helps to understand the appearance of off-shell states as a QM interference phenomenon. As can be seen from equation (A.70), an off-shell propagator is in fact a superposition of the propagation of an on-shell particle ($E_p = \sqrt{\vec{p}^{\,2}+m^2}$) from x to y for $x_0 > y_0$ (the $\Theta(t)$ part) and of an on-shell antiparticle from y to x for $y_0 > x_0$ (the $\Theta(-t)$ part).

Solving the time integral instead of using the residue theorem also works for loop contributions. Considering e.g. a simple loop containing two scalar boson propagators, the corresponding matrix element in the common form is given by

$$\begin{aligned}
\mathcal{M} &= \lim_{\epsilon\to 0^+}\int dx \int \frac{dk}{(2\pi)^4}\frac{dk'}{(2\pi)^4}\frac{i}{k^2-m_1^2+i\epsilon}\frac{i}{(k')^2-m_2^2+i\epsilon}e^{i(p-k-k')x}\\
&= \lim_{\epsilon\to 0^+} -\int \frac{dk}{(2\pi)^4}\frac{1}{k_0^2-(E_k+i\epsilon)^2}\frac{1}{(k_0-p_0)^2-(E_{p-k}+i\epsilon)^2}\\
&= -i\int\frac{d^3k}{(2\pi)^3}\left(\frac{1}{2E_k}\frac{1}{(E_k-p_0)^2-E_{p-k}^2} + \frac{1}{(E_{p-k}+p_0)^2-E_k^2}\frac{1}{2E_{p-k}}\right)\\
&= \int d\tilde{k}\frac{i}{E_{p-k}}\frac{E_k+E_{p-k}}{p_0^2-(E_k+E_{p-k})^2},
\end{aligned} \tag{A.71}$$

[3]The explanation for the substitution $E_p \to E_p - i\epsilon$ in physical processes is the assumed localization of particles – usually described as Gaussian wave packets –, implying that the wave functions of the incoming and outgoing particles in the limit $t \to \pm\infty$ do not overlap. Consequently, the probability for producing an intermediate state vanishes for large Δt. Furthermore, the limit $\epsilon \to 0^+$ leads to a good approximation as long as the time during which the two wave packets overlap is large compared to $1/(p_0 - E_p)$.

where the energy integral is evaluated using the residue theorem. Solving the time integral similarly to equation (A.70), instead, the same result is obtained:

$$\begin{aligned}
&\int dx \, \langle 0| \, T\phi_1(x+y)\phi_2(x+y)\phi_1^\dagger(y)\phi_2^\dagger(y) \, |0\rangle \, e^{ipx} \\
&= \int dx \int d\tilde{k} \int d\tilde{k}' \Big(\Theta(t) e^{-i(k+k')x} + \Theta(-t) e^{i(k+k')x} \Big) e^{ipx} \\
&= \int d\tilde{k} \frac{i}{E_{p-k}} \frac{E_k + E_{p-k}}{p_0^2 - (E_k + E_{p-k})^2} \, .
\end{aligned} \tag{A.72}$$

A.7 Detailed Calculation of the Interaction Hamiltonian for Self-Interaction Massive Vector Bosons

The Hamiltonian density corresponding to the Lagrangian density including two self-interacting massive vector boson fields, cf. equations (A.18c) and (2.42),

$$\begin{aligned}
\mathcal{L}(x) = &-\frac{1}{4} F_{A,\mu\nu}(x) F_A^{\mu\nu}(x) + \frac{m_A^2}{2} A_{H,\mu}(x) A_H^\mu(x) - \frac{1}{4} F_{B,\mu\nu}(x) F_B^{\mu\nu}(x) + \frac{m_B^2}{2} B_{H,\mu}(x) B_H^\mu(x) \\
&- J_A^\mu(x) A_{H,\mu}(x) - J_B^\mu(x) B_{H,\mu}(x) - J_{\mu\nu}(x) A_H^\mu(x) B_H^\nu(x) \, ,
\end{aligned} \tag{A.73}$$

is determined by

$$\begin{aligned}
\hat{\mathcal{H}}(x) &= \Pi_A^\mu(x) [\partial_0 A_{H,\mu}(x)] + \Pi_B^\mu(x) [\partial_0 B_{H,\mu}(x)] - \mathcal{L}(x) \\
&= -\vec{\Pi}_A [\partial_0 \vec{A}_L(x)] - \vec{\Pi}_B [\partial_0 \vec{B}_L(x)] - \mathcal{L}(x) \, .
\end{aligned} \tag{A.74}$$

Using equations (2.43) and (2.46),

$$\partial_0 \vec{A}_L(x) = -\vec{\Pi}_A(x) + \nabla A_H^0(x) = -\vec{\Pi}_A(x) + \frac{1}{m_A^2} \nabla [\nabla \vec{\Pi}_A(x) + J_A'^0(x)] \qquad \text{and} \tag{A.75}$$

$$\partial_0 \vec{B}_L(x) = -\vec{\Pi}_B(x) + \nabla B_H^0(x) = -\vec{\Pi}_B(x) + \frac{1}{m_B^2} \nabla [\nabla \vec{\Pi}_B(x) + J_B'^0(x)] \tag{A.76}$$

are obtained, meaning that the Hamiltonian density can be expressed as

$$\begin{aligned}
\hat{\mathcal{H}}(x) &= \vec{\Pi}_A(x)^2 + \frac{1}{m_A^2}[\nabla\vec{\Pi}_A(x)][\nabla\vec{\Pi}_A(x) + J'^0_A(x)] + \vec{\Pi}_B(x)^2 + \frac{1}{m_B^2}[\nabla\vec{\Pi}_B(x)][\nabla\vec{\Pi}_B(x) + J'^0_B(x)] \\
&\quad - \frac{1}{2}\vec{\Pi}_A(x)^2 + \frac{1}{2}[\nabla\times\vec{A}_L(x)]^2 + \frac{1}{2}m_A^2\vec{A}(x)^2 - \frac{1}{2}\vec{\Pi}_B(x)^2 + \frac{1}{2}[\nabla\times\vec{B}_L(x)]^2 + \frac{1}{2}m_B^2\vec{B}(x)^2 \\
&\quad - \frac{1}{2m_A^2}[\nabla\vec{\Pi}_A(x) + J'^0_A(x)]^2 - \vec{J}_A(x)\vec{A}_L(x) + \frac{1}{m_A^2}J^0_A(x)[\nabla\vec{\Pi}_A(x) + J'^0_A(x)] \\
&\quad - \frac{1}{2m_B^2}[\nabla\vec{\Pi}_B(x) + J'^0_B(x)]^2 - \vec{J}_B(x)\vec{B}_L(x) + \frac{1}{m_B^2}J^0_B(x)[\nabla\vec{\Pi}_B(x) + J'^0_B(x)] \\
&\quad + J^{ij}(x)A^i_H(x)B^j_H(x) - \frac{1}{m_A^2}J^{0j}(x)[\nabla\vec{\Pi}_A(x) + J'^0_A(x)]B^j_H(x) \\
&\quad - \frac{1}{m_B^2}J^{i0}(x)A^i_H(x)[\nabla\vec{\Pi}_B(x) + J'^0_B(x)] + \frac{1}{m_A^2m_B^2}J^{00}(x)[\nabla\vec{\Pi}_A(x) + J'^0_A(x)][\nabla\vec{\Pi}_B(x) + J'^0_B(x)] \\
&= \frac{1}{2}\vec{\Pi}_A(x)^2 + \frac{1}{2m_A^2}\big[\nabla\vec{\Pi}_A(x)\big]^2 + \frac{1}{2}\big[\nabla\times\vec{A}_L(x)\big]^2 + \frac{1}{2}m_A^2\vec{A}(x)^2 \\
&\quad + \frac{1}{2}\vec{\Pi}_B(x)^2 + \frac{1}{2m_B^2}\big[\nabla\vec{\Pi}_B(x)\big]^2 + \frac{1}{2}\big[\nabla\times\vec{B}_L(x)\big]^2 + \frac{1}{2}m_B^2\vec{B}(x)^2 \\
&\quad - \vec{J}_A(x)\vec{A}_L(x) - \vec{J}_B(x)\vec{B}_L(x) + J^{ij}(x)A^i_H(x)B^j_H(x) - \frac{1}{2m_A^2}[J'^0_A(x)]^2 - \frac{1}{2m_B^2}[J'^0_B(x)]^2 \\
&\quad + \frac{1}{m_A^2}\big[J^0_A(x) - J^{0j}(x)B^j_H(x)\big][\nabla\vec{\Pi}_A(x) + J'^0_A(x)] \\
&\quad + \frac{1}{m_B^2}\big[J^0_B(x) - J^{i0}(x)A^i_H(x)\big][\nabla\vec{\Pi}_B(x) + J'^0_B(x)] \\
&\quad + \frac{1}{m_A^2m_B^2}J^{00}(x)[\nabla\vec{\Pi}_A(x) + J'^0_A(x)][\nabla\vec{\Pi}_B(x) + J'^0_B(x)]\,. \qquad \text{(A.77)}
\end{aligned}$$

Next, changing from the Heisenberg to the interaction picture and using the definition (2.49), the interaction part of equation (A.77) becomes

$$\begin{aligned}
\hat{\mathcal{H}}_I(x) &= J^\mu_A(x)A_\mu(x) + J^\mu_B(x)B_\mu(x) + J^{\mu\nu}(x)A_\mu(x)B_\nu(x) - \frac{1}{2m_A^2}\big[J'^0_A(x)\big]^2 - \frac{1}{2m_B^2}\big[J'^0_B(x)\big]^2 \\
&\quad + \frac{1}{m_A^2}\big[J^0_A(x) + J^{0\nu}(x)B_\nu(x)\big]\,J'^0_A(x) + \frac{1}{m_B^2}\big[J^0_B(x) + J^{\mu0}(x)A_\mu(x)\big]\,J'^0_B(x) \\
&\quad + \frac{1}{m_A^2m_B^2}J^{00}(x)\,J'^0_A(x)\,J'^0_B(x) \\
&= J^\mu_A(x)A_\mu(x) + J^\mu_B(x)B_\mu(x) + J^{\mu\nu}(x)A_\mu(x)B_\nu(x) \\
&\quad + \frac{1}{2m_A^2}\big[J'^0_A(x)\big]^2 + \frac{1}{2m_B^2}\big[J'^0_B(x)\big]^2 - \frac{1}{m_A^2m_B^2}J^{00}(x)\,J'^0_A(x)\,J'^0_B(x)\,, \qquad \text{(A.78)}
\end{aligned}$$

where the relations

$$\begin{aligned}
J'^0_A(x) &= J^0_A(x) + J^{0\mu}(x)B_\mu(x) + \frac{J^{00}J'^0_B}{m_B^2}\,, \\
J'^0_B(x) &= J^0_B(x) + J^{\mu0}(x)A_\mu(x) + \frac{J^{00}J'^0_A}{m_A^2}\,, \qquad \text{(A.79)}
\end{aligned}$$

are used to derive the final form.
Substituting $J_A'^0(x)$ and $J_B'^0(x)$, cf. equation (2.46), an interaction Hamiltonian density including an infinite series of local interaction terms is obtained:

$$\begin{aligned}
\hat{\mathcal{H}}_I(x) &= J_A^\mu(x)A_\mu(x) + J_B^\mu(x)B_\mu(x) + J^{\mu\nu}(x)A_\mu(x)B_\nu(x) \\
&+ \frac{1}{2m_A^2}\left(J_A^0(x) + J^{0\nu}(x)B_\nu(x) - \frac{J^{00}(x)}{2m_B^2}\left(J_B^0(x) + J^{\mu 0}(x)A_\mu(x) + \frac{J_0{}^0(x)}{2m_A^2}\dots\right)\right)^2 \\
&+ \frac{1}{2m_B^2}\left(J_B^0(x) + J^{\mu 0}(x)A_\mu(x) - \frac{J^{00}(x)}{2m_A^2}\left(J_A^0(x) + J^{0\nu}(x)B_\nu(x) + \frac{J^0{}_0(x)}{2m_B^2}\dots\right)\right)^2 \\
&- \frac{J^{00}(x)}{m_A^2 m_B^2}\left(J_A^0(x) + J^{0\nu}(x)B_\nu(x) - \frac{J^{00}(x)}{2m_B^2}\left(J_B^0(x) + J^{\mu 0}(x)A_\mu(x) + \frac{J_0{}^0(x)}{2m_A^2}\dots\right)\right) \\
&\quad\times\left(J_B^0(x) + J^{\mu 0}(x)A_\mu(x) - \frac{J^{00}(x)}{2m_A^2}\left(J_A^0(x) + J^{0\nu}(x)B_\nu(x) + \frac{J^0{}_0(x)}{2m_B^2}\dots\right)\right) .
\end{aligned} \tag{A.80}$$

Summarizing equivalent terms, the first elements of the infinite series of local interaction terms are given by

$$\begin{aligned}
\hat{\mathcal{H}}_I(x) &= J_A^\mu(x)A_\mu(x) + J_B^\mu(x)B_\mu(x) + J^{\mu\nu}(x)A_\mu(x)B_\nu(x) + \frac{\left[J_A^0(x)\right]^2}{2m_A^2} + \frac{\left[J_B^0(x)\right]^2}{2m_B^2} \\
&\quad + \frac{J_A^0(x)J^{0\nu}(x)B_\nu(x)}{m_A^2} + \frac{J_B^0(x)J^{\mu 0}(x)A_\mu(x)}{m_B^2} + \frac{J_A^0(x)J^{00}(x)J_B^0(x)}{m_A^2 m_B^2} \\
&\quad + \frac{(J^{0\nu}(x)B_\nu(x))^2}{2m_A^2} + \frac{(J^{\mu 0}(x)A_\mu(x))^2}{2m_B^2} + \dots \quad .
\end{aligned} \tag{A.81}$$

Alternatively, using relation (A.79), one can also rewrite the interaction Hamiltonian as

$$\begin{aligned}
\hat{\mathcal{H}}_I(x) &= J_A'^\mu(x)A_\mu(x) + J_B^\mu(x)B_\mu(x) - \frac{1}{2m_A^2}\left[J_A'^0(x)\right]^2 - \frac{1}{2m_B^2}\left[J_B'^0(x)\right]^2 + \frac{1}{m_B^2}J_B^0(x)J_B'^0(x) \\
&\quad + \frac{1}{m_A^2}\left[J_A^0(x) + J^{0\nu}(x)B_\nu(x)\right]J_A'^0(x) + \frac{1}{m_A^2 m_B^2}J^{00}(x)\,J_A'^0(x)\,J_B'^0(x) \\
&= J_A'^\mu(x)A_\mu(x) + J_B^\mu(x)B_\mu(x) + \frac{1}{2m_A^2}\left[J_A'^0(x)\right]^2 - \frac{1}{2m_B^2}\left[J_B'^0(x)\right]^2 + \frac{1}{m_B^2}J_B^0(x)J_B'^0(x) \\
&= J_A'^\mu(x)A_\mu(x) + J_B^\mu(x)B_\mu(x) + \frac{1}{2m_A^2}\left[J_A'^0(x)\right]^2 + \frac{1}{2m_B^2}\left[J_B^0(x)\right]^2 - \frac{1}{2m_B^2}\left[J_B'^0(x) - J_B^0(x)\right]^2 .
\end{aligned} \tag{A.82}$$

Moreover, using

$$J_B'^0(x) - J_B^0(x) = J^{\mu 0}(x)A_\mu(x) + \frac{1}{m_A^2}J^{00}(x)J_A'^0(x)\,, \tag{A.83}$$

the interaction Hamiltonian can be rewritten into a form being useful for the investigation in the path integral formalism:

$$\begin{aligned}\hat{\mathcal{H}}_I(x) &= J_A^i(x)A_i(x) + J^{i\mu}(x)A_i(x)(B_\mu(x) + \frac{g_{\mu 0}}{m_B^2}J_B^0) + J_B^\mu(x)B_\mu(x) + \frac{1}{2m_B^2}\left[J_B^0(x)\right]^2 \\ &\quad + J_A'^0(x)A_0(x) + \frac{1}{2m_A^2}\left[J_A'^0(x)\right]^2 - \frac{1}{2m_B^2}\left[J^{00}(x)\right]^2\left(A^0(x) + \frac{1}{m_A^2}J_A'^0(x)\right)^2 \\ &= J_A^i(x)A_i(x) + J^{ij}(x)A_i(x)B_j(x) + J_B^i(x)B_i(x) + J^{i0}(x)A_i(x)\left(B^0(x) + \frac{1}{m_B^2}J_B^0(x)\right) \\ &\quad + \frac{m_B^2}{2}\left(B^0(x) + \frac{1}{m_B^2}J_B^0(x)\right)^2 - \frac{m_B^2}{2}[B_0(x)]^2 \\ &\quad + \frac{1}{2}\left(m_A^2 - \frac{1}{2m_B^2}[J^{00}(x)]^2\right)\left(A_0(x) + \frac{1}{m_A^2}J_A'^0(x)\right)^2 - \frac{m_A^2}{2}[A_0(x)]^2\,. \end{aligned} \tag{A.84}$$

A.8 Supplementary Details to Renormalization

To regularize the momentum integral, an obvious approach is to introduce a cut-off scale $\Lambda_{\text{cut-off}}$ up to which the momentum integral is evaluated, meaning that the divergences appears in the limit $\Lambda_{\text{cut-off}} \to \infty$. However, this simple method breaks Lorentz invariance and gauge symmetry so that other methods securing both are preferred. The typically used regularization method is the dimensional regularization[4] where the four-momentum integral is evaluated in $4-\epsilon$ dimensions instead, implying that the divergences appear as poles in ϵ. Because this trick reduces the mass dimension of the momentum integral, an additional arbitrary energy scale μ^2 is introduced to compensate this.

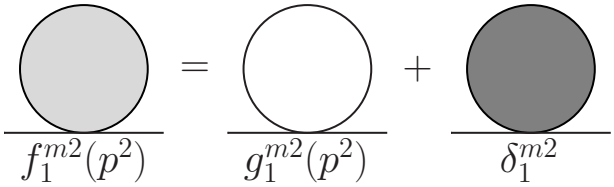

Figure A.4: Division of the full loop integral (light gray) into a finite scale dependent part that vanishes e.g. for on-shell particles (white) and the remaining constant part (dark gray)

Next, the regularized momentum integrals – which are functions of the external kinematic scales Λ_i and additional unphysical parameters induced by the regularization λ_i – are divided into a scale-dependent part $g_i\left(\Sigma_i\Lambda_i\right)$ that e.g. vanishes at the renormalization scale $\Lambda_{j,\mathrm{R}}$ and the remaining scale-independent part $\delta_i(\Sigma_i\lambda_i)$ containing the additional unphysical parameters, cf. figure A.4:

$$f_n\left(\Sigma_i\Lambda_i, \Sigma_j\lambda_j\right) := g_n\left(\Sigma_i\Lambda_i\right) + \delta_n(\Sigma_i\lambda_i)\,, \tag{A.85}$$

with $g_n\left(\Sigma_i\Lambda_{j,\mathrm{R}}\right)) = 0$ and n being the order of the considered matrix element in perturbation theory.

[4]Note that this procedure leads to other issues (e.g. defining chirality) but the result is gauge and Lorentz invariant and methods have been developed to overcome the arising problems.

Next, renormalization is used to absorb $\delta_n(\Sigma_i\lambda_i)$ into the Hamiltonian by redefining the parameters of the theory accordingly. Consequently, the renormalized parameters at the renormalization scale are given by the sum of the bare parameters and the scale-independent part of all diagrams of the perturbation series. Choosing e.g. the renormalization scale for self-energy corrections – loop corrections with only two external lines – to be the on-shell mass,

$$m^2_{\text{on-shell}} = m_0^2 + \sum_n \delta_n^{m^2}(\Sigma_i\lambda_i)\,, \tag{A.86}$$

is obtained. With this, the parameters at a different scale are given by the renormalized parameters added to the sum of all scale-dependent loop contributions:

$$m^2_{\text{eff}}(p^2) = m^2_{\text{on-shell}} + \sum_n g_n^{m^2}(p^2)\,. \tag{A.87}$$

Actually, the division of a matrix element into a scale-dependent and a scale-independent part is not as simple as indicated here. The reason for that is that each loop isolated from the remaining part of the matrix element can be divided accordingly but the hole amplitude cannot. However, this is not a problem but allows the use of the renormalized parameters for calculating the contribution of a diagram. This can be understood from the fact that exchanging any vertex or propagator of a diagram of some perturbation series by any diagram of the perturbation series of this vertex or propagator results in a diagram which is also part of the considered perturbation series.
For this reason, the divergent scale-independent contribution of any loop appearing in an amplitude can be removed by subtracting the contribution which is already taken into account by using the renormalized parameters for lower order diagrams. Consequently, the contribution of a loop in any diagram is only given by its finite scale-dependent part.

Consequently, to calculate the finite scale-dependent contribution of a certain loop, the perturbation series of each renormalized parameter is considered isolated from its appearance in amplitudes. At one-loop order, the loop integral can simply be divided into a scale-dependent and a scale-independent part as discussed before. For higher loop orders, the contribution – which is already taken into account by using the renormalized parameters for the calculation of the lower order diagrams – has to be subtracted. This can be done without difficulties because the contribution which needs to be subtracted is known from the calculation of the lower order loop correction of the considered parameter, cf. figure A.5 for an example. Thus, the scale-dependence of all renormalized parameters can be calculated order by order.

Using this procedure e.g. for the calculation of the perturbation series of the quartic scalar coupling ($\hat{\mathcal{H}}_I(x) = \frac{\lambda}{4!}\phi(x)^4$), it can be estimated that the series converges if λ is not to large ($\lambda \lesssim 16\pi^2$). In this case, the scale-dependence of λ can be approximated by only calculating lower order corrections. Furthermore, considering larger scale shifts ($\Lambda_i - \Lambda_{i,\text{R}}$), the series converges slower and, for this reason, higher order corrections become more important.

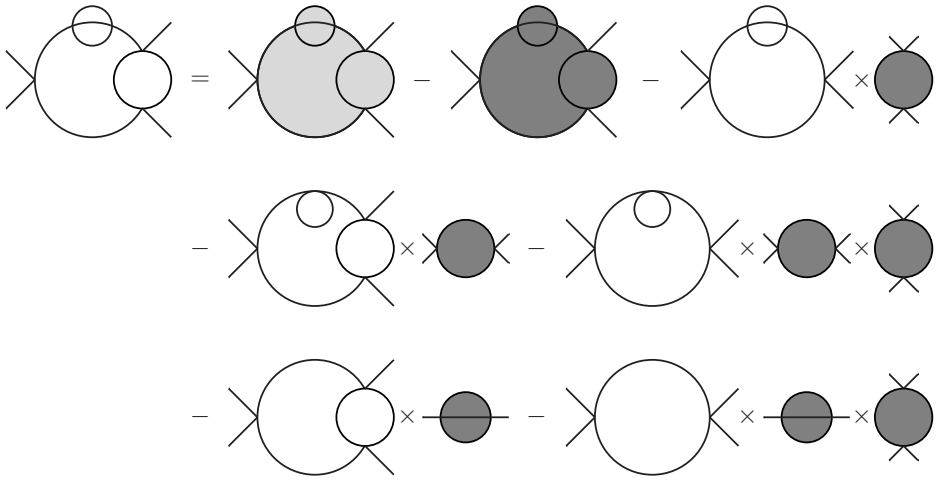

Figure A.5: The finite scale-dependent contribution of a diagram being part of the perturbation series of a renormalized parameter (white) is given by the full loop contribution (light gray) subtracted by the non-scale-dependent contribution which is adsorbed into the tree-level coupling (dark gray) and the sum of the contributions which are take into account by using the renormalized parameters for the lower order diagrams (product of lower order white and dark gray diagrams)

A.9 Renormalization Group Equations

For the SM, only taking into account the gauge couplings and the dominant Yukawa interactions (top, bottom, and tau), the RGEs at one-loop order are given by [57]

$$\frac{dg'}{d\ln\mu} = \left(\frac{4}{3}N_g + \frac{1}{10}\right)\frac{g'^3}{16\pi^2} = \frac{41}{10}\frac{g'^3}{16\pi^2}\,, \tag{A.88a}$$

$$\frac{dg}{d\ln\mu} = \left(\frac{4}{3}N_g - \frac{43}{6}\right)\frac{g^3}{16\pi^2} = -\frac{19}{6}\frac{g^3}{16\pi^2}\,, \tag{A.88b}$$

$$\frac{dg_s}{d\ln\mu} = \left(\frac{4}{3}N_g - 11\right)\frac{g_s^3}{16\pi^2} = -7\frac{g_s^3}{16\pi^2}\,, \tag{A.88c}$$

$$\frac{dy_t}{d\ln\mu} = \left(-8g_s^2 - \frac{9}{4}g^2 - \frac{17}{20}g'^2 + \frac{9}{2}y_t^2 + \frac{3}{2}y_b^2 + y_\tau^2\right)\frac{y_t}{16\pi^2}\,, \tag{A.88d}$$

$$\frac{dy_b}{d\ln\mu} = \left(-8g_s^2 - \frac{9}{4}g^2 - \frac{1}{4}g'^2 + \frac{3}{2}y_t^2 + \frac{9}{2}y_b^2 + y_\tau^2\right)\frac{y_b}{16\pi^2}\,, \tag{A.88e}$$

$$\frac{dy_\tau}{d\ln\mu} = \left(-\frac{9}{4}g^2 - \frac{9}{4}g'^2 + 3y_t^2 + 3y_b^2 + \frac{5}{2}y_\tau^2\right)\frac{y_t}{16\pi^2}\,, \tag{A.88f}$$

where N_g is the number of generations, which is 3 in the SM. Furthermore, considering the inert Higgs model, cf. section 6.1, the RGEs at one-loop order for the Higgs self couplings are given by [34,

10]

$$\frac{d\lambda_1}{d\ln\mu} = \frac{1}{16\pi^2}\Bigg[\left(12\lambda_1 - 9g^2 - \frac{9}{5}g'^2 + 12y_t^2 + 12y_b^2 + 4y_\tau^2\right)\lambda_1 + 4(\lambda_3+\lambda_4)\lambda_3 + 2\lambda_4^2 + 2|\lambda_5|^2 + \frac{9}{4}\left(g^4 + \frac{2}{5}g^2g'^2 + \frac{3}{25}g'^4\right) - 12y_t^4 - 12y_b^4 - 4y_\tau^4\Bigg], \tag{A.89a}$$

$$\frac{d\lambda_2}{d\ln\mu} = \frac{1}{16\pi^2}\Bigg[\left(12\lambda_2 - 9g^2 - \frac{9}{5}g'^2\right)\lambda_2 + 4(\lambda_3+\lambda_4)\lambda_3 + 2\lambda_4^2 + 2|\lambda_5|^2 + \frac{9}{4}\left(g^4 + \frac{2}{5}g^2g'^2 + \frac{3}{25}g'^4\right)\Bigg], \tag{A.89b}$$

$$\frac{d\lambda_3}{d\ln\mu} = \frac{1}{16\pi^2}\Bigg[\left(6\lambda_1 + 6\lambda_2 + 4\lambda_3 - 9g^2 - \frac{9}{5}g'^2 + 6y_t^2 + 6y_b^2 + 2y_\tau^2\right)\lambda_3 + 2(\lambda_1+\lambda_2)\lambda_4 + 2\lambda_4^2 + 2|\lambda_5|^2 + \frac{9}{4}\left(g^4 - \frac{2}{5}g^2g'^2 + \frac{3}{25}g'^4\right)\Bigg], \tag{A.89c}$$

$$\frac{d\lambda_4}{d\ln\mu} = \frac{1}{16\pi^2}\Bigg[\left(2\lambda_1 + 2\lambda_2 + 8\lambda_3 + 4\lambda_4 - 9g^2 - \frac{9}{5}g'^2 + 6y_t^2 + 6y_b^2 + 2y_\tau^2\right)\lambda_4 + 8|\lambda_5|^2 + \frac{9}{5}g^2g'^2\Bigg], \tag{A.89d}$$

$$\frac{d\lambda_5}{d\ln\mu} = \frac{1}{16\pi^2}\left(2\lambda_1 + 2\lambda_2 + 8\lambda_3 + 13\lambda_4 - 9g^2 - \frac{9}{5}g'^2 + 6y_t^2 + 6y_b^2 + 2y_\tau^2\right)\lambda_5\,. \tag{A.89e}$$

Note that the other SM RGEs given in equation (A.88) are unaffected by the Higgs self interaction and that the SM case is obtained by setting $\lambda_1 = \lambda$ and $\lambda_2 = \lambda_3 = \lambda_4 = \lambda_5 = 0$.
As boundary conditions for the RGEs given in equation (A.88), the values of the couplings at the Z-pole ($\mu = m_Z$) in the $\overline{\text{MS}}$ scheme are used [57]:

$$\alpha_Y(m_Z) = \frac{g'(m_Z)^2}{4\pi} = 0.0169225 \pm 0.0000039\,, \tag{A.90a}$$

$$\alpha_g(m_Z) = \frac{g(m_Z)^2}{4\pi} = 0.033735 \pm 0.000020\,, \tag{A.90b}$$

$$\alpha_s(m_Z) = \frac{g_s(m_Z)^2}{4\pi} = 0.11730 \pm 0.00069\,, \tag{A.90c}$$

$$\alpha_t(m_Z) = \frac{y_t(m_Z)^2}{4\pi} = 0.07514\,, \tag{A.90d}$$

$$\alpha_b(m_Z) = \frac{y_b(m_Z)^2}{4\pi} = 2.064 \times 10^{-5}\,, \tag{A.90e}$$

$$\alpha_\tau(m_Z) = \frac{y_\tau(m_Z)^2}{4\pi} = 8.077 \times 10^{-6}\,, \tag{A.90f}$$

$$\tag{A.90g}$$

Furthermore, for the SM case, the boundary condition for λ can be extracted from the measured Higgs boson mass and the VEV:

$$\lambda(m_h) = \frac{m_h^2}{v^2} \approx 0.258\,. \tag{A.91}$$

A.10 Standard Model Lagrangian

The SM Lagrangian density, describing the time evolution of the SM particle content, cf. section 2.8, in the Yukawa basis is given by

$$\begin{aligned}
\mathcal{L}_{\mathrm{SM}}(x) &= \overline{\Psi}_{Q_i}(x)\left(i\partial\!\!\!/ + g_s t_3^a \mathcal{G}\!\!\!/^a(x) + g t_2^3 \mathcal{W}\!\!\!/^3(x) + g' Y_{Q_i} \mathcal{B}\!\!\!/(x)\right)\Psi_{Q_i}(x) \\
&+ g\overline{\Psi}_{Q_j}(x) V_{ij}\left(t_2^1 \mathcal{W}\!\!\!/^1(x) + t_2^2 \mathcal{W}\!\!\!/^2(x)\right)\Psi_{Q_i}(x) + \overline{\Psi}_{U_i}(x)\left(i\partial\!\!\!/ + g_s t_3^a \mathcal{G}\!\!\!/^a(x) + g' Y_{U_i}\mathcal{B}\!\!\!/(x)\right)\Psi_{U_i}(x) \\
&+ \overline{\Psi}_{D_i}(x)\left(i\partial\!\!\!/ + g_s t_3^a \mathcal{G}\!\!\!/^a(x) + g' Y_{D_i}\mathcal{B}\!\!\!/(x)\right)\Psi_{D_i}(x) + \overline{\Psi}_{\ell_{R,i}}(x)\left(i\partial\!\!\!/ + g' Y_{\ell_{R,i}}\mathcal{B}\!\!\!/(x)\right)\Psi_{\ell_{R,i}}(x) \\
&+ \overline{\Psi}_{\ell_i}(x)\left(i\partial\!\!\!/ + g t_2^b \mathcal{W}\!\!\!/^b(x) + g' Y_{\ell_i}(x)\mathcal{B}\!\!\!/(x)\right)\Psi_{\ell_i}(x) - \Big[y_{U_i}\overline{\Psi}_{Q_i}(x) H^c \Psi_{U_i}(x) \\
&+ y_{D_i}\overline{\Psi}_{Q_i}(x) H \Psi_{D_i}(x) + y_{\ell_{R,i}}\overline{\Psi}_{\ell_i}(x) H \Psi_{\ell_{R,i}}(x) + h.c.\Big] - \frac{1}{4} G^a_{\mu\nu}(x) G^{a,\mu\nu}(x) \\
&- \frac{1}{4} W^b_{\mu\nu}(x) W^{b,\mu\nu}(x) - \frac{1}{4} B_{\mu\nu}(x) B^{\mu\nu}(x) - m_H^2 H^\dagger(x) H(x) - \frac{\lambda_H}{2}\left(H^\dagger(x) H(x)\right)^2 \\
&+ \left[\left(\partial_\mu - i g t_2^b W^b_\mu(x) - i g' Y_H B_\mu(x)\right) H(x)\right]^\dagger \left[\left(\partial_\mu - i g t_2^b W^b_\mu(x) - i g' Y_H B_\mu(x)\right) H(x)\right], \qquad \text{(A.92)}
\end{aligned}$$

with $H^c = i\sigma_2 H^*$. Moreover, the CKM matrix is defined as

$$V_{ij} = \begin{pmatrix} 1 & 0 & 0 \\ 0 & \cos\theta_{23} & \sin\theta_{23} \\ 0 & -\sin\theta_{23} & \cos\theta_{23} \end{pmatrix} \begin{pmatrix} \cos\theta_{13} & 0 & \sin\theta_{13} e^{-i\delta_{CP}} \\ 0 & 1 & 0 \\ -\sin\theta_{13} e^{i\delta_{CP}} & 0 & \cos\theta_{13} \end{pmatrix} \begin{pmatrix} \cos\theta_{12} & \sin\theta_{12} & 0 \\ -\sin\theta_{12} & \cos\theta_{12} & 0 \\ 0 & 0 & 1 \end{pmatrix}, \qquad \text{(A.93)}$$

cf. equation (C.5), for the observed values of the four angles. Moreover, the field strength tensors, cf. equation (A.21), associated to the $SU(3)_c$, the $SU(2)_L$, and the $U(1)_Y$ gauge symmetries are given by

$$G^a_{\mu\nu}(x) = \partial_\mu G^a_\nu(x) - \partial_\nu G^a_\mu(x) + g_s f_3^{abc} G^b_\mu(x) G^c_\nu(x), \qquad \text{(A.94a)}$$

$$W^a_{\mu\nu}(x) = \partial_\mu W^a_\nu(x) - \partial_\nu W^a_\mu(x) + g f_2^{abc} W^b_\mu(x) W^c_\nu(x), \qquad \text{(A.94b)}$$

$$B_{\mu\nu}(x) = \partial_\mu B^a_\nu(x) - \partial_\nu B^a_\mu(x). \qquad \text{(A.94c)}$$

The SM Lagrangian density in the charge conjugated picture is determined by

$$\begin{aligned}
\mathcal{L}^c_{\mathrm{SM}}(x) &= -\mathcal{L}^*_{\mathrm{SM}}(x) = \overline{\Psi^c}_{Q_i}(x)\left(i\partial\!\!\!/ - g_s t_3^a \mathcal{G}\!\!\!/^a(x) - g t_2^3 \mathcal{W}\!\!\!/^3(x) - g' Y_{Q_i}\mathcal{B}\!\!\!/(x)\right)\Psi^c_{Q_i}(x) \\
&- g\overline{\Psi^c}_{Q_j}(x) V_{ij}\left(t_2^1 \mathcal{W}\!\!\!/^1(x) + t_2^2 \mathcal{W}\!\!\!/^2(x)\right)\Psi^c_{Q_i}(x) + \overline{\Psi^c}_{U_i}(x)\left(i\partial\!\!\!/ - g_s t_3^a \mathcal{G}\!\!\!/^a(x) - g' Y_{U_i}\mathcal{B}\!\!\!/(x)\right)\Psi^c_{U_i}(x) \\
&+ \overline{\Psi^c}_{D_i}(x)\left(i\partial\!\!\!/ - g_s t_3^a \mathcal{G}\!\!\!/^a(x) - g' Y_{D_i}\mathcal{B}\!\!\!/(x)\right)\Psi^c_{D_i}(x) + \overline{\Psi^c}_{\ell_{R,i}}(x)\left(i\partial\!\!\!/ - g' Y_{\ell_{R,i}}\mathcal{B}\!\!\!/(x)\right)\Psi^c_{\ell_{R,i}}(x) \\
&+ \overline{\Psi^c}_{\ell_i}(x)\left(i\partial\!\!\!/ - g t_2^b \mathcal{W}\!\!\!/^b(x) - g' Y_{\ell_i}(x)\mathcal{B}\!\!\!/(x)\right)\Psi^c_{\ell_i}(x) - \Big[y^*_{U_i}\overline{\Psi^c}_{Q_i}(x) H \Psi^c_{U_i}(x) \\
&+ y^*_{D_i}\overline{\Psi^c}_{Q_i}(x) H^c \Psi^c_{D_i}(x) + y^*_{\ell_{R,i}}\overline{\Psi^c}_{\ell_i}(x) H^c \Psi^c_{\ell_{R,i}}(x) + h.c.\Big] - \frac{1}{4} G^a_{\mu\nu}(x) G^{a,\mu\nu}(x) \\
&- \frac{1}{4} W^b_{\mu\nu}(x) W^{b,\mu\nu}(x) - \frac{1}{4} B_{\mu\nu}(x) B^{\mu\nu}(x) - m_H^2 H^{c\dagger}(x) H^c(x) - \frac{\lambda_H}{2}\left(H^{c\dagger}(x) H^c(x)\right)^2 \\
&+ \left[\left(\partial_\mu + i g t_2^b W^b_\mu(x) + i g' Y_H B_\mu(x)\right) H^c(x)\right]^\dagger \left[\left(\partial_\mu + i g t_2^b W^b_\mu(x) + i g' Y_H B_\mu(x)\right) H^c(x)\right], \qquad \text{(A.95)}
\end{aligned}$$

meaning that all charges become negative and all Yukawa couplings complex conjugated.

B Supplementary Details to the Description of Many Body Systems

B.1 Introduction Into Basic Concepts of Thermodynamics

To quantify the distance between a state and its equilibrium state, it is convenient to define the entropy, which is minimal when a system is in a defined state. Moreover, when the entropy is maximal, a system is in its equilibrium state. Additionally, defining the entropy as an extrinsic quantity – meaning that the entropy of a state of a joined system is given be the sum of the entropies of the subsystems – the entropy can be defined as

$$S_i = -\int \rho_i \ln(\rho_i) \tag{B.1a}$$

$$\Rightarrow S_i + S_j = -\int \rho_i \rho_j (\ln(\rho_i) + \ln(\rho_j)) = -\int \rho_i \rho_j \ln(\rho_i \rho_j)\,, \tag{B.1b}$$

where ρ is the phase space density. Next, demanding an expectation value for a non-conserved quantity,

$$\langle A \rangle = \int A\rho \stackrel{!}{=} \mathcal{A}\,, \tag{B.2}$$

this additional condition can be taken into account by using the method of Lagrange multipliers:

$$S = -\int \rho \ln(\rho) - \sum_i \lambda_i \left(\int A_i \rho - \mathcal{A}_i \right). \tag{B.3}$$

Maximizing the entropy results in the equilibrium condition given by

$$\rho = \exp\left(1 - \sum_i \lambda_i A_i\right). \tag{B.4}$$

Considering e.g. a system which is thermally coupled to an environment – e.g. physically separated systems in thermal contact or single particle (species) inside a medium –, due to energy exchange, the entire system (system plus environment) equilibrates, meaning that the expectation value of the energy per particle is equivalent for all subsystems. Thus, equilibration transfers energy and therewith phase space from one system to another, where the phase space volume increases for increasing energy. In case of only demanding an expectation value for the energy,

$$\langle E \rangle = \int E\rho \stackrel{!}{=} \mathcal{E}\,, \tag{B.5}$$

instead of fixing it, the additional condition alters the phase space density after equilibration:

$$\rho = \frac{1}{Z} e^{-\beta E}\,, \tag{B.6}$$

where the so called canonical partition function Z is determined by the normalization condition:

$$\int \rho = 1 \qquad \Rightarrow \qquad Z = \int e^{-\beta E}\,. \tag{B.7}$$

At this point, defining the entropy as an extrinsic parameter is useful because it can be considered differentially in linear dependence to the energy which is also extrinsic:

$$dE = T\,dS\,, \tag{B.8}$$

where the temperature $T \geq 0$ is a factor of proportionality which is related to β:

$$\langle E \rangle = \int E\rho = -\frac{1}{Z}\frac{\partial}{\partial\beta} Z = -\frac{\partial}{\partial\beta}\ln(Z)\,, \tag{B.9a}$$

$$S = -\int \rho \ln(\rho) = -\frac{1}{Z}\int e^{-\beta E}\left[-\beta E - \ln(Z)\right] = \ln(Z) - \beta\frac{\partial}{\partial\beta}\ln(Z) \tag{B.9b}$$

$$\Rightarrow \frac{dS}{dE} = \beta \overset{!}{=} \frac{1}{T}\,. \tag{B.9c}$$

Together with equation (3.2), this implies that the average energy of a system in thermal equilibrium is proportional to T.

Next, systems with variable particle content can be considered. If an expectation value for the number of particles is demanded,

$$\langle N \rangle = \int N\rho \overset{!}{=} \mathcal{N}\,, \tag{B.10}$$

according to equation (B.4) this results in:

$$\rho = \frac{1}{\mathcal{Z}} e^{-\beta E - \gamma N}\,, \tag{B.11}$$

where the so called grand canonical partition function $\mathcal{Z}$ is again determined by the normalization condition,

$$\mathcal{Z} = \int e^{-\beta E - \gamma N}\,. \tag{B.12}$$

Because the particle number is also an extrinsic parameter, it can be set differentially in linear dependence to the energy:

$$dE = \mu\,dN\,, \tag{B.13}$$

with the chemical potential μ. As for the temperature, a similar relation among the chemical potential μ and γ can be found:

$$\langle N \rangle = \int N\rho = -\frac{\partial}{\partial\gamma}\ln(\mathcal{Z})\,, \tag{B.14a}$$

$$S = -\int \rho \ln(\rho) = \ln(\mathcal{Z}) - \beta\frac{\partial}{\partial\beta}\ln(\mathcal{Z}) - \gamma\frac{\partial}{\partial\gamma}\ln(\mathcal{Z}) \tag{B.14b}$$

$$\Rightarrow \frac{dN}{dE} = \frac{dN}{dS}\frac{dS}{dE} = \frac{\beta}{\gamma} \overset{!}{=} \frac{1}{\mu}\,. \tag{B.14c}$$

Using this, the grand canonical partition function in its common form is obtained:

$$\Rightarrow \mathcal{Z} = \int e^{-\beta(E+\mu N)} \,. \tag{B.15}$$

It might seem confusing to call μ chemical potential because only an expectation value for a particle number is assumed. However, assuming an expectation value for a number density can be done for various reasons. First of all, one can examining subsystems which can exchange particles with other subsystems. Starting from considering two subsystems which are thermally coupled and are both in an equilibrium state and assuming the particle densities of both subsystems to be different, particles will diffuse from one subsystem to the other when particle exchange is allowed, meaning that the particle densities of both subsystems becomes equivalent. Next, to obtain different particle densities for both subsystems in thermal equilibrium, one of the subsystems has to be more attractive which – according to equation (B.13) – is the case when the energy of a particle changes when it passes between the subsystems. This is e.g. the case when the considered particle reacts chemically with other particles whose densities are different in both subsystems and which are not exchanged. On the other hand, also the number densities of the product and the reactant of a chemical reaction can be considered. Because there is an energy difference between reactant and product, the reaction evolves energy in one direction and resorbs energy in the other direction, implying that the number densities of reactant and product are different in thermal equilibrium, cf. equation (3.4).
However, the chemical potential also appears in systems where an asymmetry between different particles is settled by external conditions and secured by conserved quantities. In this case, the chemical potential does not have a chemical origin, meaning that – allowing for a change of the asymmetry – it equilibrates to zero.
Furthermore, the chemical potential is relevant when considering the distribution functions of a system with constant particle number. In this case, the chemical potential is used to normalize the distribution functions such that the correct number density is obtained.

Until now, only thermally coupled systems have been considered. However, *volumes* (V) can be exchanged between subsystems as well. This case is much more intuitive because one can easily think of a movable wall separating two systems. The expectation value of the force that a system puts on the wall results from elastic scattering processes where particles are reflected on the wall. Consequently, the so called *pressure* p depends on the average energy (temperature) and the particle density. If the pressure is different on both sides of the wall, there is a net force, resulting in a motion of the wall. Due to the motion of the wall, reflected particles on the side with higher pressure lose energy, while particles on the side with lower pressure gain energy. In addition, the number densities change, implying that the pressure on both sides equilibrates. The differential equation for the energy change is thereby given by $dE = -p\,dV$ so that the well-known formula

$$dE = T\,dS - p\,dV + \mu_i\,dN_i \,, \tag{B.16}$$

is obtained.

Next, to obtain the distribution functions for particles in thermal equilibrium, it has to be taken into account that each eigenstate of a system can be either occupied or not. Consequently, the grand

canonical partition function for bosons is

$$\mathcal{Z}_{b_i} = \sum_{n=0}^{\infty} e^{-n\beta(E+\mu_{b_i})} = \frac{1}{1-e^{-\beta(E+\mu_{b_i})}}\,, \tag{B.17}$$

where each state can be occupied multiple times. Hence, the corresponding distribution function is given by the Bose-Einstein statistics:

$$f_{b_i}^{\mathrm{eq}} = \frac{1}{\mathcal{Z}_{b_i}}\frac{\partial}{\partial(\beta\mu_{b_i})}\mathcal{Z}_{b_i} = \frac{1}{e^{\beta(E+\mu_{b_i})}-1}\,, \tag{B.18a}$$

$$\Rightarrow 1 + f_{b_i}^{\mathrm{eq}} = e^{\beta(E+\mu_{b_i})} f_{b_i}^{\mathrm{eq}}\,. \tag{B.18b}$$

In contrast, for fermions, each state can only be occupied once resulting in the Fermi-Dirac statistics:

$$\mathcal{Z}_{f_i} = 1 + e^{-\beta(E+\mu_{f_i})}\,, \tag{B.19a}$$

$$f_{f_i}^{\mathrm{eq}} = \frac{1}{\mathcal{Z}_f}\frac{\partial}{\partial(\beta\mu_{f_i})}\mathcal{Z}_{f_i} = \frac{1}{e^{\beta(E+\mu_{f_i})}+1}\,, \tag{B.19b}$$

$$\Rightarrow 1 - f_{f_i}^{\mathrm{eq}} = e^{\beta(E+\mu_{f_i})} f_{f_i}^{\mathrm{eq}}\,. \tag{B.19c}$$

Only in the limit of low occupation probabilities ($\beta(E+\mu_i) \ll 1$), both statistics become equivalent to the Maxwell-Boltzmann statistics:

$$f_i^{\mathrm{eq}} = e^{-\beta(E+\mu_i)}\,. \tag{B.20}$$

For the Boltzmann statistics, the corresponding number density is given by, cf. equation (D.17),

$$n_i(T) = e^{-\beta\mu_i} m_i^3 \frac{K_2(\beta m_i)}{2\pi^2\beta m_i} \overset{T\gg m_i}{\approx} e^{-\beta\mu_i}\frac{T^3}{\pi^2}\,, \tag{B.21}$$

while the number densities for bosons and fermions in the limit $\mu_i, m_i \ll T$ become

$$n_{b_i}(T) = \frac{\zeta(3)}{\pi^2}T^3 - \frac{\mu_{b_i}}{6}T^2\,, \tag{B.22a}$$

$$n_{f_i}(T) = \frac{3\zeta(3)}{4\pi^2}T^3 - \frac{\mu_{f_i}}{12}T^2\,. \tag{B.22b}$$

B.2 Details on the Derivation of Boltzmann Equations

The time evolution of distribution functions is determined by the probability of annihilating a state from the distribution function and the probability of creating a state, which are both determined by equation (2.22). Consequently, the time evolution of the distribution function of a particle species i can be written as:

$$\begin{aligned} 2E_i\frac{df_i}{dt} = &-\int (\Pi d\tilde{k}_{f_i})(\Pi d\tilde{k}_{b_i})(\Pi d\tilde{k}_{f_f})(\Pi d\tilde{k}_{b_f})(2\pi)^4\delta(k_i + \Sigma k_{f_i} + \Sigma k_{b_i} - \Sigma k_{f_f} - \Sigma k_{b_f}) \\ &\times \Big[|M|^2_{if_{i_1}\ldots b_{i_1}\ldots\to f_{f_1}\ldots b_{f_1}\ldots} f_i(\Pi f_{f_i})(\Pi f_{b_i})(\Pi[1-f_{f_f}])(\Pi[1+f_{b_f}]) \\ &\quad - |M|^2_{f_{f_1}\ldots b_{f_1}\ldots\to if_{i_1}\ldots b_{i_1}\ldots}(\Pi f_{f_f})(\Pi f_{b_f})(1\pm f_i)(\Pi[1-f_{f_i}])(\Pi[1+f_{b_i}])\Big] := C[f_i]\,. \end{aligned} \tag{B.23}$$

Furthermore, the time evolution of a thermal plasma in the early universe is also affected by the expansion of the universe. Considering a single particle in an expanding isotropic and homogeneous universe described by the Friedmann equations (A.5), its momentum is red shifted:

$$\vec{k}_i = \vec{k}_i(t_0)\frac{a(t_0)}{a(t)} = \vec{k}_i(t_0)\exp\left(-\int_{t_0}^{t}\mathsf{H}(t')dt'\right). \tag{B.24}$$

Thus, neglecting interaction terms, the distribution function is simply shifted to lower momenta, implying that the time evolution of an isotropic and homogeneous distribution function $f_i(x,\vec{k}) = f_i(E_i,t)$ is given by

$$f_i(E_i,t) = f_i\left(\sqrt{\left(\vec{k}_i(t_0)\frac{a(t)}{a(t_0)}\right)^2 + m_i^2}, t_0\right) \tag{B.25}$$

$$\Rightarrow \frac{df_i}{dt} = \frac{1}{a(t)}\frac{da(t)}{dt}\frac{\vec{k_i}^2}{E}\frac{\partial f_i}{\partial E} = \mathsf{H}(t)\frac{\vec{k_i}^2}{E}\frac{\partial f_i}{\partial E}. \tag{B.26}$$

Consequently, the time evolution of the distribution function in general is [47]:

$$\frac{df_i}{dt} = \mathsf{H}(t)\frac{\vec{k_i}^2}{E_i}\frac{\partial f_i}{\partial E} + \frac{1}{2E_i}C[f_i]. \tag{B.27}$$

Next, the collision term $C[f_i]$ can be divided into one part $C_{\text{elastic}}[f_i]$ containing all elastic scattering processes which only change the particle momenta but not the particle species and one part $C_{\text{inelastic}}[f_i]$ containing all inelastic scattering processes changing the particle species. In many cases, it can be assumed that the elastic scattering processes are in thermal equilibrium, meaning that the distribution functions are determined by the equilibrium distribution functions (Fermi-Dirac or Bose-Einstein statistics). Under this assumption, the distribution function only depends on the particle density, meaning that the equations of motion can be rewritten in terms of particle densities [47]:

$$\frac{dn_i(t)}{dt} = -3H(t)n_i(t) + \int d\tilde{k}_i\, C_{\text{inelastic}}[f_i], \tag{B.28}$$

where the conservation of the particle number by elastic scattering processes is used:

$$\frac{dN_i(t)}{dt} = V(t)\frac{dn_i(t)}{dt} + \frac{dV(t)}{dt}n_i(t) \stackrel{!}{=} 0 \tag{B.29}$$

$$\Rightarrow \frac{dn_i(t)}{dt} = \frac{1}{V(t)}\frac{dV(t)}{dt}n_i(t) = -3\frac{1}{a(t)}\frac{da(t)}{dt}\frac{dn_i(t)}{dt} = -3\mathsf{H}(t)\frac{dn_i(t)}{dt}. \tag{B.30}$$

By normalizing the number density to the *entropy density*[1],

$$s = S/V = (\rho + p)/T, \tag{B.31}$$

with the energy density ρ and the pressure p, equation (B.28) can be further simplified to [47]

$$\frac{dY_i(t)}{dt} := \frac{d}{dt}\frac{n_i(t)}{s(t)} = \frac{1}{s}\left(\frac{dn_i(t)}{dt} - \frac{1}{s}\frac{ds}{dt}n_i(t)\right) = \frac{1}{s}\int d\tilde{k}_i\, C_{\text{inelastic}}[f_i], \tag{B.32}$$

[1] for a derivation of this relation see [47, pp.65-66]

where the conservation of the entropy S is used:

$$\frac{1}{s}\frac{ds}{dt} = V\frac{d}{dt}\frac{1}{V} + \frac{1}{S}\frac{dS}{dt} = V\frac{d}{dt}\frac{1}{V} = a(t)^3\frac{d}{dt}\frac{1}{a(t)^3} = -3\frac{1}{a(t)}\frac{da(t)}{dt} = -3\mathsf{H}(t)\,. \tag{B.33}$$

In addition, $C_{\text{inelastic}}[f_i]$ can be simplified further as well since for the equilibrium densities, the relations (B.18b) and (B.19c) can be used to obtain

$$\begin{aligned} C_{\text{inelastic}}[f_i] = -\int &(\Pi d\tilde{k}_{f_i})(\Pi d\tilde{k}_{b_i})(\Pi d\tilde{k}_{f_f})(\Pi d\tilde{k}_{b_f})(2\pi)^4\delta(k_i + \Sigma k_{f_i} + \Sigma k_{b_i} - \Sigma k_{f_f} - \Sigma k_{b_f}) \\ &\times \left[|M|^2_{if_{i_1}\dots b_{i_1}\cdots\to f_{f_1}\dots b_{f_1}\dots}e^{\Sigma\beta\mu_{f_f}+\Sigma\beta\mu_{b_f}} - |M|^2_{f_{f_1}\dots b_{f_1}\cdots\to if_{i_1}\dots b_{i_1}\dots}e^{\beta\mu_i+\Sigma\beta\mu_{f_i}+\Sigma\beta\mu_{b_i}}\right] \\ &\times e^{\beta K^0} f_i(\Pi f_{f_i})(\Pi f_{b_i})(\Pi f_{f_f})(\Pi f_{b_f})\,, \end{aligned} \tag{B.34}$$

with $K^0 = k_i^0 + \Sigma k_{f_i}^0 + \Sigma k_{b_i}^0 = \Sigma k_{f_f}^0 + \Sigma k_{b_f}^0$.

B.3 Thermal Masses

B.3.1 Second Order Thermal Self-Energy Correction

The thermal one-loop self-energy correction in ϕ^4 theory ($\hat{\mathrm{H}}_I(x) = \frac{\lambda}{4!}\phi(x)^4$) is given by

$$\begin{aligned} \Pi_T^1(p^2) &= \frac{\lambda}{2}\int\frac{d^4k}{(2\pi)^4}\left(\frac{i}{k^2-m^2} + 2\pi\big(f(E_k)\Theta(E_k) + f(-E_k)\Theta(-E_k)\big)\delta(k^2-m^2)\right) \\ &= -\frac{\lambda}{2}\frac{A(m^2)}{16\pi^2} + \lambda\int d\tilde{k}\, f(E_k)\,. \end{aligned} \tag{B.35}$$

where the divergent vacuum loop correction is completely canceled when the renormalization scale is chosen to be the on-shell mass in the vacuum. Thus, at one-loop order, the thermal mass is only determined by the remaining integral, which, in the limit $T \gg m$, can be series expand in powers of m/T ($\Pi_T^1 \approx \lambda T^2/24 + \mathcal{O}(m/T)$), cf. equation (D.11).

For the two-loop self-energy correction, the contribution of the diagram which does not contain thermal corrections to the propagator masses can be written as

$$\begin{aligned} \Pi_T^2(p^2) = i\frac{\lambda^2}{6}\int\frac{d^4\vec{k}}{(2\pi)^4}\int\frac{d^4\vec{k}'}{(2\pi)^4}&\left(\frac{i}{k^2-m^2} + 2\pi\big(f(E_k)\Theta(E_k) + f(-E_k)\Theta(-E_k)\big)\delta(k^2-m^2)\right) \\ &\times\left(\frac{i}{k'^2-m^2} + 2\pi\big(f(E_{k'})\Theta(E_{k'}) + f(-E_{k'})\Theta(-E_{k'})\big)\delta(k'^2-m^2)\right) \\ &\times\left(\frac{i}{(p+k+k')^2-m^2} + 2\pi\big(f(E')\Theta(E') + f(-E')\Theta(-E')\big)\delta((p+k+k')^2-m^2)\right). \end{aligned} \tag{B.36}$$

As for the one-loop correction, the pure vacuum contribution is canceled by choosing the renormalization scale to be the on-shell mass in the vacuum. Furthermore, the divergent contribution from

the part with one distribution function and two vacuum propagators[2]:

$$\Pi_T^{2,1}(p^2) = i\frac{\lambda^2}{2}\int d\tilde{k} f(E_k)\int \frac{d^4\vec{k}'}{(2\pi)^4}\frac{i}{k'^2-m^2} \times\left(\frac{i}{(p+k^+ +k')^2-m^2}+\frac{i}{(p+k^- +k')^2-m^2}\right), \tag{B.37}$$

is canceled by the vacuum one-loop vertex correction ($\approx \lambda/(16\pi^2)$), meaning that this correction partly takes into account vacuum one-loop corrections to λ for the thermal one-loop self-energy correction.
The contribution with two distribution functions and one vacuum propagator is given by

$$\Pi_T^{2,2}(p^2) = i\frac{\lambda^2}{4}\int d\tilde{k} f(E_k)\int d\tilde{k}' f(E_{k'})\Bigg(\frac{i}{(p+k^+ +k'^+)^2-m^2} + \frac{i}{(p+k^+ +k'^-)^2-m^2}+\frac{i}{(p+k^- +k'^+)^2-m^2}+\frac{i}{(p+k^- +k'^-)^2-m^2}\Bigg). \tag{B.38}$$

Considering $p^\mu = (m,0,0,0)$ this integral becomes

$$\begin{aligned}\Pi_T^{2,2}(m^2) &\approx \frac{\lambda^2}{64\pi^4}\int_{-1}^{1} dx \int_m^\infty dE_k\, E_k f(E_k)\int_m^\infty dE_{k'}\, E_{k'} f(E_{k'})\Bigg(\frac{1}{m(E_k+E_{k'}+m)+E_kE_{k'}(1-x)} \\ &\quad + \frac{2}{m(E_k-E_{k'}+m)-E_kE_{k'}(1+x)}+\frac{1}{m(-E_k-E_{k'}+m)+E_kE_{k'}(1-x)}\Bigg) \\ &= \frac{\lambda^2}{64\pi^4}\int_m^\infty dE_k\, f(E_k)\int_m^\infty dE_{k'}\, f(E_{k'})\Bigg[\ln\left(\frac{m(E_k+E_{k'}+m)+2E_kE_{k'}}{m(E_k+E_{k'}+m)}\right) \\ &\quad - 2\ln\left(\frac{m(E_k-E_{k'}+m)-2E_kE_{k'}}{m(E_k-E_{k'}+m)}\right)+\ln\left(\frac{m(-E_k-E_{k'}+m)+2E_kE_{k'}}{m(-E_k-E_{k'}+m)}\right)\Bigg].\end{aligned} \tag{B.39}$$

Calculating this integral in the limit $T \gg m$, $\Pi_T^{2,2}(m^2) \approx \lambda^2T^2/(32\pi^2)T^2 \approx 3\lambda/(2\pi^2)\Pi_T^1$ is obtained for $m \ll T$. Moreover, considering larger masses (e.g. $m^2 = 2\Pi_T^1 \approx \lambda T^2/12$), $\Pi_T^{2,2}(p^2)$ becomes further Boltzmann suppressed.
Finally, the contribution with three distribution function is further suppressed. Moreover, as discussed in section 3.3, it does not contribute to the thermal mass but contributes to the damping in the generalized equation of motion, cf. equation (2.117).

In contrast, considering the thermal one-loop self-energy correction ($m^2 = 2\Pi_T^1 \approx \lambda T^2/12$) for the calculation of the thermal one-loop self-energy, the result is shifted by $\Pi_T^{2'}(p^2) \approx -\sqrt{3\lambda}/(2\pi)\Pi_T^1$, cf. equation (D.11), which is by a factor $\pi/\sqrt{3\lambda}$ less suppressed than $\Pi_T^2(p^2)$.

[2]The $\pm$ index of the momentum distinguishes between positive and negative energies.

B.3.2 Leading Order Thermal Mass Corrections for the SM and Relevant Extensions

Within the SM, the thermal masses induced by the gauge interactions, the Higgs self coupling, and the top Yukawa interaction before EWSB in the high temperature limit are given by [70, 30]

$$m_H^2 = \left(\frac{3g^2+g'^2}{16} + \frac{y_t^2}{4} + \frac{\lambda}{4}\right) T^2 \,, \tag{B.40a}$$

$$m_{\ell_i}^2 = \frac{3g^2+g'^2}{32} T^2 \,, \tag{B.40b}$$

$$m_{\ell_{R,i}}^2 = \frac{g'^2}{8} T^2 \,, \tag{B.40c}$$

$$m_{Q_i}^2 = \left(\frac{g_s^2}{6} + \frac{3g^2}{32} + \frac{g'^2}{288} + \delta_{i3}\frac{y_t^2}{16}\right) T^2 \,, \tag{B.40d}$$

$$m_{U_i}^2 = \left(\frac{g_s^2}{6} + \frac{g'^2}{18} + \delta_{i3}\frac{y_t^2}{8}\right) T^2 \,, \tag{B.40e}$$

$$m_{D_i}^2 = \left(\frac{g_s^2}{6} + \frac{g'^2}{72}\right) T^2 \,, \tag{B.40f}$$

$$m_G^2 = \frac{11 g_s^2}{12} T^2 \,, \tag{B.40g}$$

$$m_W^2 = \frac{11 g^2}{12} T^2 \,, \tag{B.40h}$$

$$m_B^2 = \frac{11 g'^2}{12} T^2 \,. \tag{B.40i}$$

Extending the SM by right-chiral neutrinos – transforming as singlets under all SM gauge groups –, the induced thermal masses in the high temperature limit are

$$m_H^2 = \left(\frac{3g^2+g'^2}{16} + \frac{y_t^2}{4} + \frac{\lambda}{4}\right) T^2 + \sum_{i,j} \frac{|y_{ij}|^2}{12} T^2 \,, \tag{B.41a}$$

$$m_{\ell_j}^2 = \frac{3g^2+g'^2}{32} T^2 + \sum_i \frac{|y_{ij}|^2}{16} T^2 \,, \tag{B.41b}$$

$$m_{\nu_i^R}^2 = \sum_j \frac{|y_{ij}|^2}{8} T^2 \,. \tag{B.41c}$$

Considering the inert Higgs model, the thermal masses of the Higgs particles in the high temperature limit are given by [50]:

$$m_H^2 = \left(\frac{3g^2+g'^2}{16} + \frac{y_t^2}{4} + \frac{3\lambda_1 + 2\lambda_3 + \lambda_4}{12}\right) T^2 \,, \tag{B.42a}$$

$$m_\phi^2 = \left(\frac{3g^2+g'^2}{16} + \frac{3\lambda_2 + 2\lambda_3 + \lambda_4}{12}\right) T^2 \,. \tag{B.42b}$$

B.4 Thermal Rate for the Production of Left-Chiral Neutrinos After EWSB

The thermal interaction rate of active neutrinos can be approximated by the thermal decay rate of the $SU(2)_L$ and $U(1)_Y$ gauge bosons whose thermal masses are sufficiently large, cf. figure 3.1. The corresponding decay width can be calculated similarly to the decay width of the scalar boson considered in section 5.1. The corresponding matrix element is given by

$$i\mathcal{M}_{A_\mu\to\nu_i\bar{\ell}_i} = -ig'\epsilon^\mu_\lambda \overline{v}_{\ell_i}\gamma_\mu L u_{\nu_i} \tag{B.43}$$

$$\begin{aligned}\Rightarrow \overline{|\mathcal{M}_{A_\mu\to\nu_i\bar{\ell}_i}|^2} &= \frac{(g')^2}{3}\left(-g^{\mu\nu}-\frac{p_A^\mu p_A^\nu}{m_A^2}\right)\mathrm{Tr}\left[(\not{p}_{\ell_i}-m_{\ell_i})\gamma_\mu L \not{p}_{\nu_i}\gamma_\nu\right]\\ &= \frac{2}{3}(g')^2\left[p_{\ell_i}p_{\nu_i}+\frac{1}{m_A^2}2(p_{\ell_i}p_A)(p_A p_{\nu_i})\right],\end{aligned} \tag{B.44}$$

with $(g')^2 = g^2/2$ and $m_A = m_W$ for the decay of the $W^\pm$ boson and $(g')^2 = (g^2+g'^2)/4$ and $m_A = m_Z$ for the Z boson decay. Note that here, the decay of $W^\pm$ and Z bosons is considered because the focus is on the thermal decay rate after EWSB.
In the rest frame of the decaying particle ($E_A = m_A$ and $|\vec{p}_A| = 0$), cf. equation (D.4), the decay width, cf. equation (2.25), is

$$\begin{aligned}\Gamma_{A_\mu\to\nu_i\bar{\ell}_i} &= \frac{2(g')^2(p_{\nu_i}p_{\ell_i}+2E_{\nu_i}E_{\ell_i})}{24\pi}\frac{|\vec{p}_{\nu_i}|}{m_A^2}\\ &= \frac{g^2 m_A}{48\pi}\left(2-\frac{m_{\nu_i}^2}{m_A^2}-\frac{m_{\ell_i}^2}{m_A^2}-\frac{(m_{\nu_i}^2-m_{\ell_i}^2)}{m_A^4}\right)\lambda\left(1,\frac{m_{\nu_i}^2}{m_A^2},\frac{m_{\ell_i}^2}{m_A^2}\right).\end{aligned} \tag{B.45}$$

Thus, the corresponding thermal rate, cf. equation (3.27), becomes

$$\gamma_{W_\mu^+\to\nu_i\bar{\ell}_i^2} \approx \frac{g^2 m_W^3 T}{192\pi^3}\left(2-\frac{m_{\nu_i}^2}{m_W^2}-\frac{m_{\ell_i}^2}{m_W^2}-\frac{(m_{\nu_i}^2-m_{\ell_i}^2)}{m_W^4}\right)\lambda\left(1,\frac{m_{\nu_i}^2}{m_W^2},\frac{m_{\ell_i}^2}{m_W^2}\right)K_1\left(\frac{m_W}{T}\right), \tag{B.46a}$$

$$\gamma_{Z_\mu\to\nu_i\overline{\nu_i}} \approx \frac{(g^2+g'^2)m_Z^3 T}{384\pi^3}\left(2-\frac{m_{\nu_i}^2}{m_Z^2}-\frac{m_{\ell_i}^2}{m_Z^2}-\frac{(m_{\nu_i}^2-m_{\ell_i}^2)}{m_Z^4}\right)\lambda\left(1,\frac{m_{\nu_i}^2}{m_Z^2},\frac{m_{\ell_i}^2}{m_Z^2}\right)K_1\left(\frac{m_Z}{T}\right). \tag{B.46b}$$

Using this, the order of the thermal interaction rate of active neutrinos after EWSB can be approximated as:

$$\begin{aligned}\Gamma_{\nu_i} &\approx \frac{6}{T^3}\left(3\gamma_{W_\mu^+\to\nu_i\bar{\ell}_i^2}+3\gamma_{Z_\mu\to\nu_i\overline{\nu_i}}\right)\\ &= \frac{3}{32\pi^3}\left[\frac{g^2 m_W^3}{T^2}\left(2-\frac{m_{\nu_i}^2}{m_W^2}-\frac{m_{\ell_i}^2}{m_W^2}-\frac{(m_{\nu_i}^2-m_{\ell_i}^2)}{m_W^4}\right)\lambda\left(1,\frac{m_{\nu_i}^2}{m_W^2},\frac{m_{\ell_i}^2}{m_W^2}\right)K_1\left(\frac{m_W}{T}\right)\right.\\ &\quad\left.+\frac{(g^2+g'^2)m_Z^3}{2T^2}\left(2-\frac{m_{\nu_i}^2}{m_Z^2}-\frac{m_{\ell_i}^2}{m_Z^2}-\frac{(m_{\nu_i}^2-m_{\ell_i}^2)}{m_Z^4}\right)\lambda\left(1,\frac{m_{\nu_i}^2}{m_Z^2},\frac{m_{\ell_i}^2}{m_Z^2}\right)K_1\left(\frac{m_Z}{T}\right)\right].\end{aligned} \tag{B.47}$$

This production rate in the region of interest ($T_{Sph} \lesssim T \lesssim T_c$) is shown in figure B.1. Thus, the thermal interaction rate for active neutrinos is roughly of the order $\Gamma_{\nu_i} \sim T \times 10^{-3}$.

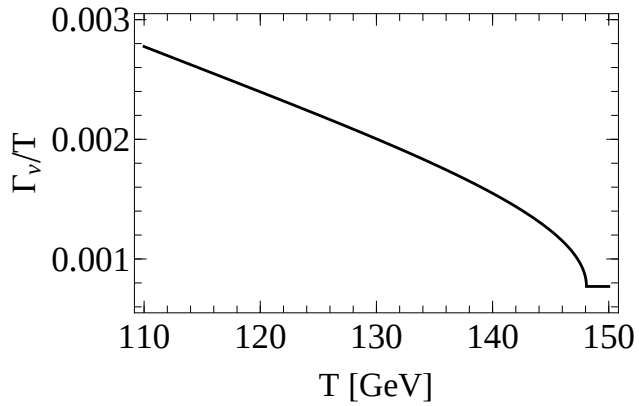

Figure B.1: Approximate thermal interaction rate of neutrinos normalized with respect to the temperature as a function of the temperature.

C Relevant Measured Observables

The measured masses of the Higgs and the massive gauge bosons are given by [76]:

$$m_W = 80.379 \pm 0.012 \text{ GeV}\,, \tag{C.1}$$
$$m_Z = 91.1876 \pm 0.0021 \text{ GeV}\,, \tag{C.2}$$
$$m_h = 125.10 \pm 0.14 \text{ GeV}\,. \tag{C.3}$$

The neutrino mass differences observed in neutrino oscillation experiments are [76]:

$$\Delta m^2_{\text{atm}} = \Delta m^2_{32} = (-2.546^{+0.034}_{-0.040}) \times 10^{-3}\text{eV}^2 \qquad \text{inverted order}\,, \tag{C.4a}$$
$$\Delta m^2_{\text{atm}} = \Delta m^2_{32} = (2.453 \pm 0.034) \times 10^{-3}\text{eV}^2 \qquad \text{normal order}\,, \tag{C.4b}$$
$$\Delta m^2_{\text{sol}} = \Delta m^2_{21} = (7.53 \pm 0.18) \times 10^{-5}\text{eV}^2\,. \tag{C.4c}$$

The measured angles of the CKM matrix are [76]:

$$\sin^2(\Theta_{12}) = 0.22650 \pm 0.00048\,, \tag{C.5a}$$
$$\sin^2(\Theta_{13}) = 0.00361^{+0.00011}_{-0.00009}\,, \tag{C.5b}$$
$$\sin^2(\Theta_{23}) = 0.04053^{+0.00083}_{-0.00061}\,, \tag{C.5c}$$
$$\delta_{\text{CP}} = 1.196^{+0.045}_{-0.043}\,, \tag{C.5d}$$

and for the PMNS matrix [76]:

$$\sin^2(\Theta_{12}) = 0.307 \pm 0.013\,, \tag{C.6a}$$
$$\sin^2(\Theta_{13}) = (2.18 \pm 0.07) \times 10^{-2}\,, \tag{C.6b}$$
$$\sin^2(\Theta_{23}) = 0.547 \pm 0.021 \qquad \text{inverted order}\,, \tag{C.6c}$$
$$\sin^2(\Theta_{23}) = 0.545 \pm 0.021 \qquad \text{normal order}\,, \tag{C.6d}$$
$$\delta_{\text{CP}} = (1.36 \pm 0.17) \times \pi\,. \tag{C.6e}$$

The bound on the sum of all active neutrino masses at 95 % CL is given by [2][1]

$$\sum m_\nu < 0.12 \text{ eV}\,. \tag{C.7}$$

The observed relic baryon and DM abundance for the base-ΛCDM model at 68 % CL are [2][2]

$$\Omega_B h^2 = (2.242 \pm 0.014) \times 10^{-2}\,, \tag{C.8a}$$
$$\Omega_{\text{DM}} h^2 = 0.11933 \pm 0.00091\,. \tag{C.8b}$$

The measured temperature of the CMB is [22]

$$T_0 = (2.72548 \pm 0.00057) K\,. \tag{C.9}$$

[1] The strongest bound from combining multiple measurements taken from p. 48 of reference [2].
[2] The values for $\Omega_B h^2$ and Ω_{DM} are taken from Table 2 of reference [2].

D Kinematics and Integrals

D.1 Kinematics of $2 \to 2$ Scattering Processes

The Mandelstam variables are defined as

$$s = p_s^2 := (p_1 + p_2)^2 = (p_3 + p_4)^2\,, \tag{D.1a}$$
$$t = p_t^2 := (p_1 - p_3)^2 = (p_4 - p_2)^2\,, \tag{D.1b}$$
$$u = p_u^2 := (p_1 - p_4)^2 = (p_3 - p_2)^2\,, \tag{D.1c}$$

and fulfill the relation

$$s + t + u = p_1^2 + p_2^2 + p_3^2 + p_4^2 = m_1^2 + m_2^2 + m_3^2 + m_4^2\,. \tag{D.2}$$

In the limit of negligible small masses ($m_1^2 + m_2^2 + m_3^2 + m_4^2 \ll s, t, u$), all relevant kinematic variables can be expressed in terms of s and $x = \cos\theta$:

$$t = -\frac{s}{2}(1 - x)\,, \tag{D.3a}$$
$$u = -\frac{s}{2}(1 + x)\,, \tag{D.3b}$$
$$p_1 p_2 = p_3 p_4 = \frac{s}{2}\,, \tag{D.3c}$$
$$p_1 p_3 = p_2 p_4 = \frac{s}{4}(1 - x)\,, \tag{D.3d}$$
$$p_1 p_4 = p_2 p_3 = \frac{s}{4}(1 + x)\,, \tag{D.3e}$$

with θ being the angle between $\vec{p}_1$ and $\vec{p}_3$.

On the other hand, considering sizable masses, the energies and momenta of the single particles in the center-of-mass frame are given by

$$E_{1,2} = \frac{s + m_{1,2}^2 - m_{2,1}^2}{2\sqrt{s}}\,, \qquad E_{3,4} = \frac{s + m_{3,4}^2 - m_{4,3}^2}{2\sqrt{s}}\,, \tag{D.4a}$$
$$|\vec{p}_1| = |\vec{p}_2| = \frac{\lambda[s, m_1^2, m_2^2]}{2\sqrt{s}}\,, \qquad |\vec{p}_3| = |\vec{p}_4| = \frac{\lambda[s, m_3^2, m_4^2]}{2\sqrt{s}}\,, \tag{D.4b}$$

with

$$\lambda\,[a, b, c] = \sqrt{a^2 + b^2 + c^2 - 2ab - 2ac - 2bc}\,. \tag{D.5}$$

If both incoming and both outgoing particles have the same masses ($m_1 = m_2 = m_i$ and $m_3 = m_4 = m_f$), this further simplifies to

$$E_1 = E_2 = E_3 = E_4 = \frac{\sqrt{s}}{2} \qquad |\vec{p}_1| = |\vec{p}_2| = \frac{1}{2}\sqrt{s - 4m_i^2}\,, \qquad |\vec{p}_3| = |\vec{p}_4| = \frac{1}{2}\sqrt{s - 4m_f^2}\,, \tag{D.6}$$

and

$$t = (p_1 - p_3)^2 = m_i^2 + m_f^2 - \frac{1}{2}\left(s - \sqrt{s - 4m_i^2}\sqrt{s - 4m_f^2}\,x\right), \tag{D.7a}$$

$$u = (p_1 - p_4)^2 = m_i^2 + m_f^2 - \frac{1}{2}\left(s + \sqrt{s - 4m_i^2}\sqrt{s - 4m_f^2}\,x\right), \tag{D.7b}$$

is obtained.

Considering $m_1 = m_3$ and $m_2 = m_4$ instead, t simplifies to

$$t = (p_1 - p_3)^2 = 2m_1^2 - \frac{1}{2s}\left((s + m_1^2 - m_2^2)^2 - \lambda[s, m_1^2, m_2^2]^2 x\right) = -\lambda[s, m_1^2, m_2^2]^2 \frac{(1-x)}{2s}. \tag{D.8}$$

D.2 Integrals and Functions

The Heaviside function is defined as

$$\Theta(x) := \begin{cases} 0, & \text{for } x < 0 \\ 1, & \text{for } x \geq 0 \end{cases}. \tag{D.9}$$

The series expansion of the contribution of a single particle to the free energy density in powers of the particle masses divided by the temperature for vanishing chemical potentials is given by[20]:

$$\begin{aligned} \frac{F_{\text{boson}}}{V} &= T\int \frac{d^3k}{(2\pi)^3} \ln\left[1 - \exp(-\sqrt{k^2 + m_i^2}/T)\right] \\ &\approx -\frac{\pi^2 T^4}{90} + \frac{m_i^2 T^2}{24} - \frac{m_i^3 T}{12\pi} - \frac{m_i^4}{64\pi^2}\left[\ln\left(\frac{m_i^2}{T^2}\right) + 2\gamma - \frac{3}{2} - 2\ln(4\pi)\right], \end{aligned} \tag{D.10a}$$

$$\begin{aligned} \frac{F_{\text{fermion}}}{V} &= T\int \frac{d^3k}{(2\pi)^3} \ln\left[1 + \exp(-\sqrt{k^2 + m_i^2}/T)\right] \\ &\approx \frac{7\pi^2 T^4}{720} - \frac{m_i^2 T^2}{48} - \frac{m_i^4}{64\pi^2}\left[\ln\left(\frac{m_i^2}{T^2}\right) + 2\gamma - \frac{3}{2} - 2\ln(\pi)\right], \end{aligned} \tag{D.10b}$$

with the Euler-Mascheroni constant $\gamma \approx 0.577$. Using this, the following integral occurring in thermal self-energy corrections is given by

$$\int d\tilde{k}_i\, f_i(E_k) = \frac{d}{dm_i^2}\frac{F}{V} = \begin{cases} \frac{T^2}{24} - \frac{mT}{8\pi} - \frac{m^2}{32\pi^2}\left[\ln\left(\frac{m^2}{T^2}\right) + 2\gamma - 1 - 2\ln(4\pi)\right] & \text{for bosons} \\ \frac{T^2}{48} - \frac{m^2}{32\pi^2}\left[\ln\left(\frac{m^2}{T^2}\right) + 2\gamma - 1 - 2\ln(\pi)\right] & \text{for fermions}. \end{cases} \tag{D.11}$$

Using the Boltzmann approximation and equation (D.16), the thermal decay rate can by evaluated analytically:

$$\begin{aligned} \gamma_{i\to f_1\cdots f_n} = \gamma_{f_1\cdots f_n\to i} &= \int d\tilde{k}_i(\Pi d\tilde{k}_{f_i})(2\pi)^4\delta(k_i - \Sigma k_{f_i})|M|^2_{i\to f_1\cdots f_n} e^{-\beta E_i} \\ &= \int d\tilde{k}_i\, 2m_i\Gamma_{i\to f_1\ldots f_n} e^{-\beta E_i} = \frac{m_i^2}{2\pi^2}\sqrt{a_{\Gamma_{i\to f_1\cdots f_n}}}\int_{m_i}^{\infty} dE_i\sqrt{E_i^2 - m_i^2}\, e^{-\beta E_i} \\ &= \frac{m_i^4}{2\pi^2}\sqrt{a_{\Gamma_{i\to f_1\cdots f_n}}}\int_1^{\infty} dx\sqrt{x^2-1}\, e^{-zx} = \frac{m_i^4}{2\pi^2}\sqrt{a_{\Gamma_{i\to f_1\cdots f_n}}}\frac{K_1(z)}{z}, \end{aligned} \tag{D.12}$$

where equation (2.23) and the Lorentz invariance of $d\tilde{k}_{f_i}$ is used to rewrite the thermal rate in terms of the decay width $\Gamma_{i\to f_1\dots f_n}$. Moreover, using equation (2.24), the thermal rate for $2\to 2$ scattering processes can be expressed as

$$\begin{aligned}\gamma_{i_1i_2\to f_1f_2} &= \int d\tilde{k}_{i_1}d\tilde{k}_{i_2}d\tilde{k}_{f_1}d\tilde{k}_{f_1}(2\pi)^4\delta(k_{i_1}+k_{i_2}-k_{f_1}-k_{f_2})|M|^2_{i_1i_2\to f_1f_2}e^{-\beta k_0}\\ &= \int \frac{dk}{(2\pi)^4}d\tilde{k}_{i_1}d\tilde{k}_{i_2}(2\pi)^4\delta(k-k_{i_1}-k_{i_2})\frac{\hat{\sigma}_{i_1i_2\to f_1f_2}}{\lambda\left[1,\frac{m_{i_1}}{s},\frac{m_{i_2}}{s}\right]}e^{-\beta k_0}\\ &= \frac{1}{8\pi}\int\frac{dk}{(2\pi)^4}\hat{\sigma}_{i_1i_2\to f_1f_2}e^{-\beta k_0}\,,\end{aligned} \tag{D.13}$$

which, in case of a reduced cross section only depending on the Mandelstam variable s, further simplifies to

$$\begin{aligned}\gamma_{i_1i_2\to f_1f_2} &= \frac{1}{64\pi^4}\int\limits_{s_{\min}}^{\infty}ds\,\hat{\sigma}(s)\int\limits_0^\infty d|\vec{k}|\frac{\vec{k}^2}{\sqrt{s+\vec{k}^2}}e^{-\beta\sqrt{s+\vec{k}^2}}\\ &= \frac{m_i^2}{64\pi^4}\int\limits_{u_{\min}}^{\infty}du\,\hat{\sigma}(u)\,u\int\limits_1^\infty dx\sqrt{x^2-1}\,e^{-z\sqrt{u}x}\\ &= \frac{m_i^4}{64\pi^4}\int\limits_{u_{\min}}^{\infty}du\sqrt{u}\,\hat{\sigma}(u)\frac{K_1\left(\sqrt{u}z\right)}{z}\,.\end{aligned} \tag{D.14}$$

The non-Lorentz invariant part of the massive vector boson propagator can be rewritten as

$$\begin{aligned}-\int\frac{dk}{(2\pi)^4}\frac{k_A^\mu k_A^\nu}{m_A^2}\frac{i}{k^2-m_A^2}e^{-ikx} &= \int\frac{dk}{(2\pi)^4}\left[\frac{k^\mu k^\nu-k_A^\mu k_A^\nu}{m_A^2}-\frac{k^\mu k^\nu}{m_A^2}\right]\frac{i}{k^2-m_A^2}e^{-ikx}\\ &= i\int\frac{dk}{(2\pi)^4}\left[\frac{(k_0^2-E_k^2)g^{\mu0}g^{\nu0}-(k_0-E_k)k^i(g^{\mu0}g^{\nu i}+g^{\mu i}g^{\nu0})}{m_A^2(k_0^2-E_k^2)}-\frac{k^\mu k^\nu}{m_A^2}\frac{1}{k^2-m_A^2}\right]e^{-ikx}\\ &= i\int\frac{dk}{(2\pi)^4}\left[\frac{g^{\mu0}g^{\nu0}}{m_A^2}-\frac{k^\mu k^\nu}{m_A^2}\frac{1}{k^2-m_A^2}\right]e^{-ikx}\,.\end{aligned} \tag{D.15}$$

Further integrals used in this thesis are

$$\int\limits_1^\infty dx\sqrt{x^2-1}\,e^{-ax} = K_1(a)\,, \tag{D.16}$$

$$\int\limits_0^\infty dx\,x^2e^{-a\sqrt{1+x^2}} = \frac{K_2(a)}{a}\,, \tag{D.17}$$

$$\int\limits_{-1}^{1}dx\,\frac{1}{a+bx} = \frac{1}{b}\ln\left(\frac{a-b}{a+b}\right)\,, \tag{D.18}$$

$$\int\limits_{x_1}^{x_2}dx\,\frac{1}{x^2+a} = \frac{1}{\sqrt{a}}\left[\arctan\left(\frac{x_2}{\sqrt{a}}\right)-\arctan\left(\frac{x_1}{\sqrt{a}}\right)\right]\,. \tag{D.19}$$

Bibliography

[1] K. Abe et al., *Solar neutrino results in Super-Kamiokande-III*, Phys. Rev. D **83** (2011) p. 052010, arXiv: 1010.0118 [hep-ex].

[2] N. Aghanim et al., *Planck 2018 results. VI. Cosmological parameters*, (2018), arXiv: 1807.06209 [astro-ph.CO].

[3] Evgeny K. Akhmedov, V. A. Rubakov, and A. Yu. Smirnov, *Baryogenesis via neutrino oscillations*, Phys. Rev. Lett. **81** (1998) p. 1359, arXiv: hep-ph/9803255.

[4] E. Aprile et al., *Dark Matter Search Results from a One Ton-Year Exposure of XENON1T*, Phys. Rev. Lett. **121** (2018) p. 111302, arXiv: 1805.12562 [astro-ph.CO].

[5] Peter Brockway Arnold and Larry D. McLerran, *Sphalerons, Small Fluctuations and Baryon Number Violation in Electroweak Theory*, Phys. Rev. **D36** (1987) p. 581.

[6] Dietrich Bodeker and Wilfried Buchmuller, *Baryogenesis from the weak scale to the GUT scale*, (2020), arXiv: 2009.07294 [hep-ph].

[7] M. Bohm, Ansgar Denner, and H. Joos, *Gauge theories of the strong and electroweak interaction*, 2001, ISBN: 978-3-519-23045-8, 978-3-322-80162-3, 978-3-322-80160-9.

[8] Debasish Borah, Arnab Dasgupta, and Sin Kyu Kang, *TeV Scale Leptogenesis via Dark Sector Scatterings*, Eur. Phys. J. C **80** (2020) p. 498, arXiv: 1806.04689 [hep-ph].

[9] D. Boyanovsky and Chiu Man Ho, *Sterile neutrino production via active-sterile oscillations: The Quantum Zeno effect*, JHEP **07** (2007) p. 030, arXiv: hep-ph/0612092.

[10] G. C. Branco et al., *Theory and phenomenology of two-Higgs-doublet models*, Phys. Rept. **516** (2012) p. 1, arXiv: 1106.0034 [hep-ph].

[11] W. Buchmuller, P. Di Bari, and M. Plumacher, *Leptogenesis for pedestrians*, Annals Phys. **315** (2005) p. 305, arXiv: hep-ph/0401240.

[12] W. Buchmuller, P. Di Bari, and M. Plumacher, *Some aspects of thermal leptogenesis*, New J. Phys. **6** (2004) p. 105, arXiv: hep-ph/0406014.

[13] Y. Burnier, M. Laine, and M. Shaposhnikov, *Baryon and lepton number violation rates across the electroweak crossover*, JCAP **0602** (2006) p. 007, arXiv: hep-ph/0511246.

[14] M.E. Carrington, *The Effective potential at finite temperature in the Standard Model*, Phys. Rev. D **45** (1992) p. 2933.

[15] James M. Cline, Kimmo Kainulainen, Pat Scott, and Christoph Weniger, *Update on scalar singlet dark matter*, Phys. Rev. D **88** (2013) p. 055025, [Erratum: Phys.Rev.D 92, 039906 (2015)], arXiv: 1306.4710 [hep-ph].

[16] Sidney R. Coleman and Erick J. Weinberg, *Radiative Corrections as the Origin of Spontaneous Symmetry Breaking*, Phys. Rev. D **7** (1973) p. 1888.

[17] Laura Covi, Esteban Roulet, and Francesco Vissani, *CP violating decays in leptogenesis scenarios*, Phys. Lett. B **384** (1996) p. 169, arXiv: hep-ph/9605319.

[18] Yanou Cui, Lisa Randall, and Brian Shuve, *A WIMPy Baryogenesis Miracle*, JHEP **04** (2012) p. 075, arXiv: 1112.2704 [hep-ph].

[19] Michela D'Onofrio, Kari Rummukainen, and Anders Tranberg, *Sphaleron Rate in the Minimal Standard Model*, Phys. Rev. Lett. **113** (2014) p. 141602, arXiv: 1404.3565 [hep-ph].

[20] L. Dolan and R. Jackiw, *Symmetry Behavior at Finite Temperature*, Phys. Rev. **D9** (1974) p. 3320.

[21] Glennys R. Farrar and M.E. Shaposhnikov, *Baryon asymmetry of the universe in the minimal Standard Model*, Phys. Rev. Lett. **70** (1993) p. 2833, [Erratum: Phys.Rev.Lett. 71, 210 (1993)], arXiv: hep-ph/9305274.

[22] D.J. Fixsen, *The Temperature of the Cosmic Microwave Background*, Astrophys. J. **707** (2009) p. 916, arXiv: 0911.1955 [astro-ph.CO].

[23] Marion Flanz, Emmanuel A. Paschos, Utpal Sarkar, and Jan Weiss, *Baryogenesis through mixing of heavy Majorana neutrinos*, Phys. Lett. B **389** (1996) p. 693, arXiv: hep-ph/9607310.

[24] Robert Foot and R.R. Volkas, *Studies of neutrino asymmetries generated by ordinary sterile neutrino oscillations in the early universe and implications for big bang nucleosynthesis bounds*, Phys. Rev. D **55** (1997) p. 5147, arXiv: hep-ph/9610229.

[25] Harald Fritzsch and Peter Minkowski, *Universality of the Basic Interactions*, Phys. Lett. B **53** (1974) p. 373.

[26] M. Fukugita and T. Yanagida, *Baryogenesis Without Grand Unification*, Phys. Lett. **B174** (1986) p. 45.

[27] M. Fukugita and T. Yanagida, *Resurrection of grand unified theory baryogenesis*, Phys. Rev. Lett. **89** (2002) p. 131602, arXiv: hep-ph/0203194.

[28] Camilo Garcia-Cely, Michael Gustafsson, and Alejandro Ibarra, *Probing the Inert Doublet Dark Matter Model with Cherenkov Telescopes*, JCAP **02** (2016) p. 043, arXiv: 1512.02801 [hep-ph].

[29] H. Georgi and S.L. Glashow, *Unity of All Elementary Particle Forces*, Phys. Rev. Lett. **32** (1974) p. 438.

[30] G. F. Giudice, A. Notari, M. Raidal, A. Riotto, and A. Strumia, *Towards a complete theory of thermal leptogenesis in the SM and MSSM*, Nucl. Phys. **B685** (2004) p. 89, arXiv: hep-ph/0310123.

[31] S.L. Glashow, *Partial Symmetries of Weak Interactions*, Nucl. Phys. **22** (1961) p. 579.

[32] J. Gluza and M. Zralek, *Feynman rules for Majorana neutrino interactions*, Phys. Rev. D **45** (1992) p. 1693.

[33] Eugene Golowich, *SCALAR MEDIATED PROTON DECAY*, Phys. Rev. D **24** (1981) p. 2899.

[34] Walter Grimus and Luis Lavoura, *Renormalization of the neutrino mass operators in the multi-Higgs-doublet standard model*, Eur. Phys. J. C **39** (2005) p. 219, arXiv: hep-ph/0409231.

[35] David J. Gross, Robert D. Pisarski, and Laurence G. Yaffe, *QCD and Instantons at Finite Temperature*, Rev. Mod. Phys. **53** (1981) p. 43.

[36] Jeffrey A. Harvey and Michael S. Turner, *Cosmological baryon and lepton number in the presence of electroweak fermion number violation*, Phys. Rev. **D42** (1990) p. 3344.

[37] Gerard 't Hooft, *Renormalizable Lagrangians for Massive Yang-Mills Fields*, Nucl. Phys. B **35** (1971) p. 167, ed. by J.C. Taylor.

[38] Gerard 't Hooft, *Symmetry Breaking Through Bell-Jackiw Anomalies*, Phys. Rev. Lett. **37** (1976) p. 8.

[39] Wei-Chih Huang, Heinrich Päs, and Sinan Zeißner, *Scalar Dark Matter, GUT baryogenesis and Radiative neutrino mass*, Phys. Rev. **D98** (2018) p. 075024, arXiv: 1806.08204 [hep-ph].

[40] Wei-Chih Huang, Heinrich Päs, and Sinan Zeissner, *Neutrino assisted GUT baryogenesis - revisited*, Phys. Rev. **D97** (2018) p. 055040, arXiv: 1608.04354 [hep-ph].

[41] Thomas Hugle, Moritz Platscher, and Kai Schmitz, *Low-Scale Leptogenesis in the Scotogenic Neutrino Mass Model*, Phys. Rev. **D98** (2018) p. 023020, arXiv: 1804.09660 [hep-ph].

[42] Gerard Jungman, Marc Kamionkowski, and Kim Griest, *Supersymmetric dark matter*, Phys. Rept. **267** (1996) p. 195, arXiv: hep-ph/9506380.

[43] Shoichi Kashiwase and Daijiro Suematsu, *Leptogenesis and dark matter detection in a TeV scale neutrino mass model with inverted mass hierarchy*, Eur. Phys. J. C **73** (2013) p. 2484, arXiv: 1301.2087 [hep-ph].

[44] S. Yu. Khlebnikov and M. E. Shaposhnikov,
The Statistical Theory of Anomalous Fermion Number Nonconservation,
Nucl. Phys. **B308** (1988) p. 885.

[45] Frans R. Klinkhamer and N. S. Manton,
A Saddle Point Solution in the Weinberg-Salam Theory, Phys. Rev. **D30** (1984) p. 2212.

[46] Edward W. Kolb, Andrei D. Linde, and Antonio Riotto, *GUT baryogenesis after preheating*,
Phys. Rev. Lett. **77** (1996) p. 4290, arXiv: `hep-ph/9606260`.

[47] Edward W. Kolb and Michael S. Turner, *The Early Universe*, Front. Phys. **69** (1990) p. 1.

[48] Edward W. Kolb and Stephen Wolfram, *Baryon Number Generation in the Early Universe*,
Nucl. Phys. B **172** (1980) p. 224, [Erratum: Nucl.Phys.B 195, 542 (1982)].

[49] V.A. Kuzmin, V.A. Rubakov, and M.E. Shaposhnikov,
On the Anomalous Electroweak Baryon Number Nonconservation in the Early Universe,
Phys. Lett. B **155** (1985) p. 36.

[50] M. Laine, M. Meyer, and G. Nardini,
Thermal phase transition with full 2-loop effective potential, Nucl. Phys. B **920** (2017) p. 565,
arXiv: `1702.07479 [hep-ph]`.

[51] Mikko Laine and Aleksi Vuorinen, *Basics of Thermal Field Theory*, vol. 925, Springer, 2016,
arXiv: `1701.01554 [hep-ph]`.

[52] Andrei D. Linde, *Infrared Problem in Thermodynamics of the Yang-Mills Gas*,
Phys. Lett. **B96** (1980) p. 289.

[53] Jiang Liu, *Phenomenological description of an unstable fermion*, (1993),
arXiv: `hep-ph/9304213`.

[54] Ernest Ma, *Verifiable radiative seesaw mechanism of neutrino mass and dark matter*,
Phys. Rev. **D73** (2006) p. 077301, arXiv: `hep-ph/0601225`.

[55] Takeo Matsubara, *A New approach to quantum statistical mechanics*,
Prog. Theor. Phys. **14** (1955) p. 351.

[56] Alexander Merle and Moritz Platscher, *Parity Problem of the Scotogenic Neutrino Model*,
Phys. Rev. **D92** (2015) p. 095002, arXiv: `1502.03098 [hep-ph]`.

[57] Luminita N. Mihaila, Jens Salomon, and Matthias Steinhauser, *Renormalization constants and beta functions for the gauge couplings of the Standard Model to three-loop order*,
Phys. Rev. **D86** (2012) p. 096008, arXiv: `1208.3357 [hep-ph]`.

[58] S. P. Mikheyev and A. Yu. Smirnov, *Resonant neutrino oscillations in matter*,
Prog. Part. Nucl. Phys. **23** (1989) p. 41.

[59] Peter Minkowski, $\mu \to e\gamma$ *at a Rate of One Out of* 10^9 *Muon Decays?*,
Phys. Lett. B **67** (1977) p. 421.

[60] Michael E. Peskin and Daniel V. Schroeder, *An Introduction to quantum field theory*,
Addison-Wesley, 1995, ISBN: 978-0-201-50397-5.

[61] Werner Rodejohann, *Neutrino-less Double Beta Decay and Particle Physics*,
Int. J. Mod. Phys. E **20** (2011) p. 1833, arXiv: `1106.1334 [hep-ph]`.

[62] A. D. Sakharov,
Violation of CP Invariance, c Asymmetry, and Baryon Asymmetry of the Universe,
Pisma Zh. Eksp. Teor. Fiz. **5** (1967) p. 32, [Usp. Fiz. Nauk161,61(1991)].

[63] Matthew D. Schwartz, *Quantum Field Theory and the Standard Model*,
Cambridge University Press, 2014, ISBN: 978-1-107-03473-0, 978-1-107-03473-0.

[64] M. Srednicki, *Quantum field theory*, Cambridge University Press, 2007,
ISBN: 978-0-521-86449-7, 978-0-511-26720-8.

[65] Steven Weinberg, *A Model of Leptons*, Phys. Rev. Lett. **19** (1967) p. 1264.

[66] Steven Weinberg, *Gauge and Global Symmetries at High Temperature*,
Phys. Rev. D **9** (1974) p. 3357.

[67] Steven Weinberg, *Perturbative Calculations of Symmetry Breaking*,
Phys. Rev. D **7** (1973) p. 2887.

[68] Steven Weinberg, *The Quantum theory of fields. Vol. 1: Foundations*,
Cambridge University Press, 2005, ISBN: 978-0-521-67053-1, 978-0-511-25204-4.

[69] Steven Weinberg, *The quantum theory of fields. Vol. 2: Modern applications*,
Cambridge University Press, 2013,
ISBN: 978-1-139-63247-8, 978-0-521-67054-8, 978-0-521-55002-4.

[70] H. Arthur Weldon, *Effective Fermion Masses of Order gT in High Temperature Gauge Theories with Exact Chiral Invariance*, Phys. Rev. **D26** (1982) p. 2789.

[71] H. Arthur Weldon, *Simple Rules for Discontinuities in Finite Temperature Field Theory*,
Phys. Rev. D **28** (1983) p. 2007.

[72] R. Wendell et al., *Atmospheric neutrino oscillation analysis with sub-leading effects in Super-Kamiokande I, II, and III*, Phys. Rev. D **81** (2010) p. 092004,
arXiv: `1002.3471 [hep-ex]`.

[73] L. Wolfenstein, *Neutrino Oscillations in Matter*, Phys. Rev. D **17** (1978) p. 2369.

[74] Sinan Zeißner, "Majorana-Neutrino unterstützte GUT Baryogenese",
MA thesis: Fakultät Physik, Technische Univerität Dortmund.

[75] Clarence Zener, *Nonadiabatic crossing of energy levels*,
Proc. Roy. Soc. Lond. **A137** (1932) p. 696.

[76] P.A. Zyla et al., *Review of Particle Physics*, PTEP **2020** (2020) p. 083C01.